Reflood Experiments With a 4-Rod Bundle

EPRI

EPRI NP-1277
Project 1118-1
Interim Report
December 1979

Keywords:
LWR
Safety
Reflood
Data
Zircaloy
Heat Transfer

Prepared by
University of California, Los Angeles
Los Angeles, California

ELECTRIC POWER RESEARCH INSTITUTE

Reflood Experiments With a 4-Rod Bundle

NP-1277
Research Project 1118-1

Interim Report, December 1979

Prepared by

UNIVERSITY OF CALIFORNIA, LOS ANGELES
Chemical, Nuclear and Thermal Engineering Department
Los Angeles, California 90024

Principal Investigators
V. K. Dhir
I. Catton

Student Participants
R. Ornedo
M. Drucker
J. Yaung
J. Murrin

Prepared for

Electric Power Research Institute
3412 Hillview Avenue
Palo Alto, California 94304

EPRI Project Manager
R. B. Duffey
Nuclear Power Division

ORDERING INFORMATION

Requests for copies of this report should be directed to Research Reports Center (RRC), Box 50490, Palo Alto, CA 94303, (415) 961-9043. There is no charge for reports requested by EPRI member utilities and affiliates, contributing nonmembers, U.S. utility associations, U.S. government agencies (federal, state, and local), media, and foreign organizations with which EPRI has an information exchange agreement. On request, RRC will send a catalog of EPRI reports.

NOTICE

This report was prepared by the organization(s) named below as an account of work sponsored by the Electric Power Research Institute, Inc. (EPRI). Neither EPRI, members of EPRI, the organization(s) named below, nor any person acting on their behalf: (a) makes any warranty or representation, express or implied, with respect to the accuracy, completeness, or usefulness of the information contained in this report, or that the use of any information, apparatus, method, or process disclosed in this report may not infringe privately owned rights; or (b) assumes any liabilities with respect to the use of, or for damages resulting from the use of, any information, apparatus, method, or process disclosed in this report.

Prepared by
University of California, Los Angeles
Los Angeles, California

EPRI PERSPECTIVE

PROJECT DESCRIPTION

For convenience, it is traditional in light water reactor safety analysis to use heat transfer data and correlations derived from experiments using steel-clad bundles. However, the thermal properties of steel are significantly different from Zircaloy cladding, and this particularly manifests itself in the quenching behavior. Since the position of the quench front is a reference point for the development of the post-dryout and film boiling heat transfer, it is important to estimate correctly its velocity and position. The thermal stresses on quenching are also important for estimating fuel rod integrity (cf. Three Mile Island).

PROJECT OBJECTIVE

The primary objective of this project was to investigate the quenching and heat transfer behavior relevant to Zircaloy-clad nuclear fuel.

PROJECT RESULTS

The experiments reported here show that Zircaloy cladding quenches faster than stainless steel cladding (up to twice as fast in a Zircaloy-clad bundle and 1.3 times as fast in a mixed bundle containing both steel- and Zircaloy-clad rods). This translates as an increase of up to 20% in core reflood rate for postulated accident conditions.

This work is coordinated with other EPRI reflooding and film boiler heat transfer studies, including pressurized water reactor and boiling water reactor bundle experiments (Research Project [RP] 959-1, RP1377-1), fundamental single tube work (RP248-1), and studies of various emergency cooling systems (RP341-2). Related analytic development has been reported in EPRI Special Report NP-1027-SR and in Nuclear Technology, 1979, 43, 22-27.

R. B. Duffey, Project Manager
Nuclear Power Division

Blank Page

ABSTRACT

Experiments are reported on the reflooding of a four-rod bundle in a new radio-frequency heating facility. A range of flowrates and surface temperatures have been covered.

The results show significant differences in the quenching rates of stainless-steel and zircaloy clad, and significant interaction between them in a mixed bundle. The results have beeen correlated utilizing conduction theory. Comments are made on the nature of the transient boiling curve.

Blank Page

CONTENTS

ILLUSTRATIONS

NOMENCLATURE

Bi	Biot number, $h\delta/k$
C	circumference of a rod, cm
D_h	hydraulic diameter
G	mass flow rate period, gm/s
h	heat transfer coefficient, W/cm^2 K
k	thermal conductivity of cladding material, W/cm K
Re	Reynolds number, UD_h/ν
T_o	quenching temperature
T_{sat}	saturation temperature at one atmosphere pressure
T_w	surface temperature
T*	dimensionless temperature, $(T_o-T_{sat})/(T_w-T_o)$
U	flooding velocity
u	quenching velocity
u*	dimensionless quenching velocity, $U\delta/\alpha$
α	thermal diffusivity of cladding material
δ	cladding thickness
ν	kinematic viscosity of water

SUMMARY

Quenching data for zircaloy and stainless steel clad 4-rod bundles have been obtained to supplement the data already existing in the literature. In particular, a filling material (Al_2O_3) with thermophysical properties comparable to UO_2 is used. The rods which are 1.1 mm in outside diameter, and are 1.2 meters high, are arranged in a square grid and are inductively heated. The experiments have been performed with initial rod surface temperatures up to 1140 K and flooding velocity varying over the range 1-30 cm/s. The subcooling of water at inlet has been either 75 K or 50 K.

Under identical flow conditions zircaloy is observed to quench faster than stainless steel. The difference in quenching times is seen to depend on the initial temperature of the rods, the flow velocity and on the liquid subcooling. Precursory cooling due to entrained droplets is observed to play a very important role in rod bundles, as the heat transfer associated with it is much higher than with normal film boiling. The quench front velocity data obtained on stainless steel rod bundles are compared with existing correlations by properly defining the quench front temperature and wall temperature ahead of the quench front. At an initial rod temperature of about 1000 K, complete oxidation of zircaloy is observed to take place in about three successive quenching experiments.

Section 1

INTRODUCTION

During off normal operation of a light water reactor, many situations may arise when the time variations in the heat flux and/or temperature of the surface of the fuel rod are very rapid. For example, during the blowdown phase of a hypothetical loss of coolant accident (LOCA), the rapid changes in coolant flowrate and thermodynamic conditions may lead to a rapid decrease in heat flux and an increase in the temperature of the fuel rods. In BWR's and PWR's, the ultimate cooling of the fuel rods following a LOCA is by quenching. Maintaining the integrity of the fuel rods until they are quenched is a major safety constraint. At present our knowledge of film and transition boiling heat fluxes during quenching of a bundle of tubes is limited and a better understanding of the transient boiling process needs to be gained, particularly for zircaloy clad bundles. The objective of this study is to provide such data.

BACKGROUND

Most experimental studies that bear on this work have been of heat transfer phenomena in simplified geometries. Boiling heat transfer during quenching of spheres in saturated liquid was found by Bergles and Thompson (1) to be different than previously measured. Subsequently, Veres and Florschuetz (2) claimed that the differences in heat fluxes observed by Bergles and Thompson were a manifestation of surface effects. Tachibana and Enya (3) have studied boiling from cylinders both in steady state as well as during quenching. Subcooled pool and forced flow film boiling during quenching of stainless steel, copper and silver spheres has been investigated by Dhir and Purohit (4).

Re-wetting experiments on single stainless steel and zircaloy tubes and rods subjected to falling water film and bottom flooding were performed by Piggott and Duffey (5). The experiments were conducted at one atmosphere pressure with water subcooling of 80 K. From their work, it was shown that zircaloy quenched faster than stainless steel. This is primarily due to smaller thermal capacity of zircaloy and axial conduction effects at the quench front. A model was developed by Duffey and Porthouse (6) for the conduction controlled re-wetting and improved by Sun et al. (7) to consider the heat transfer phenomena in three

distinct regions - a sputtering region between the wet and adiabatic regions. In a subsequent paper Sun et al. (8) further improved their model by including the prequench cooling ahead of the quench front as it occurs in emergency core cooling.

Film and transition boiling on hot rods subjected to cooling by a water jet have been investigated by Piggott, White and Duffey (9). They observed that the time needed to achieve wetting of the rods was strongly dependent on water subcooling, jet velocity, heat generation rate in the rod, jet impact angle and surface temperature. Surface finish and rod size were found to have little effect.

Iloeje, Plummer, Griffith and Rohsenow (10) studied film boiling and surface re-wetting in forced flow through a vertical tube. In their experiments, water in the quality range 30-100% and at 1000 psi was forced through an electrically heated 1 cm diameter inconel tube. Data for the minimum tube temperature to accomplish re-wetting and the transient heat fluxes in film, transition and nucleate boiling were obtained. Recently a detailed investigation of quenching of a vertical stainless steel tube, 14.4 mm inside diameter and 3.66 m long was carried out at UC Berkeley (11). In these experiments conducted at one atmosphere pressure, water was injected at the bottom and water subcoolings and inlet velocities were varied systematically. Data for the tube wall temperature as a function of time, the equivalent height of water in the tube and the exiting fluid temperature and quality and apparent heat transfer coefficient ahead of the quench front are reported.

Thus, except for the FLECHT experiments (12), very little quenching data on zircaloy tube bundles cooled from outside are available. Unfortunately, the high conductivity filler used in the heaters for the FLECHT experiments is atypical of reactor fuel rods. Further, the gap conductance is not properly simulated. Pearson et al. (13) have shown that filler properties can affect the quenching behavior. Currently, reactor safety analysis is based on the FLECHT data, and an arbitrary limit is imposed on the amount of clad oxidation to avoid fragmentation due to embrittlement and thermal shock.

PURPOSE OF THE PRESENT WORK

One of the major tasks of this work is to study quenching of zircaloy rods during reflooding and to compare it with stainless steel rods. The experiments are conducted in a 4-rod bundle to obtain data for quench front velocity, with additional information on pre-quench cooling. How the quenching rate depends

on variables such as high surface temperature, thermal capacity and oxidation of the surface of the rod is investigated for a prescribed liquid subcooling, flow velocity and initial temperature of the rod. The filler material in the rods is chosen such that it simulates the thermophysical properties of UO_2 that are relevant to the quenching process.

The second chapter of the report contains a description of the apparatus and the experimental procedure. The results of quenching of a 4-rod stainless steel bundle, of a 4-rod bundle having two stainless steel and two zircaloy rods, and of a 4-rod zircaloy bundle are discussed in Section 3. In this chapter a brief description of quenching behavior of a 4-rod bundle containing two zircaloy and two rods from FLECHT experiments is also given. Tabulation of all the data and graphical presentation of quench front locations and quench front velocity are done in Appendices A, B, C and D. The thermophysical properties of the Al_2O_3 fillers are compared with UO_2 in Appendix E.

Section 2

EXPERIMENTAL APPARATUS AND PROCEDURE

The experimental apparatus is designed so that thermal-hydraulic phenomena associated with quenching of rod bundles can be investigated. The rods are arranged in a square grid and the bundle is housed in a quartz tube. Vertical tubes (≃120 cm in height and about 1.1 cm in outer diameter) made of different materials and different wall thicknesses (0.71-0.88 mm) are used to simulate the fuel rods. Fillers made of Al_2O_3 and having the same diameter (0.91 cm) as that of UO_2 pellets are used. This leaves a gap of 0.07-0.24 mm between the filler and the cladding. Filler material is chosen such that thermophysical properties important in the quenching process are properly simulated. The properties of UO_2, zircaloy and the filler material are compared in Appendix E. The tubes are heated inductively to the desired temperature with power supply from a 450 kHz, 25 kw induction heater. Apart from the induction heater, the test equipment consists of an induction coil, a pneumatic cylinder to move the induction coil in the vertical direction, a nitrogen or argon gas supply system, a flow loop and the test section. A magnetic flowmeter, two Houston X-Y recorders, and a Sanborn 8 channel recorder comprise the necessary instrumentation.

DESCRIPTION OF THE APPARATUS

Schematic diagram of the experimental apparatus used in the quenching tests is shown in Fig. 2-1. The reservoir, which was designed as a pressure vessel, is made of stainless steel plate and is capable of safe operation at a pressure of 790 kPa (100 psig) and a temperature of 177°C (350°F). The pressure vessel has a volume of 49 liters (1.74 ft^3) and provision is made to heat the water by four 0.62 kw strip heaters placed on the outside of the pressure vessel. The pressure vessel is connected through a 25 mm (1 in) nominal size schedule 80, stainless steel pipe. About 60 cm downstream of the pressurizer, another line is taken off the main line so as to be able to charge or drain the pressure vessel. To avoid fluctuations in the reflood velocity under gravity flow conditions (≃1 atmosphere pressure), a centrifugal pump is placed between solenoid valve and the pressurizer. The flow rate through the pump is controlled by a

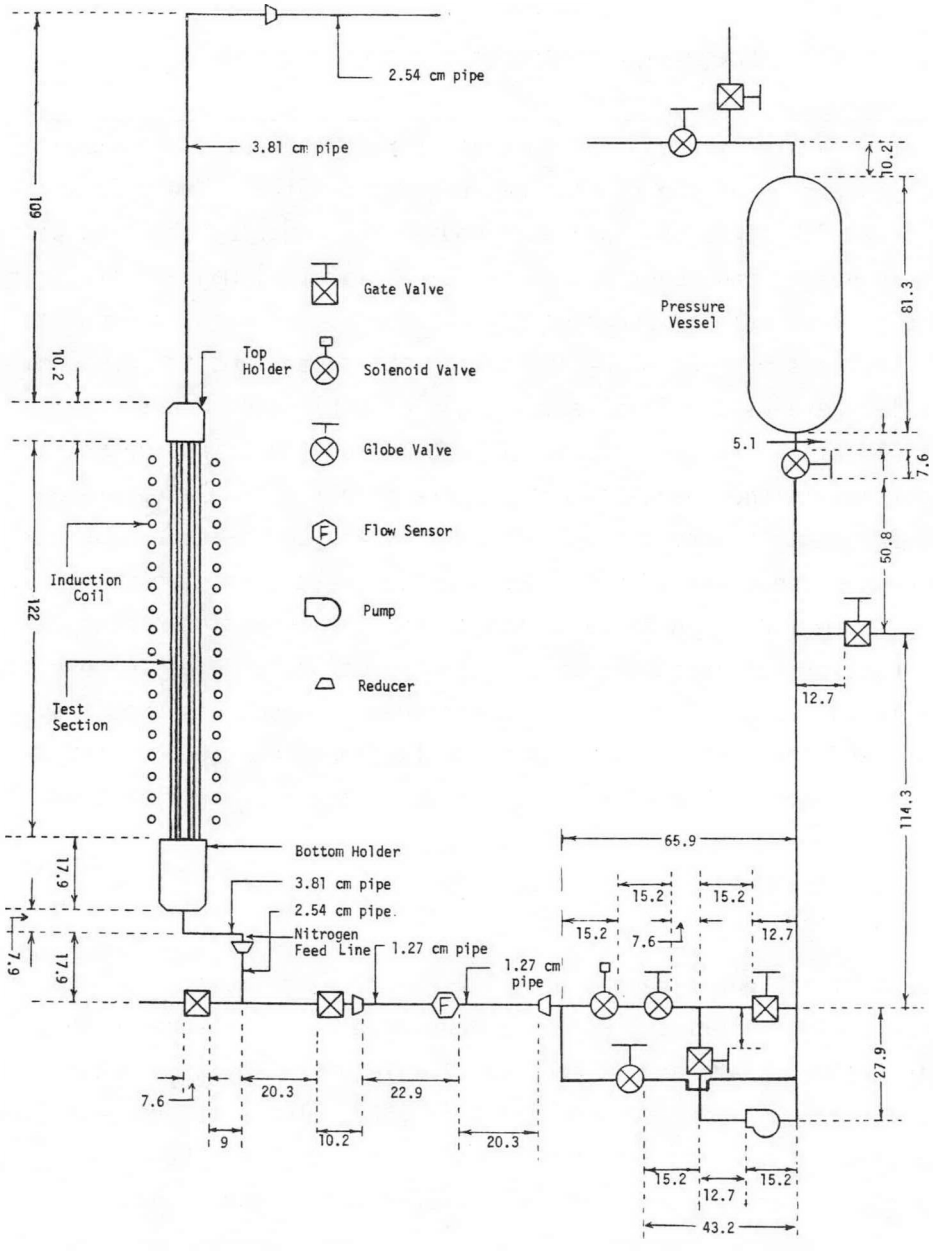

Figure 2-1 Schematic Diagram of the Experimental Setup (Dimensions Given in Centimeters)

metering globe valve. Flow rate in the pipeline connecting the test section is measured with a magnetic flow sensor, type Signet MK 315. Figure 2-2 shows the reflood velocity in the test section as a function of globe valve opening. The flow velocity increases linearly with valve opening for openings varying from 60° to 120°. Minimum flow velocity of 6 cm/s occurs for valve opening of 60°. Below this opening the pump starts to stall causing the flow in the test section to oscillate. To obtain flow velocities less than 6 cm/s in the test section, a by-pass loop is installed.

A 5.5 cm outer diameter and 0.1 cm wall thickness quartz tube serves as housing of the rod bundle. Figure 2-3 shows the test section and details of how the thermocouples are mounted on the stainless steel tubes. Chromel alumel, 26 gage thermocouples are spot welded 15 cm apart in the mid-portion of the tube. The bare thermocouple wires are carried through six hole 0.79 cm diameter alumina insulators (fillers). The alumina insulators are stacked one on another in the stainless steel tubes. To measure the representative temperature of the alumina insulators, the top thermocouple in one of the tubes (1) is fixed to the insulator with adhesive cement.

Details of the top and bottom rod holders are shown in Figs. 2-4 and 2-5 respectively. The holders are made out of 302 stainless steel stock. The outer quartz tube sits in the steps provided in the holder. Leakage of water from the tube is avoided by pushing the stainless steel sleeves against the top and bottom O-rings. The stainless steel tubes are held in a square grid with multihole orifice plates, which also serve to provide flow of coolant through the test section. The bottom orifice plate sits in the bottom holder, while the top plate is free floating. The free floating orifice plate is held in position with a light spring. Figure 2-6 shows a detailed view of the orifice plate.

To avoid bowing of the tubes due to uneven thermal expansion and contraction during preheating and quenching periods, pieces of 1.5 mm diameter tantalum wire were welded to the tubes as shown in Fig. 2-7. The tantalum wire did not overheat with respect to the stainless steel or zircaloy tubes and also it did not affect the flow area in any significant way. However, difficulty was encountered in spot welding the tantalum wire to the stainless steel or zircaloy tubes. The tantalum grid spacers are placed about 22.5 cm and 38 cm from the lower and upper ends of the tube bundle respectively.

An inert gas feed line is installed about 30 cm below the entrance to the test section to purge the test section prior to or during induction heating of the

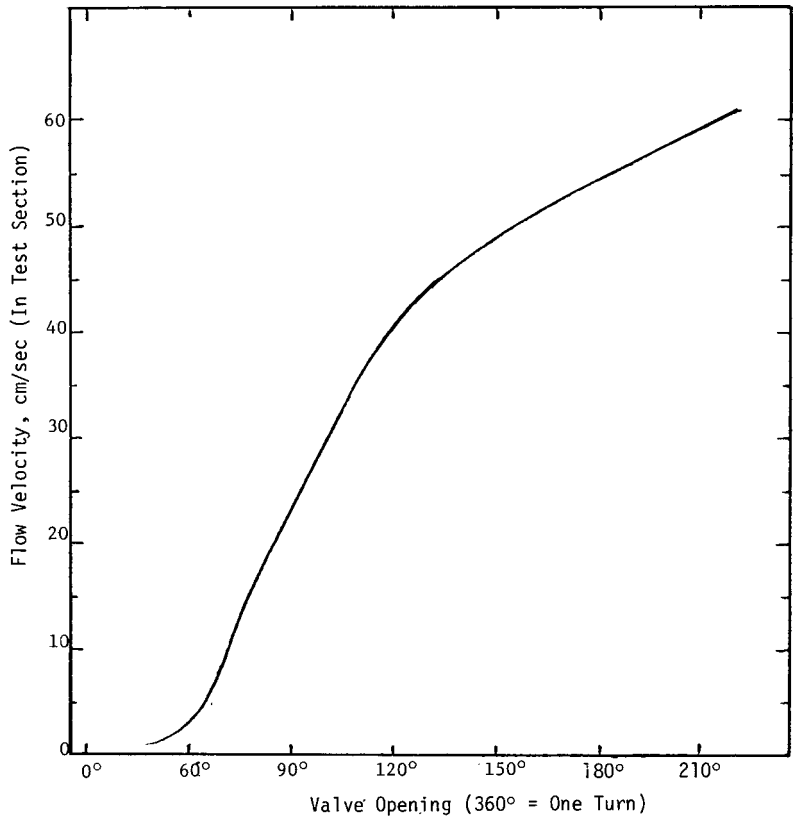

Figure 2-2 Calibration Curve of the Flow Rate with Respect to the Opening of the Globe Valve

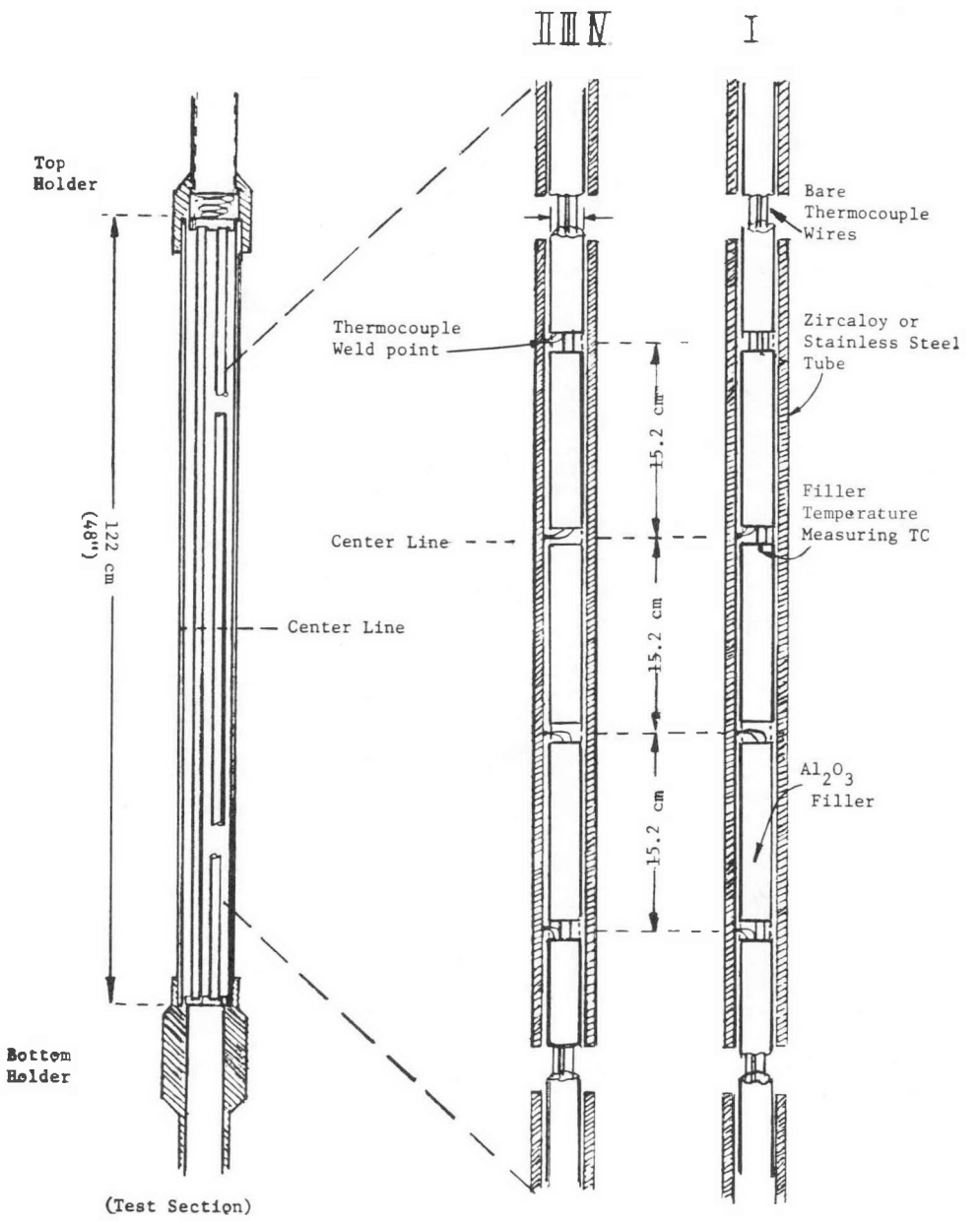

Figure 2-3 Detailed View of the Test Section and the Approximate Location of the Thermocouples in Four Rods

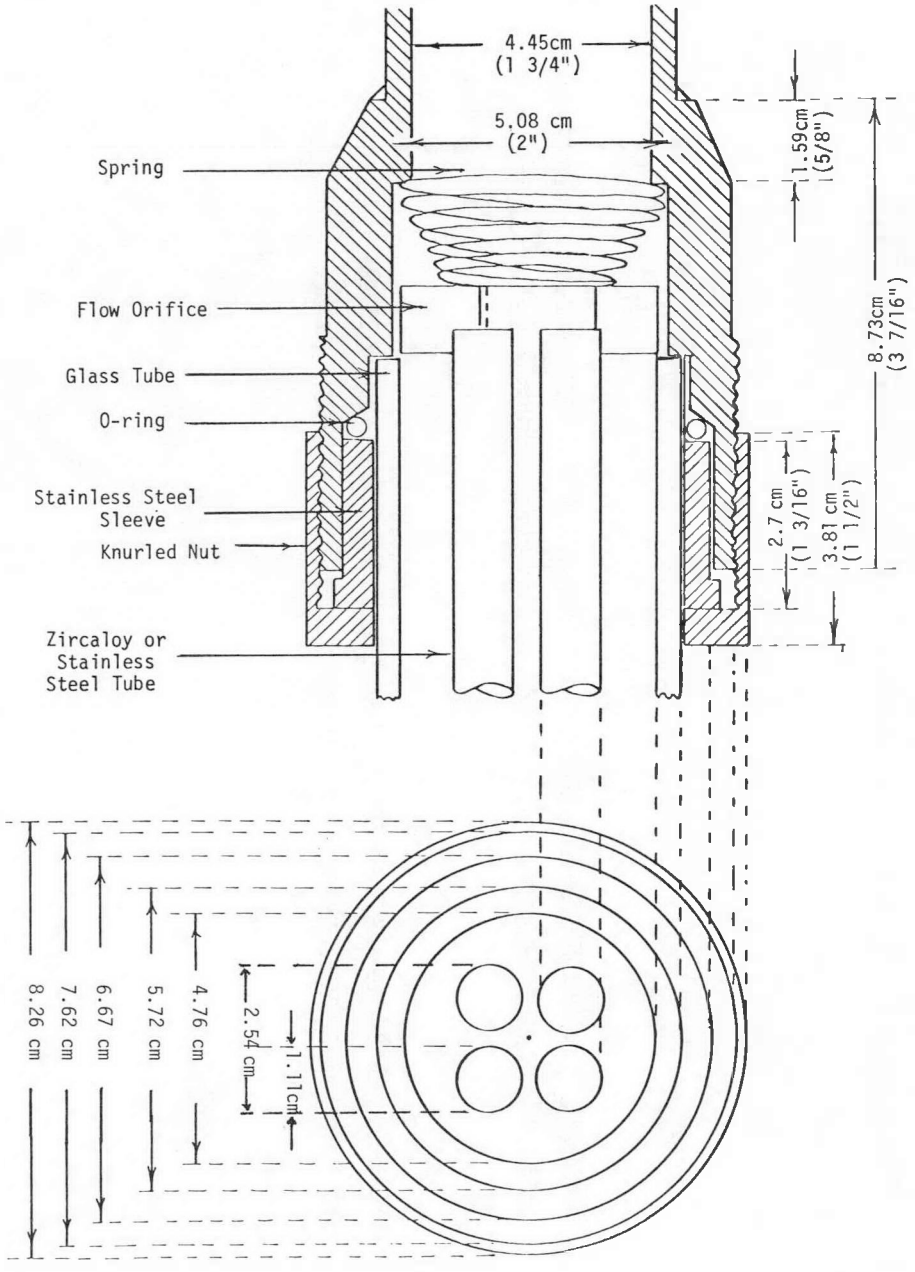

Figure 2-4 Details of the Top Holder

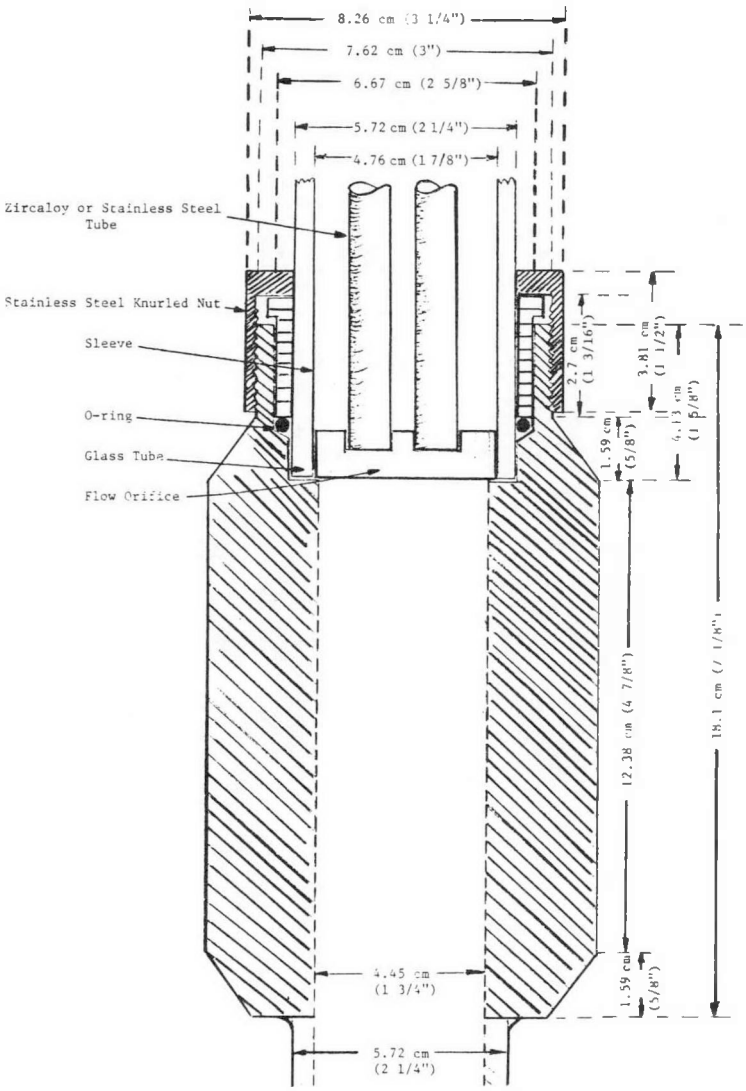

Figure 2-5 Details of the Bottom Holder

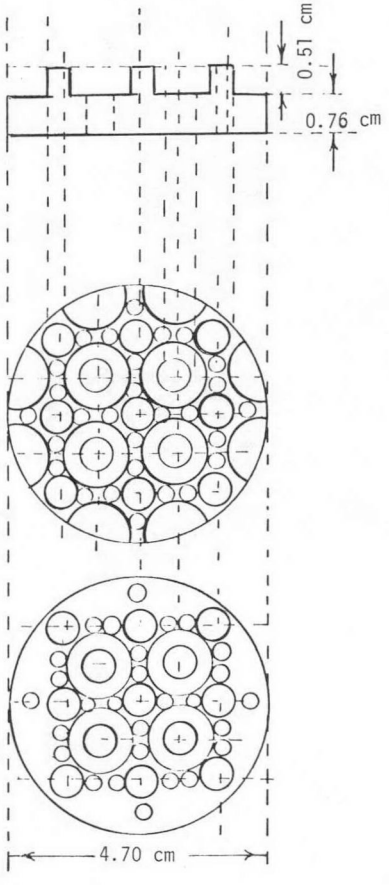

Figure 2-6 Orifice Plate

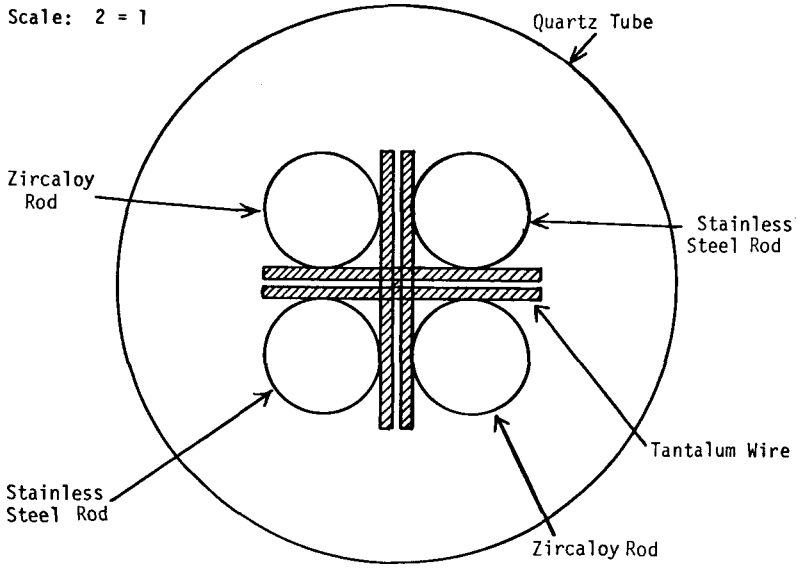

Figure 2-7 Tantalum Wire Grid Spacers

tubes. A solenoid operated pneumatic cylinder is used to move the induction coil over or away from the test section.

EXPERIMENTAL PROCEDURE

Prior to start of the experiment, various accessories and instruments are checked for their operability. De-ionized water is added to the pressurizer and heated to about the temperature at which a particular test run is to be made. Meanwhile, thermocouples are checked for electrical continuity and are hooked to various temperature recorders (2 Houston Single Channel X-Y Recorders and 2 Sanborn 8 channel recorders). The R-F generator and the recorders are switched on and are allowed to warm up for about 20 minutes. In the experiments in which a movie is to be made, Hycam movie camera is positioned and proper illumination of the test section is assured. Thereafter, the opening of the metering globe valve is adjusted to have the desired flow rate in the test section. The drain valve is opened while the valve connecting the water feed line to the test section is closed. This is done to facilitate preheating of the pipeline and this procedure is followed only in the experiments in which water is hotter than the ambient temperature.

Now nitrogen gas is allowed to flow through the test section and induction coil is properly located around the tube bundle. Thereafter, the work coil is energized. During the heating period, the temperature of at least three thermocouples located on three different rods are monitored. The water feed line is pre-heated by allowing water from the storage tank to flow through it and on to the drain. The radio frequency generator is switched off, when the tube temperature reaches a pre-determined value. The induction coil is then moved away from the field of view. The valve connecting the pump to the storage tank is opened and the pump is started. The solenoid valve in the water feed line is opened while the solenoid valve in the inert gas line is closed and the recorders are started. At the same time the movie camera is activated and the quenching phenomena on the rod bundle is captured on a TRI-X film running at 100 frames/s.

DATA REDUCTION

The main output of a quenching experiment is the temperature time traces of the inner surface of zircaloy or stainless steel cladding. A typical temperature-time trace corresponding to little or no precursory cooling is shown in Fig. 2-8. Here precursory cooling implies cooling of the rod by entrained water droplets.

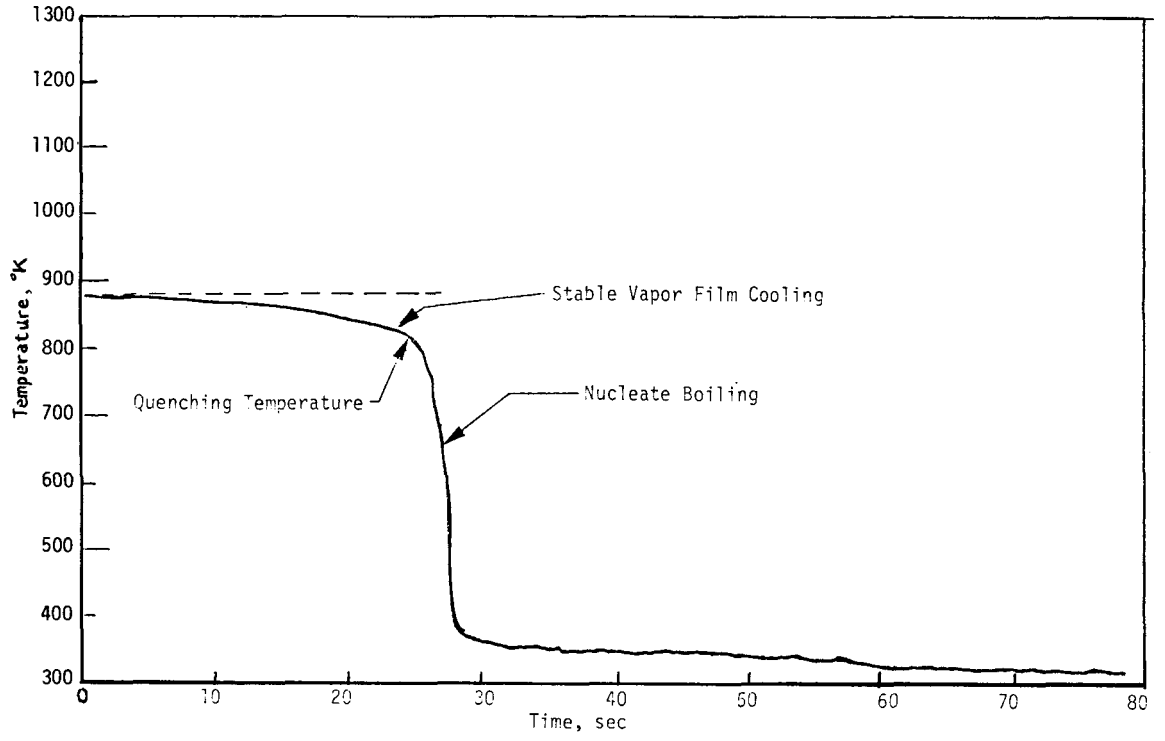

Figure 2-8 Temperature History of a Thermocouple in the Absence of Precursory Cooling

The temperature at which the slope of the temperature-time trace increased sharply was taken as the quenching temperature, T_Q. As the film boiling Biot number for the zircaloy and stainless steel cladding is very small (<0.06), little error is made in assuming T_Q as the surface temperature.

The quenching temperature is generally highest near the rod bundle where the water is at its coldest and decreases in the vertical direction as the liquid enthalpy increases. The wall temperature ahead of the quench front strongly affects the quench front velocity. This temperature varies both with time and axial position. In the present work, while correlation quench front velocity data, the temperature indicated by the thermocouple closest but ahead of the quench front was taken as the wall temperature, T_W.

The temperature histories when precursory cooling as a result of droplets hitting the rod surface ahead of the quench front occurs are shown in Figs. 2-9 and 2-10. The temperature history shown in Fig. 2-9 corresponds to the situation when droplets with short contact periods hit the cladding surface. The oscillations in the surface temperature are caused by repeated cooling of the surface by evaporation and subsequent insulation of it by the vapor. Figure 2-10 shows the case when the rod surface is cooled below the quenching temperature by precursory cooling alone. In this case the temperature history is indicative of cooling of the rod surface because of some sort of continued contact of liquid with the surface. No clear quenching temperature can be defined in this case.

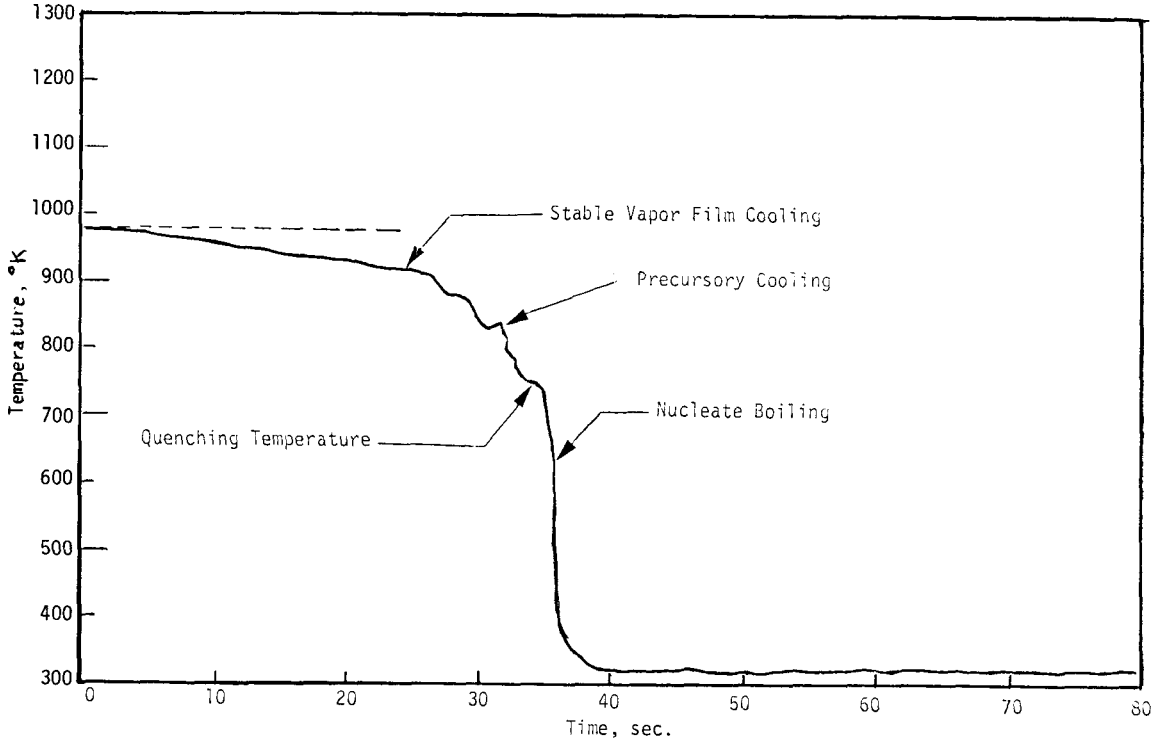

Figure 2-9 Temperature History of a Thermocouple in the Presence of Precursory Cooling (High Frequency Small Liquid Contact)

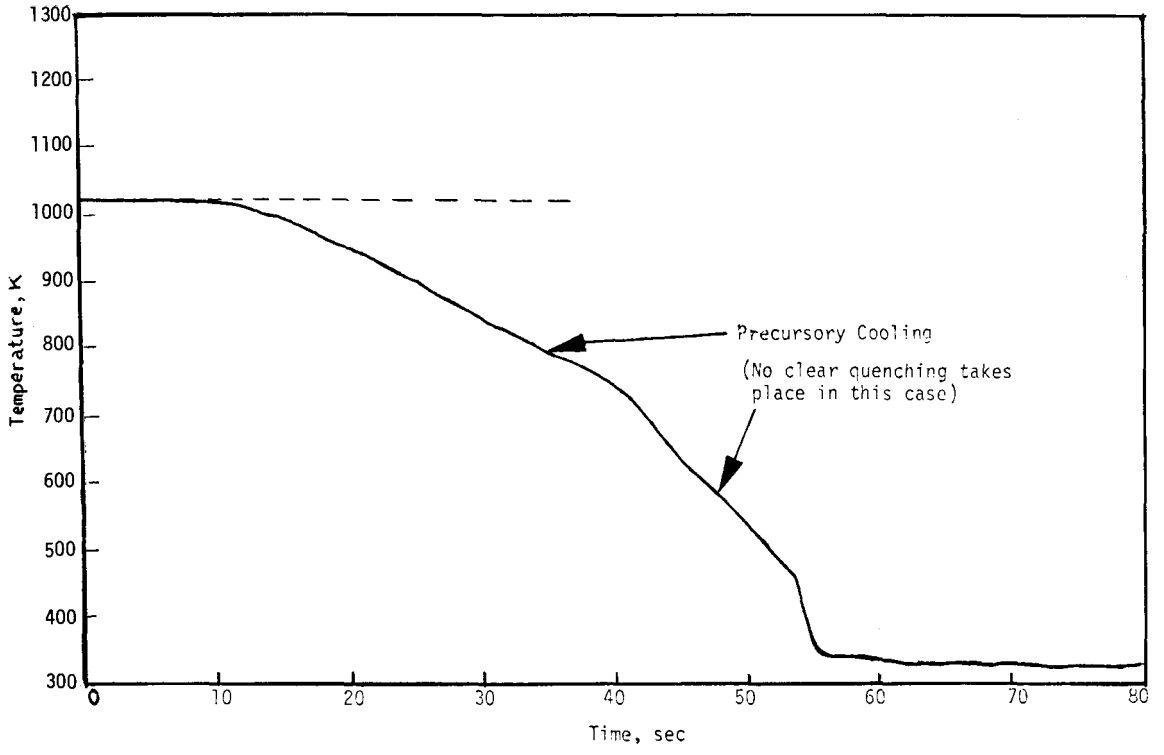

Figure 2-10 Temperature History of a Thermocouple in the Presence of Precursory Cooling (Low Frequency Large Liquid Contact)

Section 3

RESULTS AND DISCUSSION

A total of fifty-seven runs with all zircaloy, all stainless steel and a mixed bundle containing two zircaloy rods and two stainless steel rods were made. Out of these, three runs were made with all zircaloy bundles, thirteen runs with all stainless steel bundles and ten runs were made with a mixed bundle containing two zircaloy rods and two used rods from the FLECHT experiments. The remaining thirty-one runs were made with a 4 rod bundle containing two zircaloy and two stainless steel rods. In these experiments initial rod temperature varied from 900 to 1100 K and flooding velocities varied from 2-30 cm/s. For all of the runs, inlet water subcoolings were either about 75 K or about 50 K. All the data are tabulated and plotted in Appendices A through D.

The specific goals of these experiments were to understand the role of the following variables on the quenching behavior of the rods:

1. rod material properties
2. liquid subcooling and flooding velocity
3. initial rod temperature
4. precursory cooling
5. oxidation, especially in the case of zircaloy rods.

QUENCHING OF A 4 ROD STAINLESS STEEL BUNDLE

The temperature histories plotted in Appendix A show that the quenching temperature increases with liquid subcooling, but decreases because of the increase of enthalpy of the liquid as the liquid moves upward. In the lower region of the rod bundle, the quenching temperature is observed to increase with flow velocity, however at high flooding velocities, precursory cooling results in early cooling of the upper regions of the rod surface. This in turn leads to rapid rewetting of the rod bundle.

Typical quench front locations as a function of time for flooding velocity of 3 cm/s and 30 cm/s are plotted in Figs. 3-1 and 3-2. It is noted that quenching of different rods at the same vertical location may differ by a few seconds. The difference in quenching times is observed to decrease somewhat with increased flooding velocity. This observation is consistent with that reported

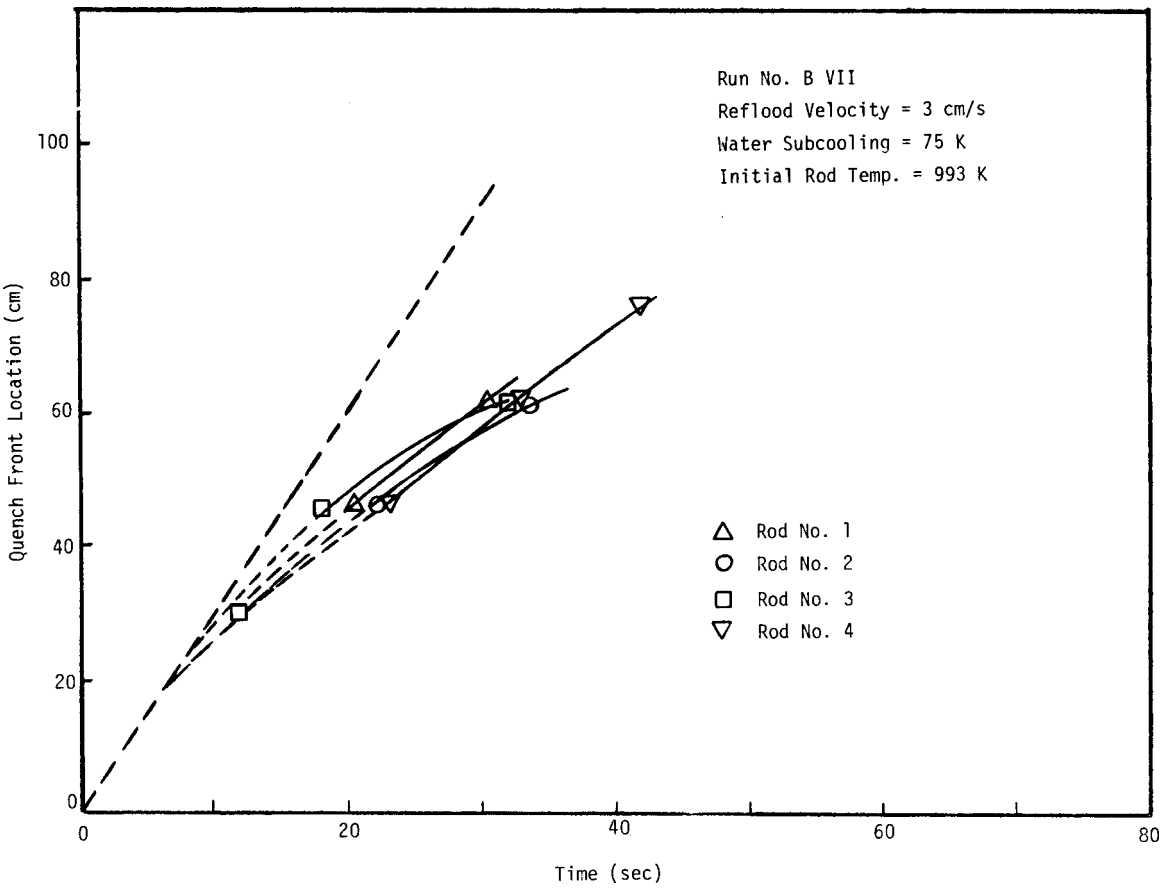

Figure 3-1 Quench Front Location as a Function of Time

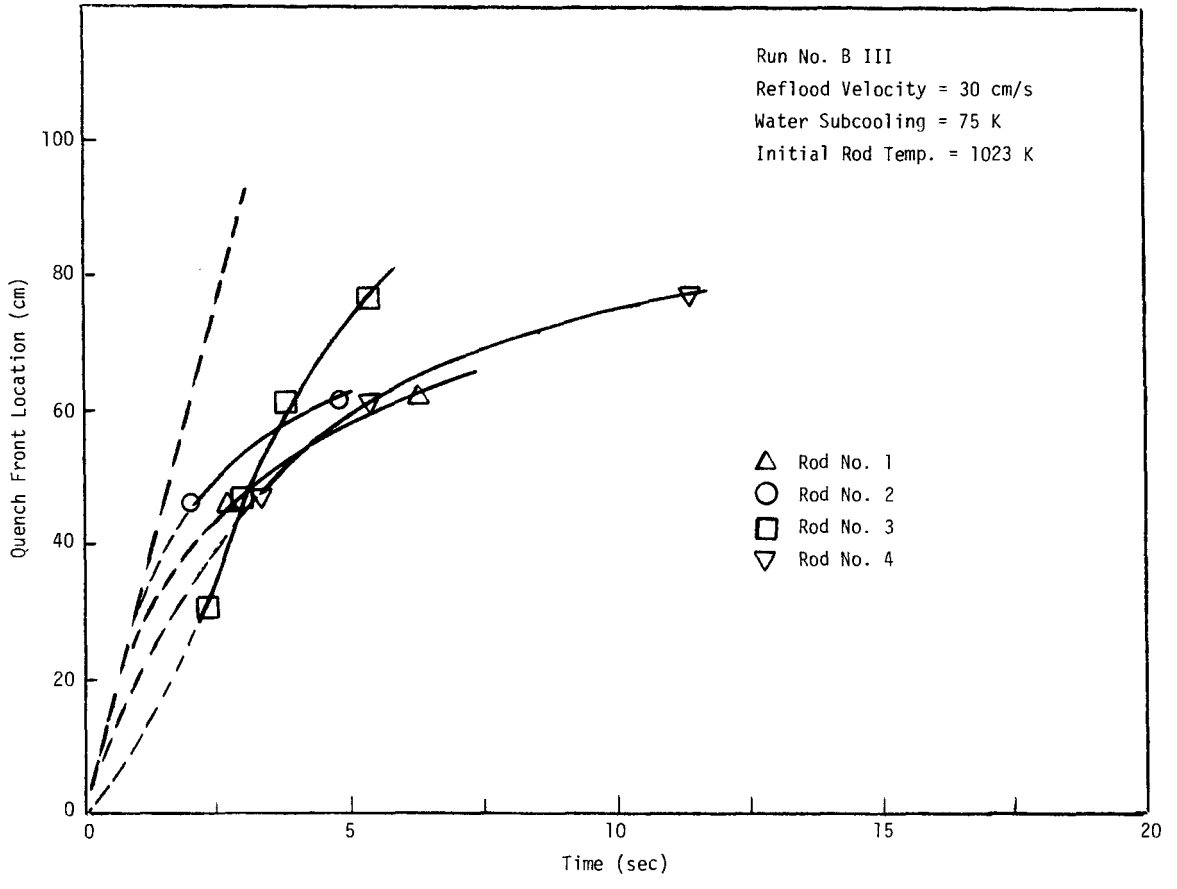

Figure 3-2 Quench Front Location as a Function of Time

in the literature by various other investigators. Increased subcooling of the liquid is also found to have similar effect. The initial temperature of the rods at the ends were generally less than that at the middle section because of nonuniform heat input to the rods as well as due to conduction of heat into the rod bundle holder. For this reason, quench front did not form in the first 15-20 cm of the rod bundle. Also, in certain instances, especially at higher flooding velocities, the precursory cooling resulted in early quenching of the upper end regions. This, in turn, caused a second quench front to move from top to bottom.

The quench front velocities as deduced from quench front location data indicate that quench front velocities generally increase with flooding velocity and inlet subcooling. For flooding velocities of 9 cm/s or higher, the quench front velocities are significantly higher in the lowermost and uppermost parts of the rod bundle. The quench front velocity is minimum in the middle portion of the rod bundle. Figure 3-3 shows one such case. Higher quench front velocities in the lower region of the rod bundle are due to larger subcoolings whereas in the upper region, the rods quench faster because of precursory cooling. In the middle portion of the rod bundle, the liquid is nearly saturated and inverse annular flow conditions exist. Quench front velocity in the middle portion of the rod bundle is plotted in Fig. 3-4 as a function of flooding velocity. The inlet water subcooling for the data plotted in Fig. 3-4 was 75°C whereas the initial rod temperature was 1000 ± 25 K. It is noted that for a flooding rate of 1 cm/s, the quench front velocity is about the same as the flooding velocity. For higher flooding rates, quench front velocity increases slowly with flooding velocity. The subcooling of liquid at inlet has little effect on the total quenching time as long as flooding velocities are small ($\simeq$2 cm/s). However, at higher flooding velocities liquid subcooling tends to reduce the total quenching time. This reduction in quenching time results from higher quenching velocities in the lower regions of the rod bundle where liquid is still subcooled.

QUENCHING OF THE 4 ROD BUNDLE CONTAINING TWO STAINLESS STEEL AND TWO ZIRCALOY RODS

The quench front location data on stainless steel and zircaloy rods as obtained from one of the movies are shown in Fig. 3-5. In this figure, the quench front location, as interpreted from the temperature-time traces of thermocouple output in the manner described in Section 2, is also plotted. It is noted from Fig. 3-5 and other data plotted in Appendix B that zircaloy quenches faster than

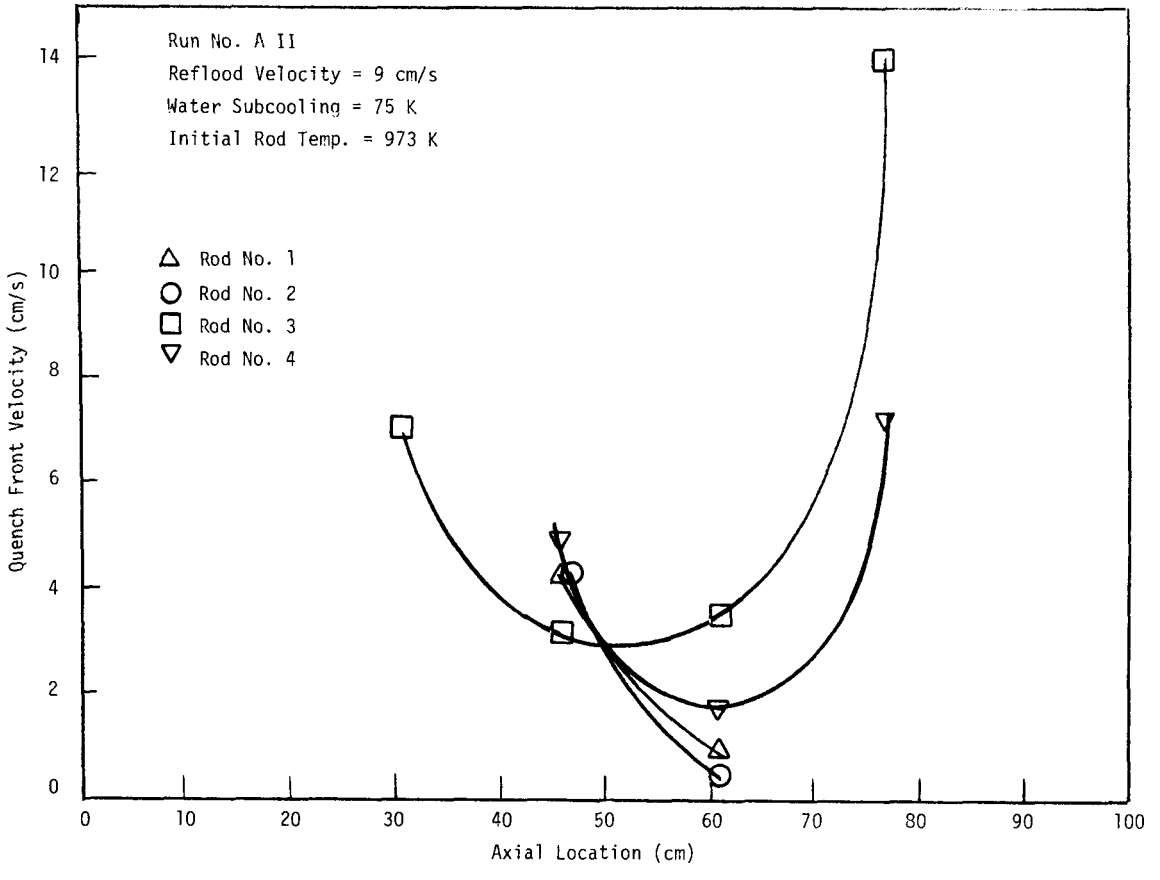

Figure 3-3 Quench Front Velocity as a Function of Height

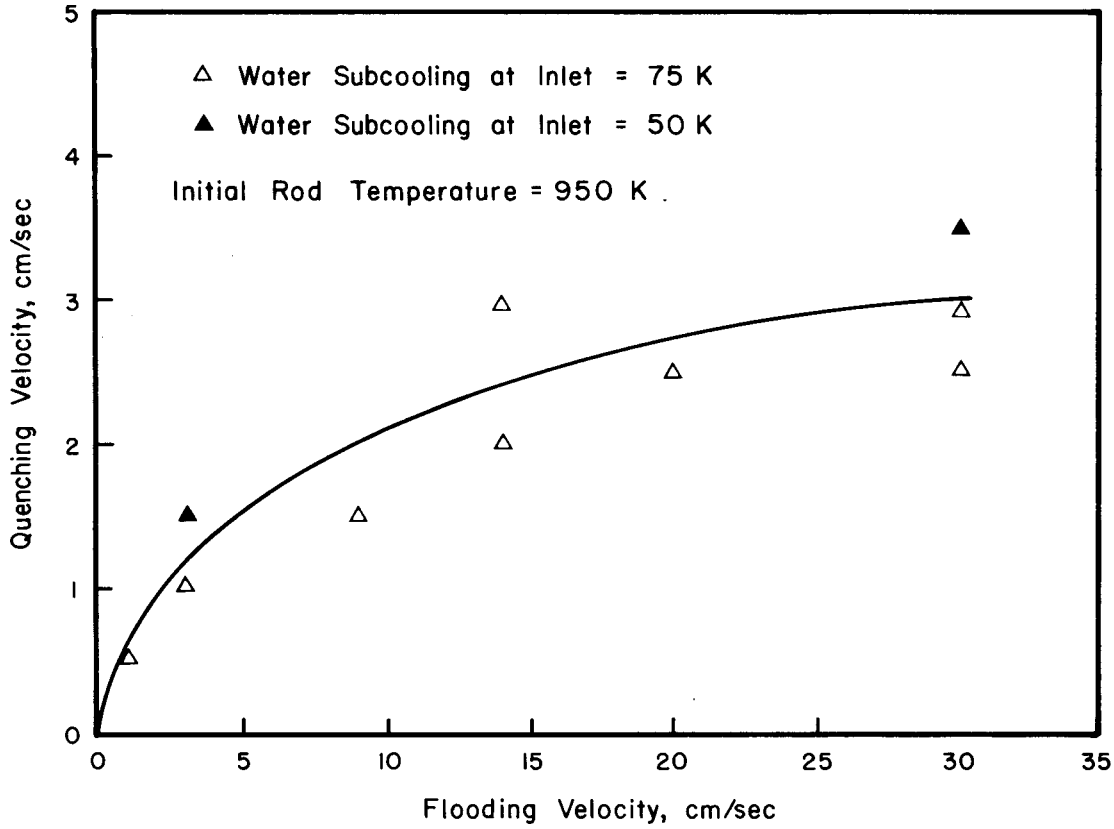

Figure 3-4 Quench Front Velocity in the Middle Portion of All Stainless Steel Rod Bundle

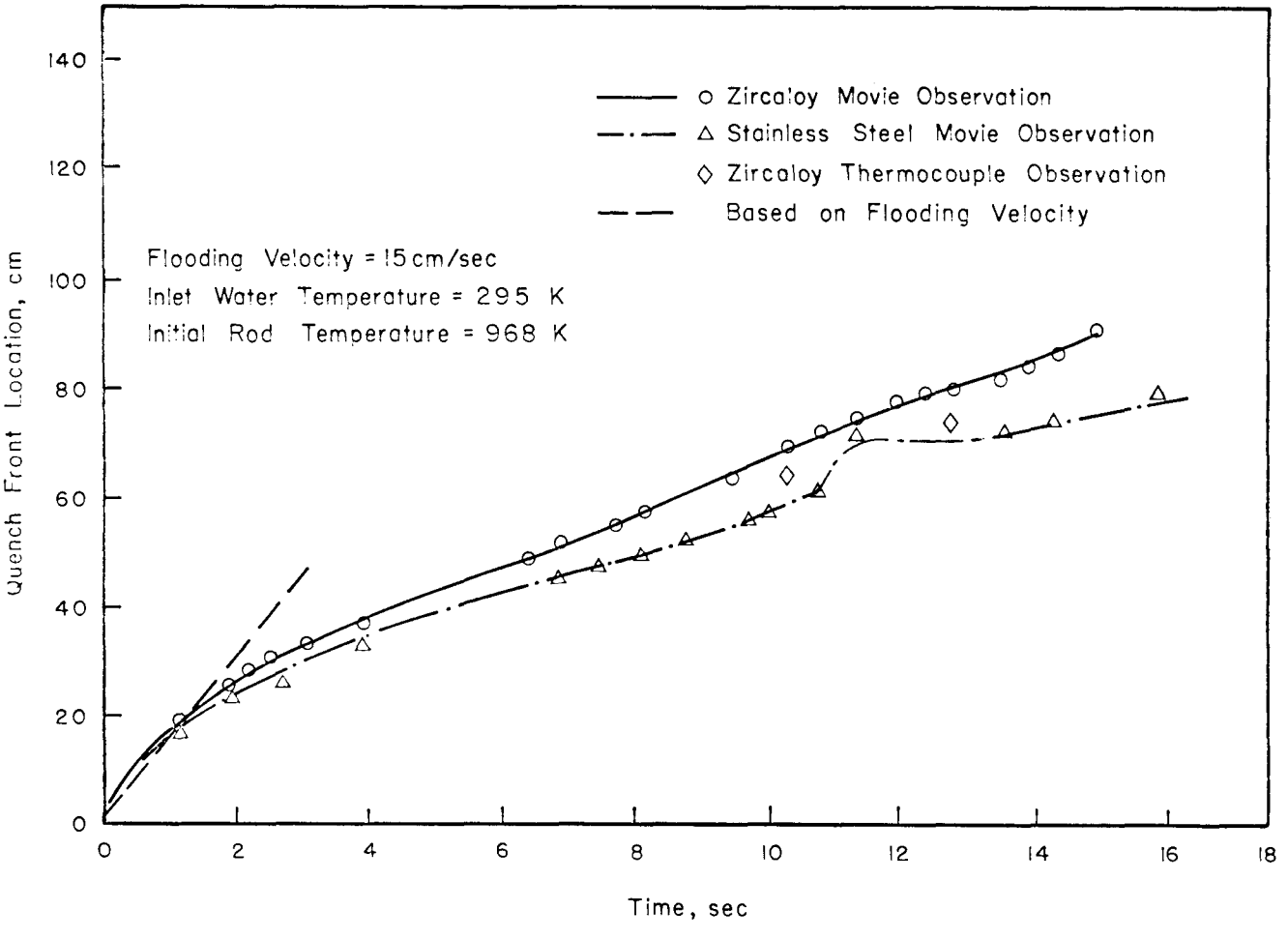

Figure 3-5 Quench Front Location as a Function of Time on Zircaloy and Stainless Steel Rods

stainless steel. The thermocouple observations are generally in agreement with the observations from the movies during the early periods of quenching or when the flooding velocity is small. However, at higher elevations where precursory cooling becomes important, thermocouple observations can be misleading. This is mostly because of difficulty in defining a quenching temperature on the temperature time trace. Many times the agitation (breakup of liquid droplets) created by the faster moving quench front was observed to cause local breakup of vapor film on the rod with a slower moving quench front. This led to a kind of step process during which the slower moving quench front caught up with the faster moving quench front. Such a trend can clearly be seen from the data plotted in Fig. 3-5.

Different phases of the quenching process as observed in the movies are reproduced in Figs. 3-6 through 3-11. Zircaloy (right) and stainless steel rods (left) prior to heating are shown in Fig. 3-6. Figure 3-7 shows precursory droplet motion well ahead of the free surface of the coolant two phase mixture. The slug flow conditions below the free surface and droplet motion above the free surface of coolant can be seen in Fig. 3-8. Fully developed slug flow below the free surface and well ahead of the quench front is shown in Fig. 3-9. Figure 3-10 shows film boiling immediately ahead of the quench front. It is interesting to note the existence of a highly ripply vapor film on the stainless steel rod. Figure 3-11 shows the quench front locations on the stainless steel and zircaloy rods. The quench front on the zircaloy rod is well ahead of that on the stainless steel rod. Nucleate boiling just behind the quench front can be clearly seen on both ends.

Typical quench front velocities as reduced from quench front location data are plotted in Figs. 3-12 and 3-13. The data in Fig. 3-12 was reduced from thermocouple observations. It is noted from these figures as well as from the data plotted in Appendix B that quench front velocity in the middle portion of the rod bundle where coolant is saturated and inverse annular flow conditions exist is higher on zircaloy rods as compared to stainless steel rods. Quench front velocities on zircaloy and stainless steel rods for different flooding velocities are shown in Fig. 3-14. For the data plotted in Fig. 3-14, the initial rod temperature was 950 ± 20 K while the subcooling of water at the inlet to the rod bundle was 78 ± 2 K. It must be pointed out that the quench front velocities plotted in Fig. 3-14 are only for the mid-plane region of the rod bundle. It is noted from Fig. 3-14 that difference in quenching velocities for zircaloy and stainless steel increases with flooding velocity. In the mixed bundle, the

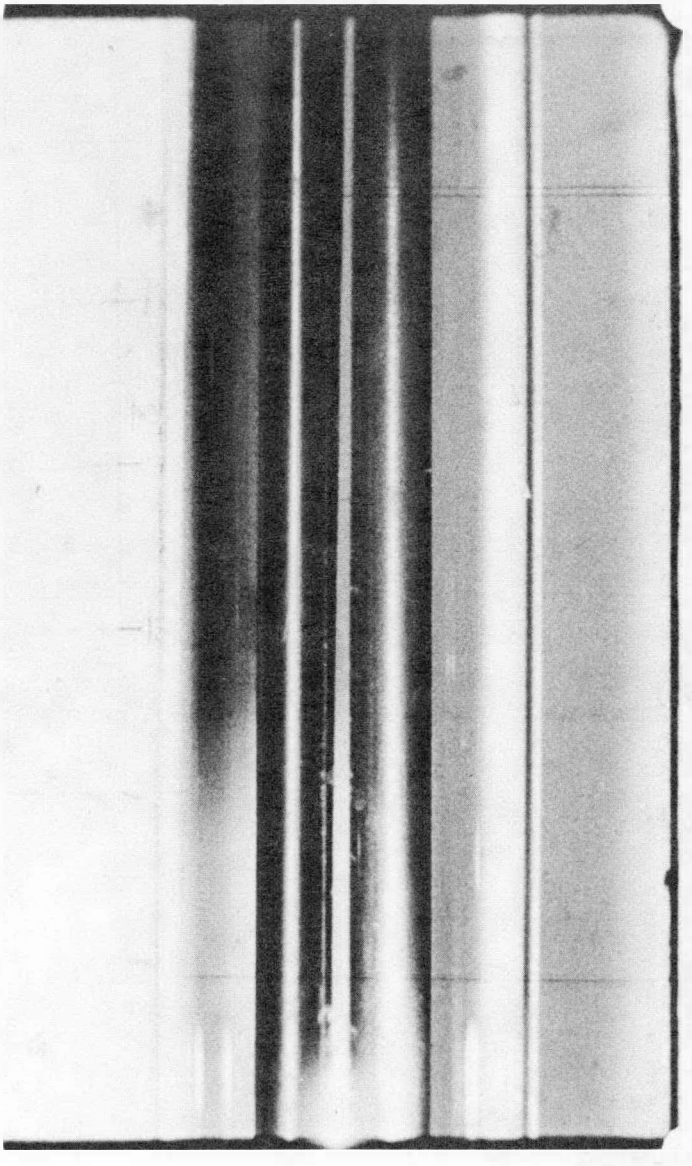

Figure 3-6 Relative Locations of Stainless Steel (Left) and Zircaloy (Right) Rods in the 4 Rod Bundle

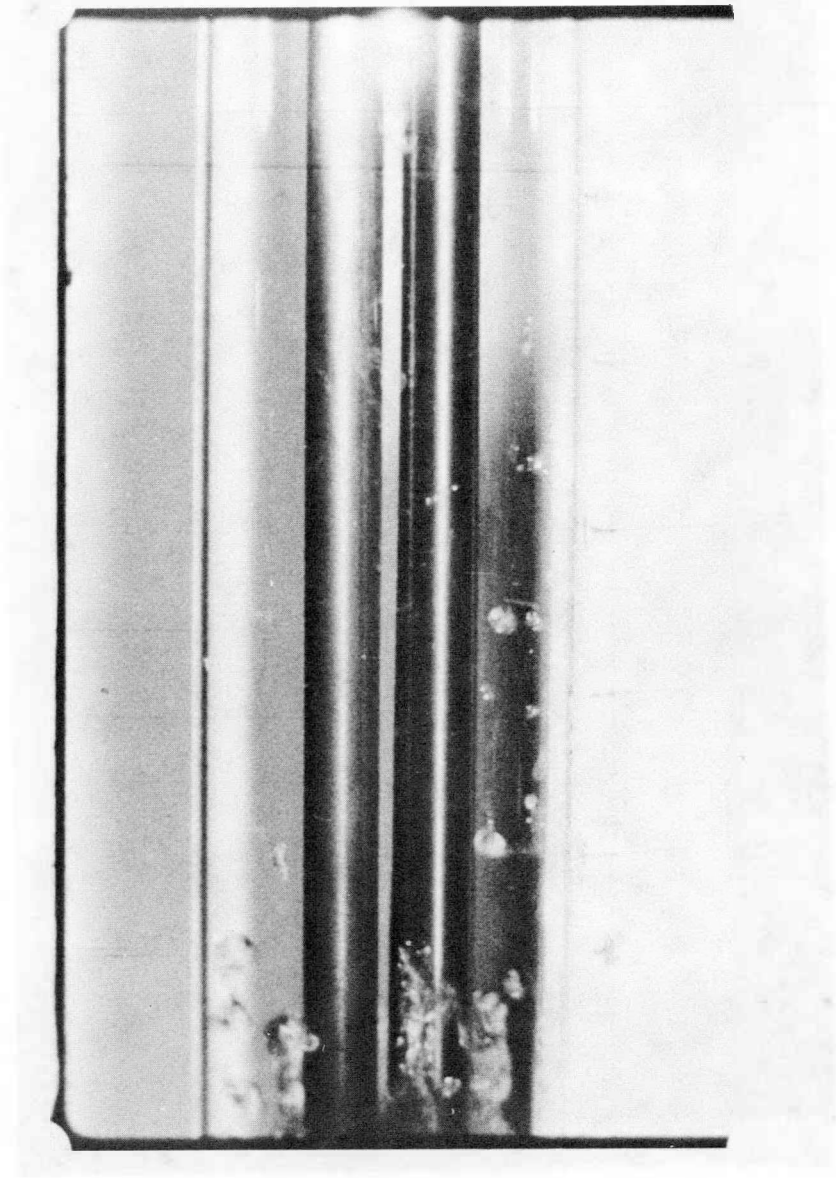

Figure 3-7 Precursory Droplet Motion Well Ahead of Free Surface. Run No. D-II; Flooding Velocity 3 cm/s; Initial Rod Temperature 968 K

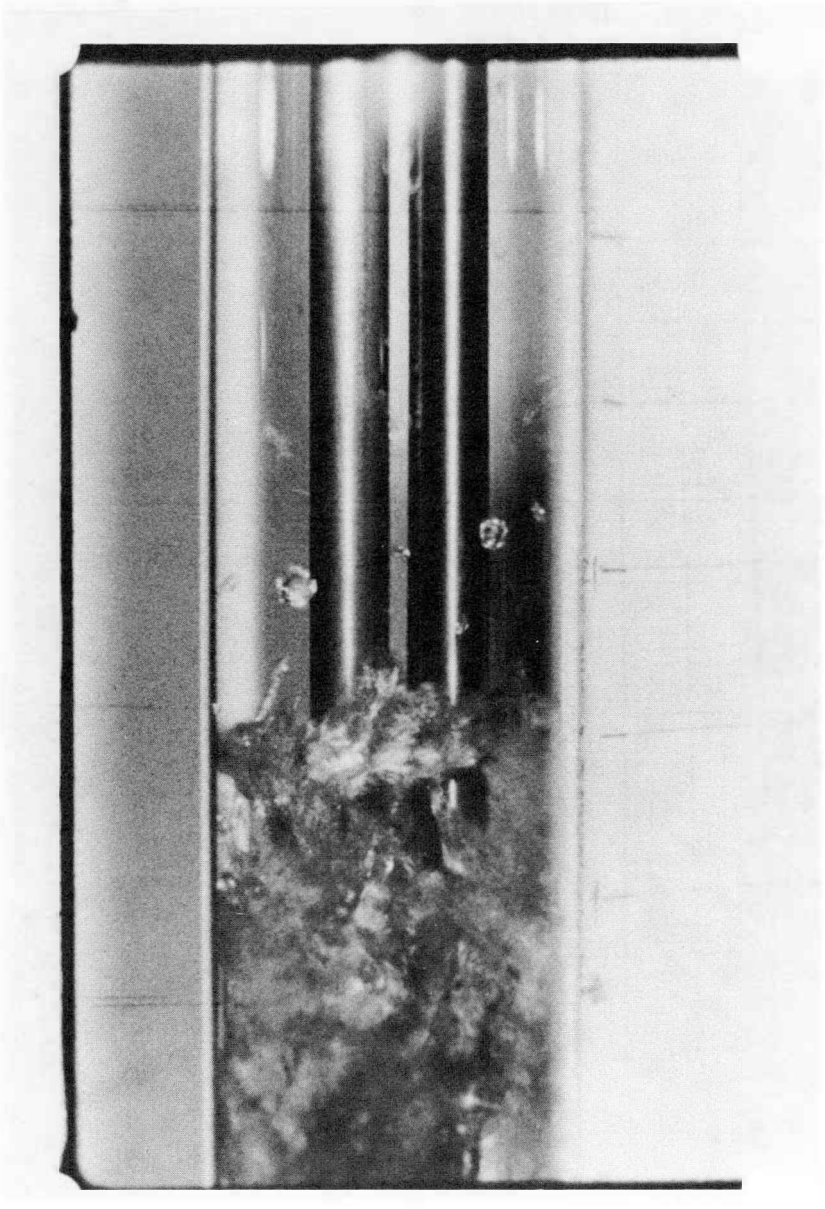

Figure 3-8 Free Surface of the Two Phase Mixture. Run No. D-II; Flooding Velocity 3 cm/s; Initial Rod Temperature 968 K

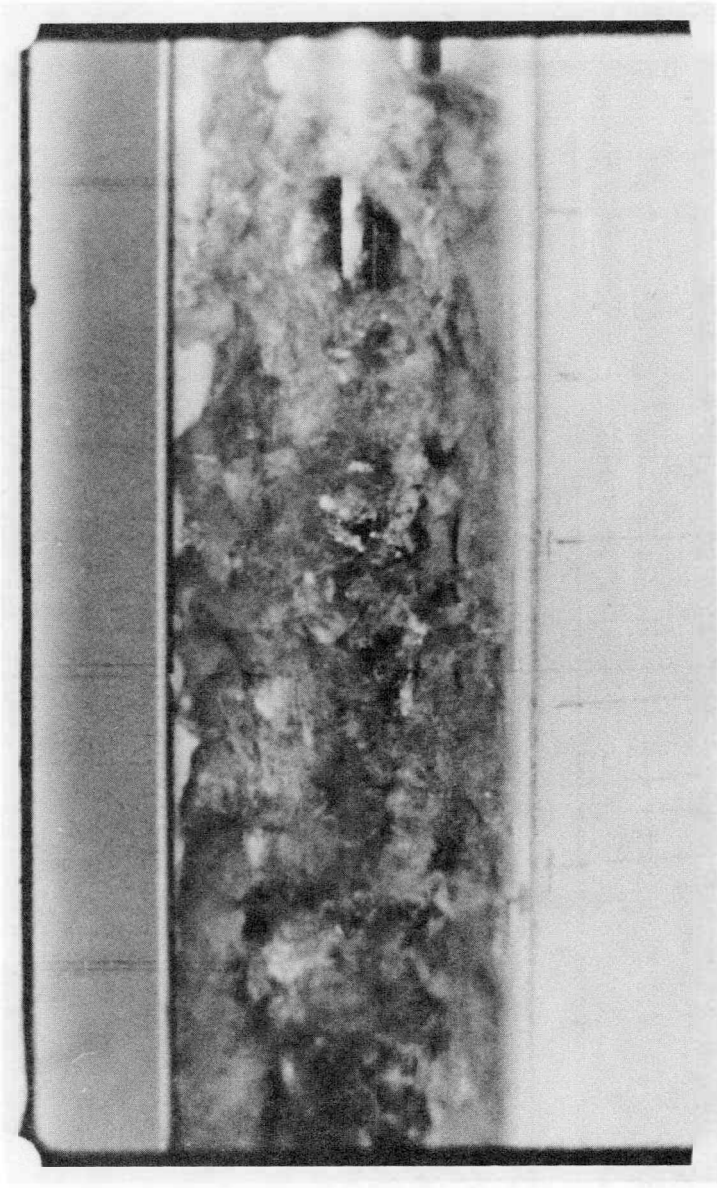

Figure 3-9 Churn Turbulent Flow. Run No. D-II; Flooding Velocity 3 cm/s; Initial Rod Temperature 968 K

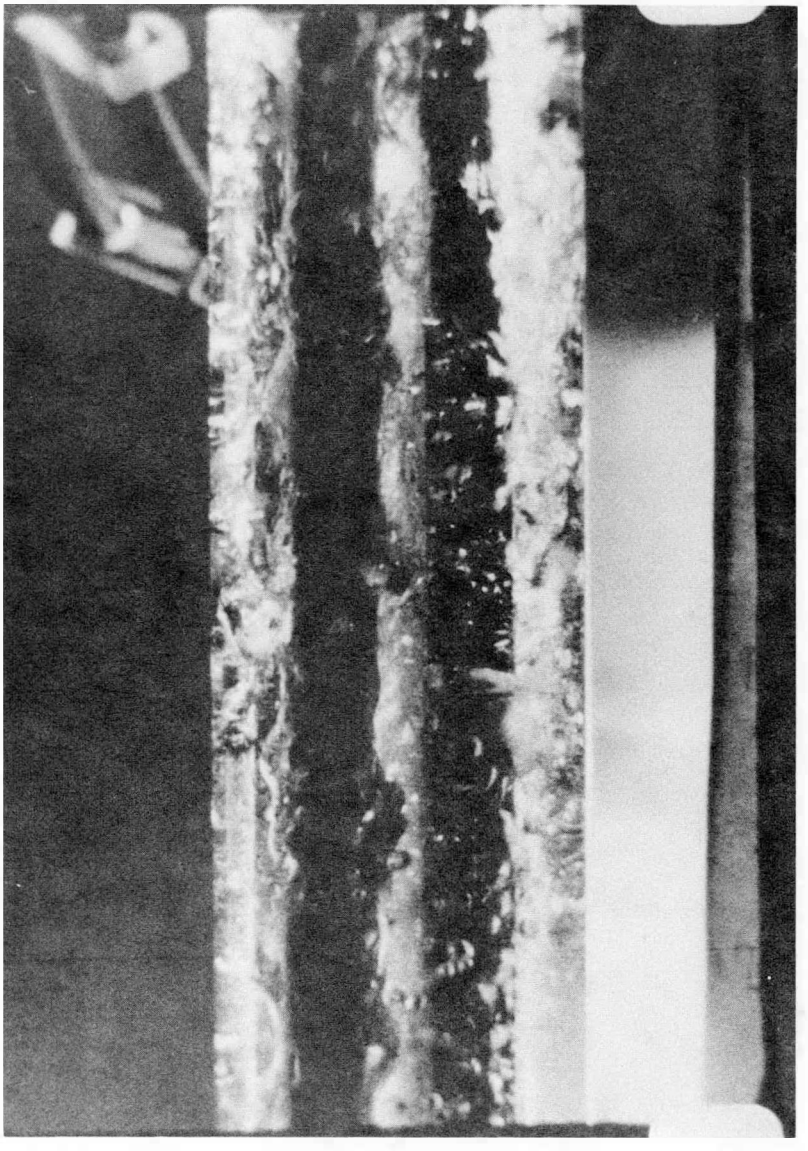

Figure 3-10 Film Boiling on Stainless Steel and Zircaloy Rods, Run No. D-II; Flooding Velocity 3 cm/s; Initial Rod Temperature 968 K

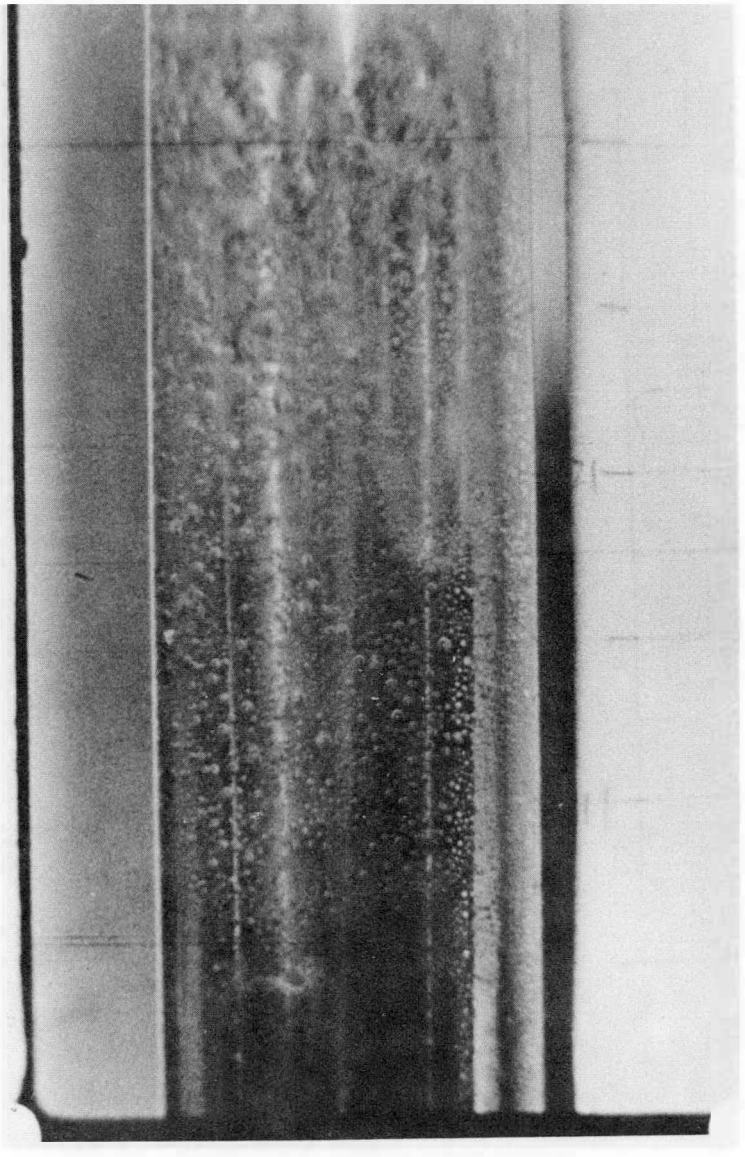

Figure 3-11 Quench Front Location on Stainless Steel and Zircaloy Rods; Run No. D-II; Flooding Velocity 3 cm/s; Initial Rod Temperature 968 K

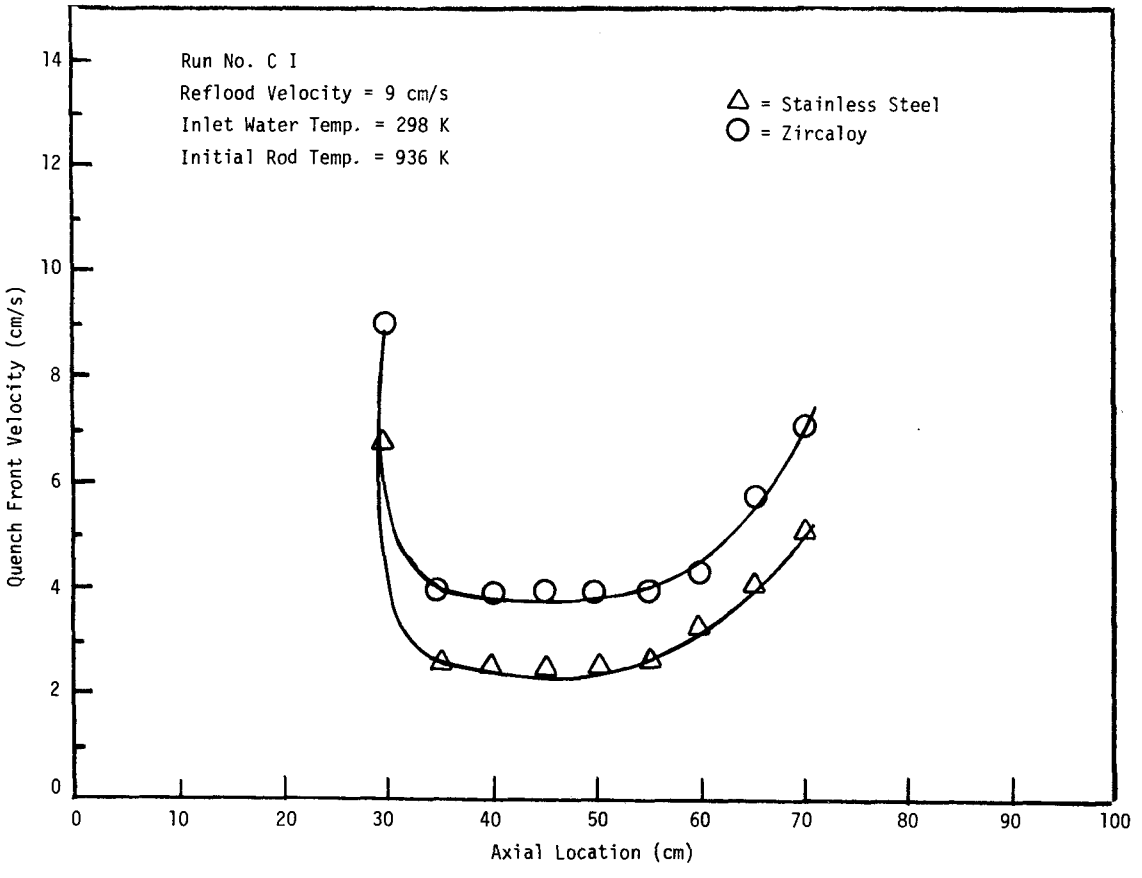

Figure 3-12 Quench Front Velocity as a Function of Height

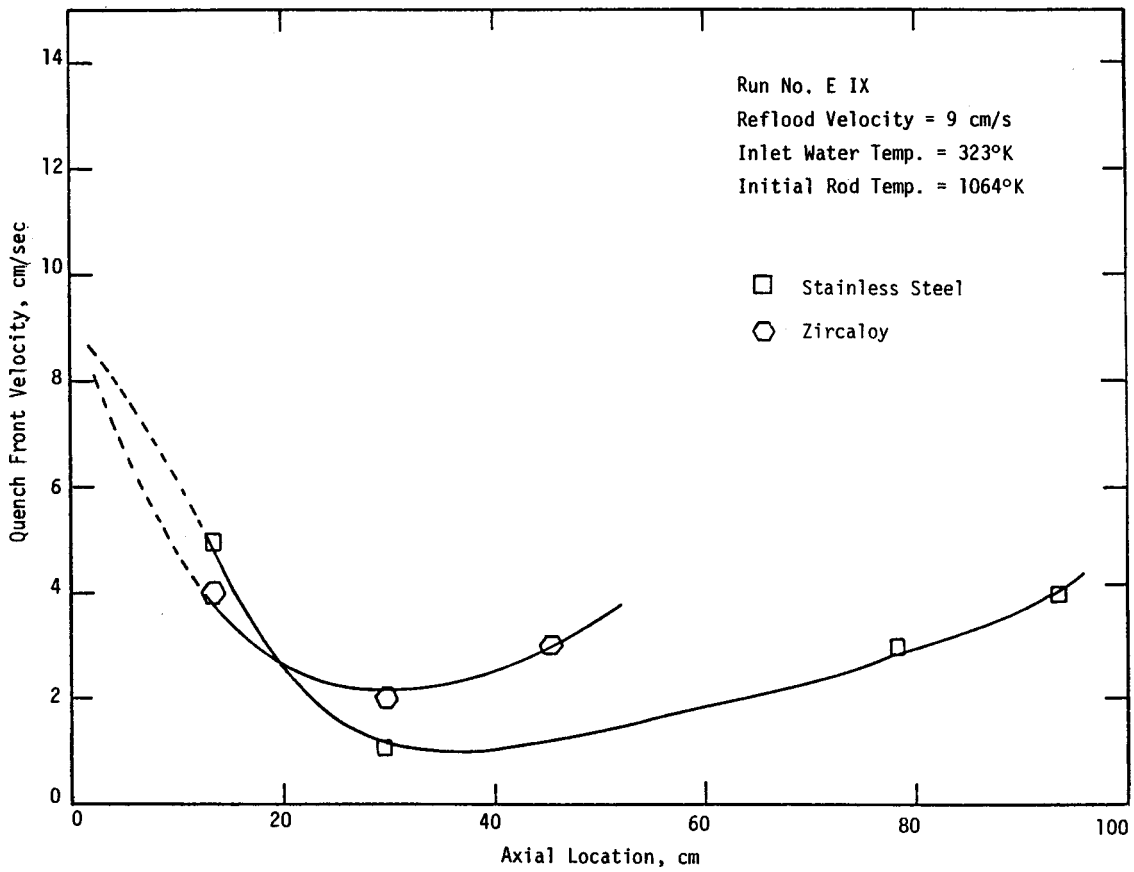

Figure 3-13 Quench Front Velocity as a Function of Axial Location

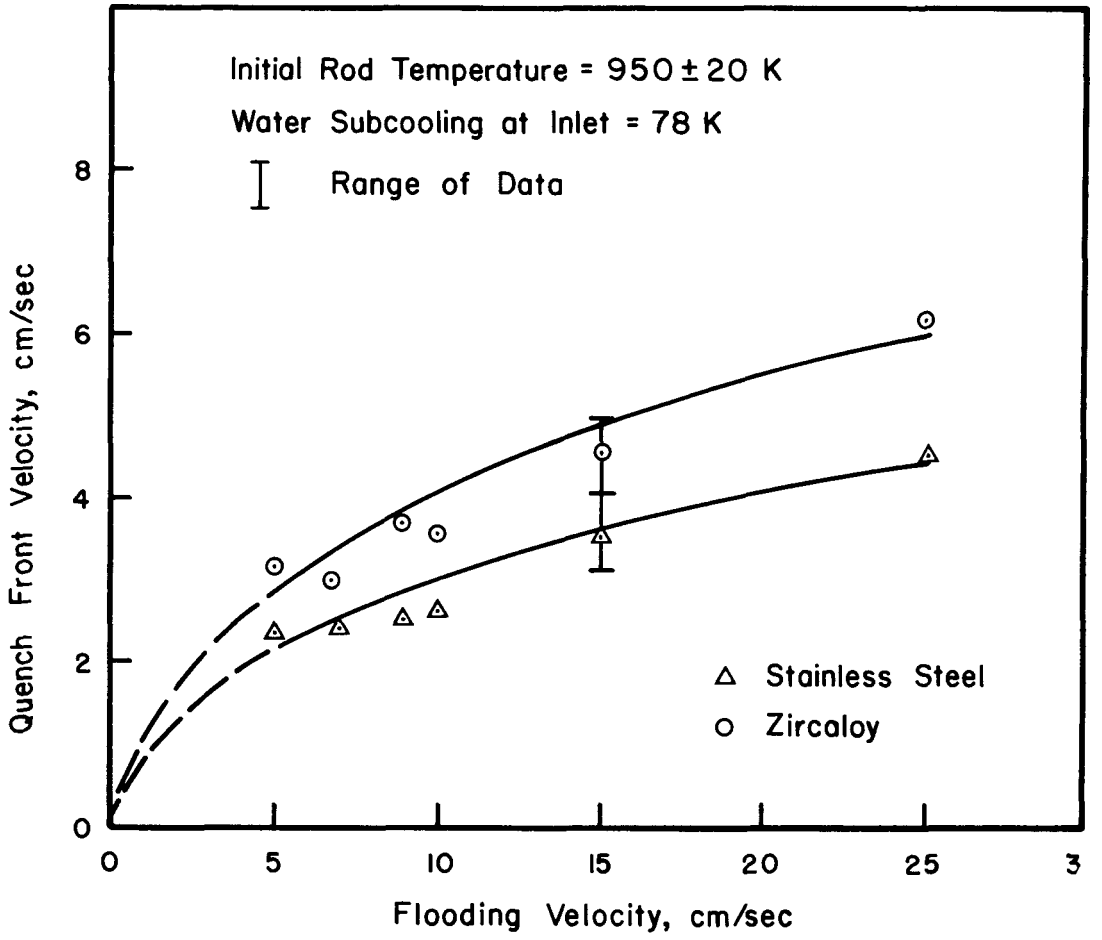

Figure 3-14 Quench Front Velocity Under Inverse Annular Flow Conditions on a 4 Rod Bundle Containing Two Zircaloy and Two Stainless Steel Rods

quench front on zircaloy is observed to move about 33% faster than on stainless steel when flooding velocity is 25 cm/s. Piggott and Duffey (5), in their single rod tests noted that with filler and quenching rate of zircaloy was about 20-25% faster than stainless steel. However, when filler was removed, zircaloy tended to quench at about twice the velocity for stainless steel. The difference in quench velocities has been found to decrease with increase in initial temperature of the rod. At higher temperatures the filler probably plays a more important role.

The quench front velocities near the entrance and the upper half region of the bundle were generally significantly higher than in the middle portion because of the liquid subcooling and precursory cooling respectively. An increase in liquid subcooling increased the quench front velocity in the entrance region but had little effect in the upper regions of the rod bundle where the liquid temperature had already reached saturation. Faster quenching of zircaloy caused the stainless steel rods to quench earlier also.

QUENCHING OF ALL ZIRCALOY BUNDLE

In the all zircaloy rod bundle, determination of the effect of oxidation during quenching was one of the major considerations. For this reason an 18 inch long zircaloy tube cut as a half cylinder was used as a test specimen. This tube was placed in the test section such that it preserved the square grid spacing of the rod bundle. Also, the exposure of both the inside and outside surface of the tube to the test section environment resulted in the same surface area as for a rod of the same length. This test specimen was removed from the test bundle after each run and was weighed. Starting with a fresh test sample, Table 3-1 lists the weights of the test section before and after each run in which the rod bundle was heated to about 1000 K and quenched at the flooding velocity of 2 cm/s. It is noted that the amount of oxide deposited on the rod decreases after two runs. This is mainly due to uncertainty in determining the weight.

The quench front location data, a fresh rod bundle (Run G-I) and a heavily oxidized bundle (Run G-III) are plotted in Figs. 3-15 and 3-16 for a flooding velocity of 2 cm/s. The oxidation seems to increase the difference in quenching times between various rods at the same vertical locations. This is especially true at higher vertical locations where precursory cooling becomes important. The presence of an oxide layer would improve the wettability of the surface. An examination of the temperature-time traces of thermocouples indicated that the quenching temperature of the oxidized rods was about 50-100 K higher than

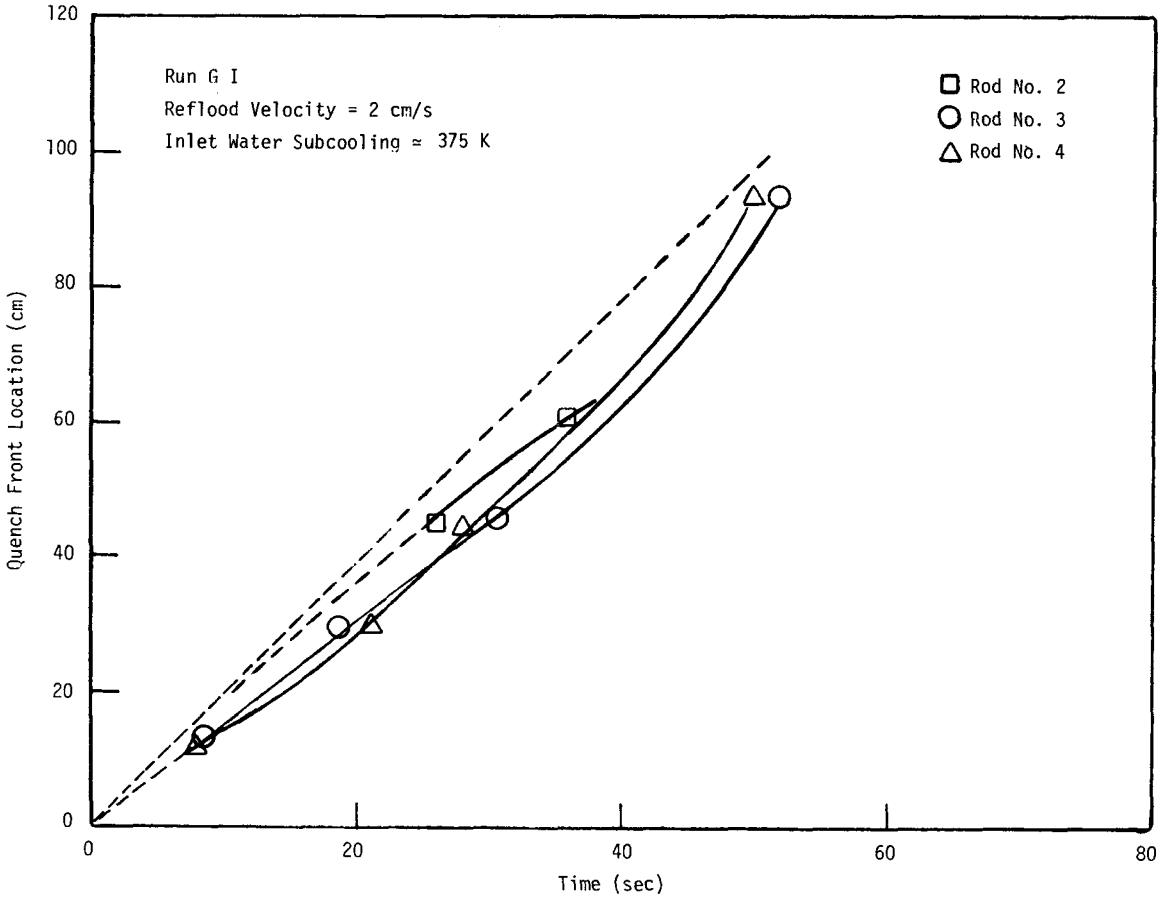

Figure 3-15 Quench Front Location as a Function of Time for a Fresh Zircaloy 4 Rod Bundle

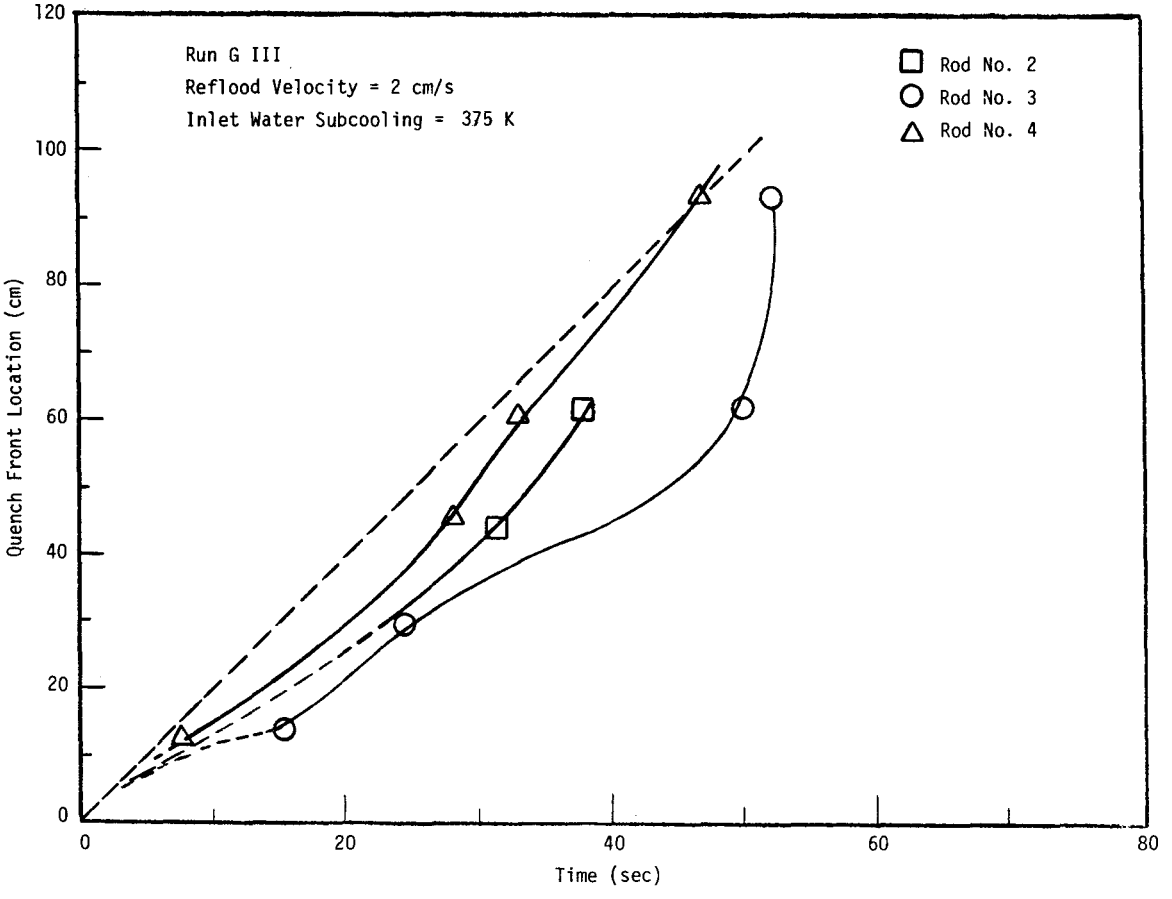

Figure 3-16 Quench Front Location as a Function of Time for Highly Oxidized Zircaloy 4 Rod Bundle

Table 3-1

WEIGHT OF ZIRCALOY TEST SPECIMEN AFTER EACH RUN

Run	Initial Weight gm	Final Weight gm	Weight Gain gm
G-I	29.5910	29.5933	0.0023
G-II	29,5933	29.5941	0.0008
G-III	29.5941	29.5940	-0.0001
G-IV	29.9940	-	-

for the fresh rods. Quench front velocities in the fresh and heavily oxidized rod bundles as obtained from the quench front location data are plotted in Figs. 3-17 and 3-18. In the lower half region, the quench front velocities in the fresh and heavily oxidized rod bundle are about the same, however in the upper half region, the quench front velocity on the oxidized rod bundle is much higher than on a fresh (presumably non-oxidized) bundle. Enhancement in quenching velocity is thought to be due to higher wettability of the oxidized surfaces which allows for longer periods of good heat transfer during each contact of precursory cooling droplets.

The quenching process at different axial locations on a fresh zircaloy rod bundle as observed from the movies is shown in Figs. 3-19 through 3-22. In the inverse annular flow conditions, the neighboring rods are clearly seen to quench at about the same time.

QUENCHING OF THE 4 ROD BUNDLE CONTAINING TWO ZIRCALOY RODS AND TWO USED RODS FROM FLECHT EXPERIMENTS

Ten quenching experiments at a variety of flooding conditions were made on a four rod bundle consisting of two used rods from FLECHT program and two zircaloy rods. The FLECHT rods which were heavily oxidized were cut into 1.2 meter long pieces. These rods could not be instrumented from the inside because of the presence of electrical heating elements and related insulating material. Quench front locations on the FLECHT stainless steel rods could thus only be ascertained from the movies.

Figures 3-23 - 3-25 show the quench front location on stainless steel and zircaloy rods as obtained from the movies and also the thermocouples placed on zircaloy clad rods. The flooding velocity for the data plotted in Figures 3-23 - 3-25 was 2, 10 and 30 cm/s while subcooling of water at the inlet was 78 K. The data

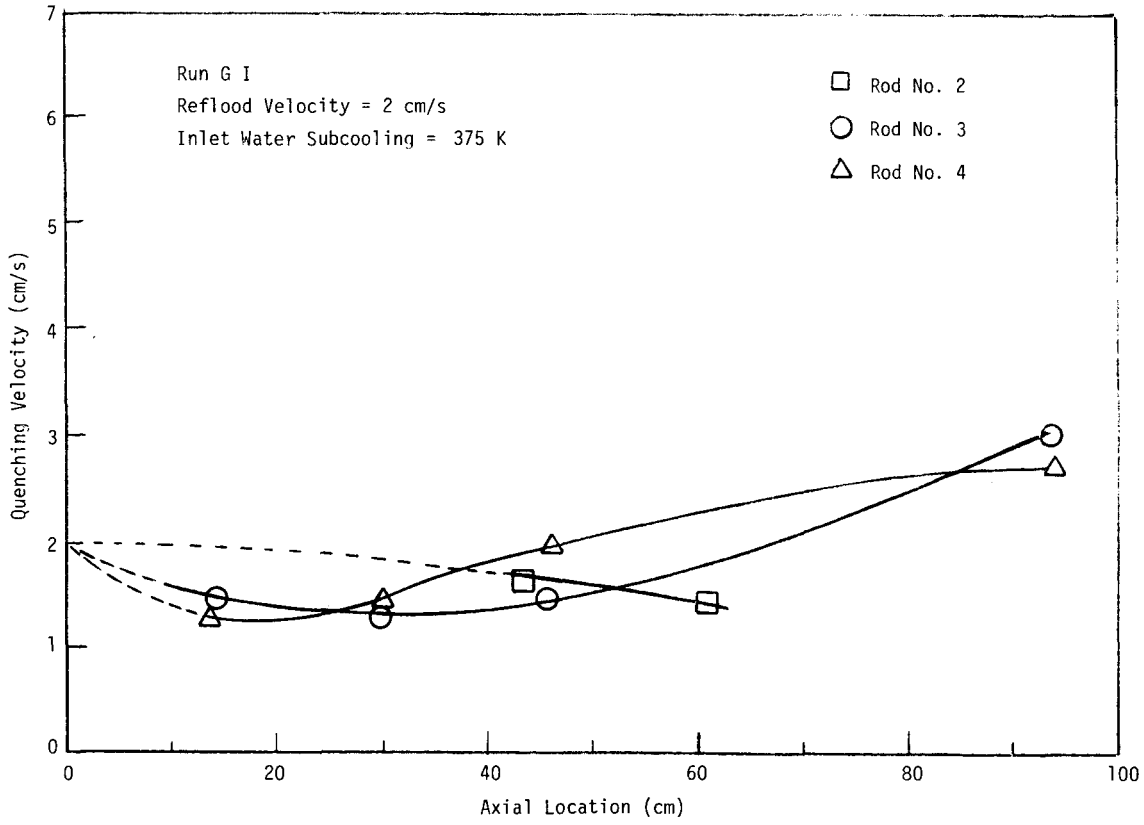

Figure 3-17 Quench Front Velocity as a Function of Axial Location for a Fresh Zircaloy 4 Rod Bundle

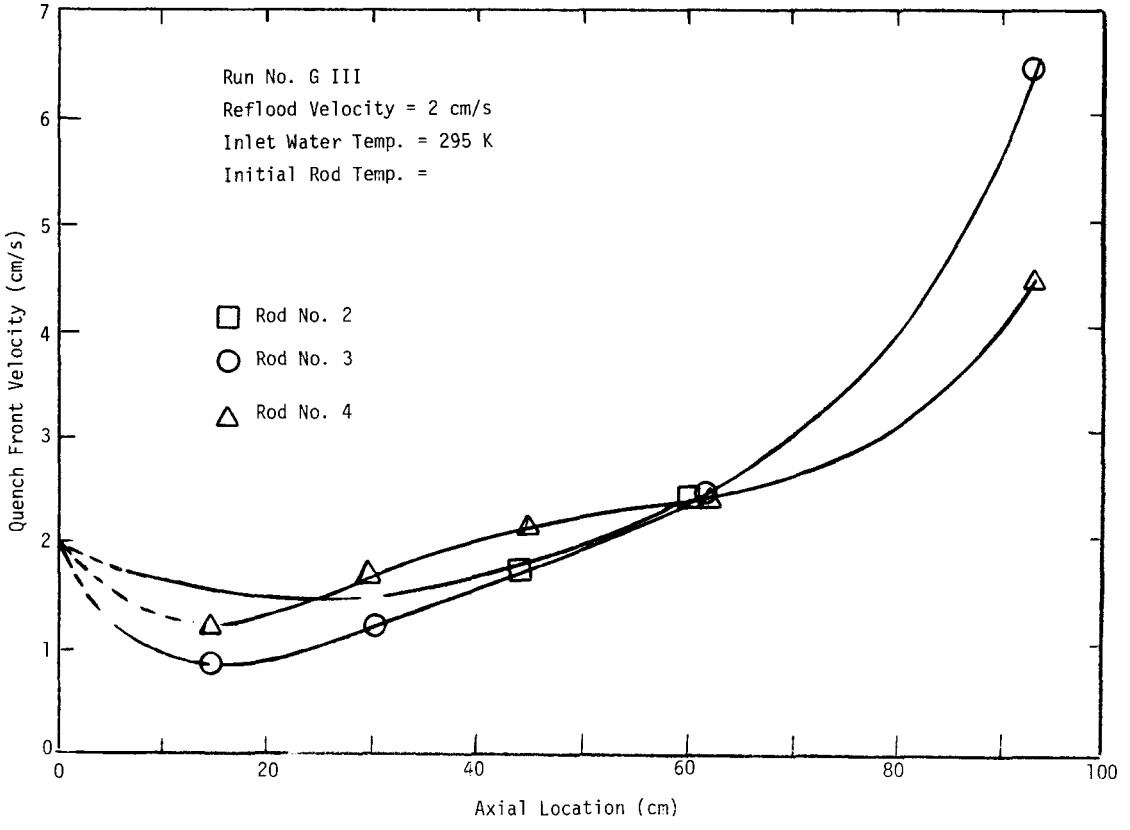

Figure 3-18 Quench Front Velocity as a Function of Axial Location in a Heavily Oxidized Zircaloy 4 Rod Bundle

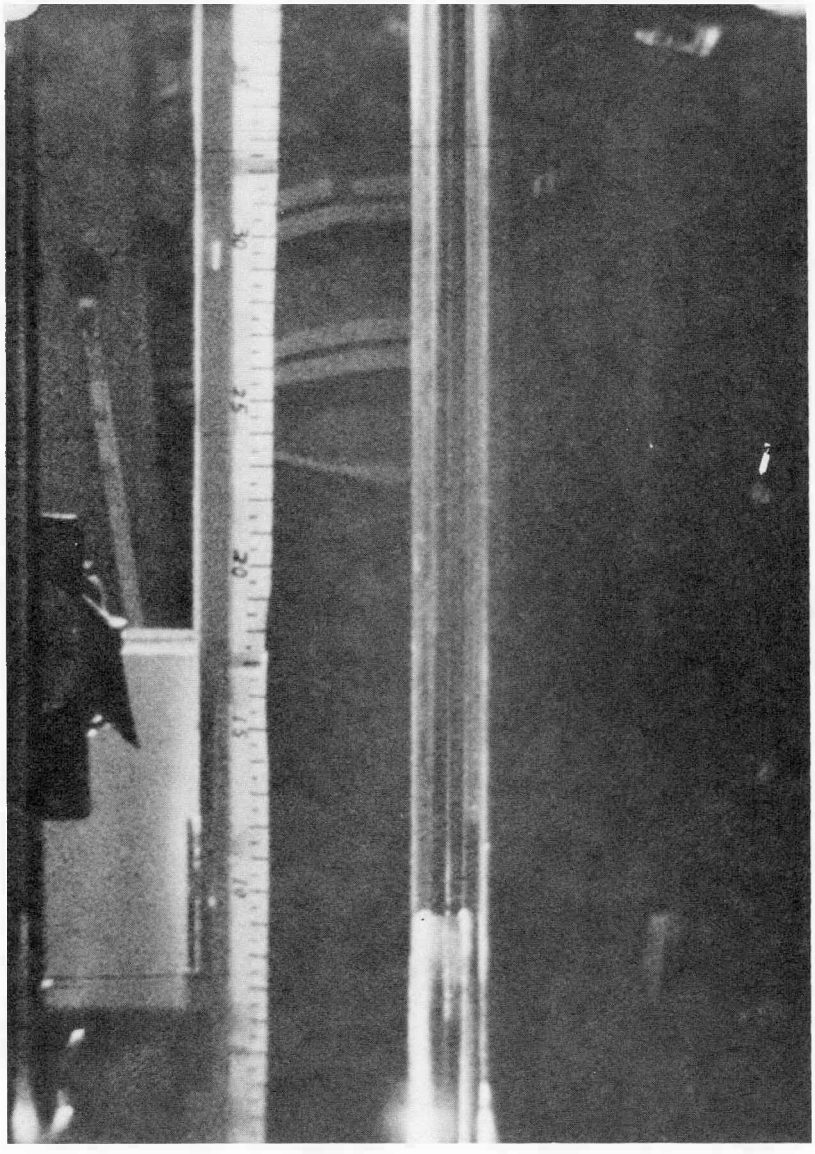

Figure 3-19 Quench Front Location on All Zircaloy Bundle Near the Entrance Region when Liquid is Still Subcooled, Run No. G-I; Flooding Velocity 2 cm/s; Initial Rod Temperature 1000 K

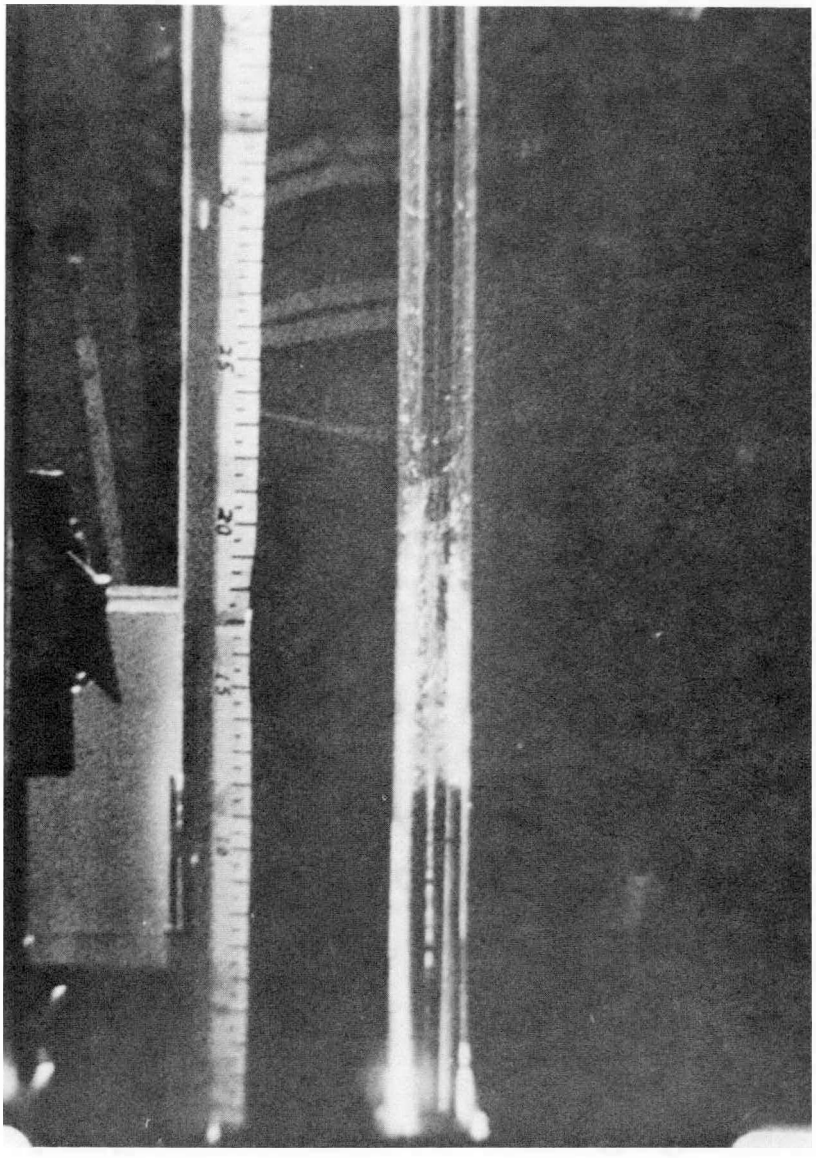

Figure 3-20 Quench Front in the Lower Middle Portion of All Zircaloy Bundle when Liquid is Nearly Saturated; Flooding Velocity 2 cm/s; Initial Rod Temperature 1000 K

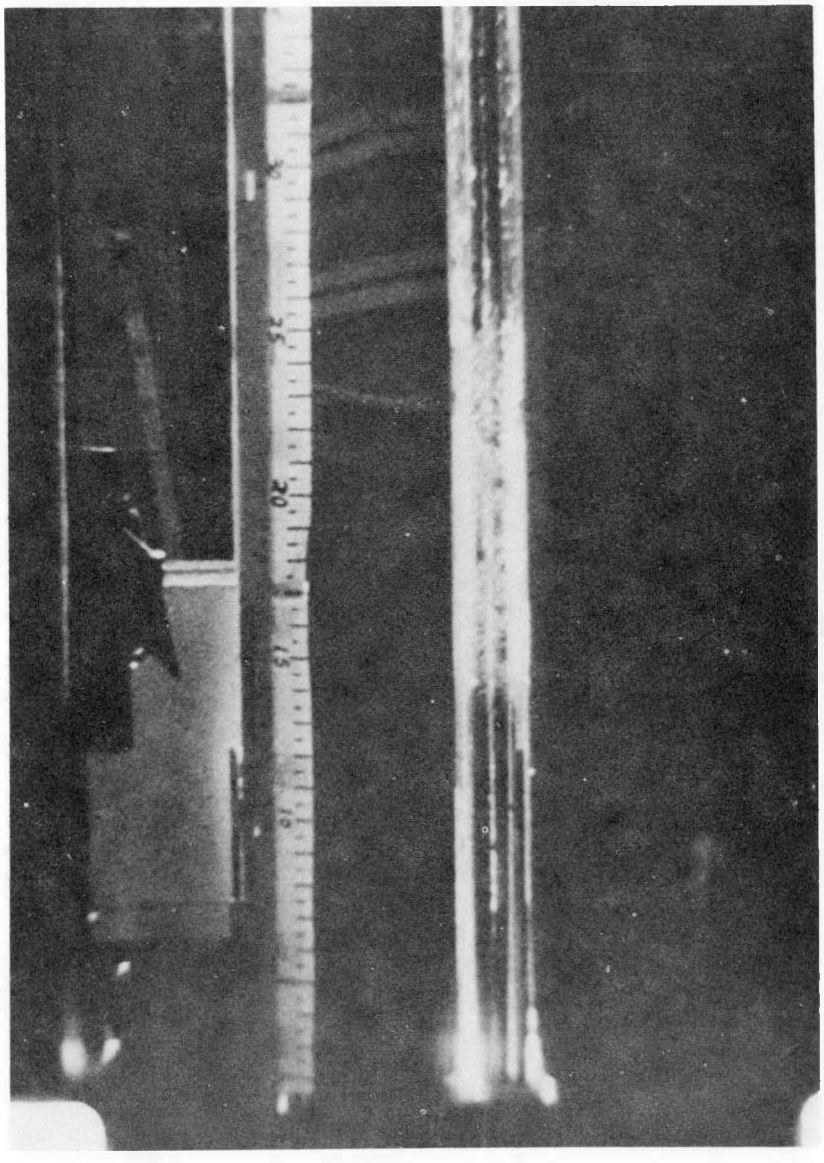

Figure 3-21 Quench Front Location on All Zircaloy Bundle with Well Developed Two Phase Mixture Ahead of the Quench Front; Run No. G-I; Flooding Velocity 2 cm/s; Initial Rod Temperature 1000 K

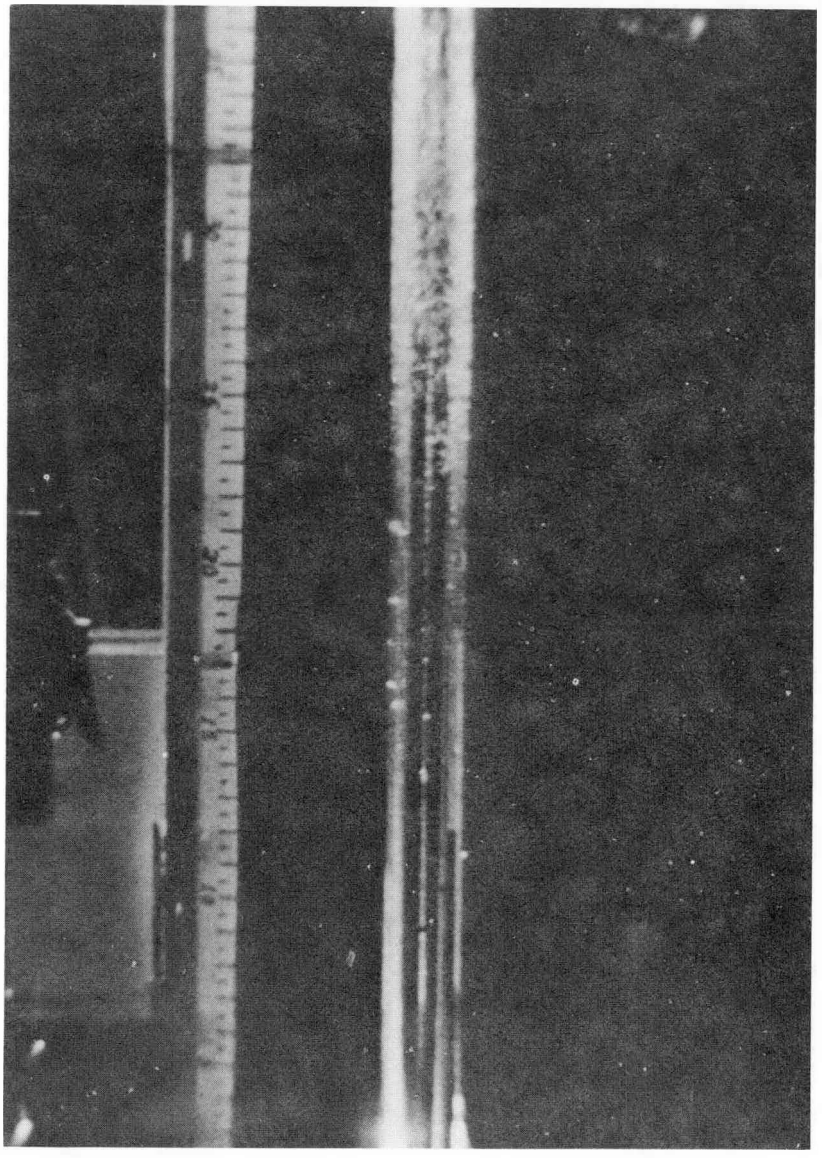

Figure 3-22 Quench Front Location on All Zircaloy Bundle with Near Slug Flow Ahead of Quench Front; Run No. G-I; Flooding Velocity 2 cm/s; Initial Rod Temperature 1000 K

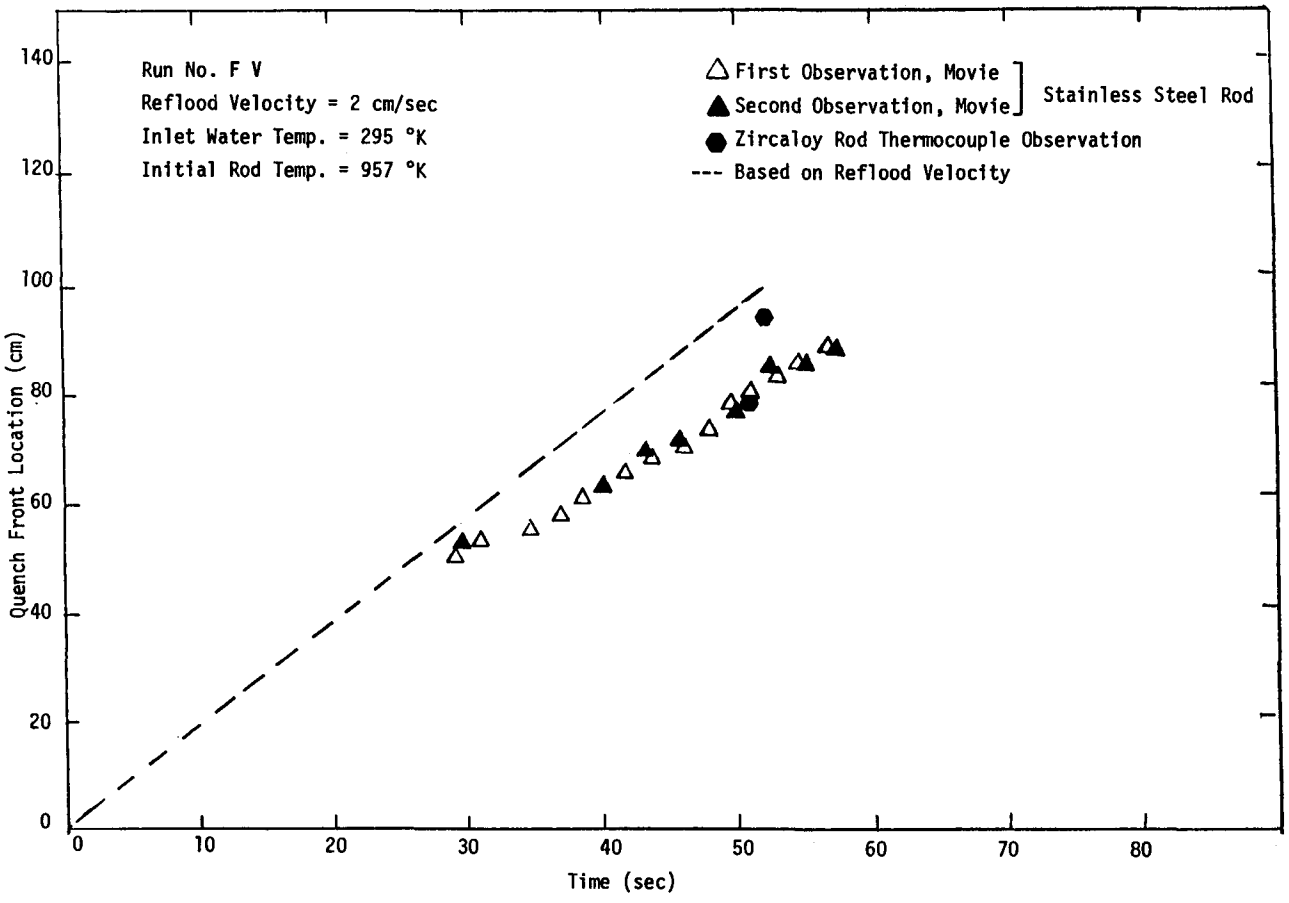

Figure 3-23 Quench Front Location as a Function of Time

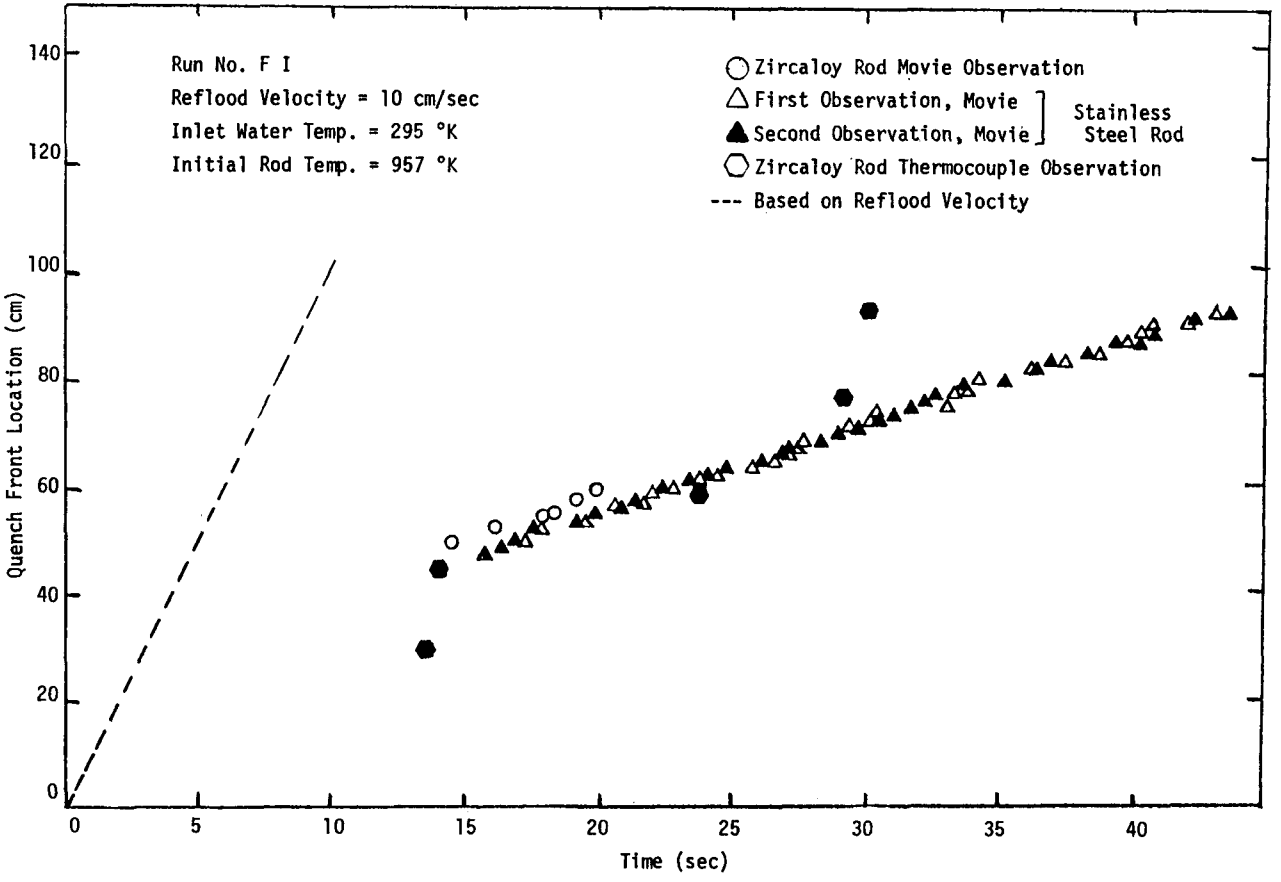

Figure 3-24 Quench Front Location as a Function of Time

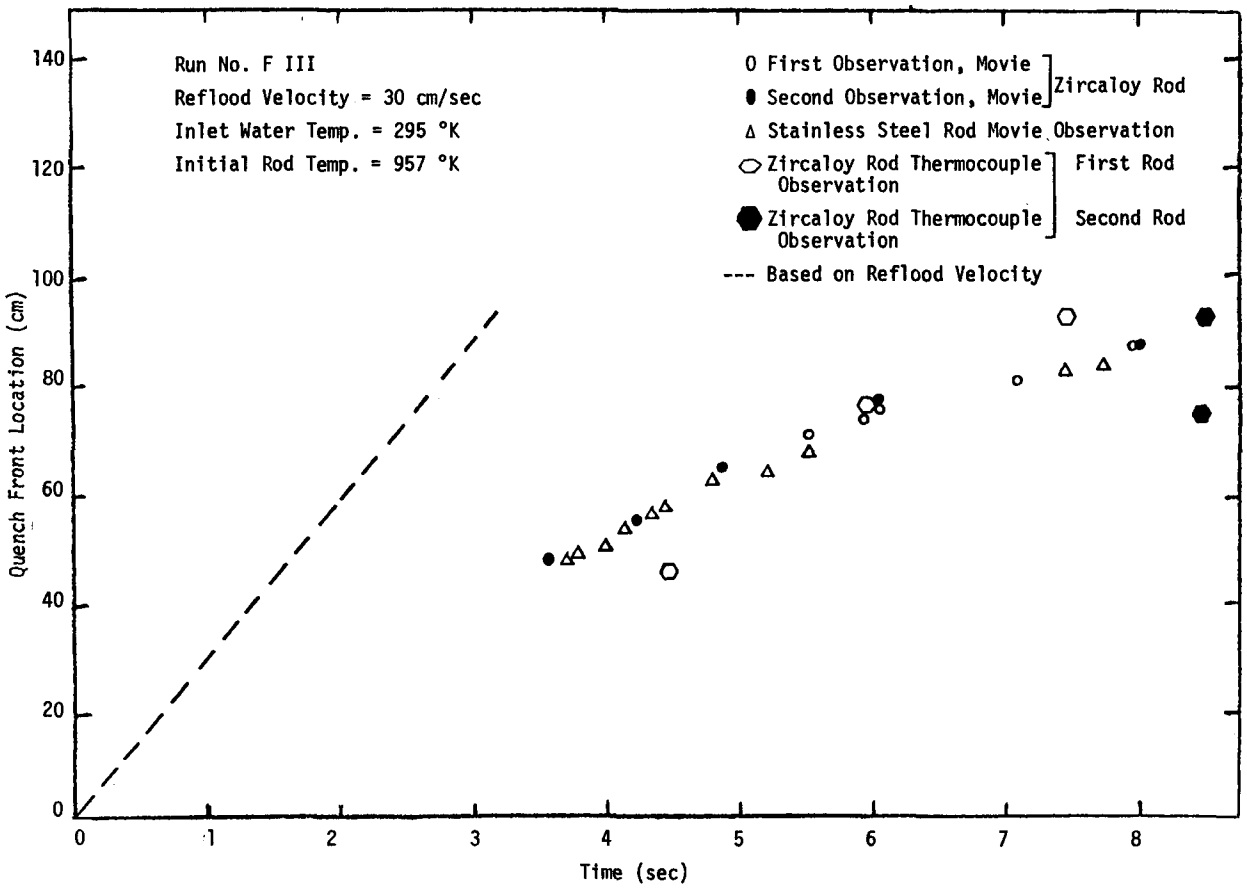

Figure 3-25 Quench Front Location as a Function of Time

plotted in Figure 3-24 show that quenching of zircaloy rods occurred somewhat faster than stainless steel rods from FLECHT program. This is consistent with the conclusions drawn earlier. However, the data plotted in Figures 3-23 and 3-25 does not show as large a difference between quenching rates of zircaloy and stainless steel rods from FLECHT experiments. This could be due to the 15-20% higher thermal capacity of the FLECHT rods which caused these rods to be relatively cooler at the start of the quenching process.

BOILING CURVES

The coiling curves as deduced from the temperature time traces for the case when quench front was well defined on the rod surface and for the case when cooling of the rod mainly occurred by precursory droplets are compared in Figure 3-26. The dependence of heat flux on temperature was obtained by solving one dimensional inverse transient conduction equation in the cladding as well as in the insulators. The boiling curve obtained with the assumption of no filler but an insulated cladding inner surface was not much different except in the lower end of the nucleate boiling region. Slight modification in the boiling curve, however, may occur if two-dimensional inverse transient conduction equation was solved or an approach similar to that of reference (14) was taken instead.

The transition boiling region in the boiling curve corresponding to a well defined quench front is extremely narrow. In fact, it suggests that boiling process directly goes from film to nucleate boiling and that in quenching models, heat transfer just behind the quench front should be evaluated from peak heat flux rather than from average of minimum and maximum heat fluxes. The observed shape of the boiling curve confirms the recent conceptualization of the boiling process by Murao (15). The transition boiling data obtained by Cheng et al. (16) on an inconel tube embedded in a copper block and also plotted in Figure 3-26, show a much different dependence of heat flux on wall superheat. It is possible that in their experiments copper block acted to smooth out any large temperature gradients and thus caused the tube wall temperature to vary slowly with time.

The heat transfer associated with precursory cooling is significantly higher than for film-boiling region ahead of the well defined quench front. The advantage of precursory cooling in terms of reduction in overall quenching times becomes more clear if one integrates the heat flux over the time precursory cooling instead of classical film boiling prevails on the rod surface. It is interesting to note that maximum heat flux achieved with precursory cooling is much less than that for well defined quenching. This is most probably due to lower rod temperature at the time of complete wetting.

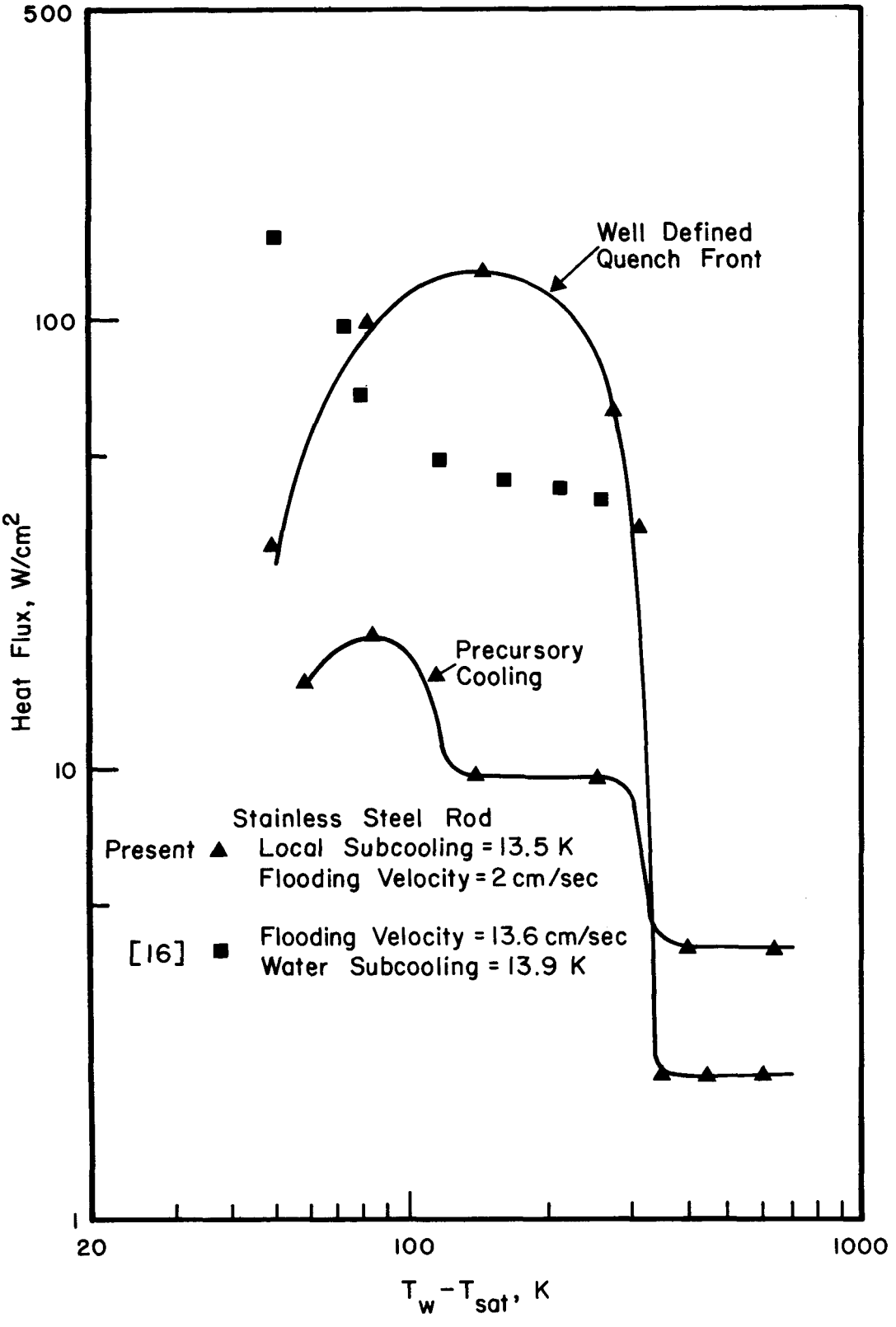

Figure 3-26 Boiling Curves Obtained During Quenching of Stainless Steel Rods

For a well defined quench front, the quenching temperatures as obtained from the temperature time traces, and generally confirmed by visual observations, have been found to decrease very rapidly with axial height before reaching an asumptotic value. The decrease in quenching temperature is presumably associated with increase in enthalpy of liquid as it moves upwards. Figure 3-27 shows the quenching temperatures (as defined earlier) on a stainless steel rod bundle as a function of axial height. The quenching temperatures in Figure 3-27 have not been plotted as a function of local liquid subcooling because of insufficient water temperature data. Also, no data are plotted for upper regions of the rod bundle because under precursory cooling conditions, a quenching temperature could not be defined from the temperature time traces. In this figure, the quenching temperatures as would be obtained by using the correlation suggested in reference (4) for stainless spheres as well as those suggested by Henry (17) have also been plotted. In plotting the correlations, liquid enthalpy based on stored energy considerations has been assumed to increase linearly, until the liquid becomes saturated. It is noted that the quenching temperatures are represented well by the correlation of reference (4). Henry's correlation (17) also fairs well when the liquid is saturated but underpredicts the quenching temperatures in the subcooled region. Interestingly, the range of quenching temperatures observed in the FLECHT (18) experiments is about the same as in the present case.

CORRELATION OF QUENCHING DATA

Figure 3-28 shows the dimensionless inverse quench front velocities as a function of Reynolds number based on the flooding velocity. The data plotted in Figure 3-28 is for a stainless steel rod bundle and is only for the middle portion of the rod bundle where coolant was nearly saturated and inverse annular flow conditions existed. The data are correlated within ±20% as

$$\frac{T^*}{u^*} = 11.5 Re^{-1/2} \tag{3-1}$$

The one-dimensional correlation of Duffey and Porthouse (6)

$$\frac{T^*}{u^*} = \frac{1}{3} \left(\frac{k}{\delta}\right)^{1/2} \left(\frac{C}{G}\right)^{1/2} \tag{3-2}$$

is also seen to compare quite favorably with the data. Two-dimensional solution for quench front velocity on a cylinder has been given by Blair (19) and Duffey and Porthouse as

$$\frac{T^*}{u^*} = \frac{\pi}{2} \frac{1}{Bi} \tag{3-3}$$

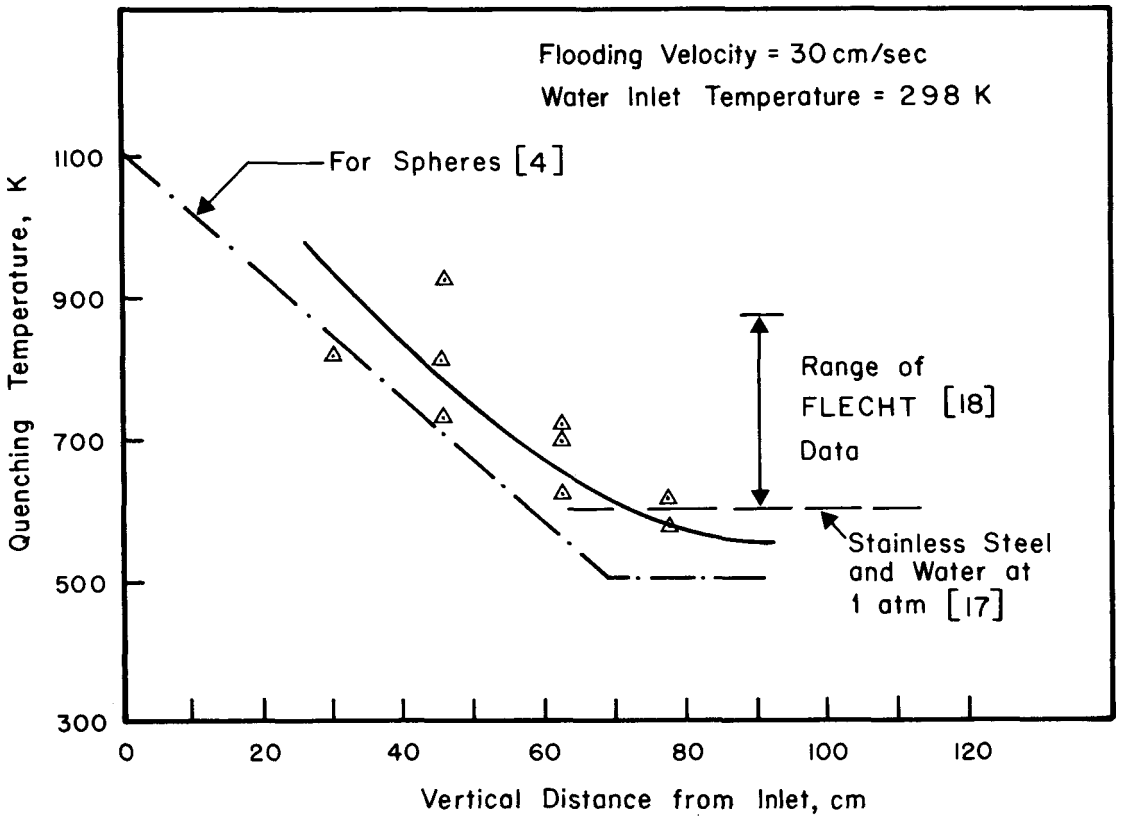

Figure 3-27 Variation of Quenching Temperature on a 4 Rod Stainless Steel Bundle

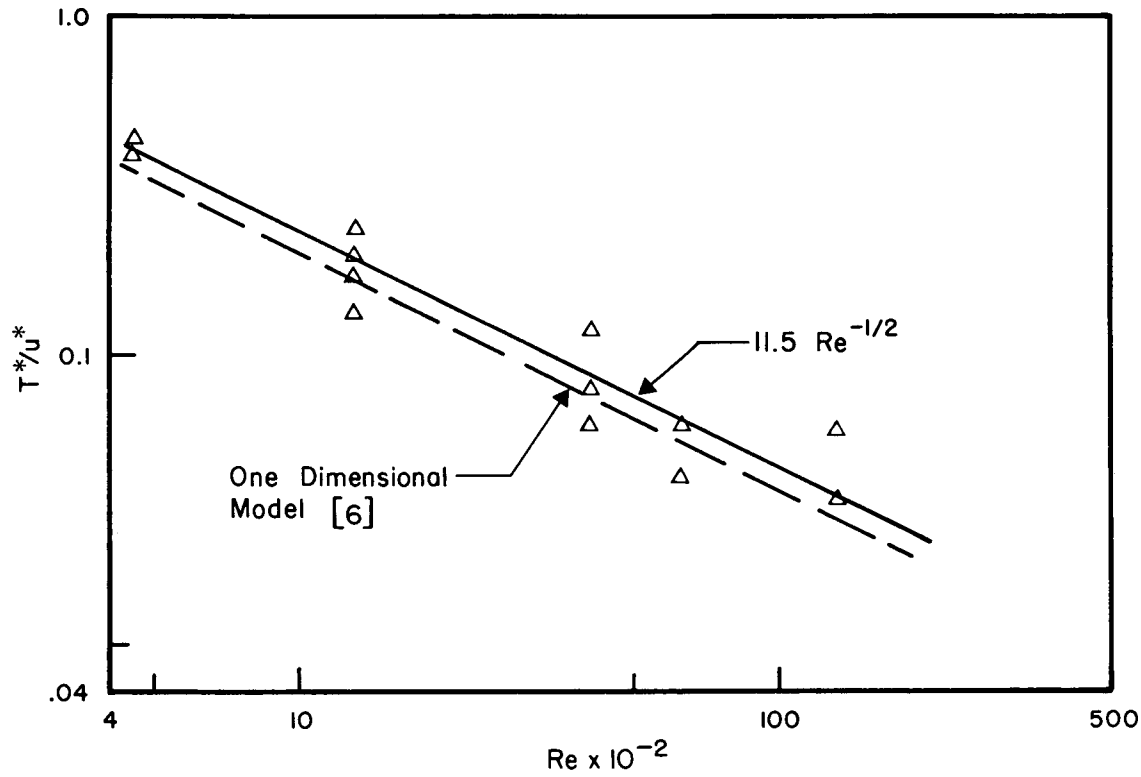

Figure 3-28 Correlation of Quenching Data Obtained on Stainless Steel Rod Bundle Under Saturated Inverse Annular Flow Conditions

The flooding velocity dependence in Eq. 3-3 is carried through Biot number. If it is assumed that Biot number would be a function of Reynolds number, Eqs. 3-1 and 3-3 can be equated to yield

$$Bi \simeq 0.14Re^{1/2} \tag{3-4}$$

This translates to heat transfer coefficients of 5.7 and 31.2 W/cm^2 for flooding velocities of 1 and 30 cm/s respectively. Corresponding values obtained by using Yamanouchi's (20) correlation would be 44.8 and 245.4 W/cm^2 K. Very high heat transfer coefficients given by Yamanouchi's correlation are probably due to his use of a too simplistic model for the quenching process.

For flooding rates of about 1 cm/s, the heat transfer coefficient given by Eq. 3-4 is consistent with the boiling curve if the heat transfer coefficient is evaluated near the peak heat flux on the nucleate boiling side. However, for higher flooding velocities the predicted heat transfer coefficient is significantly higher than would be obtained from the boiling curve. It only suggests that the thermocouples are giving a smeared output and are not reflecting the actual heat transfer at the surface under extreme transient conditions. Further efforts are continuing to resolve this discrepancy in observed heat transfer coefficient and the heat transfer coefficient needed to explain the observed quenching velocities.

SECTION 4

CONCLUSIONS

1. Under similar flooding conditions, zircaloy has been observed to quench faster than stainless steel. For example, in a mixed bundle containing both zircaloy and clad rods, the quench front moves about 33% faster on zircaloy than on stainless steel. The difference in quenching velocities is even higher for an all zircaloy bundle, and has been found to decrease with increase in initial temperature of the rod. At higher temperatures, the filler probably plays a more important role.

2. For a given rod surface temperature and flooding velocity, liquid subcooling increases quenching temperature as well as quench front temperature.

3. Quench front velocity under saturated inverse annular flow conditions has been found to increase as square root of flooding velocity.

4. At flooding velocities of 10 cm/s or higher, precursory cooling plays an important role in quenching the upper regions of the rod bundle.

5. Oxidation of zircaloy has been observed to reach an asymptotic state after about 3 runs. During flooding, oxidized rods quench somewhat differently than a fresh rod.

6. The transition boiling region of the transient boiling curve obtained in the presence of well defined quench front is nearly nonexistent.

7. At low flooding velocities ($\simeq$ 2 cm/s), the quench front velocities are consistent with the heat transfer coefficient corresponding to maximum heat flux. However, at higher flooding velocities, the heat transfer coefficient obtained from boiling curve is much less than needed to explain the observed quench front velocities. This is probably due to smeared output of the thermocouple which does not reflect the actual heat flux at the surface.

SECTION 5
REFERENCES

1. Bergles, A. E., and W. G. Thompson, "The Relationship of Quench Data to Steady State Pool Boiling Data", Int. J. Heat Mass Transfer, Vol. 13, 1970.

2. Veres, D. R., and L. W. Florschuetz, "A Comparison of Transient and Steady State Pool Boiling Data Using the Same Heating Surface", J. Heat Transfer, Vol. 93, No. 2, 1971.

3. Tachibana, F., and S. Enya, "Heat Transfer Problems in Quenching", Bulletin of Japanese Society of Mechanical Engineers, Vol. 16, No. 81, 1973.

4. Dhir, V. K., and G. P. Purohit, "Subcooled Film Boiling Heat Transfer from Spheres", Nucl. Eng. and Design, Vol. 47, 1978.

5. Piggott, B. D. G., and Duffey, R. B., "The Quenching of Irradiated Fuel Pins", Nucl. Eng. and Design, Vol. 32, 1975.

6. Duffey, R. B., and D. T. C. Porthouse, "The Physics of Rewetting in Water Reactor Emergency Core Cooling", Nucl. Eng. and Design, Vol. 25, 1973.

7. Sun, K. M., G. E. Dix and C. L. Tien, "Cooling of a Very Hot Vertical Surface by a Falling Liquid Film", J. Heat Transfer, Vol. 96, 1974.

8. Sun, K. M., G. E. Dix and C. L. Tien, "Effect of Precursory Cooling on Falling-Film Rewetting", J. Heat Transfer, Vol. 97, 1975.

9. Piggott, W. G., E. P. White and R. B. Duffey, "Wetting Delay Due to Film and Transition Boiling on Hot Surfaces", Nucl. Eng. and Design, Vol. 36, 1976.

10. Iloeje, O. C., D. N. Plummer, P. Griffith and W. M. Rohsenow, "An Investigation of the Collapse and Surface Rewet in Film Boiling in Forced Vertical Flow", ASME Paper No. 73-WA/HT-20. Presented at the ASME Winter Annual Meeting, Detroit, Michigan, November 1973.

11. "UC-B Reflood Program: Experimental Data Report", EPRI NP-743, April 1978.

12. Blaisdell, J. A., L. E. Hochreiter and J. D. Waring, "PWR FLECHT-SET Phase BI Data Report", USAEC Report WCAP-8238, Westinghouse Electric Corp., NTIS, 1973.

13. Pearson, K. G., B. D. G. Piggott and R. B. Duffey, "The Effect of Thermal Diffusion from Fuel Pellets on Rewetting of Overheated Water Reactor Pins", Nucl. Eng. and Design, Vol. 41, 1977.

14. Elias, E., and G. Yadigaroglu, "A General One Dimensional Model for Conduction Controlled Rewetting of a Surface", Nucl. Eng. and Design, Vol. 42, 1977.

15. Murao, Y., "Correlation of Quench Phenomena for Bottom Flooding During Loss of Coolant Accidents", J. Nucl Science and Technology, Vol. 15, 1978.

16. Cheng, S. C., and M. Ragheb, "Transition Effect of Heated Surface Thermal Properties on Transition Boiling", International Multiphase Symposium, Miami, April 1979.

17. Henry, R. E., "A Correlation for the Minimum Film Boiling Temperature", Chem. Eng. Prog. Symp. Series, Vol. 70, 1974.

18. Kirchner, W. L., "Reflood Heat Transfer in a Light Water Reactor", MIT, NUREG-0106, NRC-24, 1976.

19. Blair, J. M., "An Analytical Solution to a Two Dimensional Model of the Rewetting of a Hot Dry Rod", Nucl. Eng. and Design, Vol. 32, 1975.

20. Yamanouchi, A., "Effect of Core Spray Cooling in Transient State After Loss of Coolant Accident", J. Nucl. Science and Technology, Vol. 5, 1968.

APPENDIX A

TABULATION AND GRAPHICAL PRESENTATION OF DATA FOR QUENCHING TEMPERATURE, QUENCH FRONT LOCATION AND QUENCH FRONT VELOCITY FOR ALL STAINLESS STEEL BUNDLE

A total of thirteen runs were made with initial rod temperatures varying from 650°C to 760°C and flooding velocity from 1-30 cm/s. For these runs the inlet water subcooling was either 75°C or about 50°C. Table A-1 lists all the runs (Series A and B) made with stainless steel rod bundles. Data from Run AII and AIII could not be reduced because of the malfunction of the recorders during the runs.

TEMPERATURE HISTORIES

Temperature time traces at different vertical distances from the inlet for four of the thirteen runs are shown in Figures A-1 - A-4. It should be mentioned that zero time in these figures corresponds to the time at which the recorder is started and may be different by a few seconds from the time at which water entered the test section.

QUENCH FRONT LOCATION

Figures A-5 - A-16 show the quench front location as a function of time. The curve joining different quenching locations has been drawn by hand.

QUENCH FRONT VELOCITIES

Quench front velocities at the quenching location as obtained by noting the slope of the quench front locations versus time plots are plotted in Figures A-17 - A-38.

Table A-1

TEST RUNS WITH 4 STAINLESS STEEL ROD BUNDLE

Serial Number	Run Number	Inlet Water Temp.(K)	Reflood Velocity (cm/s)	Initial Rod Temp.(K)	Water Subcooling (K)	Movie
1	B-VIII	298	1	1033	75	No
2	B-VII	298	3	993	75	No
3	A-II	298	9	973	75*	No
4	A-V	298	14	983	75	No
5	B-I	298	20	1023	75	No
6	B-III	298	30	1023	75	No
7	B-V	323	3	1023	50	No
8	B-VI	323	30	993	50	No
9	A-I	298	9	923	75	No
10	A-III	298	9	998	75*	No
11	A-IV	298	14	1013	75	No
12	B-II	298	30	1033	75	No
13	B-IV	298	3	1008	75	No

*Data could not be reduced because of malfunction of recorders.

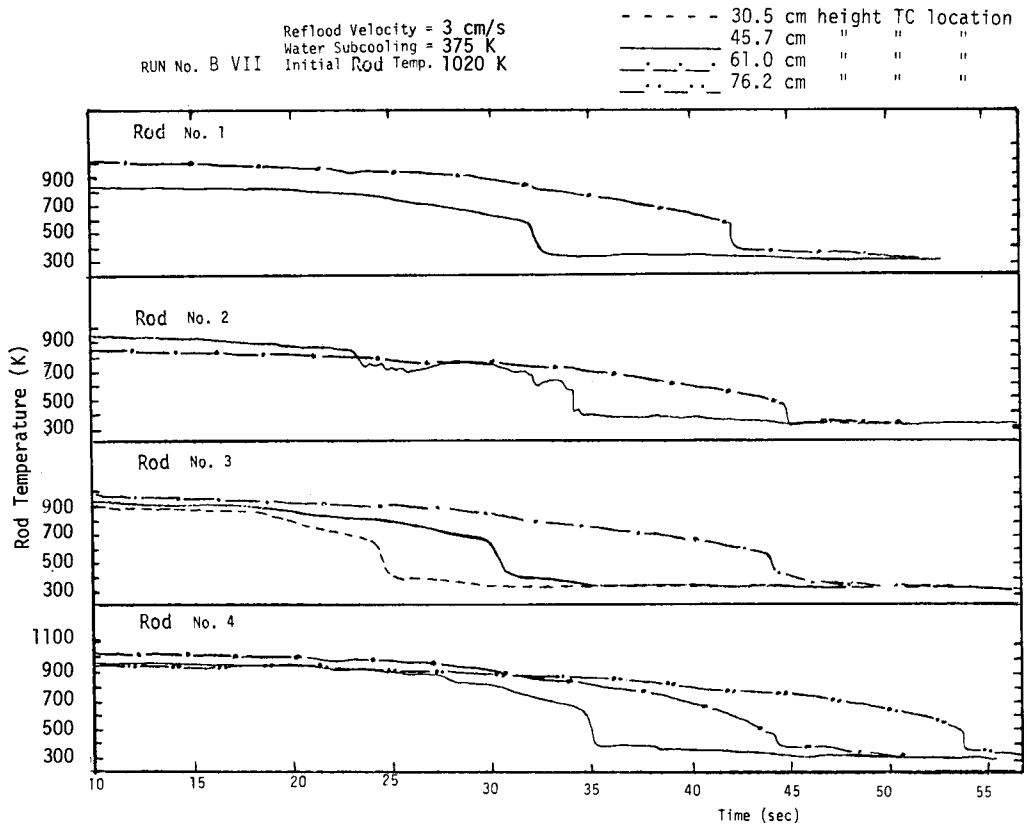

Figure A-1 Temperature Histories at Different Locations During Quenching of All Stainless Steel Rod Bundle

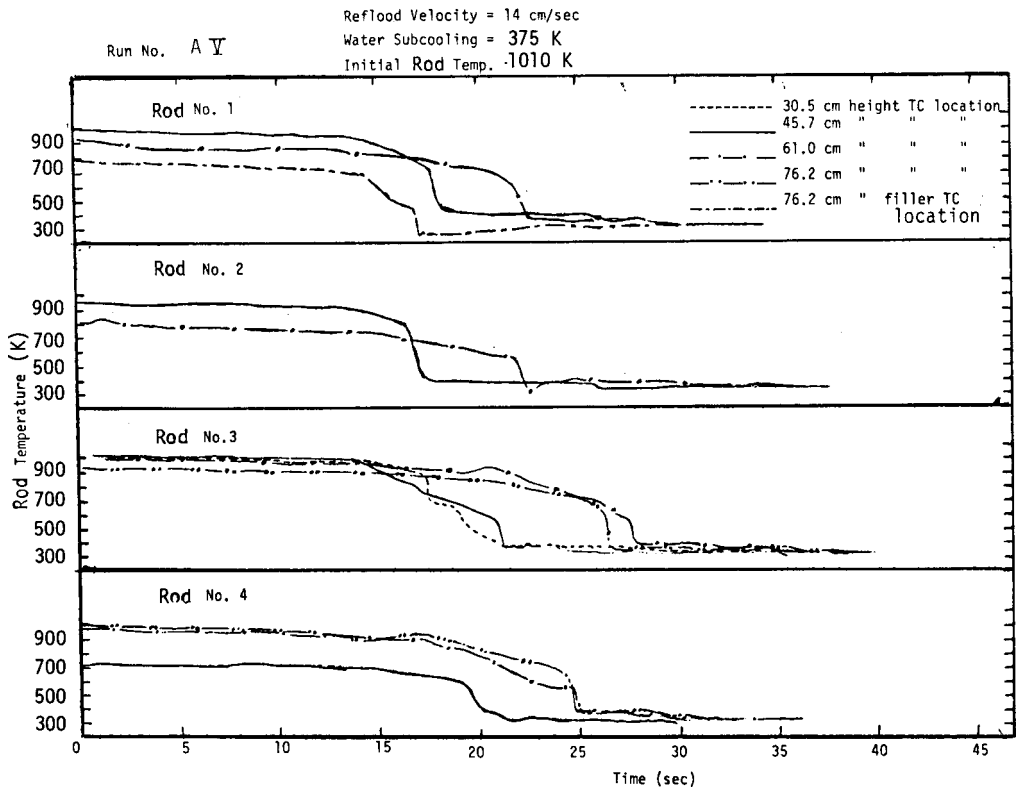

Figure A-2 Temperature Histories at Different Locations During Quenching of All Stainless Steel Rod Bundle

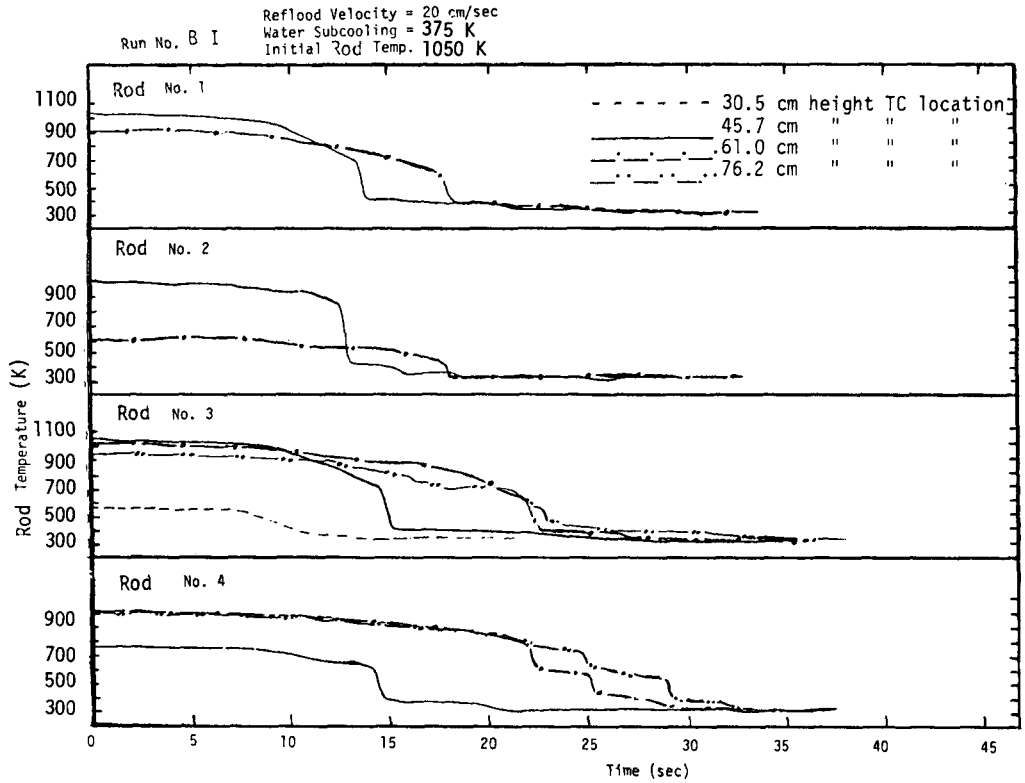

Figure A-3 Temperature Histories at Different Locations During Quenching of All Stainless Steel Rod Bundle

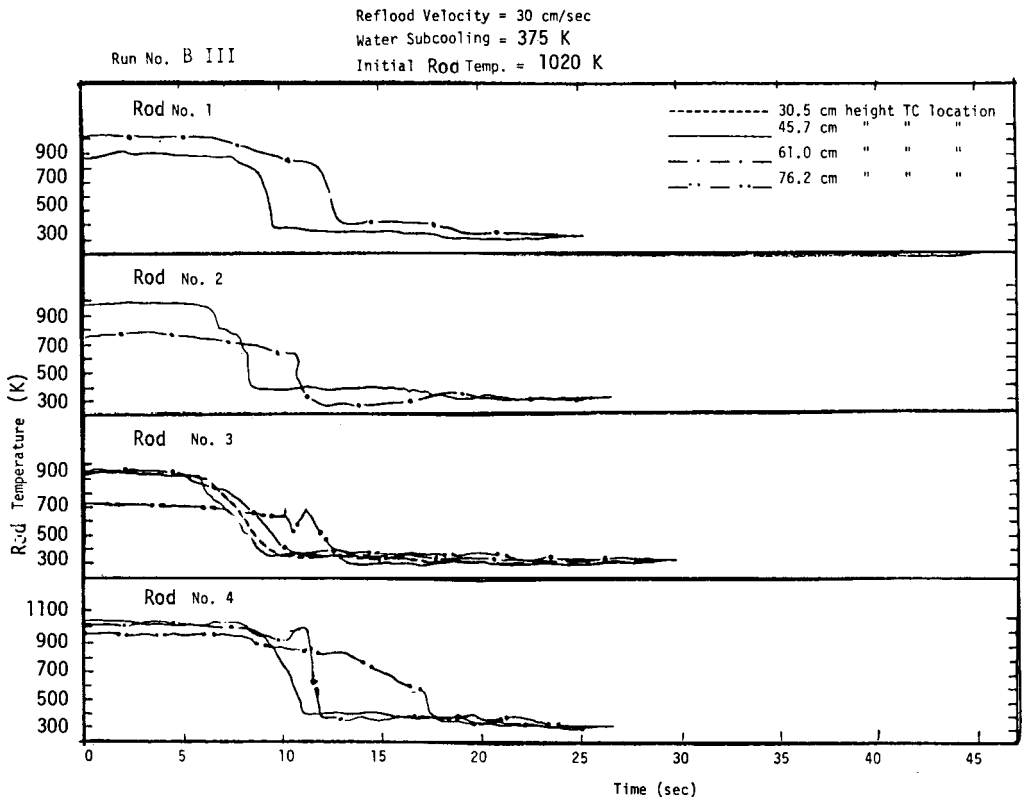

Figure A-4 Temperature Histories at Different Locations During Quenching of All Stainless Steel Rod Bundle

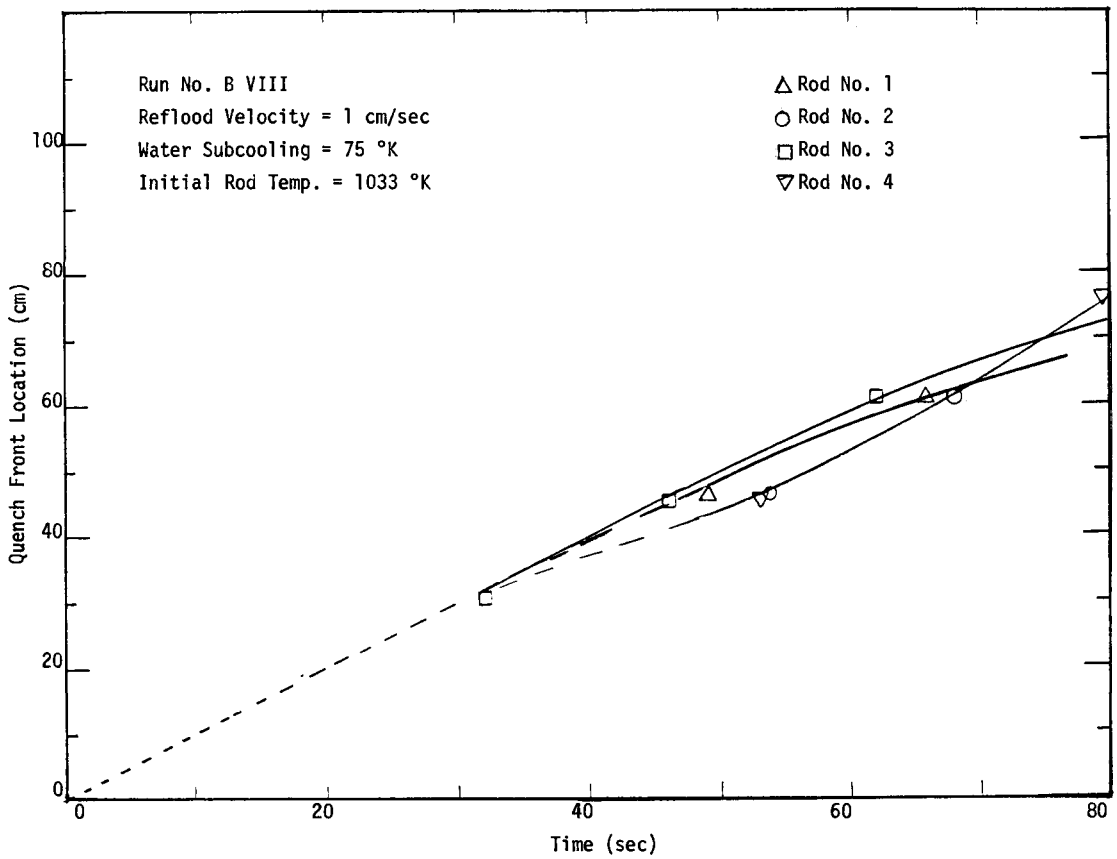

Figure A-5 Quench Front Location as a Function of Time

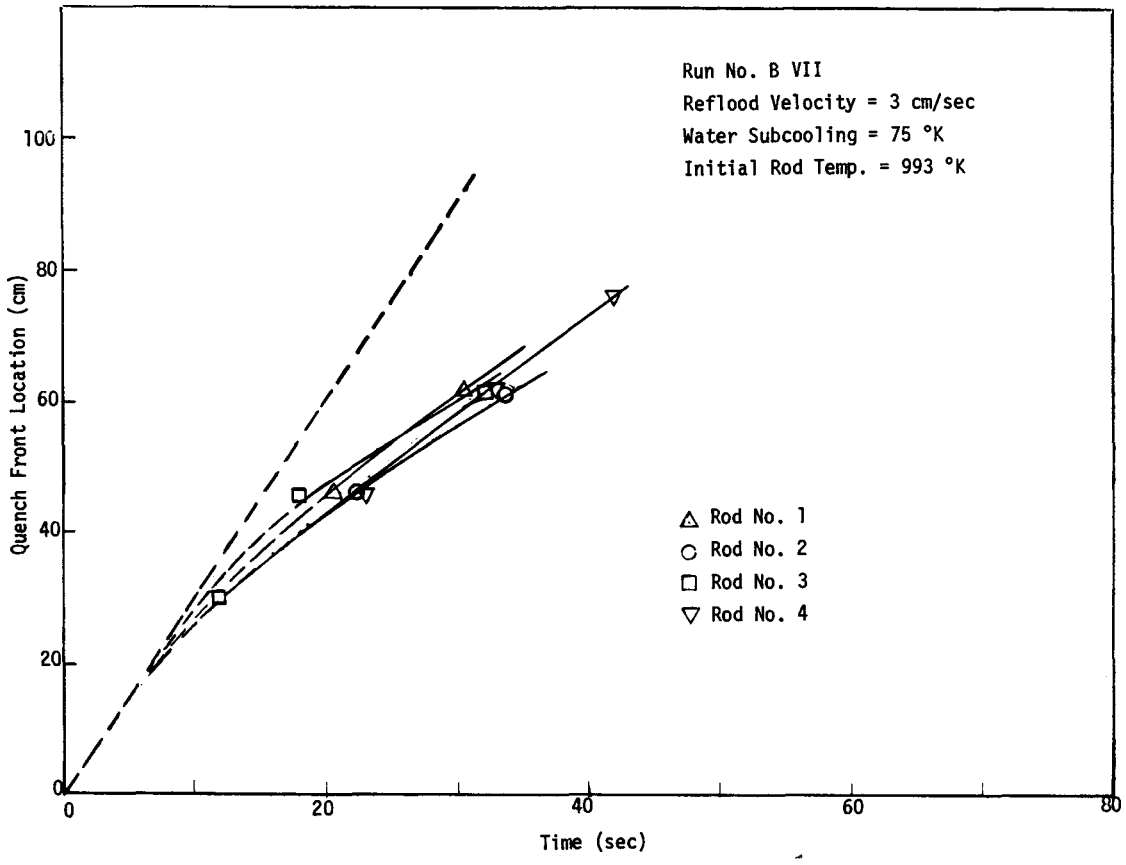

Figure A-6 Quench Front Location as a Function of Time

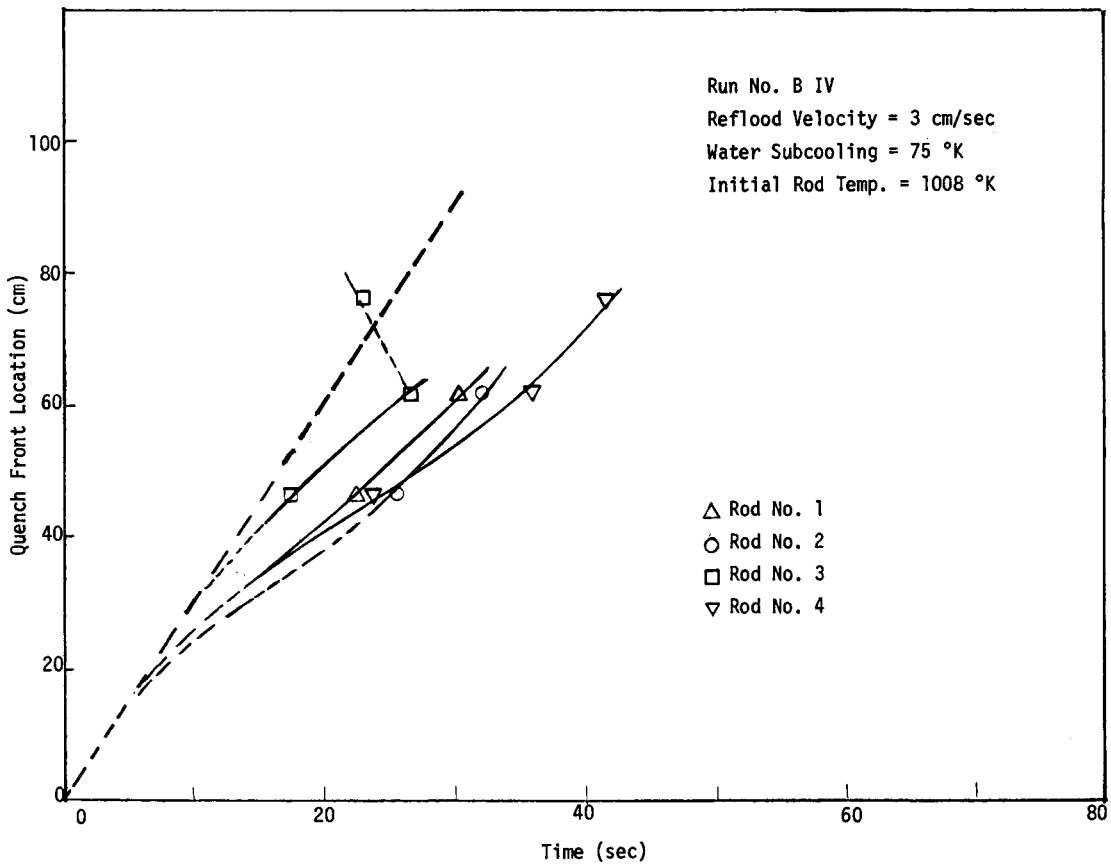

Figure A-7 Quench Front Location as a Function of Time

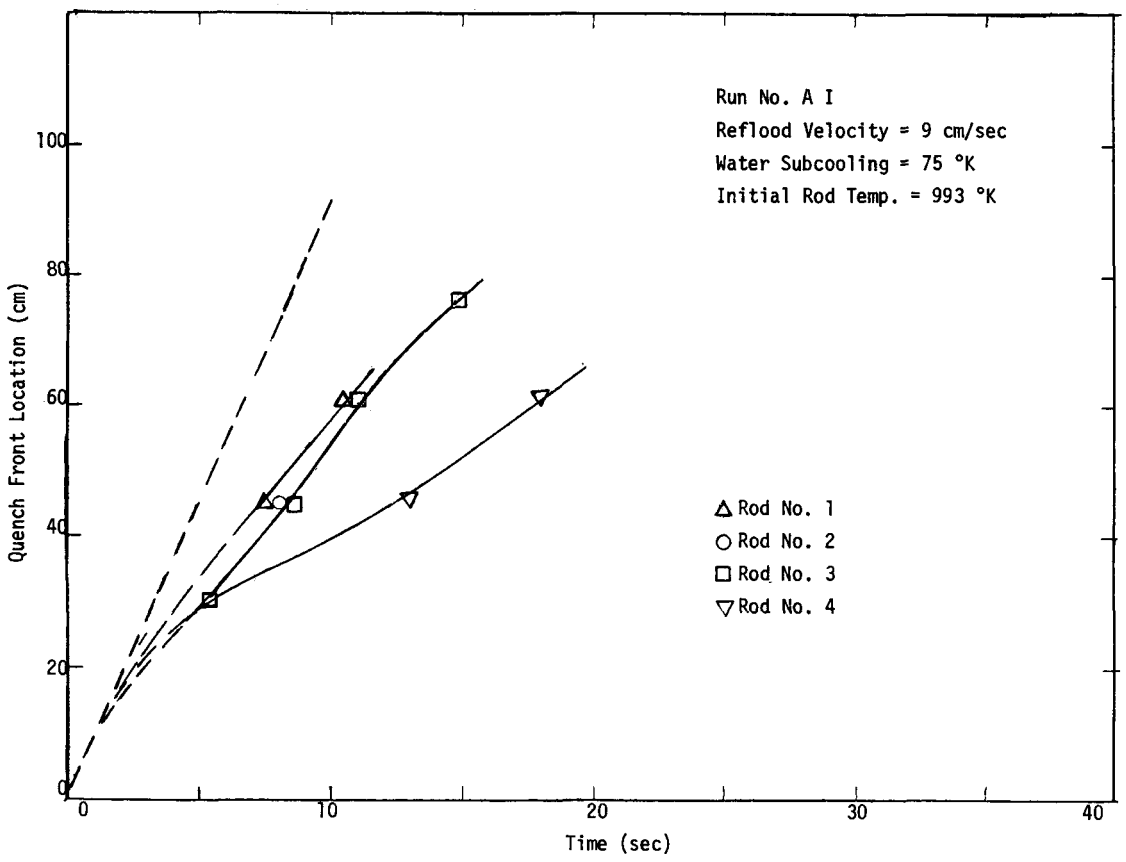

Figure A-8 Quench Front Location as a Function of Time

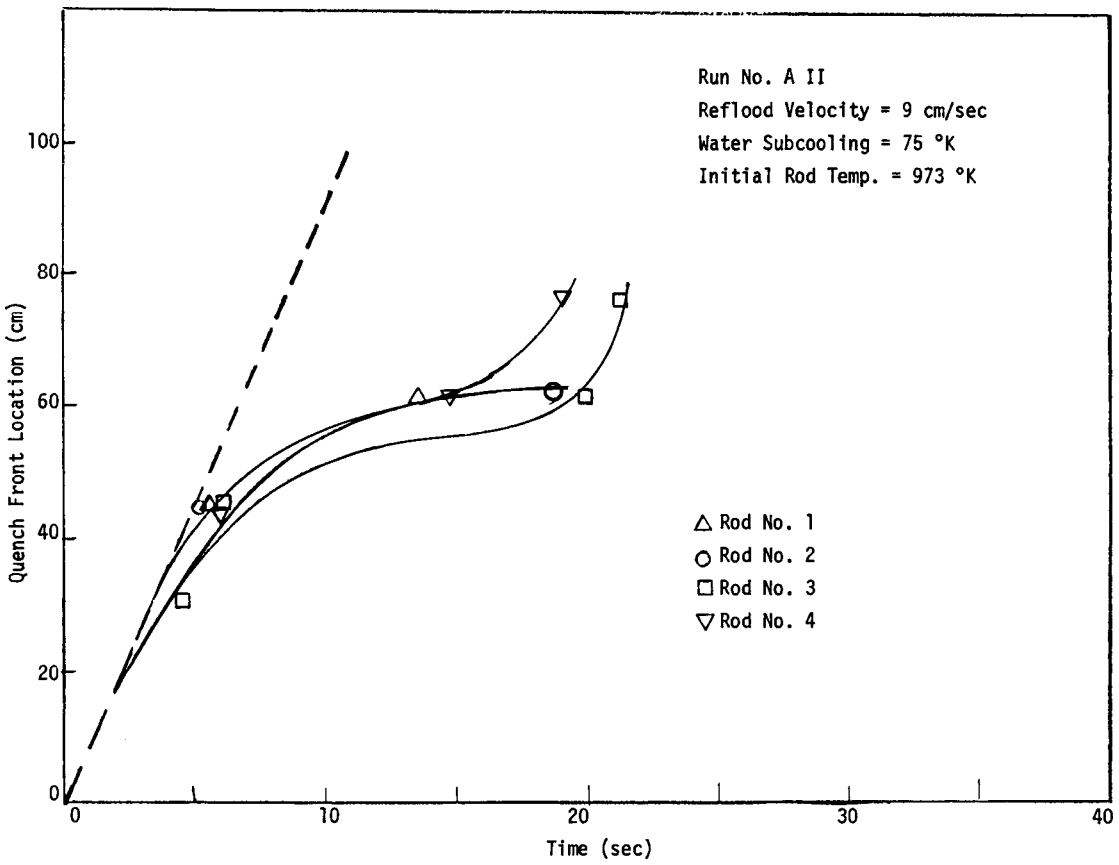

Figure A-9 Quench Front Location as a Function of Time

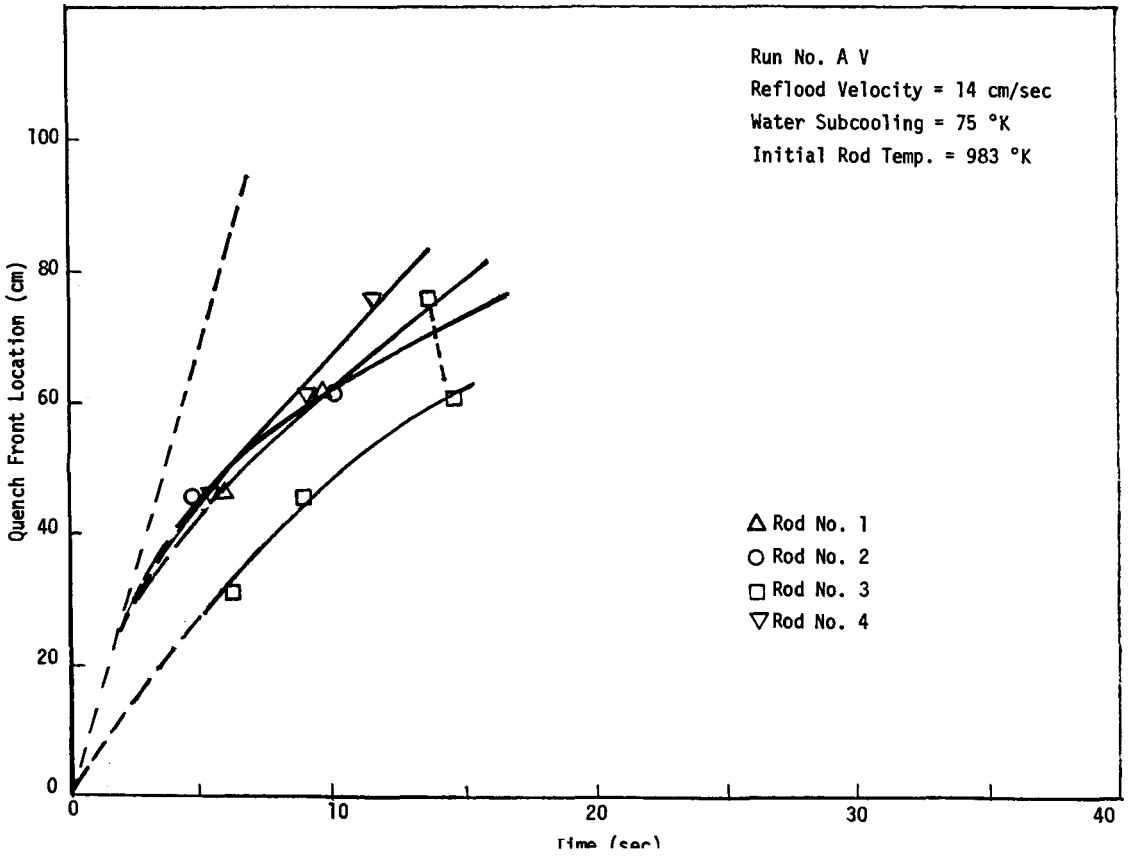

Figure A-10 Quench Front Location as a Function of Time

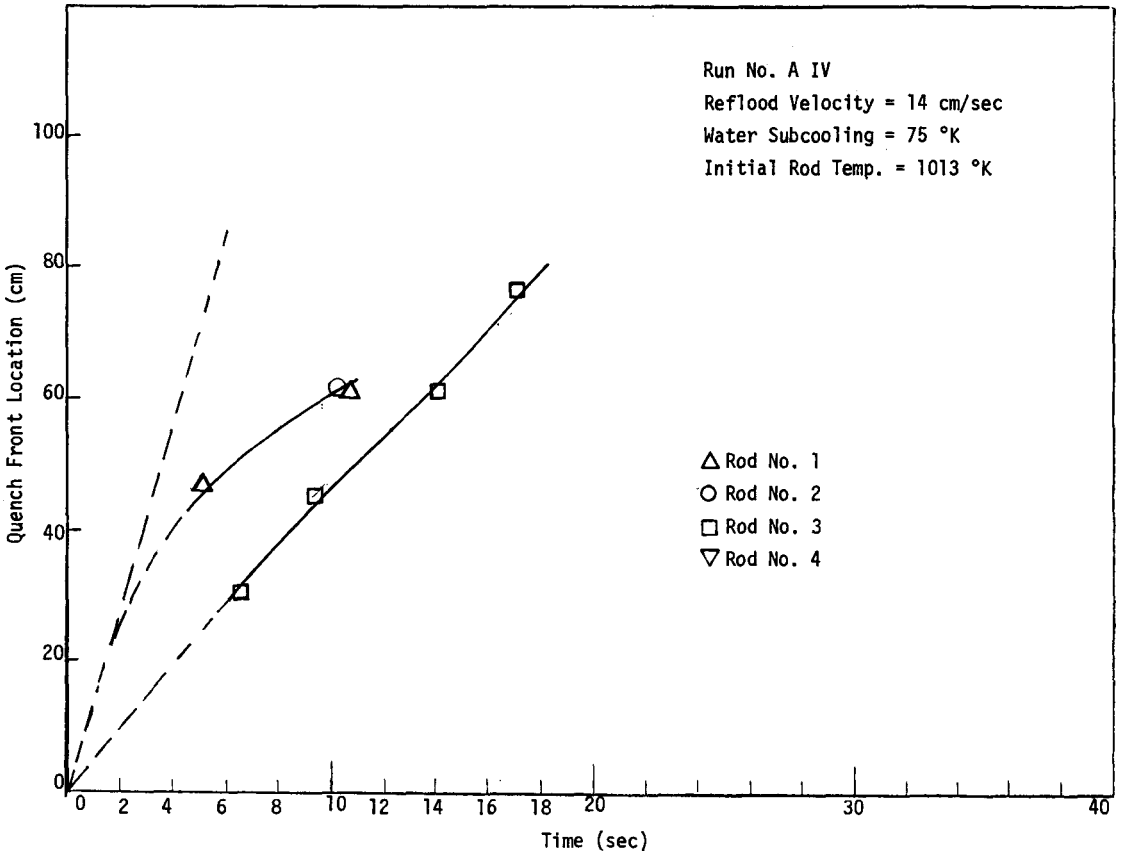

Figure A-11 Quench Front Location as a Function of Time

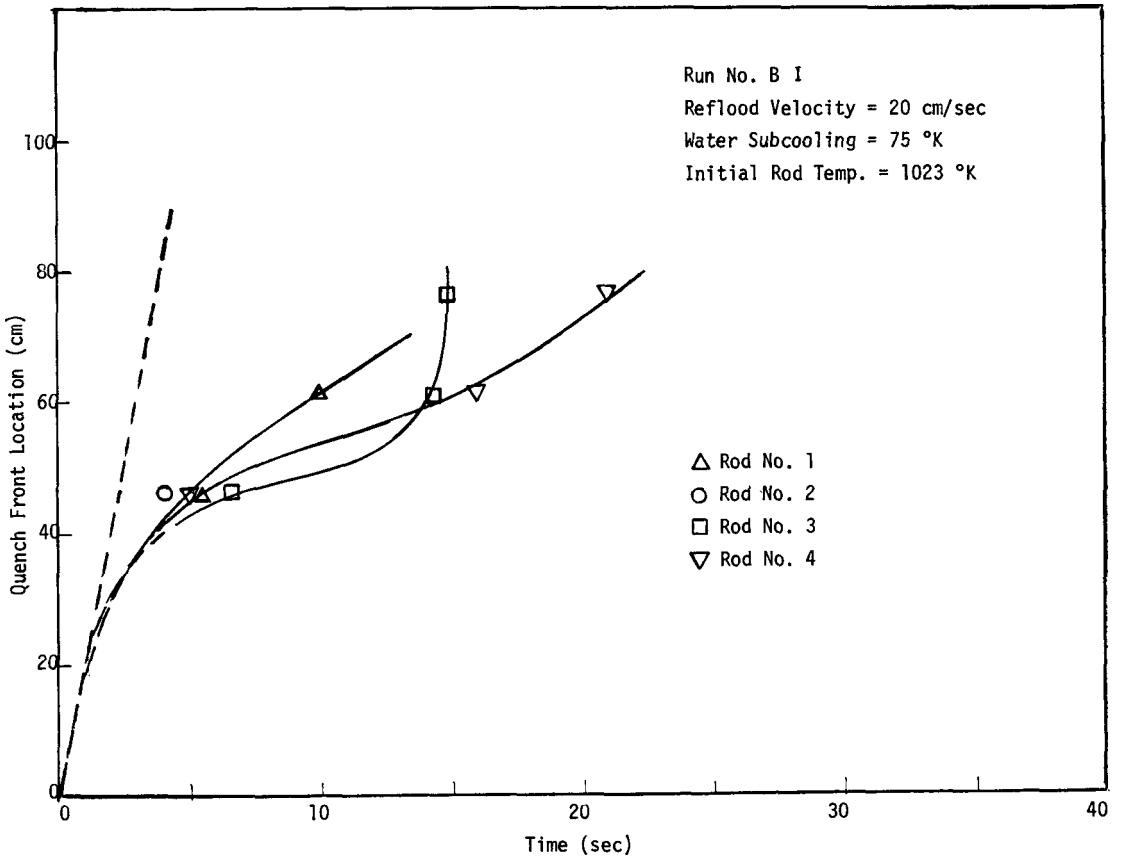

Figure A-12 Quench Front Location as a Function of Time

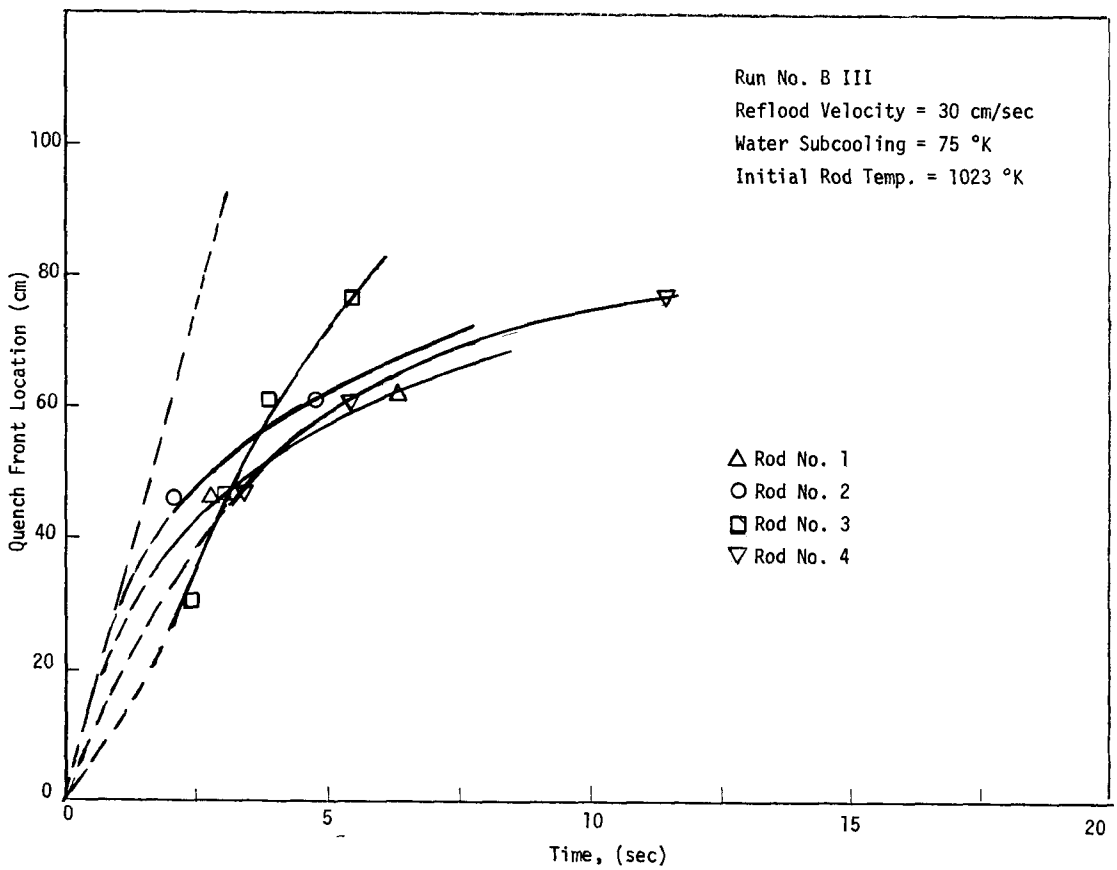

Figure A-13 Quench Front Location as a Function of Time

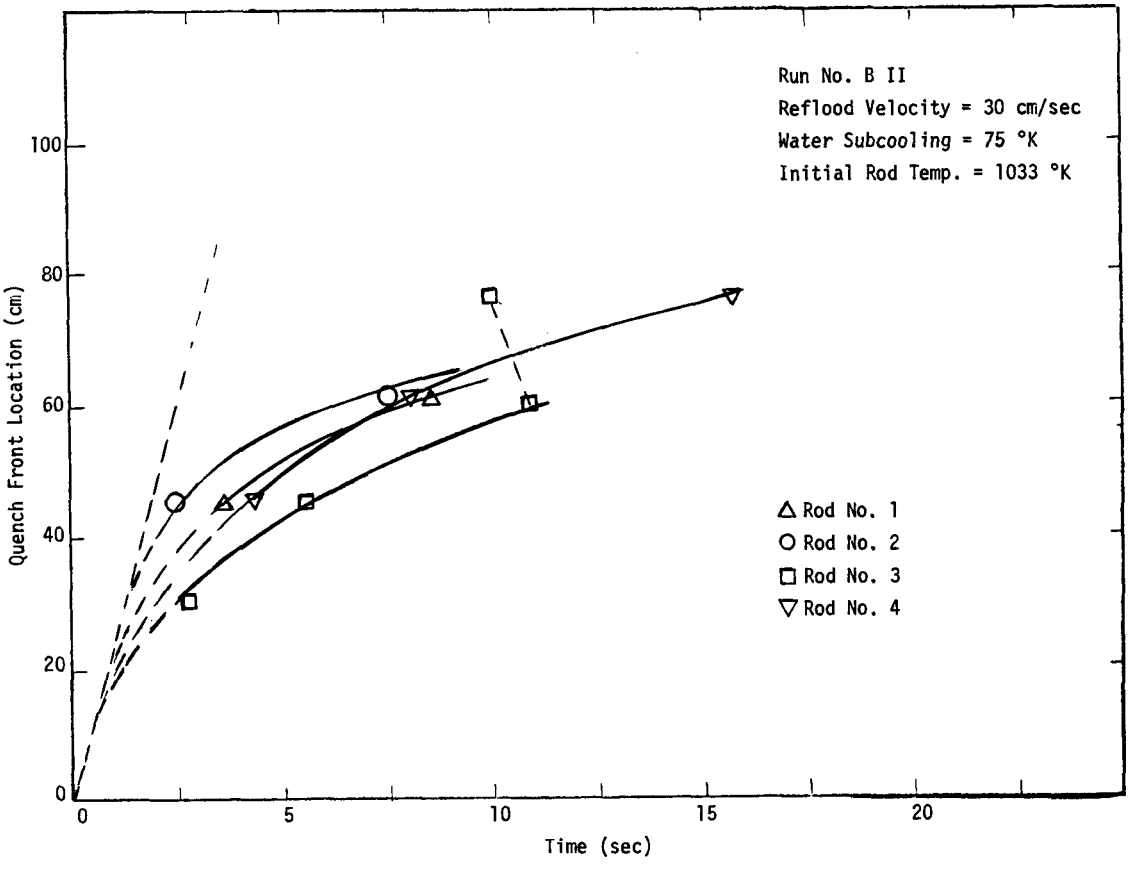

Figure A-14 Quench Front Location as a Function of Time

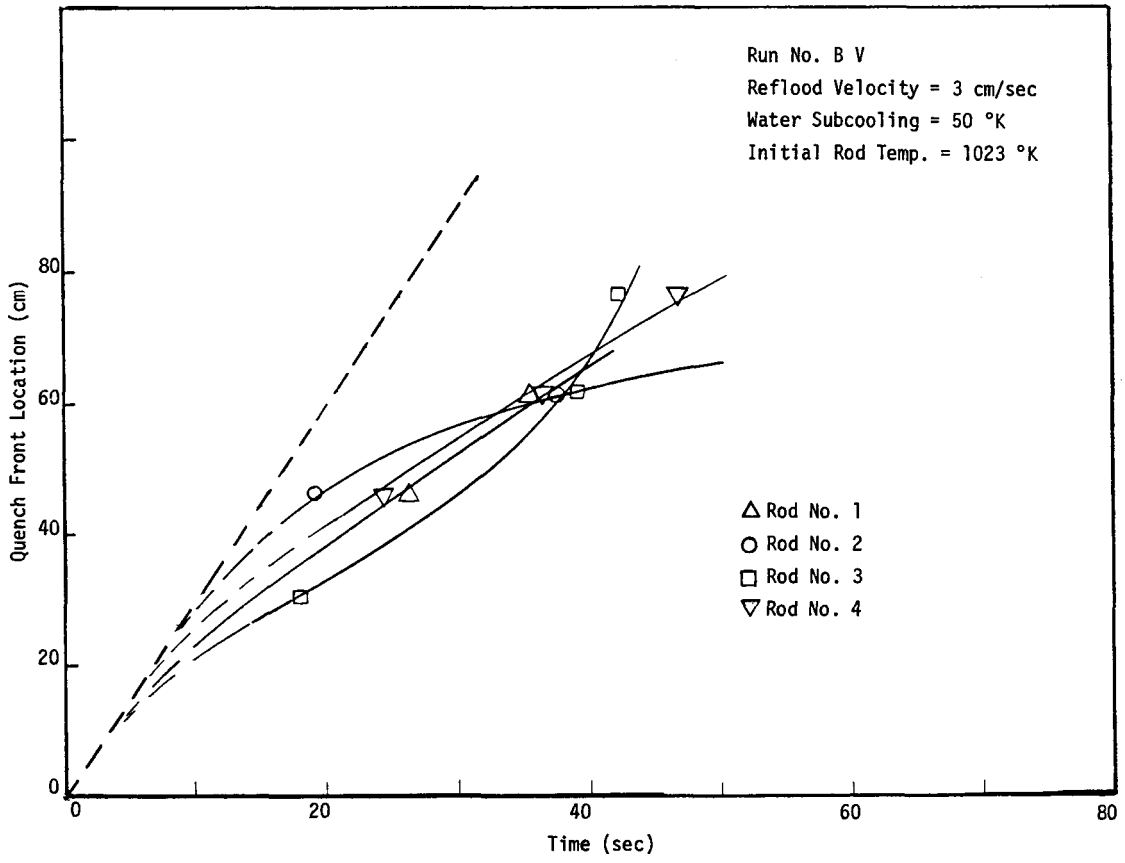

Figure A-15 Quench Front Location as a Function of Time

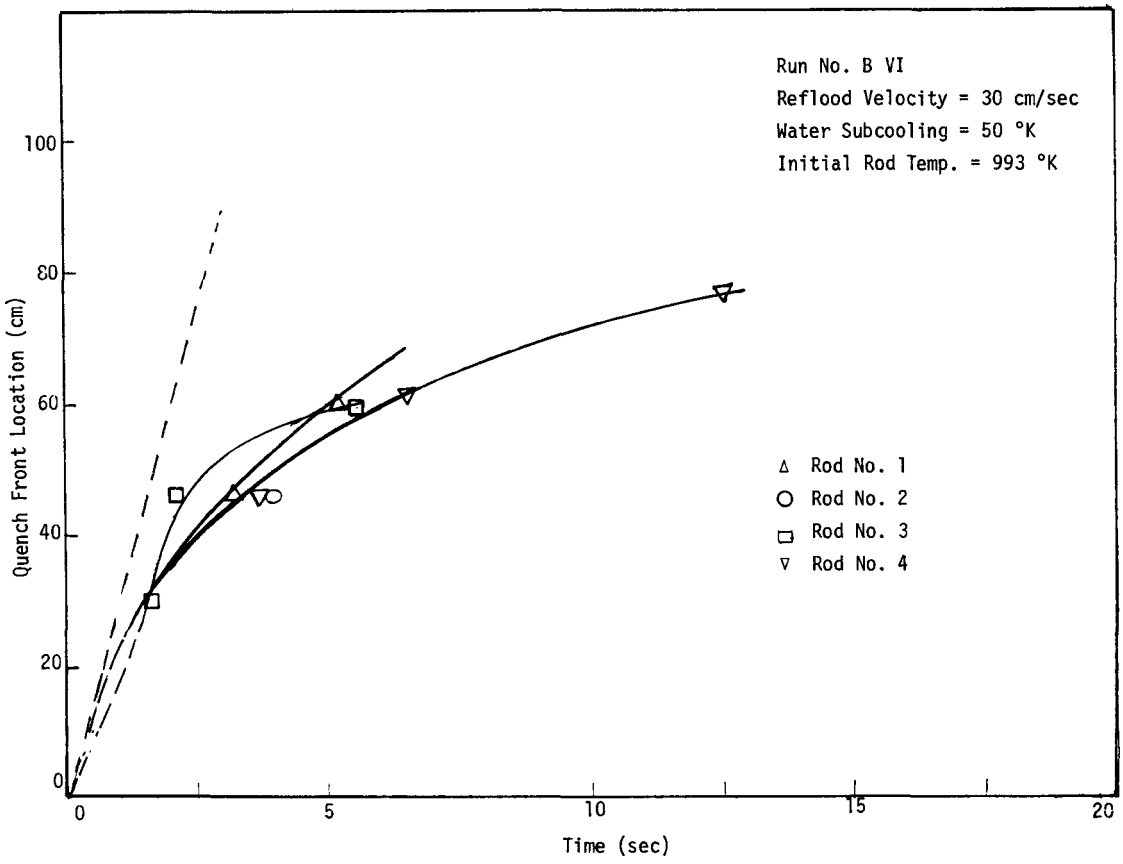

Figure A-16 Quench Front Location as a Function of Time

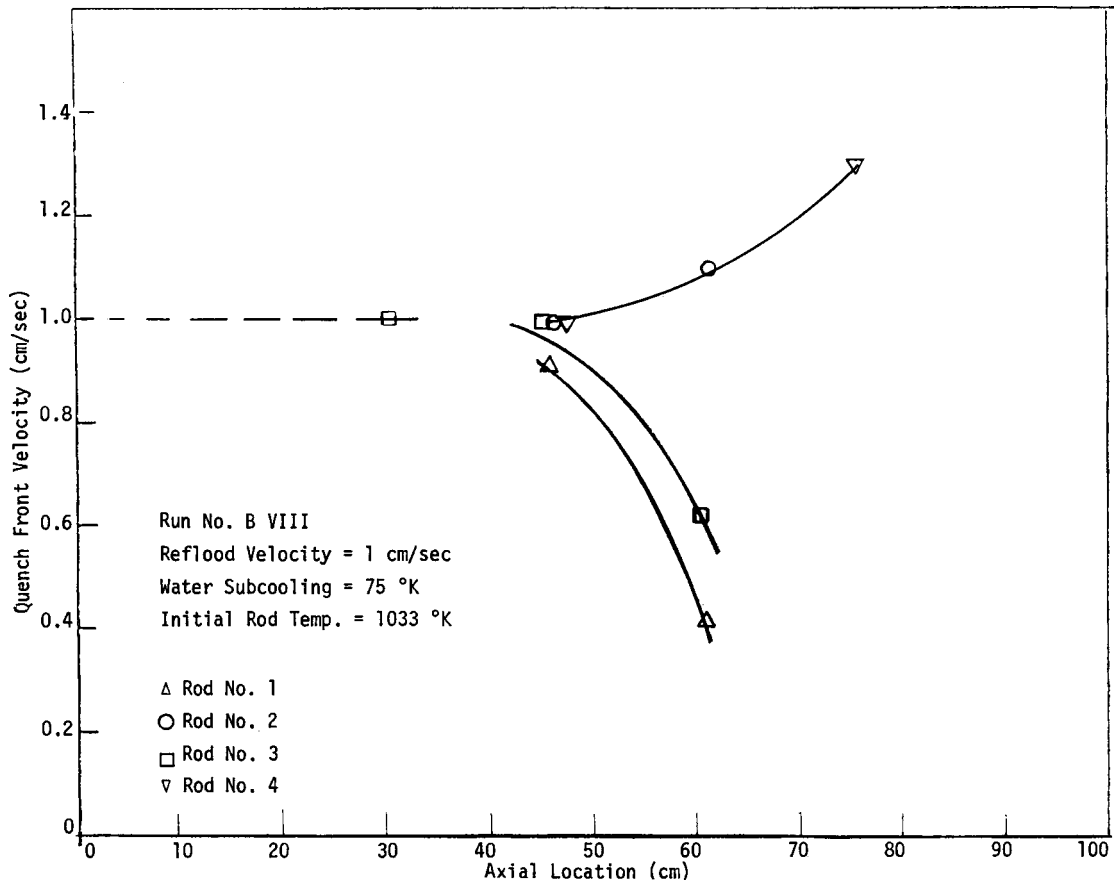

Figure A-17 Quench Front Velocity as a Function of Height

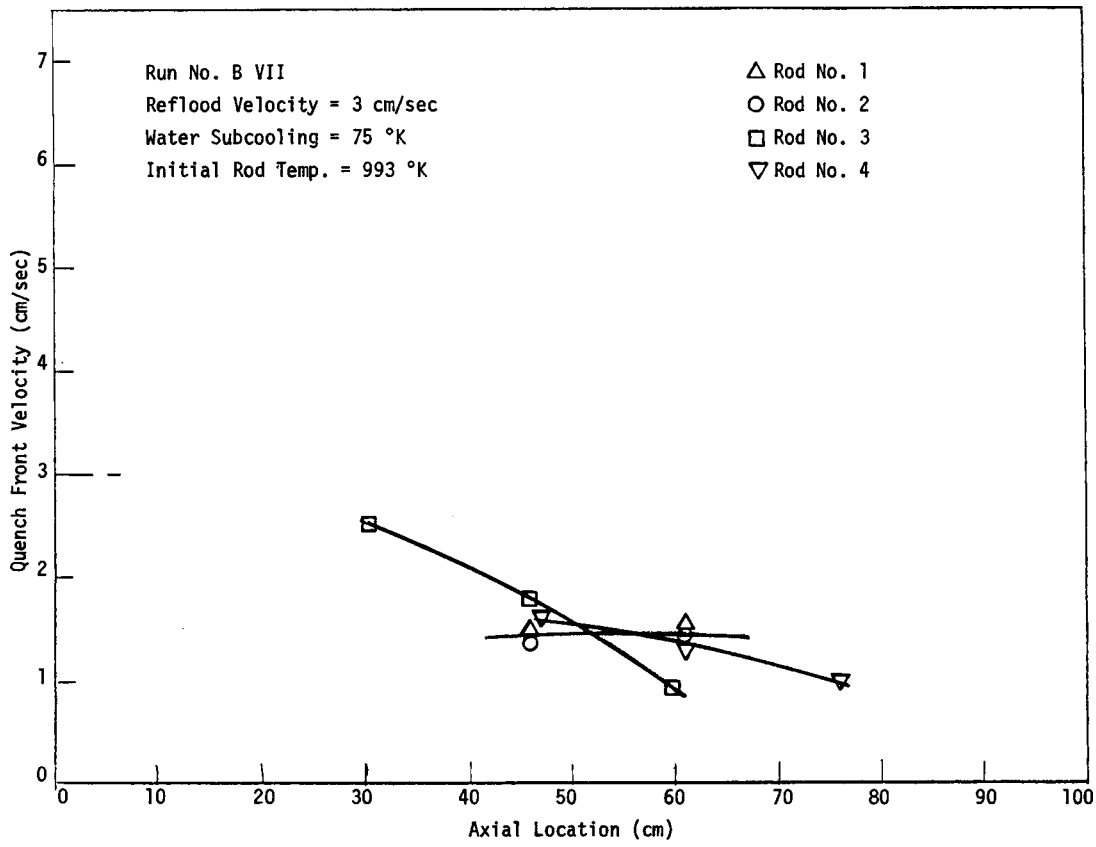

Figure A-18 Quench Front Velocity as a Function of Height

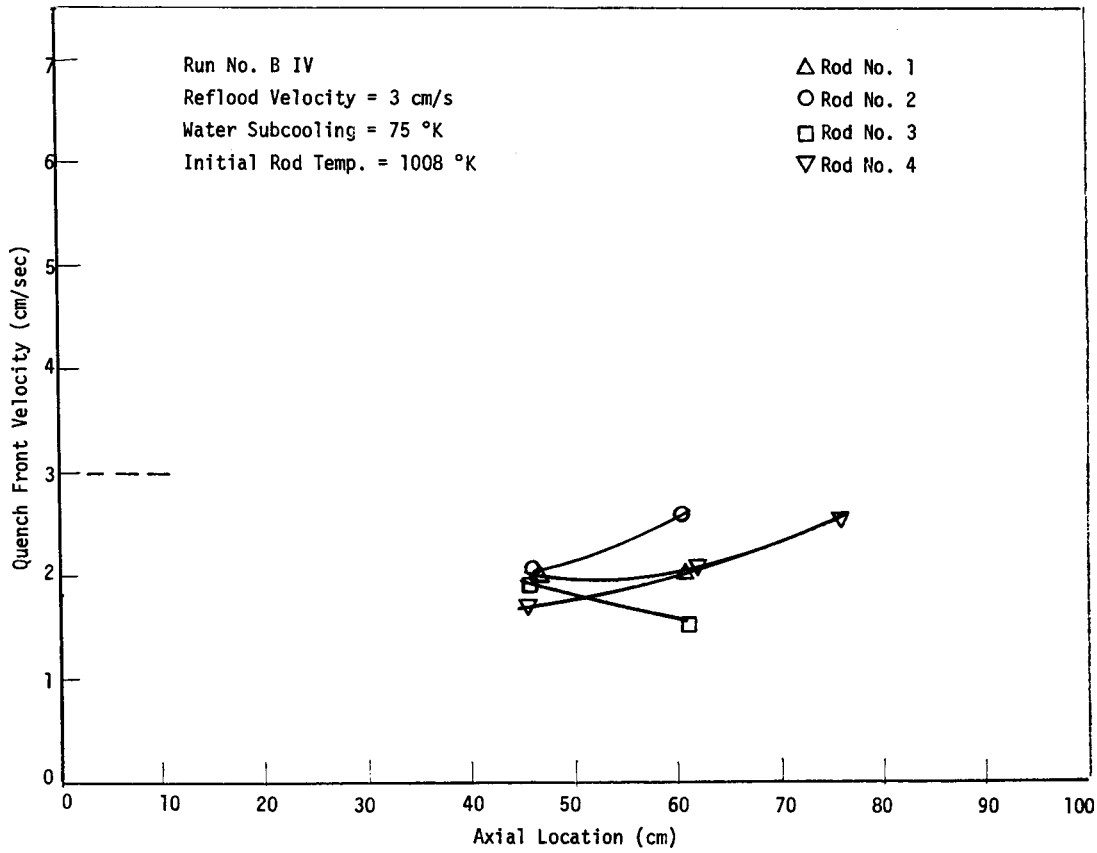

Figure A-19 Quench Front Velocity as a Function of Height

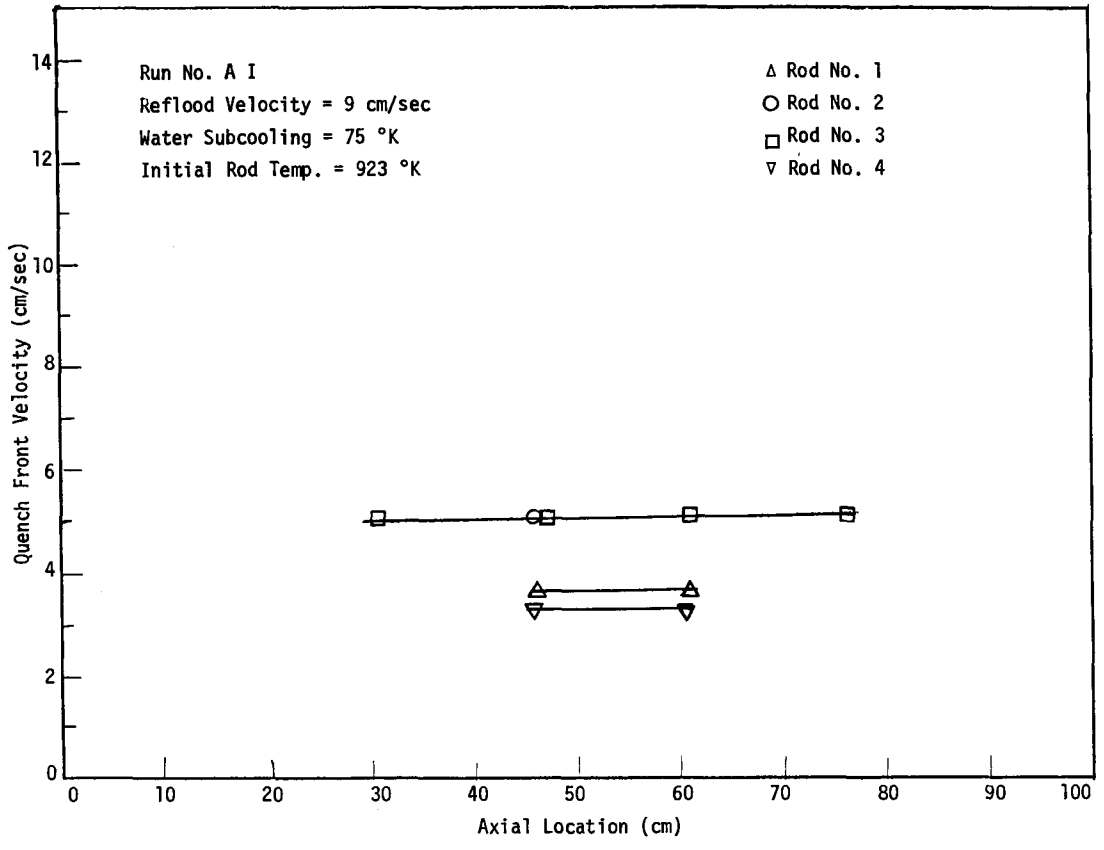

Figure A-20 Quench Front Velocity as a Function of Height

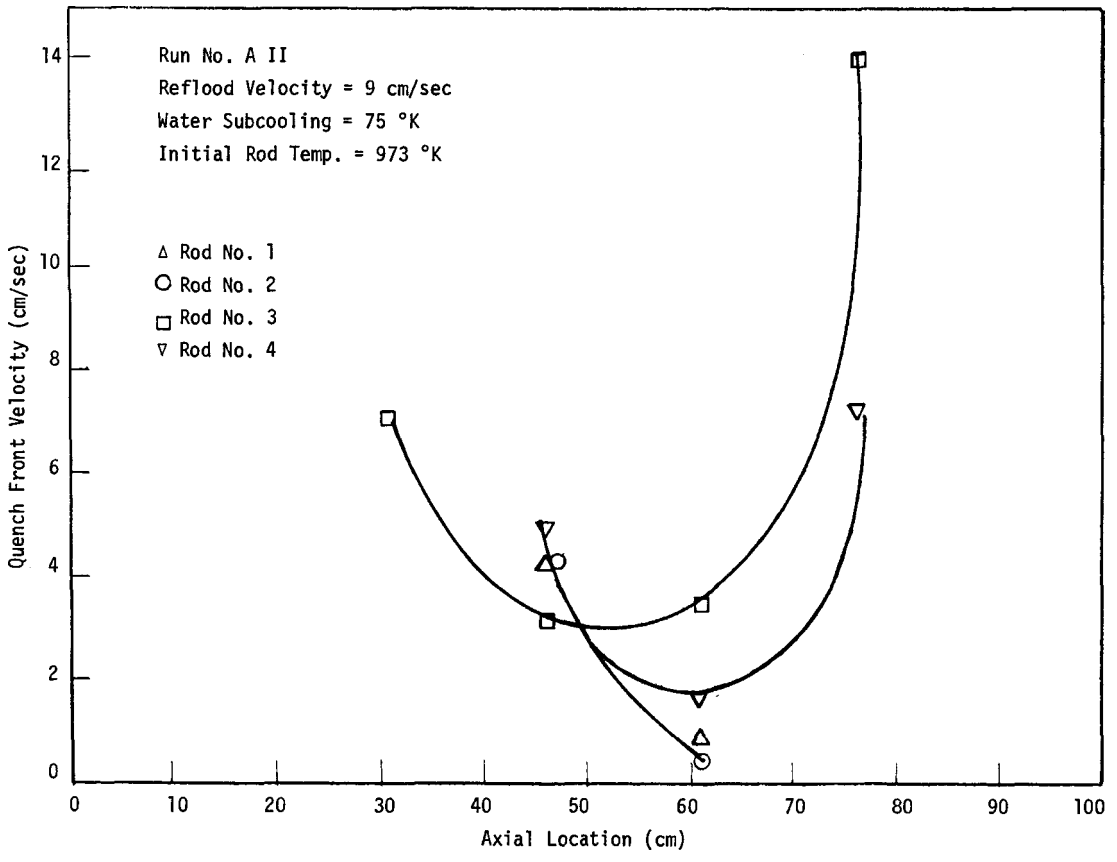

Figure A-21 Quench Front Velocity as a Function of Height

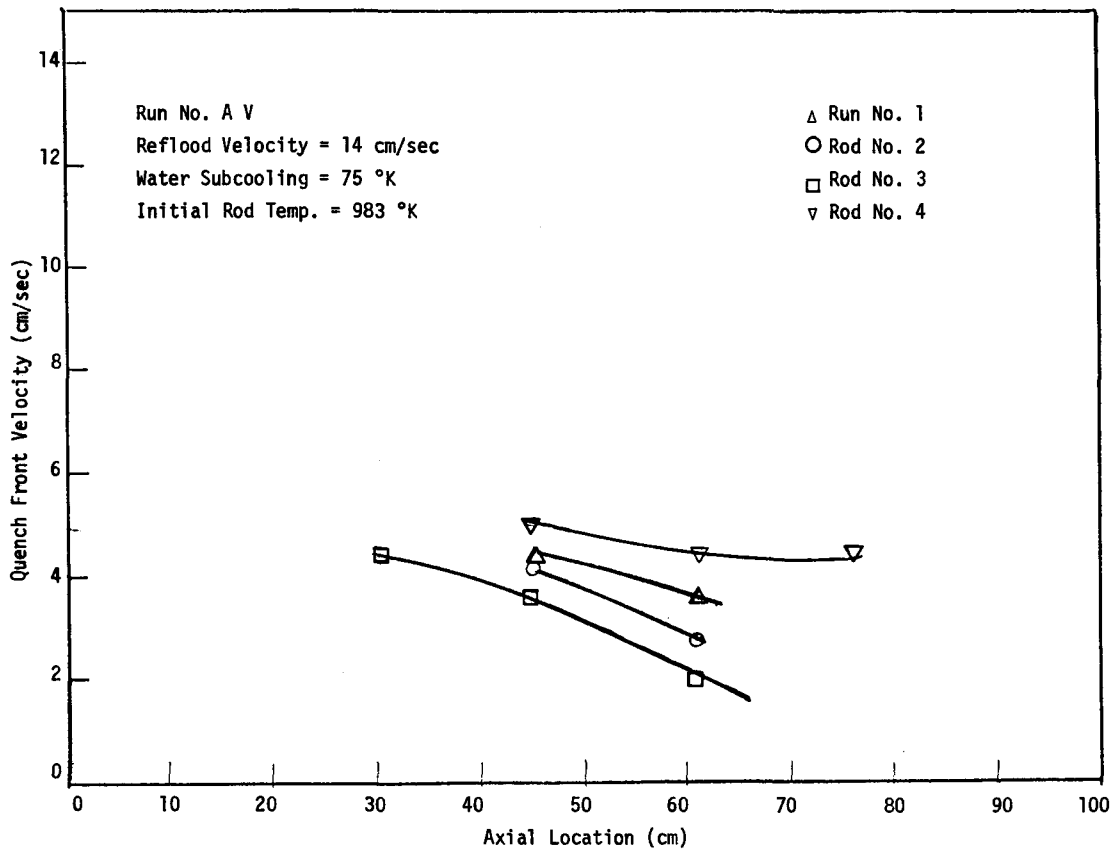

Figure A-22 Quench Front Velocity as a Function of Height

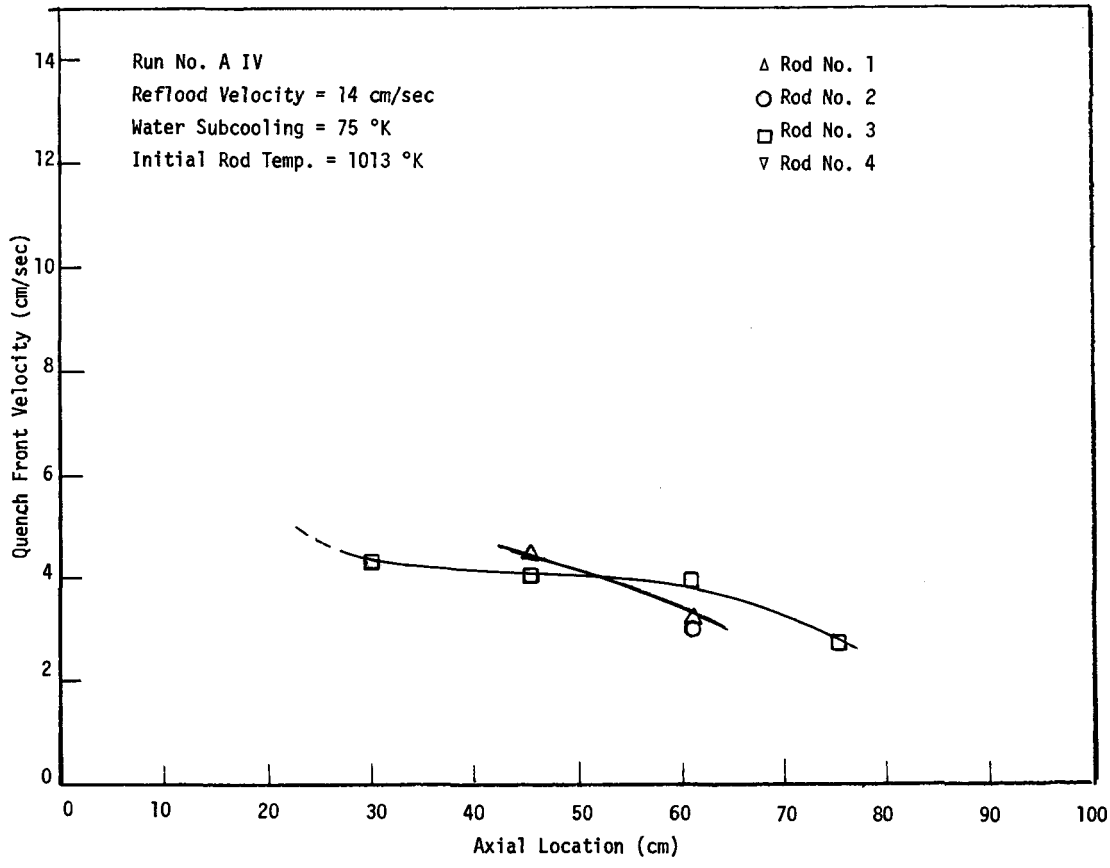

Figure A-23 Quench Front Velocity as a Function of Height

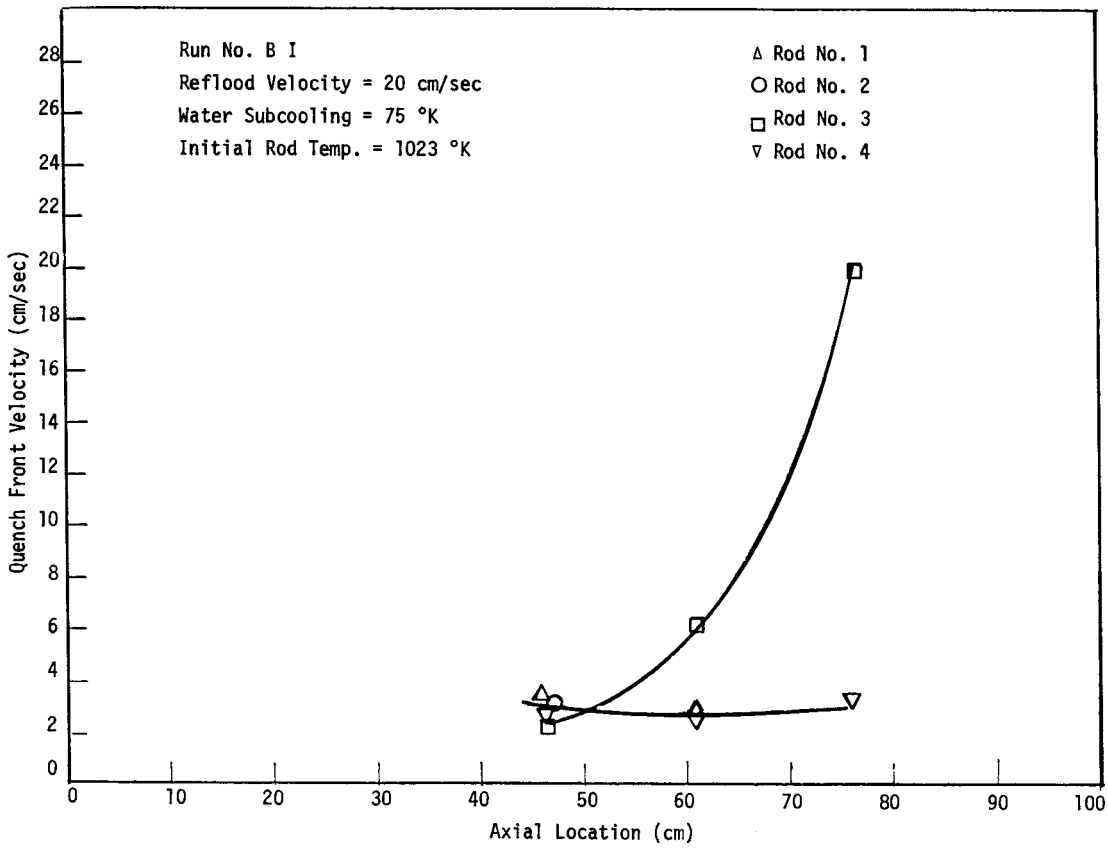

Figure A-24 Quench Front Velocity as a Function of Height

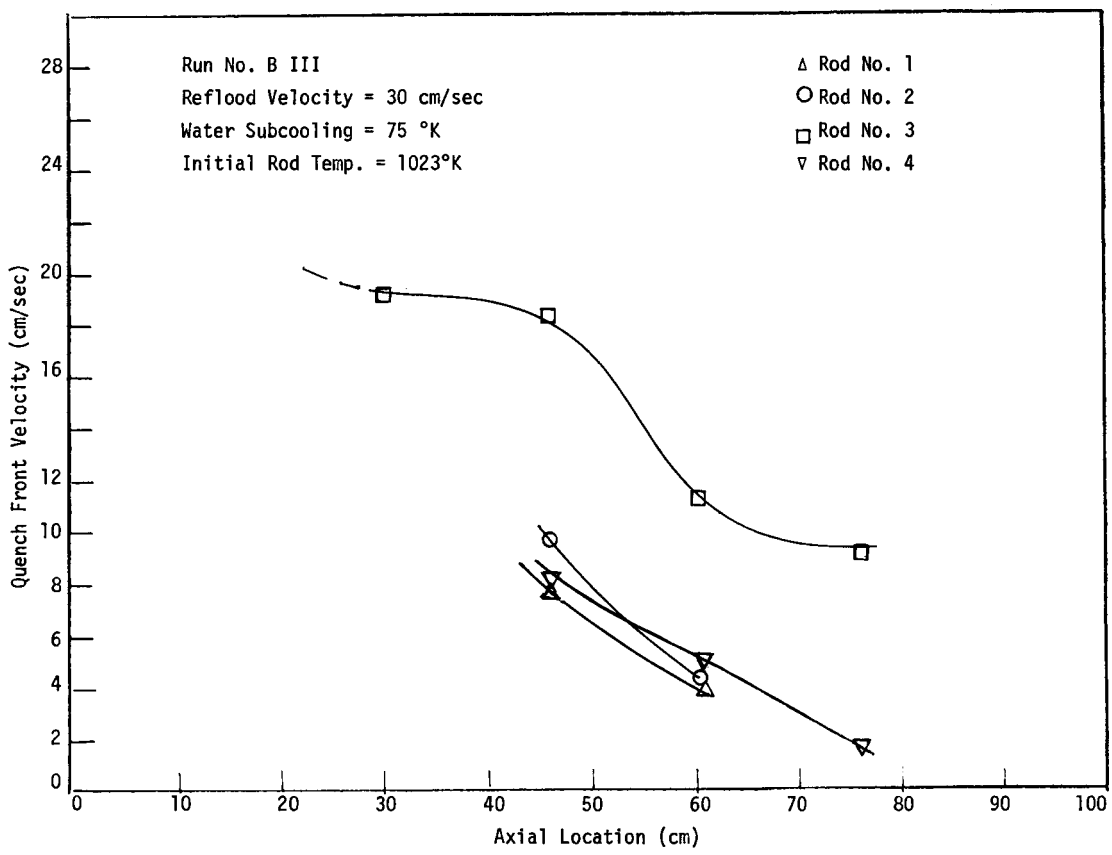

Figure A-25 Quench Front Velocity as a Function of Height

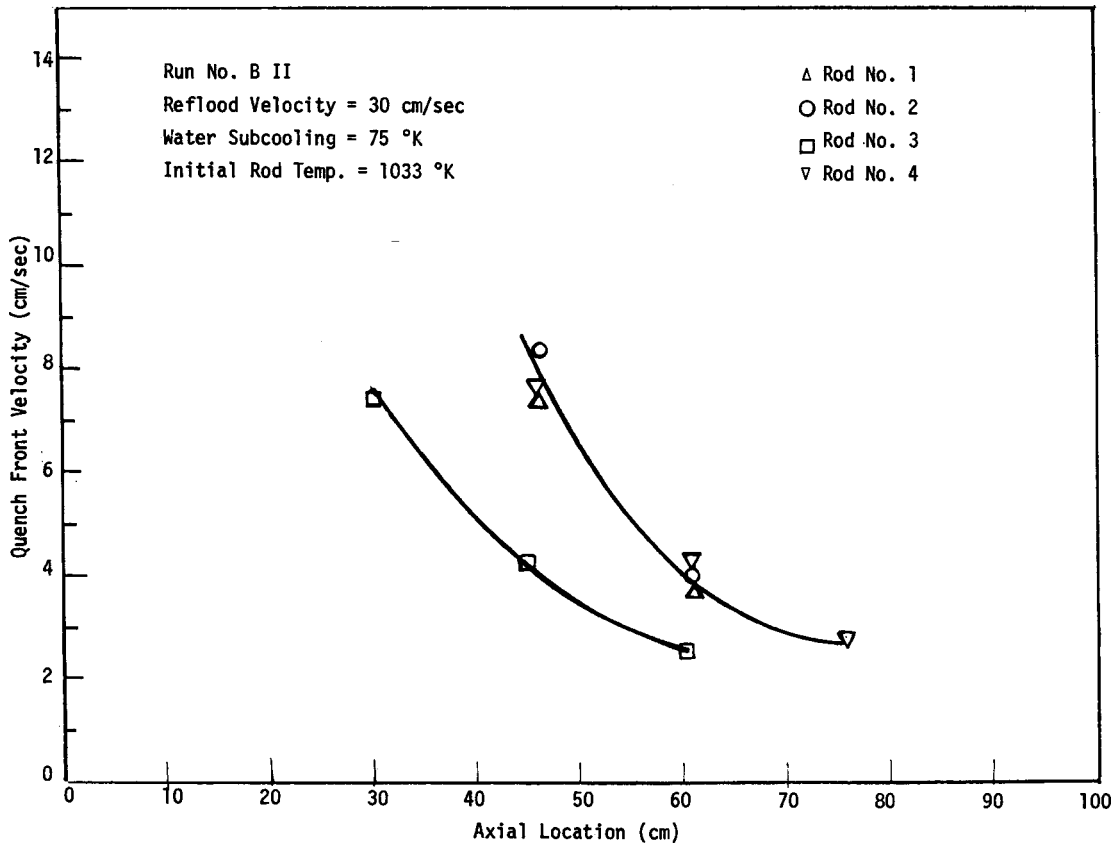

Figure A-26 Quench Front Velocity as a Function of Height

APPENDIX B

TABULATION AND GRAPHICAL PRESENTATION OF DATA FOR QUENCHING TEMPERATURE, QUENCH FRONT LOCATION AND QUENCH FRONT VELOCITY FOR A 4 ROD BUNDLE CONTAINING TWO STAINLESS STEEL AND TWO ZIRCALOY RODS

A total of thirty-one runs were made to compare the behavior of zircaloy cladding with the stainless steel cladding under identical flooding conditions. In these experiments the initial wall temperatures varied from 873-1133 K and flooding velocities varied from 2-30 cm/s. For all of the runs, inlet water subcooling was either about 75 K or about 50 K. Tables B-1 and B-2 list all the runs made with the mixed bundle containing two zircaloy and two stainless steel rods.

QUENCH FRONT LOCATION

Quench front locations obtained from movies for both zircaloy and stainless steel are shown in Figures B-1 - B-6 as a function of time. In these figures, the quench front locations, as interpreted from the temperature time traces of thermocouple output by using the procedure described in Section 2, are also marked. The figures are arranged in order of increasing flooding velocity and zero time in these figures corresponds to the time at which liquid entered the test section. Liquid subcooling at inlet for these data was about 75 K. The other quench front location data obtained from thermocouples for the cases in which no movies were made and subcooling of water at inlet was 75 K are plotted in Figures B-7 - B-12. Figures B-13 and B-14 show the quench front location data as obtained from movies whereas Figures B-15 - B-26 show the data obtained from thermocouples when subcooling of water at inlet was reduced to about 50 K.

QUENCH FRONT VELOCITIES

The quench front velocities as reduced from the quench front location data obtained from movies as well as thermocouples are plotted in Figures B-27 - B-52.

Table B-1

TEST RUNS WITH TWO ZIRCALOY AND TWO STAINLESS STEEL RODS

Serial Number	Run Number	Reflood Velocity (cm/s)	Inlet Water Temp.(K)	Initial Tube Temp.(K)	Movie Data
1	C-I	9	295	957	Yes
2	C-II	5	295	980	Yes
3	C-III	9	298	876	No
4	C-IV	20	298	899	No
5	C-V	30	298	973	No
6	D-I	5	295	933	No
7	D-II	3	295	968	Yes
8	D-III	1	295	968	Yes
9	D-IV	15	295	968	Yes
10	D-V	7	295	973	Yes
11	D-VI	15	295	973	Yes
12	D-VII	25	295	973	Yes

Table B-2

TEST RUNS WITH TWO ZIRCALOY AND TWO STAINLESS STEEL RODS

Serial Number	Run Number	Reflood Velocity (cm/s)	Inlet Water Temp.(K)	Initial Tube Temp.(K)	Movie Data
13	E-I*	9	295	-	No
14	E-II	20	323	-	No
15	E-III	9	323	980	No
16	E-IV	8	323	909	No
17	E-V	8.5	335	1040	No
18	E-VI	7	323	1040	Yes
19	E-VII	20	323	992	Yes
20	E-VIII	4	323	874	Yes
21	E-IX	9	323	1064	Yes
22	E-X	20	320	1088	Yes
23	E-XI	3	320	1113	Yes
24	E-XII	30	323	1137	No
25	E-XIII	2	321	1137	No
26	E-XIV	15	330	992	No
27	E-XV	15	316	1137	No
28	E-XVI*	30	295	1016	No
29	E-XVII*	20	295	992	No
30	E-XVIII*	9	295	968	No
31	E-XIX*	4	295	968	No

*Data could not be reduced because of malfunction of recorders.

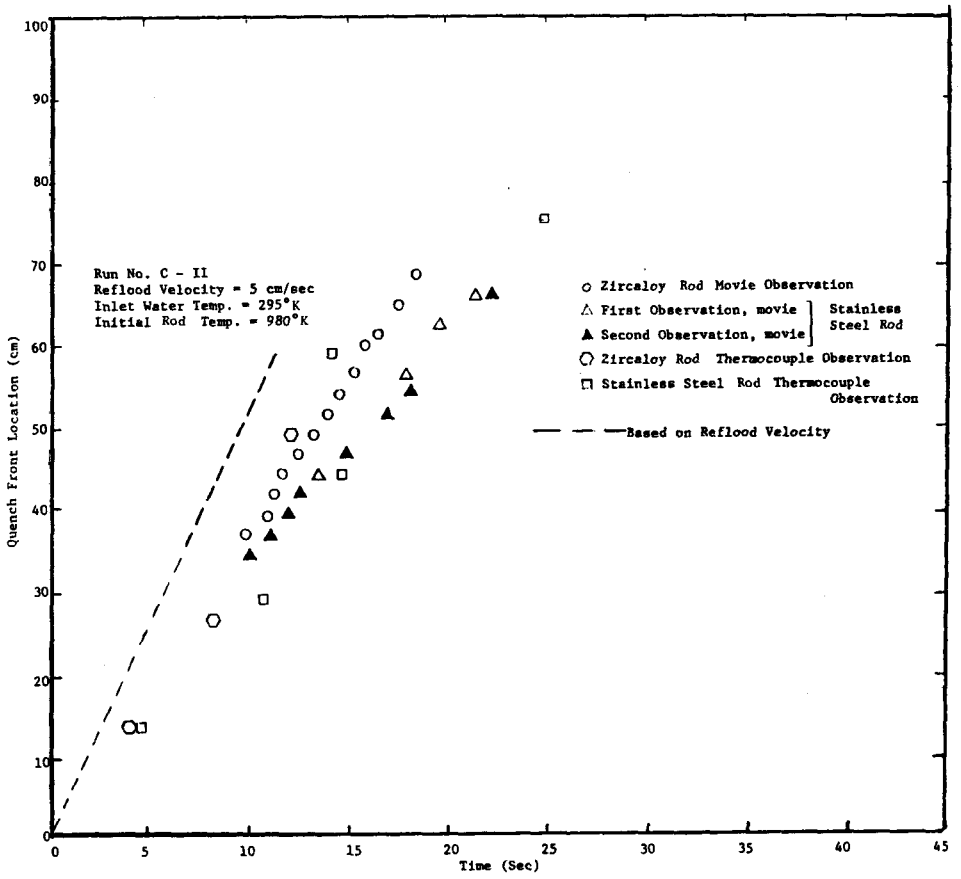

Figure B-1 Quench Front Location as a Function of Time

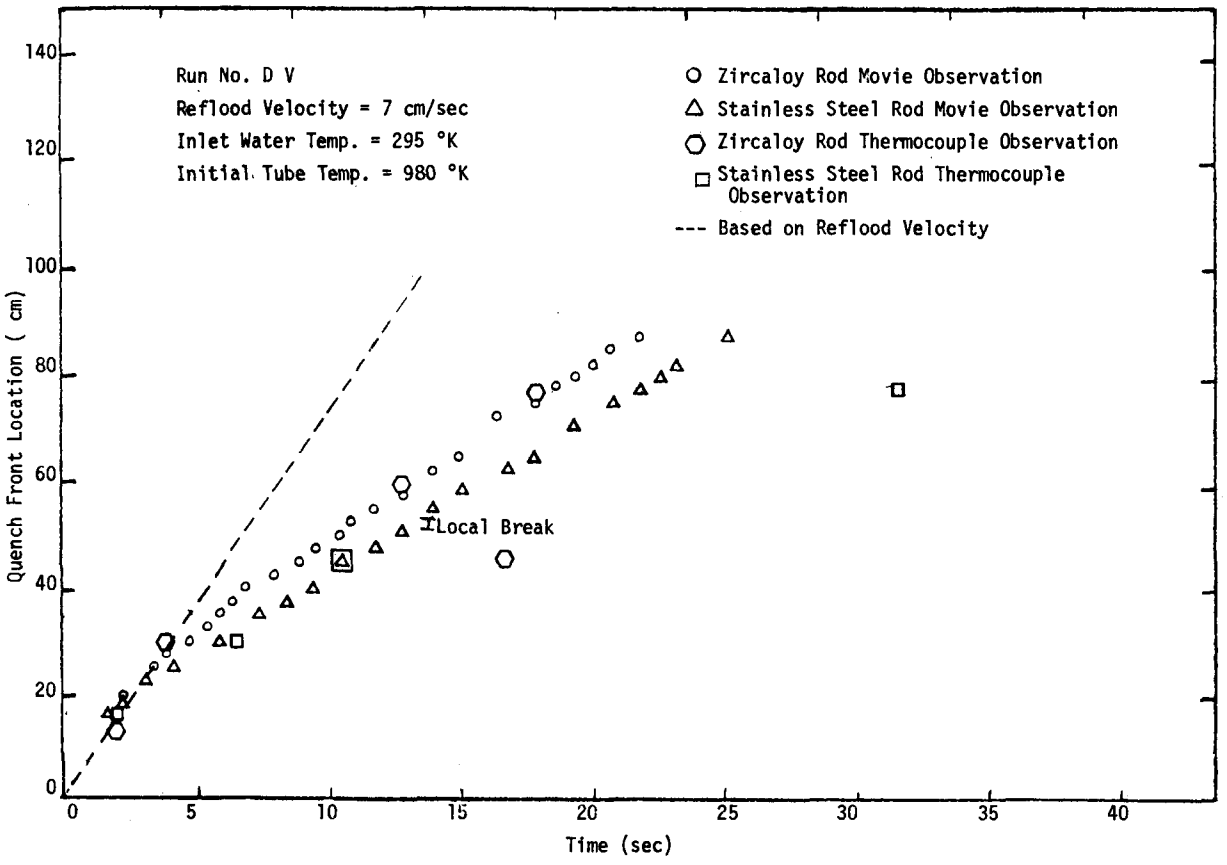

Figure B-2 Quench Front Location as a Function of Time

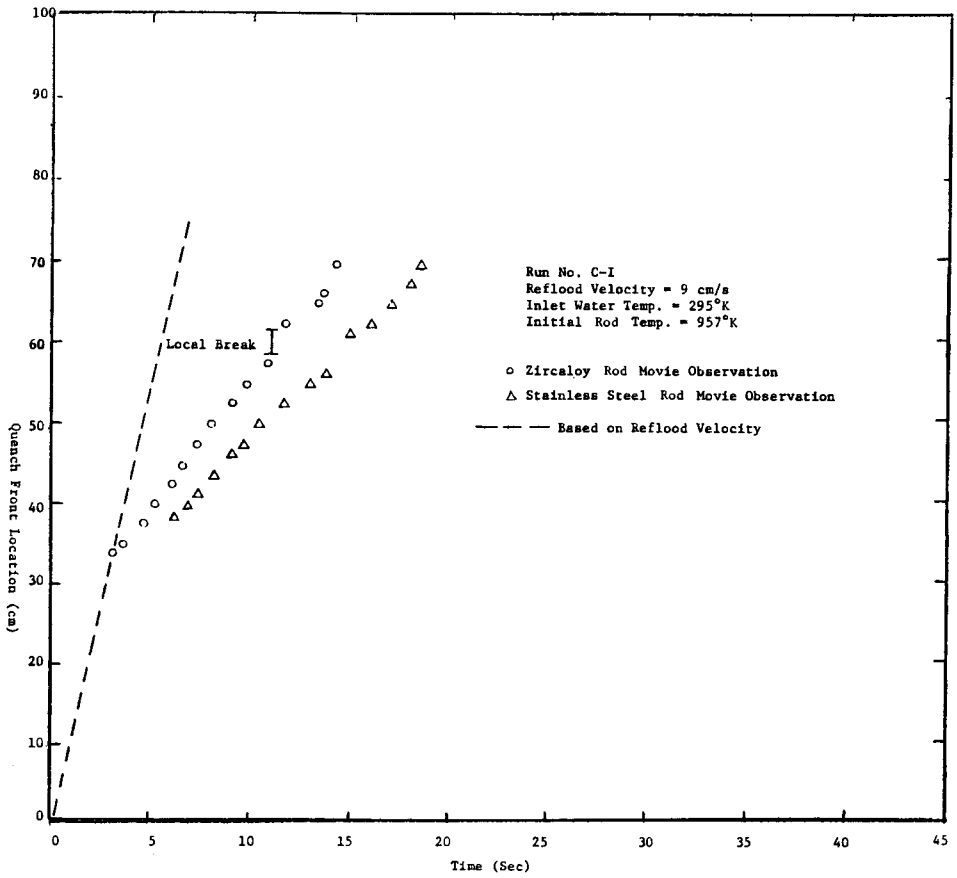

Figure B-3 Quench Front Location as a Function of Time

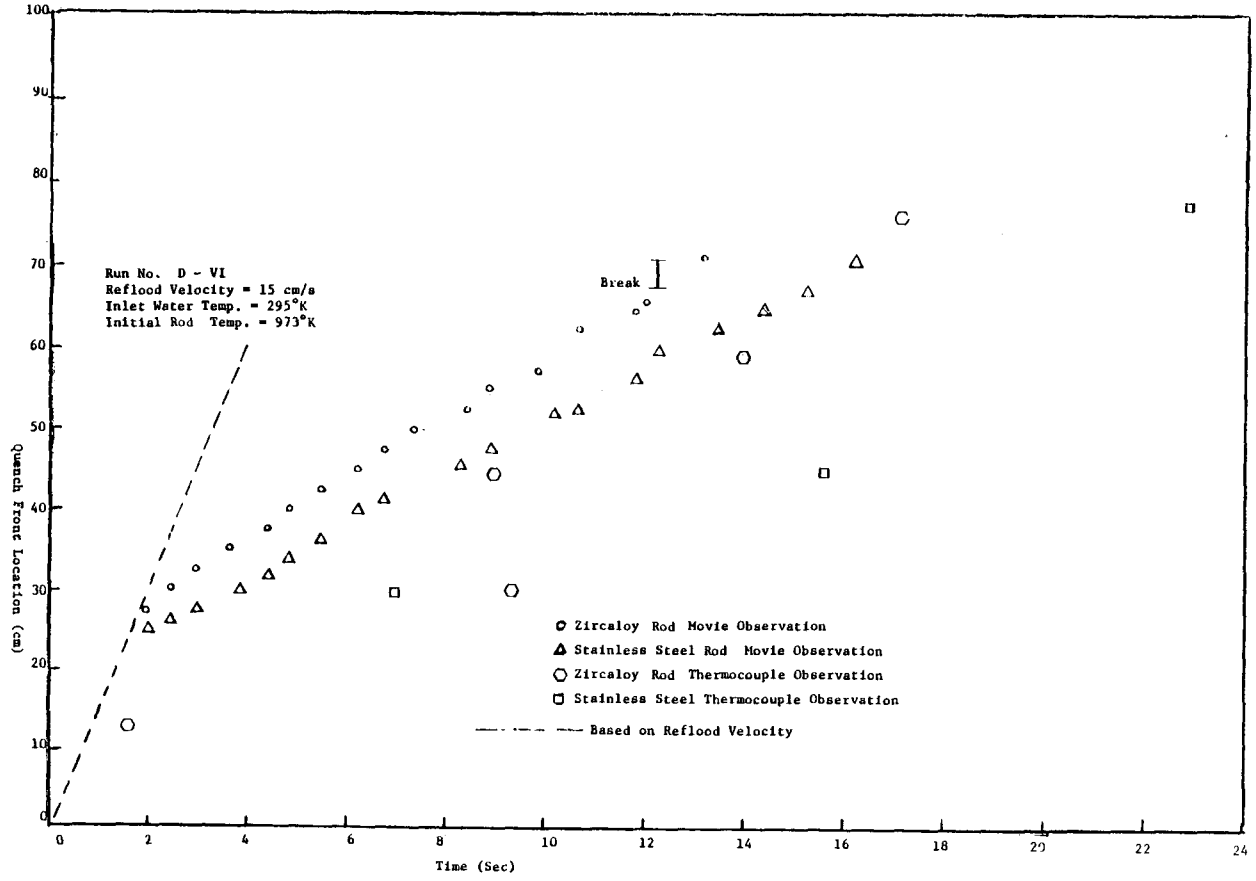

Figure B-4 Quench Front Location as a Function of Time

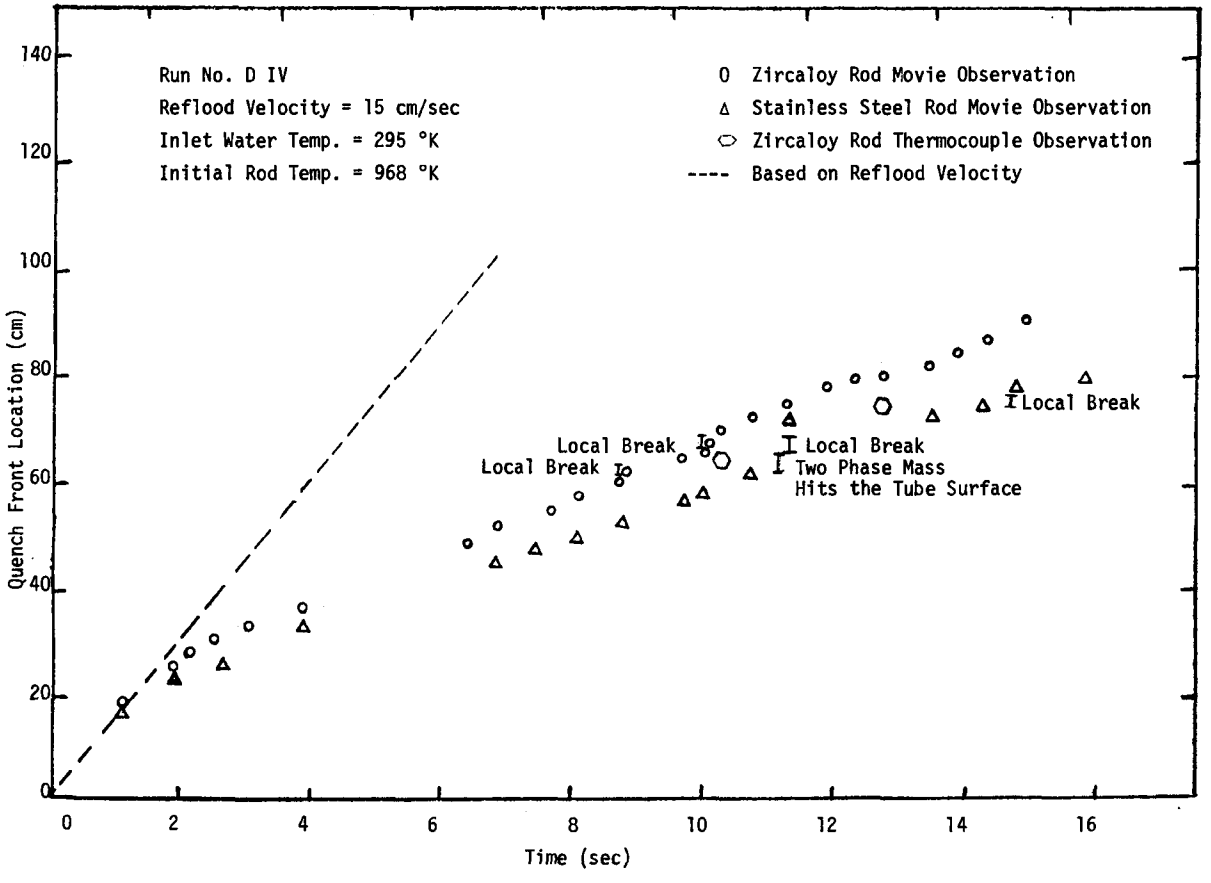

Figure B-5 Quench Front Location as a Function of Time

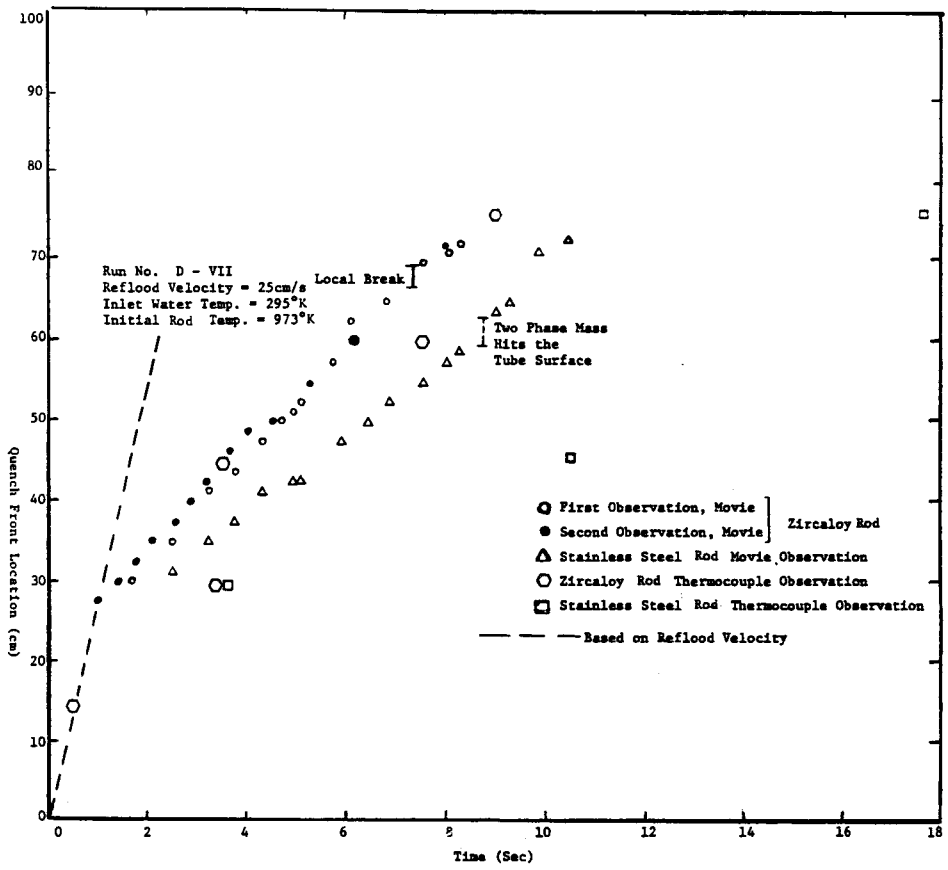

Figure B-6 Quench Front Location as a Function of Time

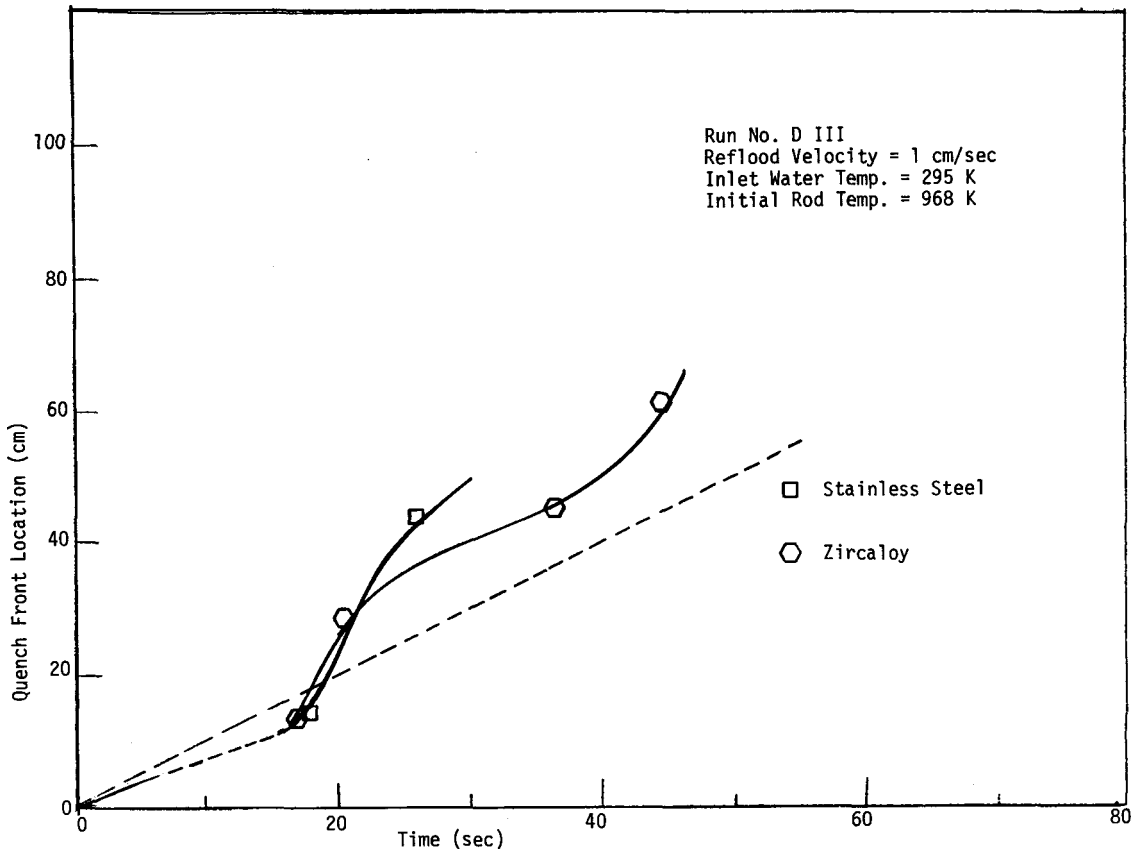

Figure B-7 Quench Front Location as a Function of Time

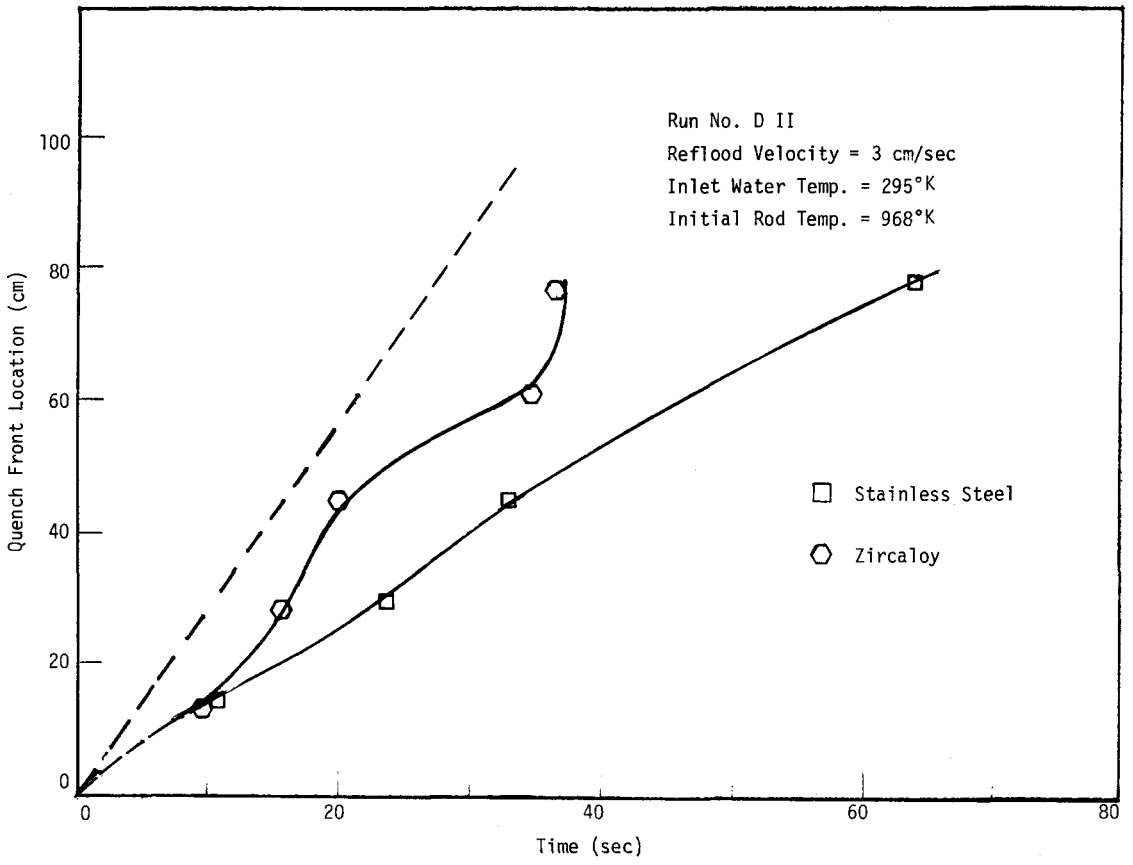

Figure B-8 Quench Front Location as a Function of Time

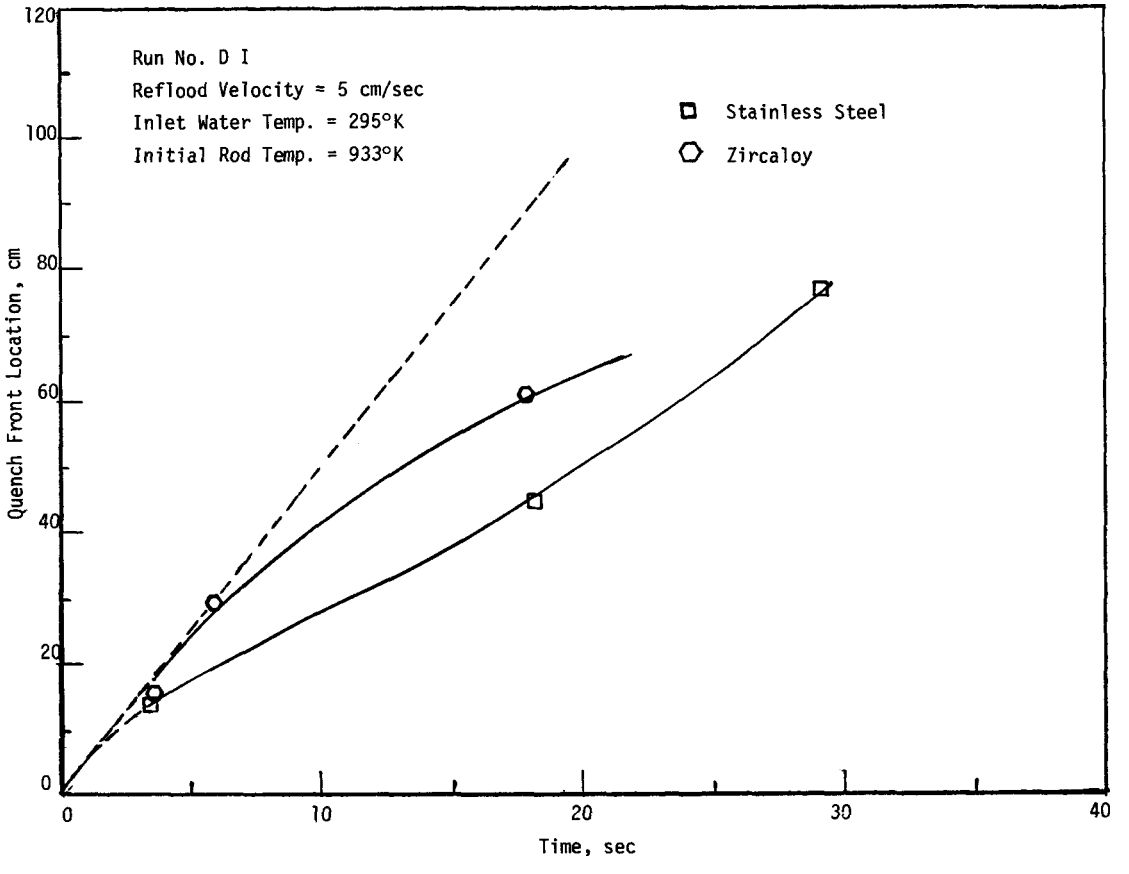

Figure B-9 Quench Front Location as a Function of Time

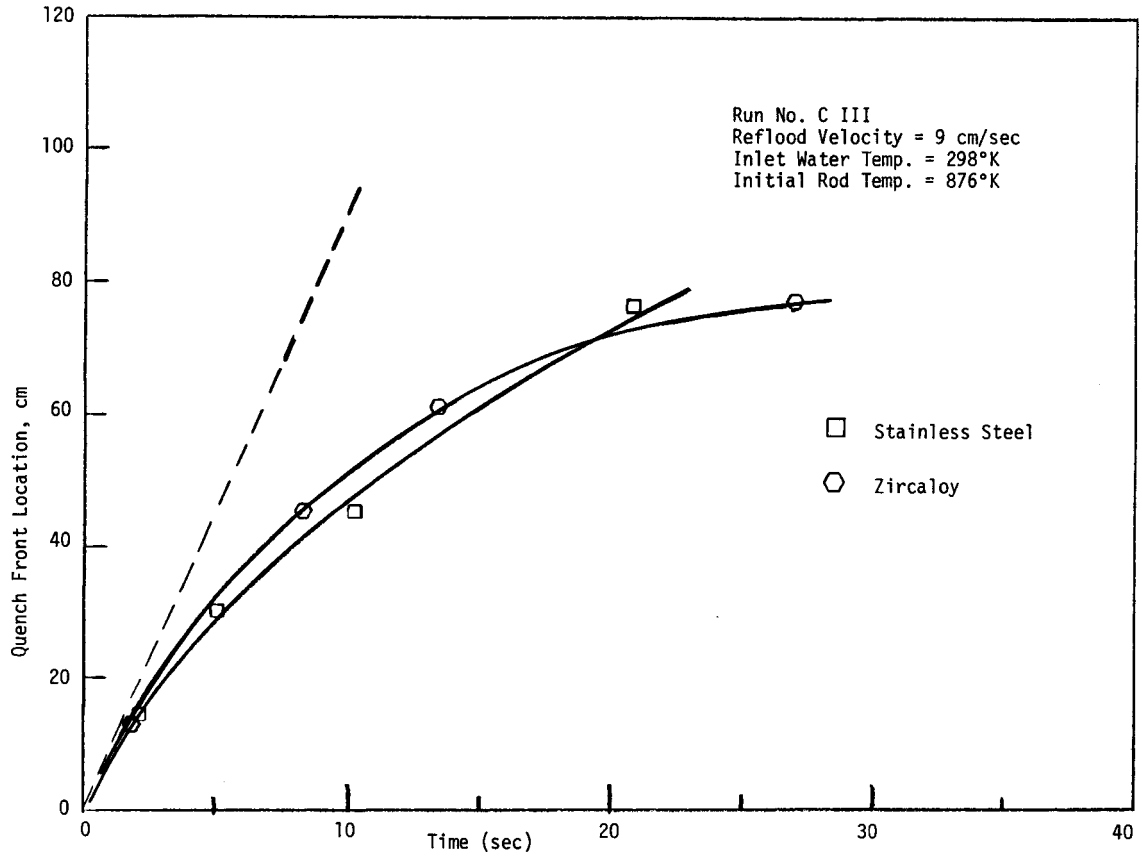

Figure B-10 Quench Front Location as a Function of Time

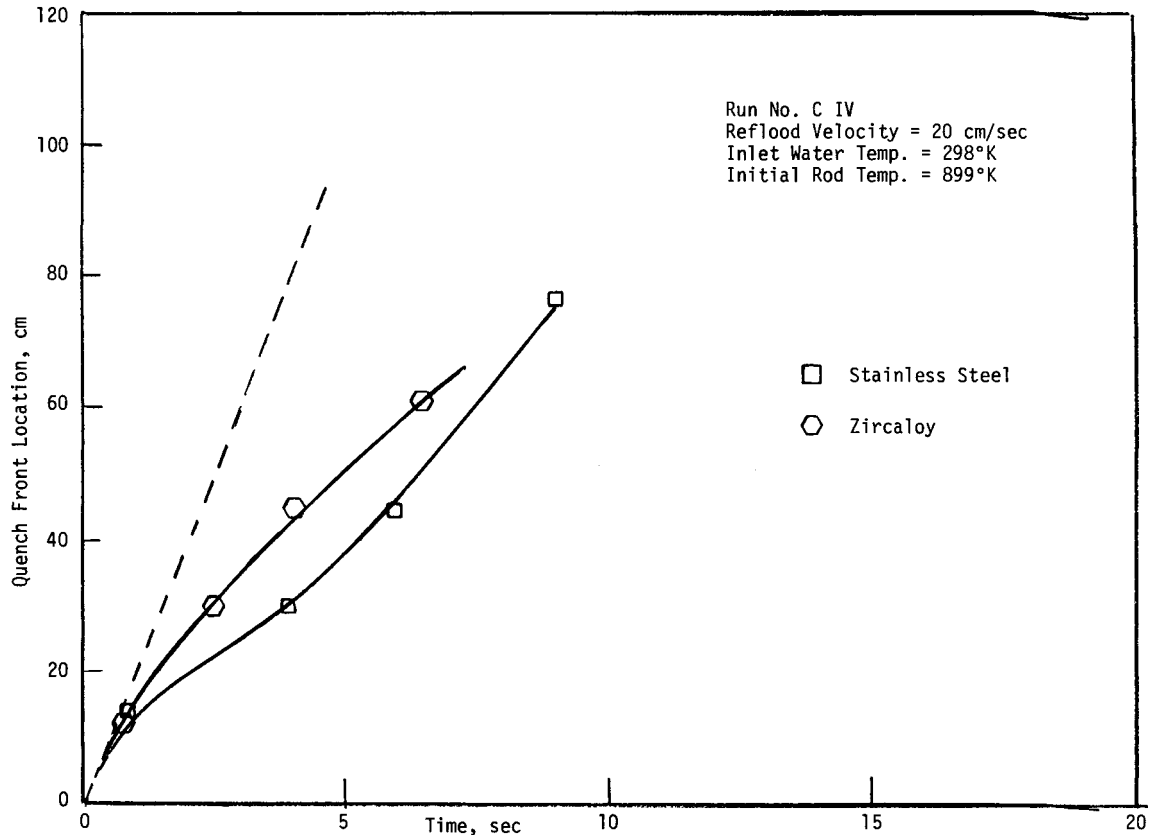

Figure B-11 Quench Front Location as a Function of Time

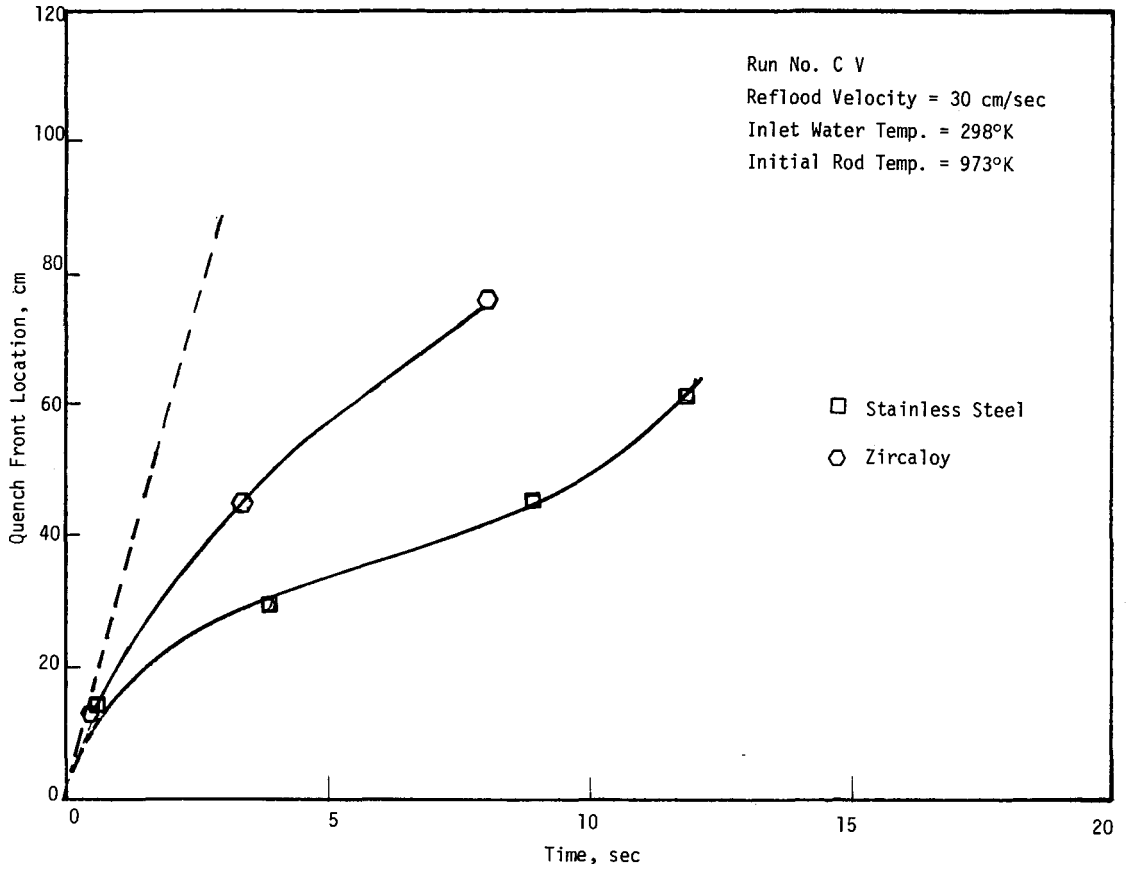

Figure B-12 Quench Front Location as a Function of Time

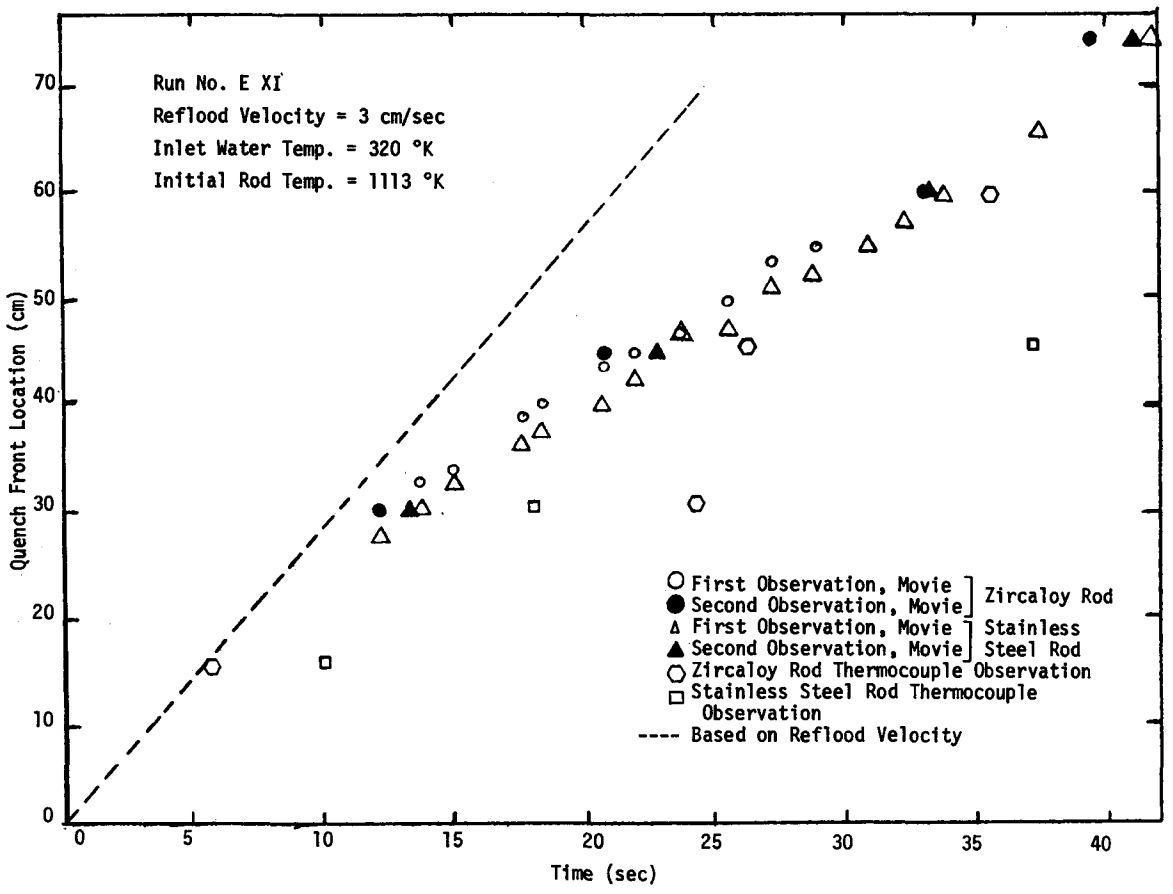

Figure B-13 Quench Front Location as a Function of Time

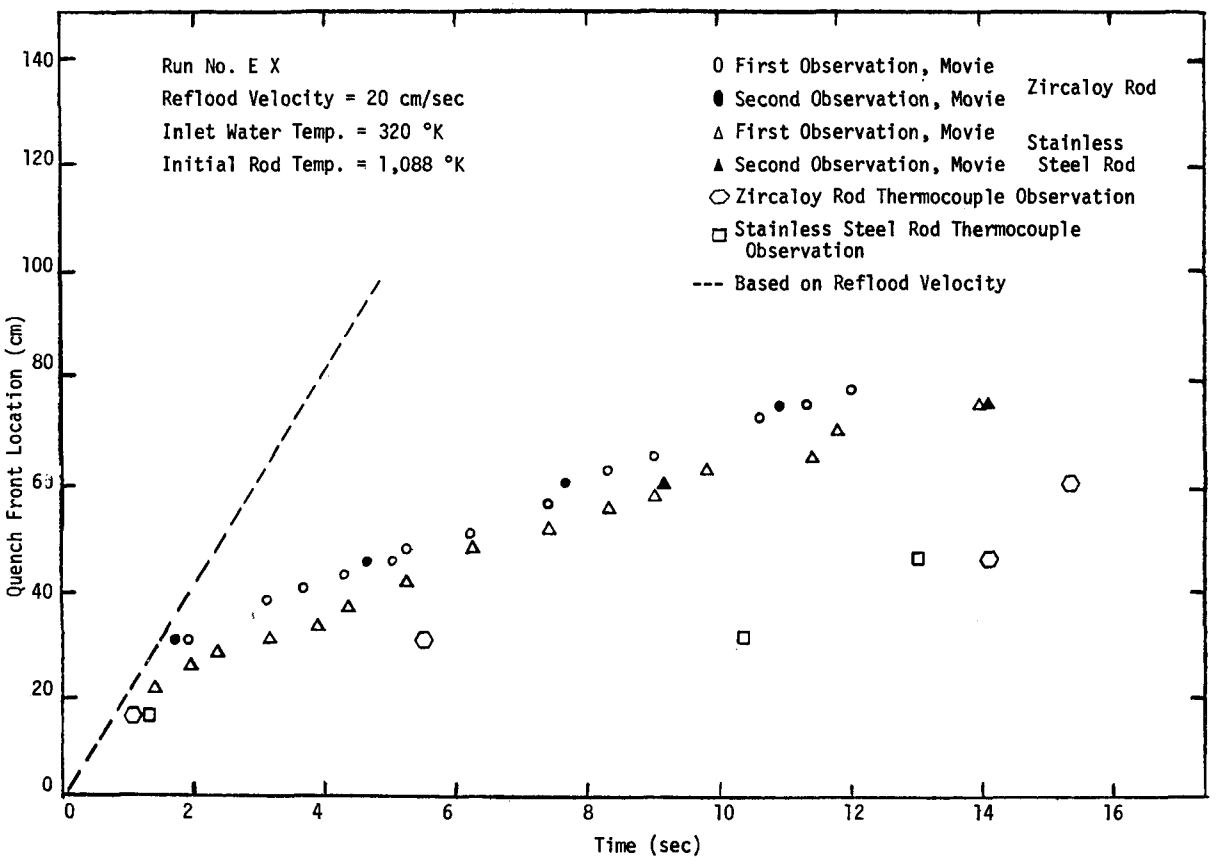

Figure B-14 Quench Front Location as a Function of Time

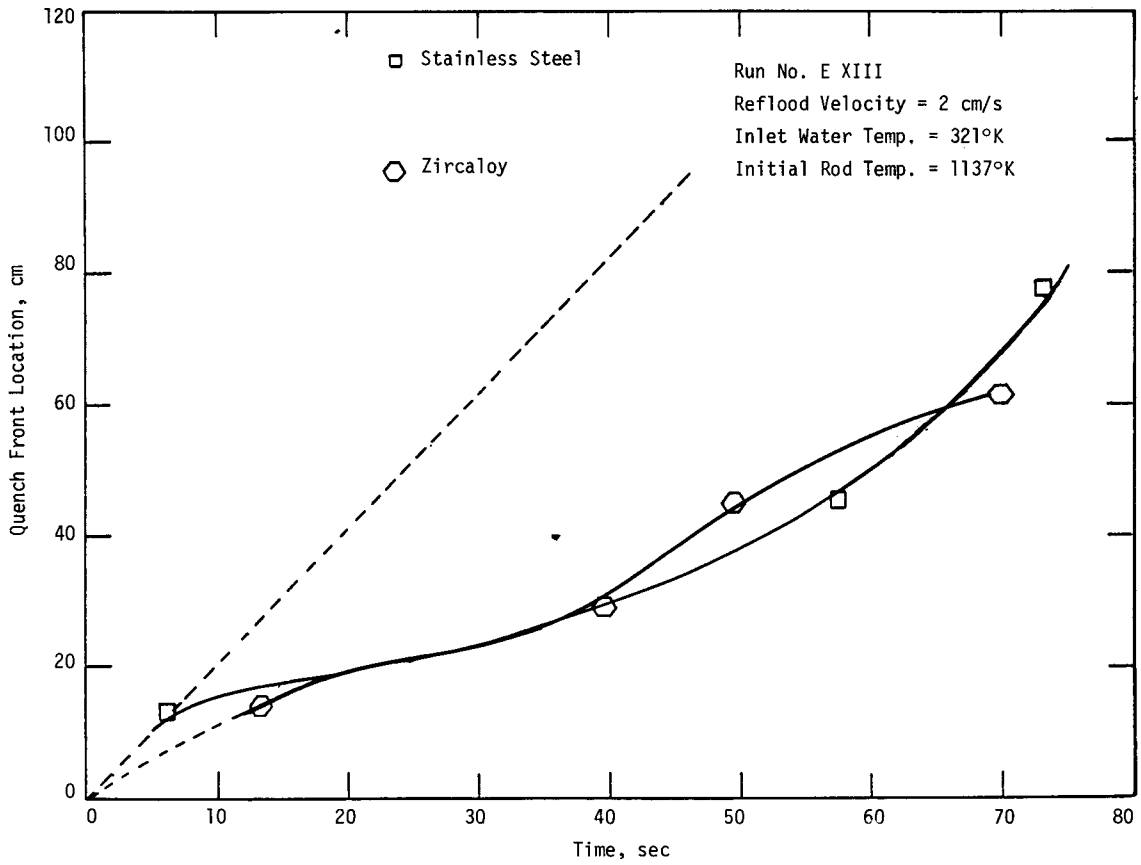

Figure B-15 Quench Front Location as a Function of Time

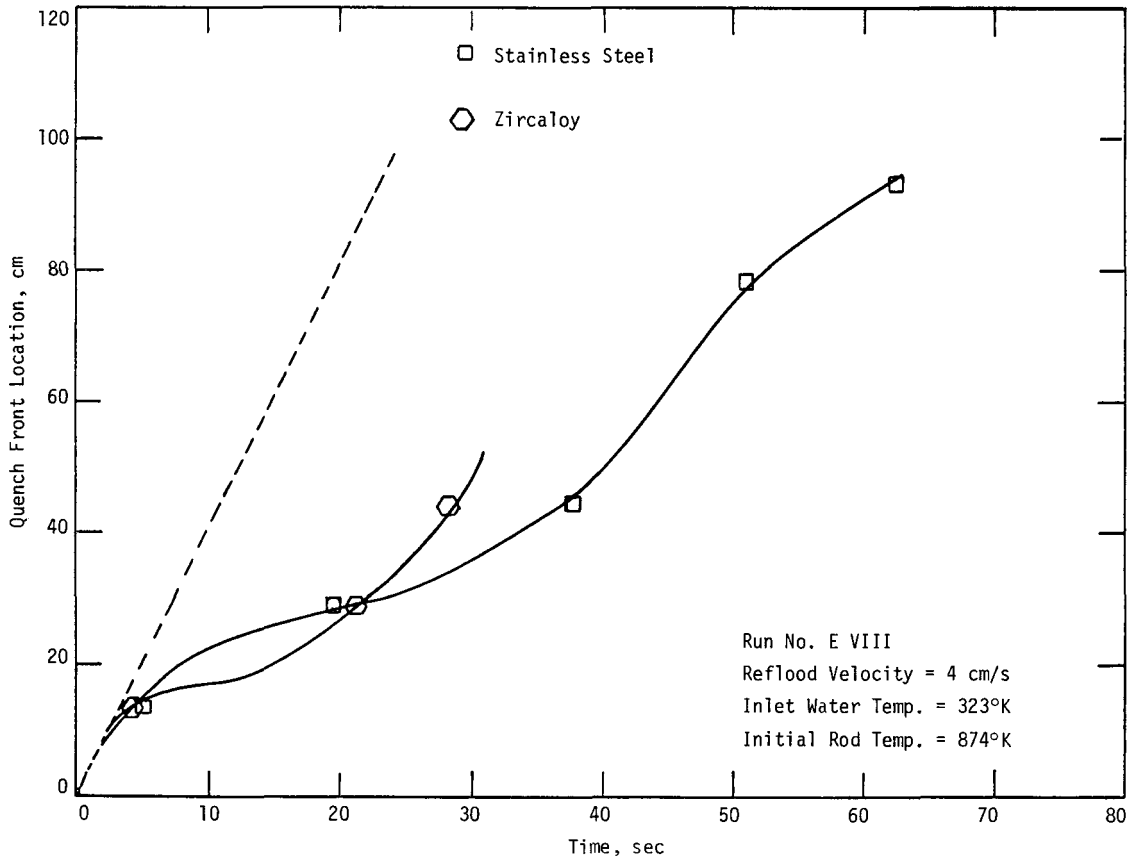

Figure B-16 Quench Front Location as a Function of Time

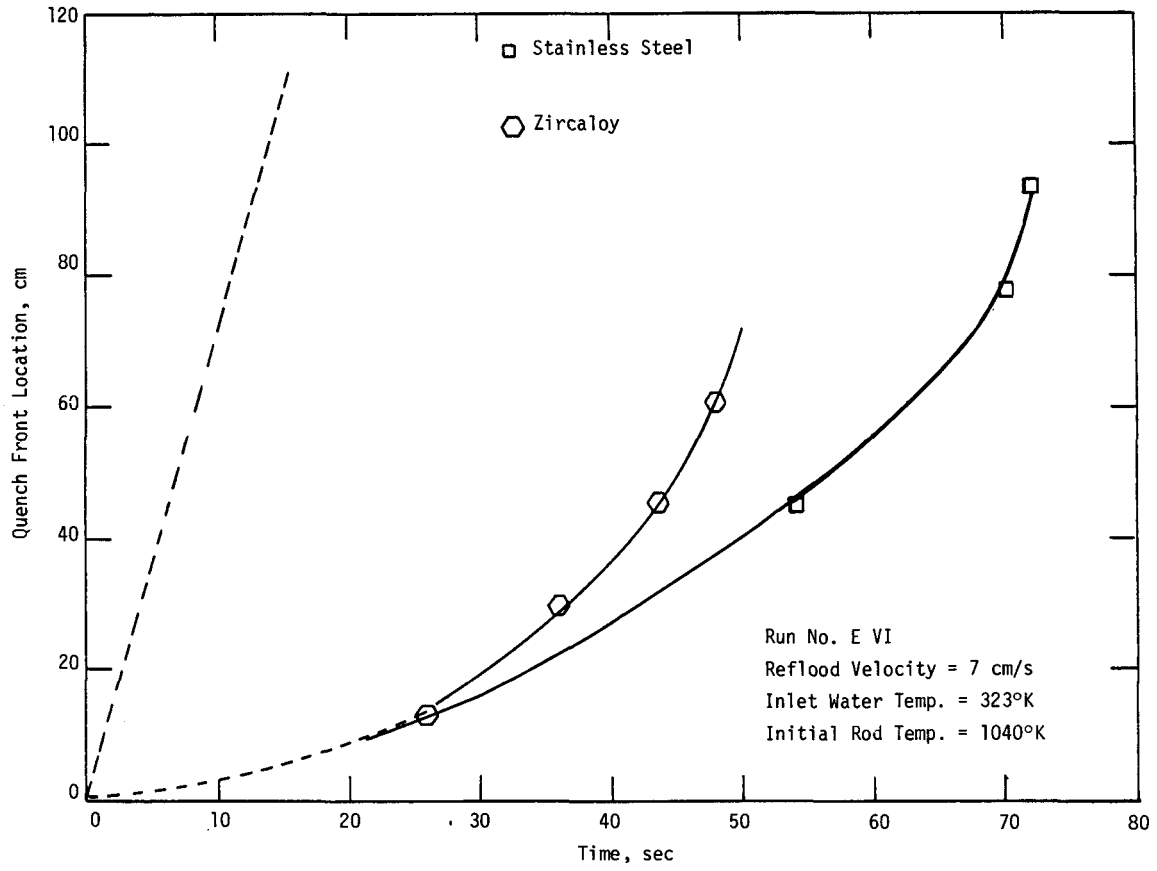

Figure B-17 Quench Front Location as a Function of Time

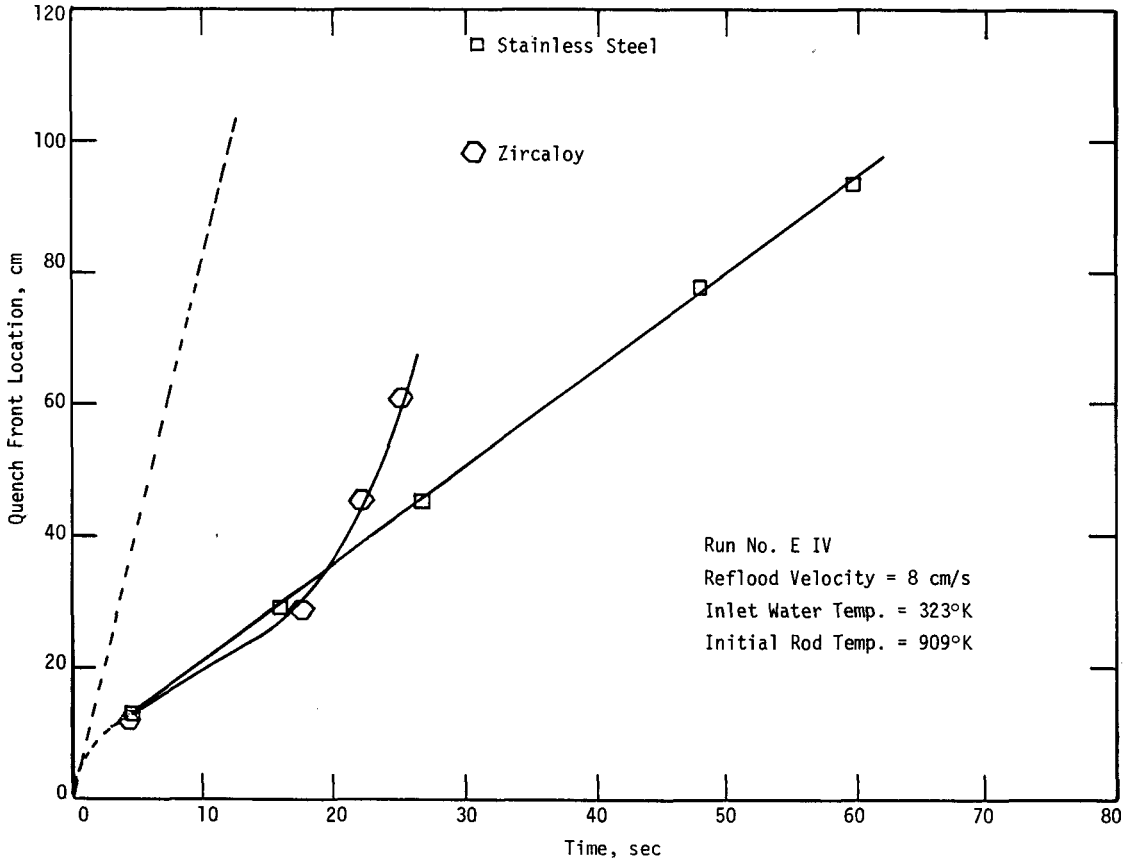

Figure B-18 Quench Front Location as a Function of Time

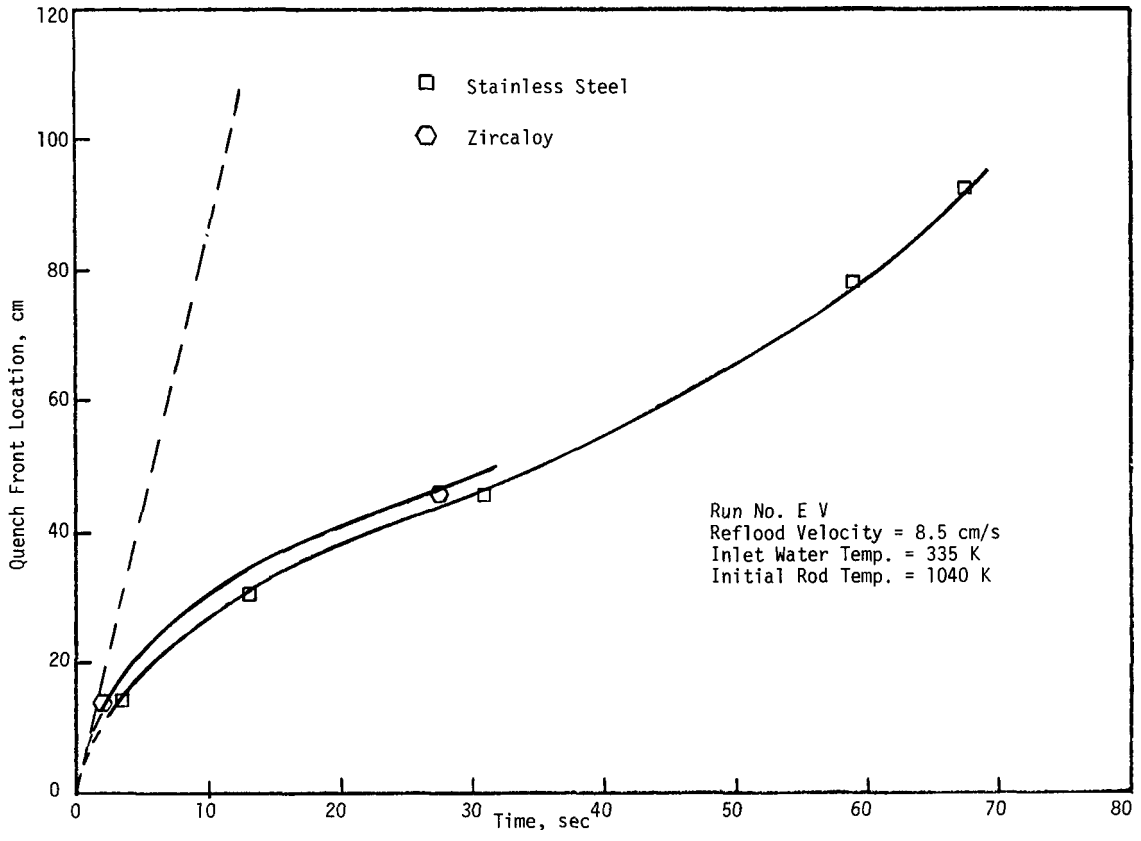

Figure B-19 Quench Front Location as a Function of Time

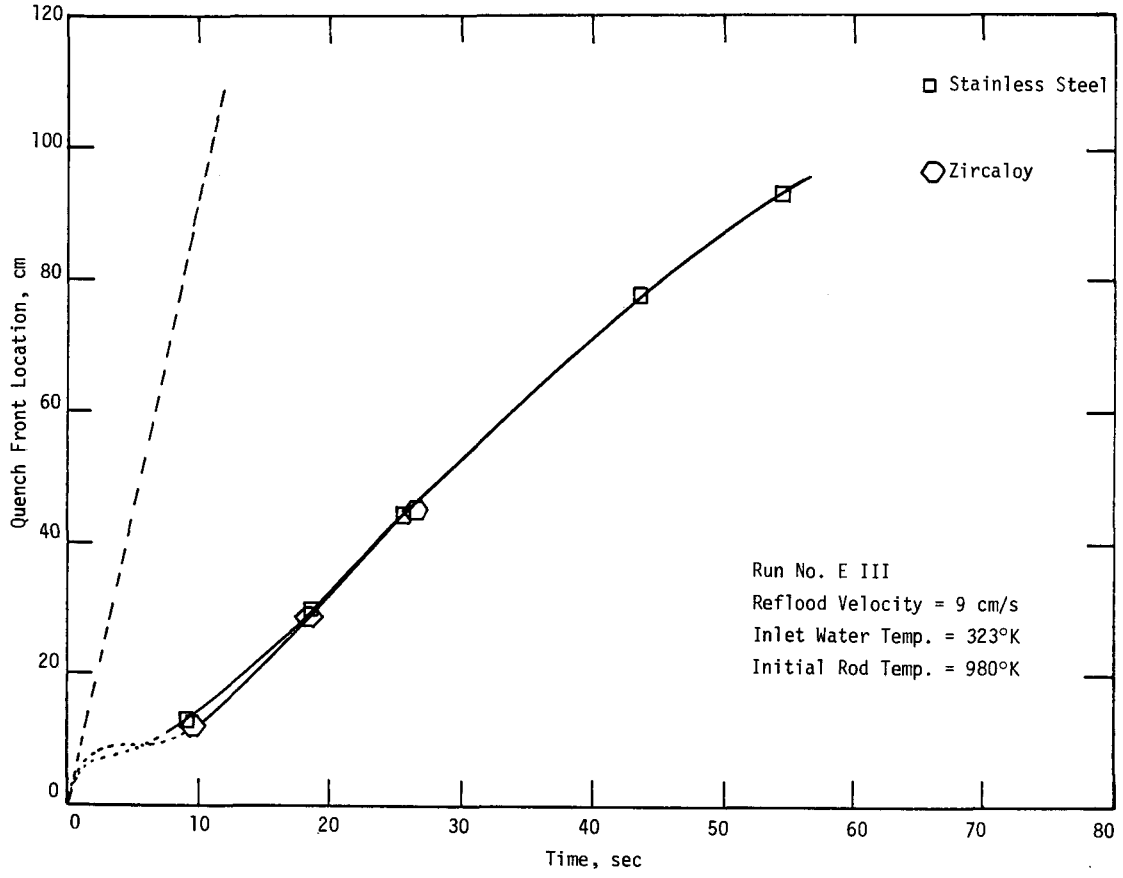

Figure B-20 Quench Front Location as a Function of Time

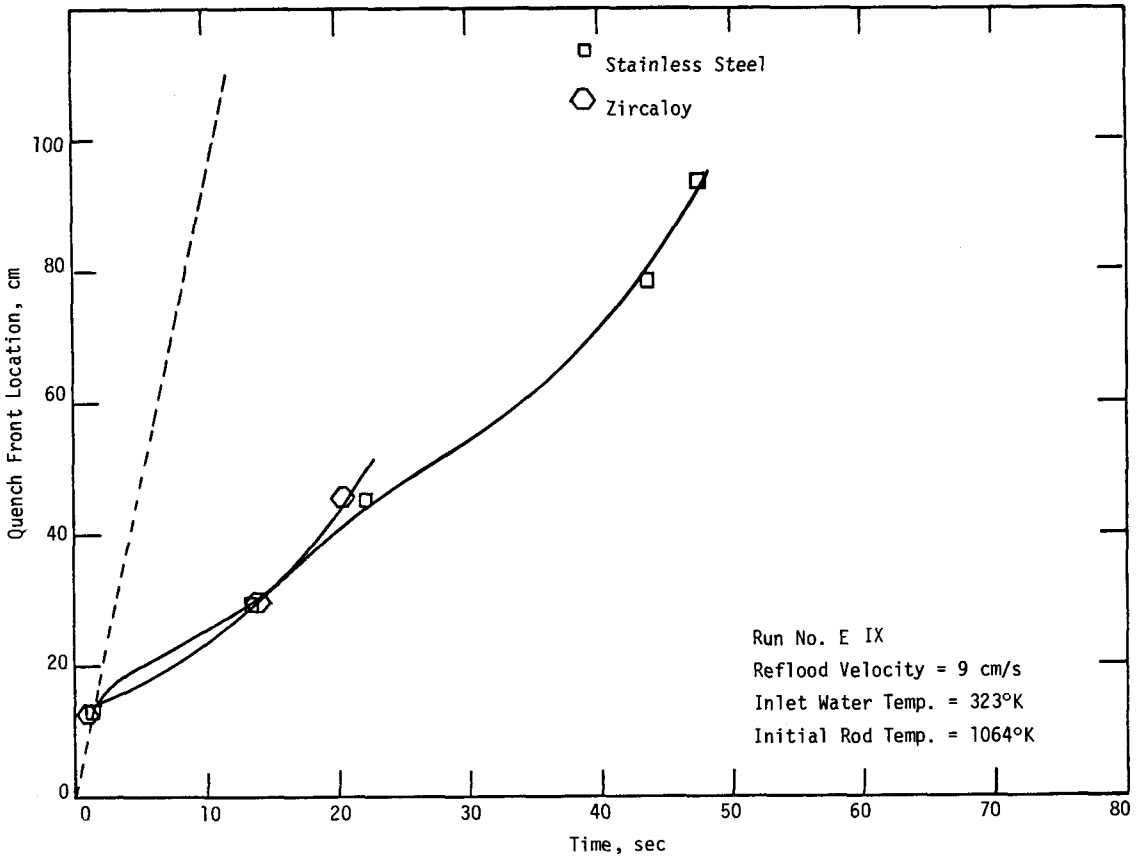

Figure B-21 Quench Front Location as a Function of Time

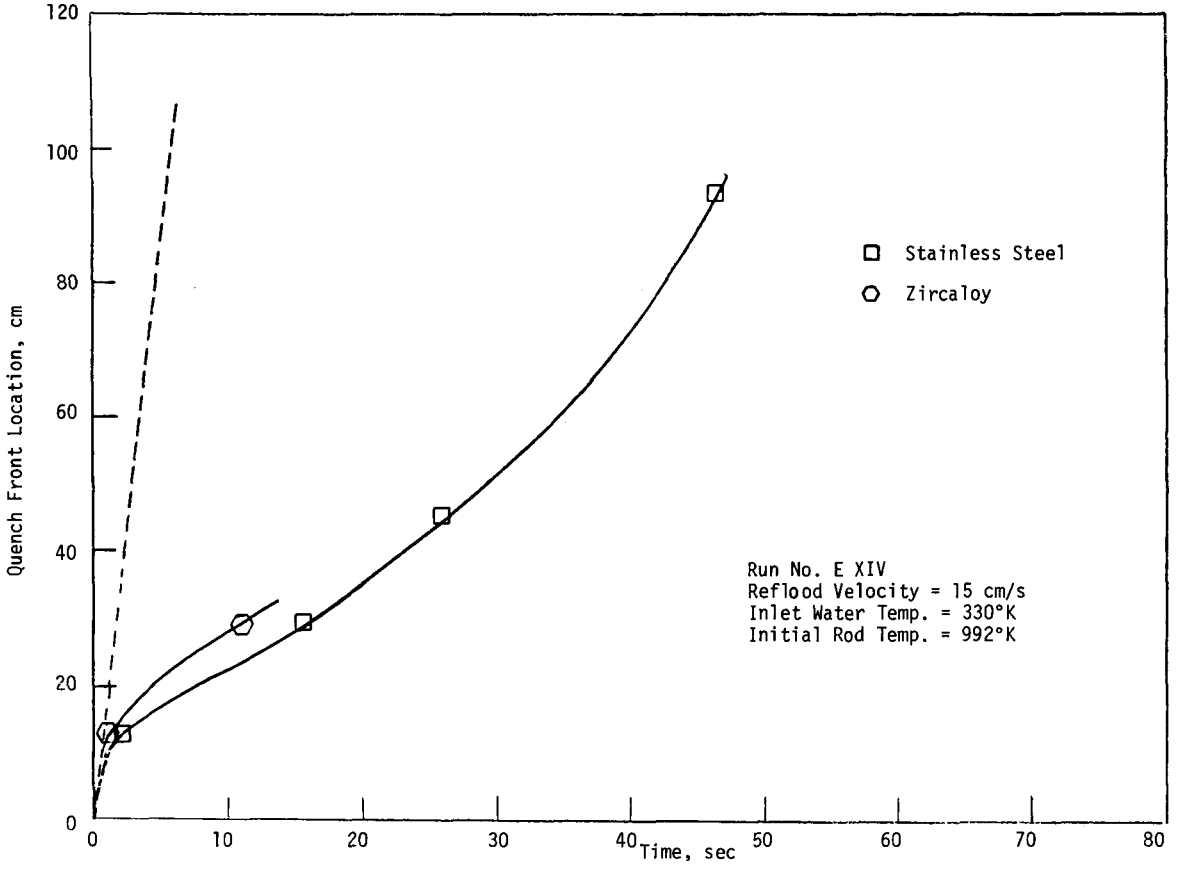

Figure B-22 Quench Front Location as a Function of Time

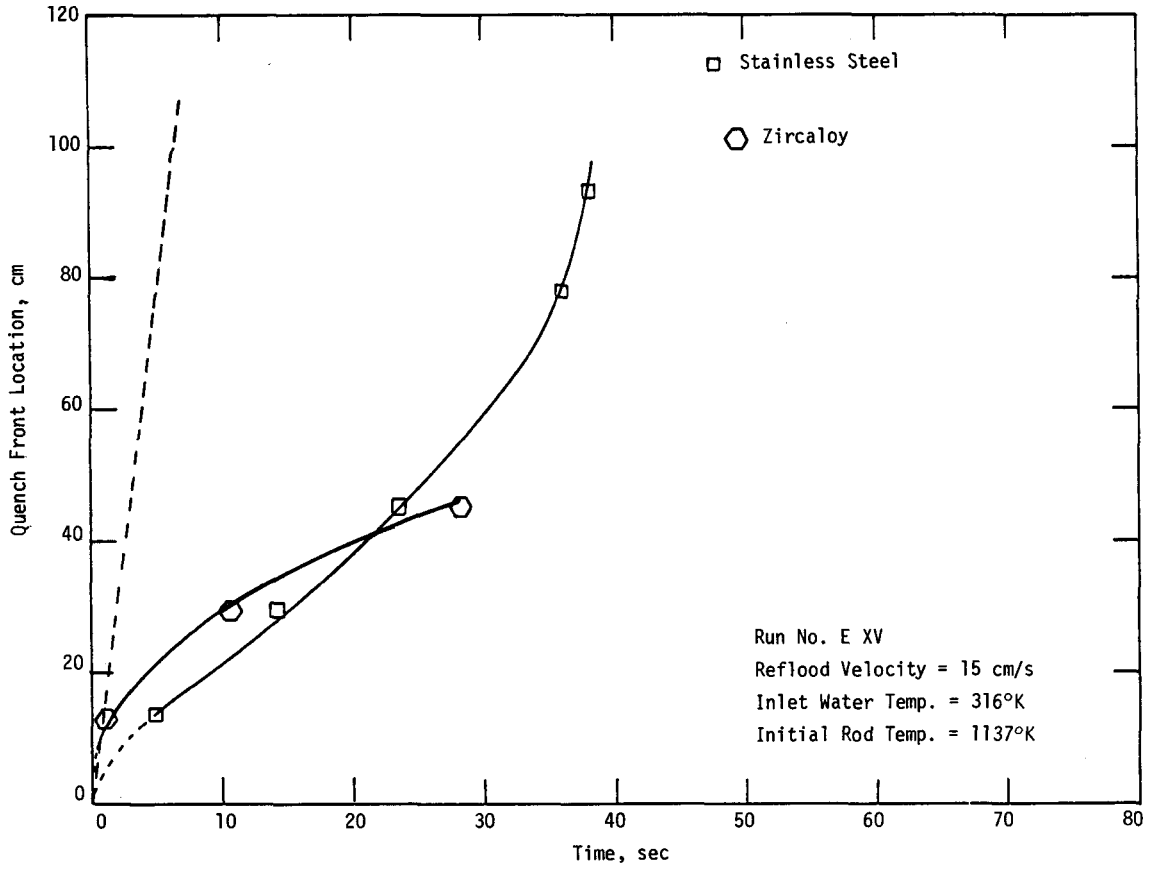

Figure B-23 Quench Front Location as a Function of Time

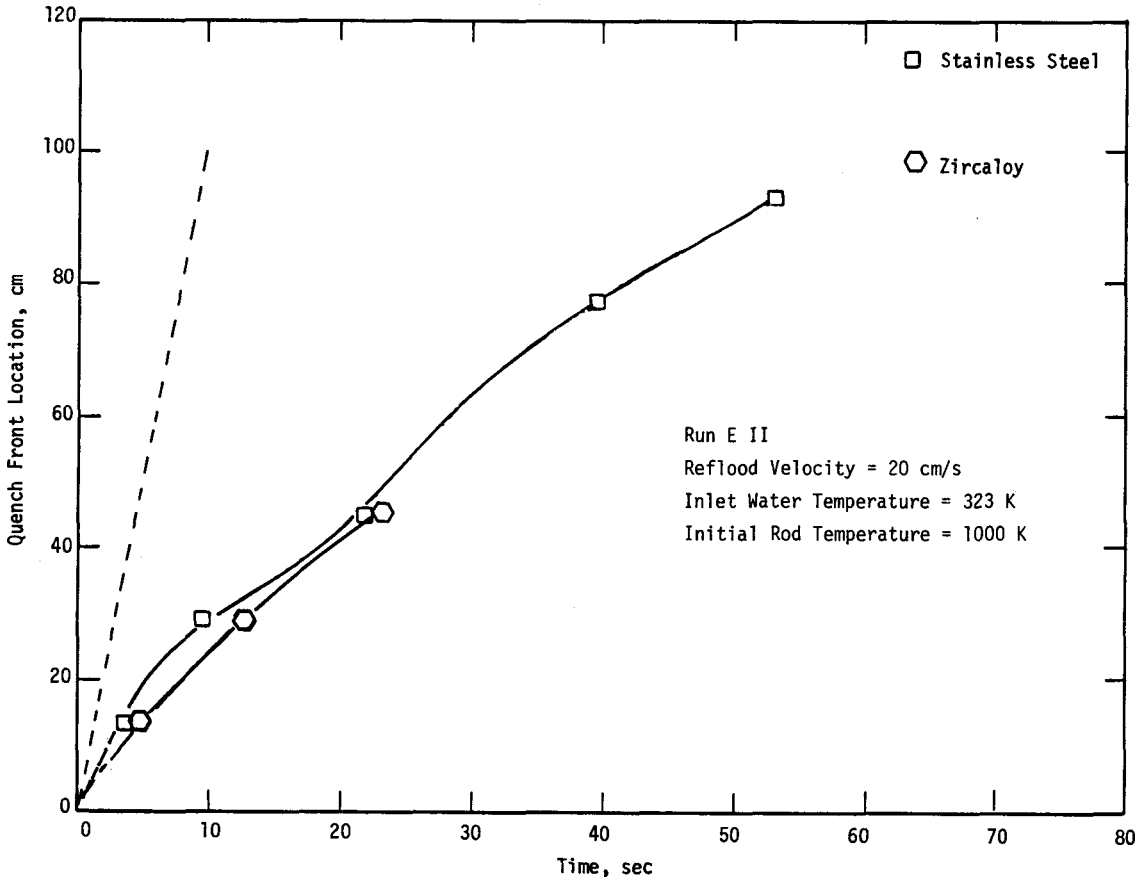

Figure B-24 Quench Front Location as a Function of Time

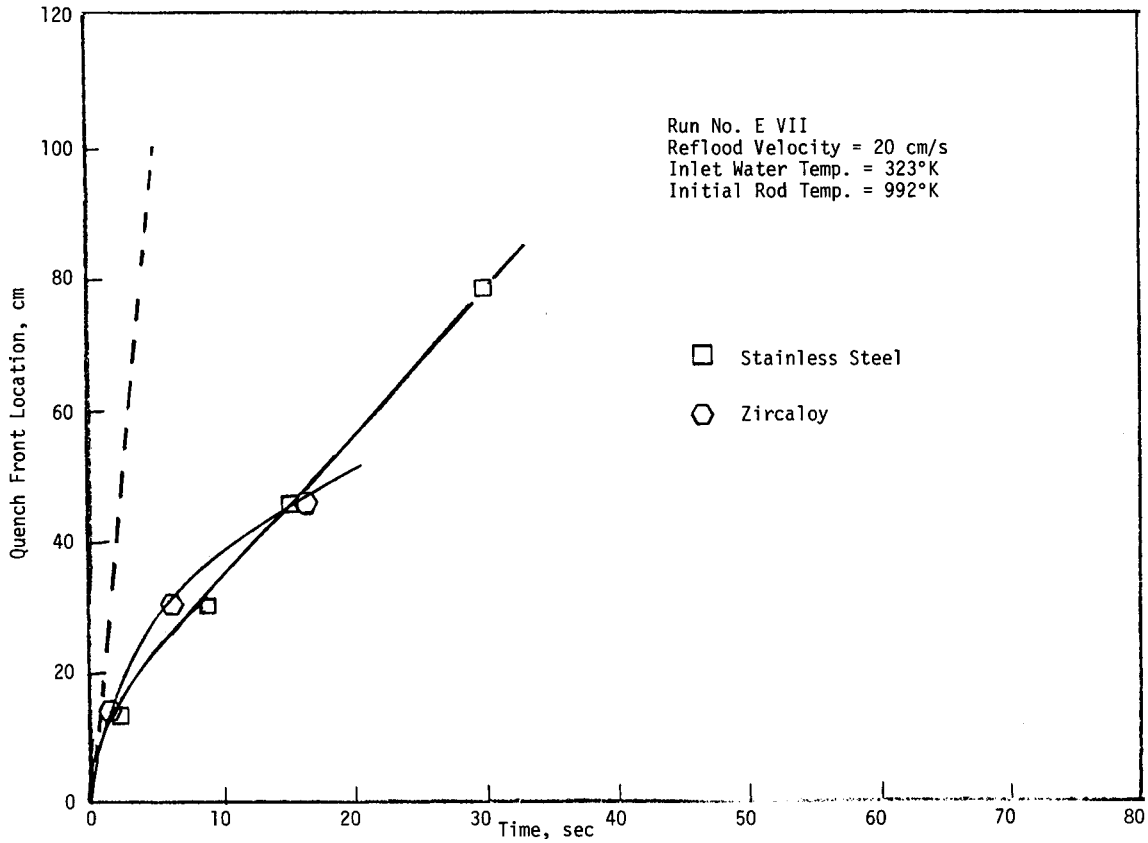

Figure B-25 Quench Front Location as a Function of Time

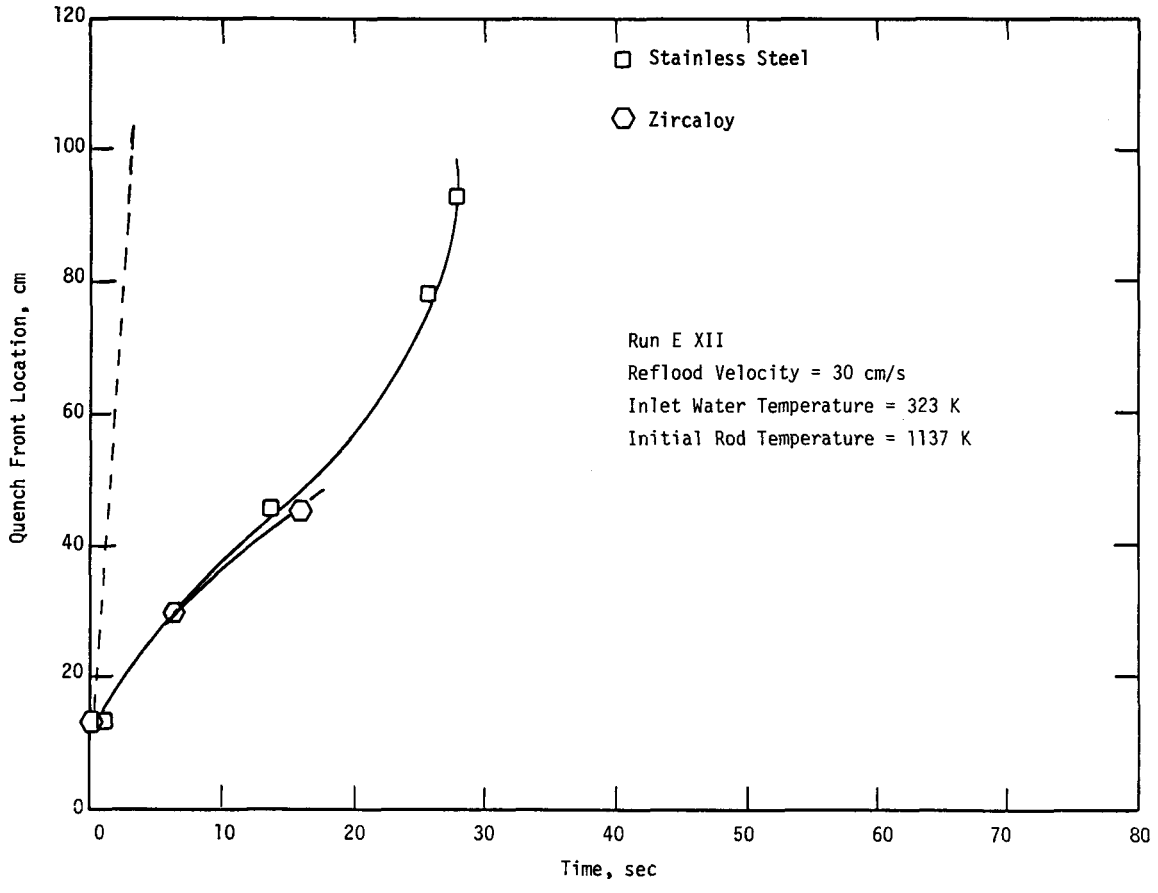

Figure B-26 Quench Front Location as a Function of Time

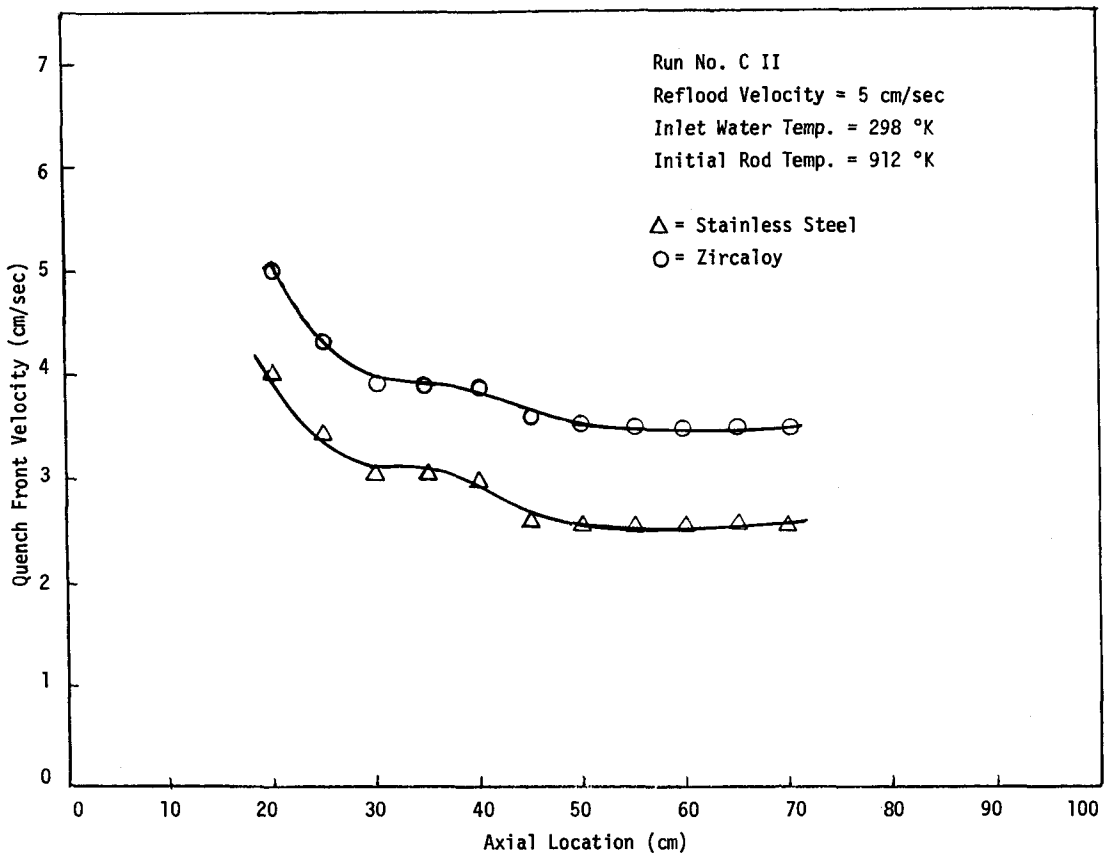

Figure B-27 Quench Front Velocity as a Function of Height

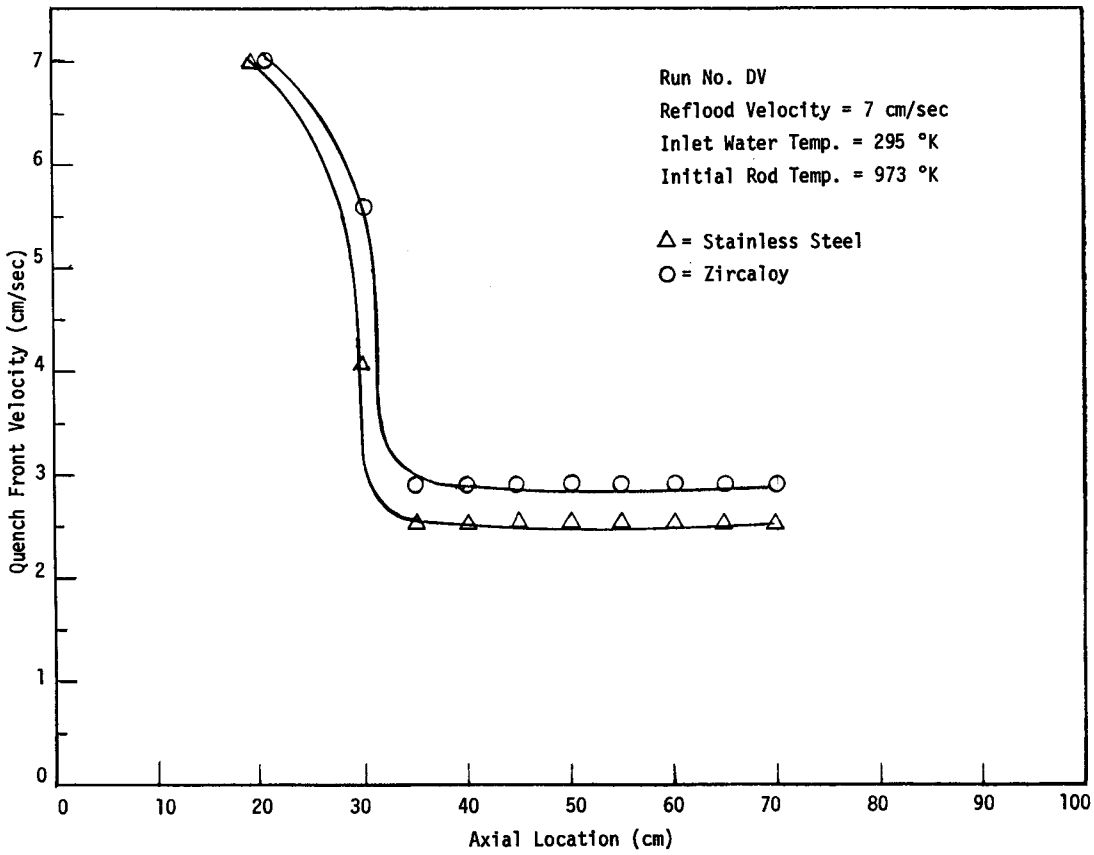

Figure B-28 Quench Front Velocity as a Function of Height

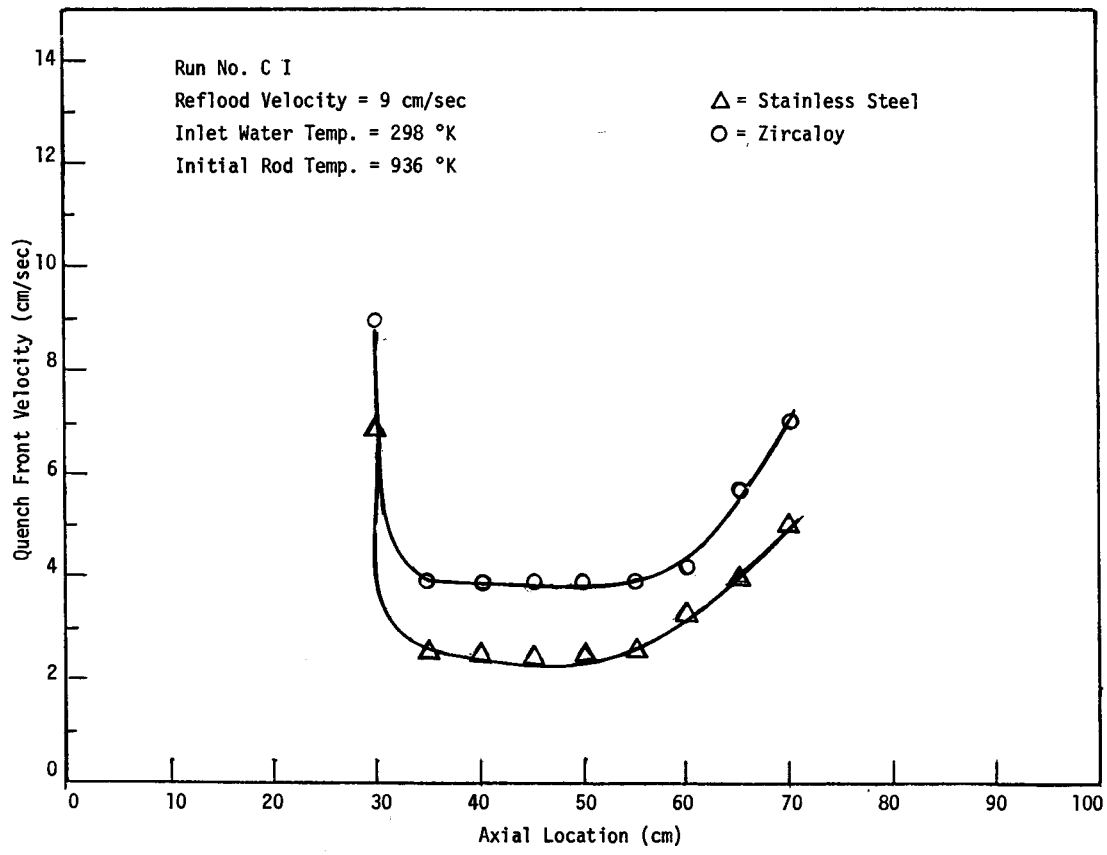

Figure B-29 Quench Front Velocity as a Function of Height

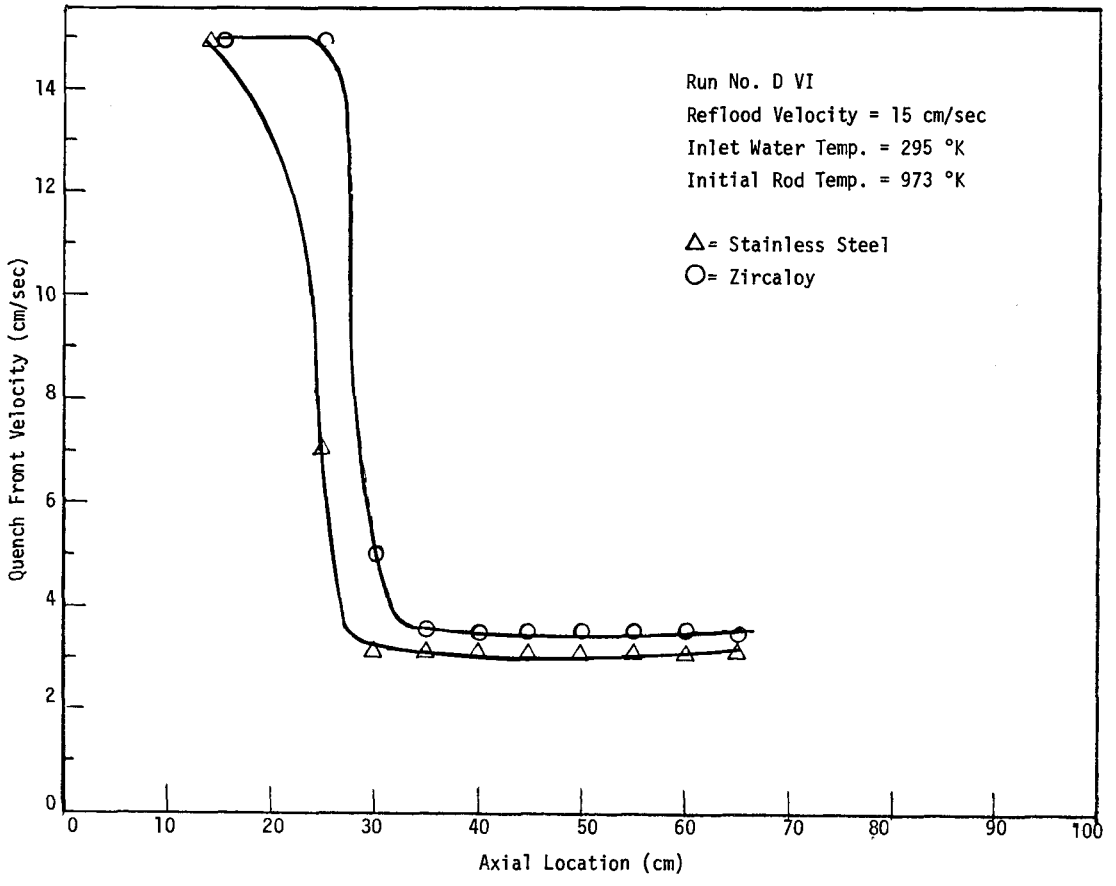

Figure B-30 Quench Front Velocity as a Function of Height

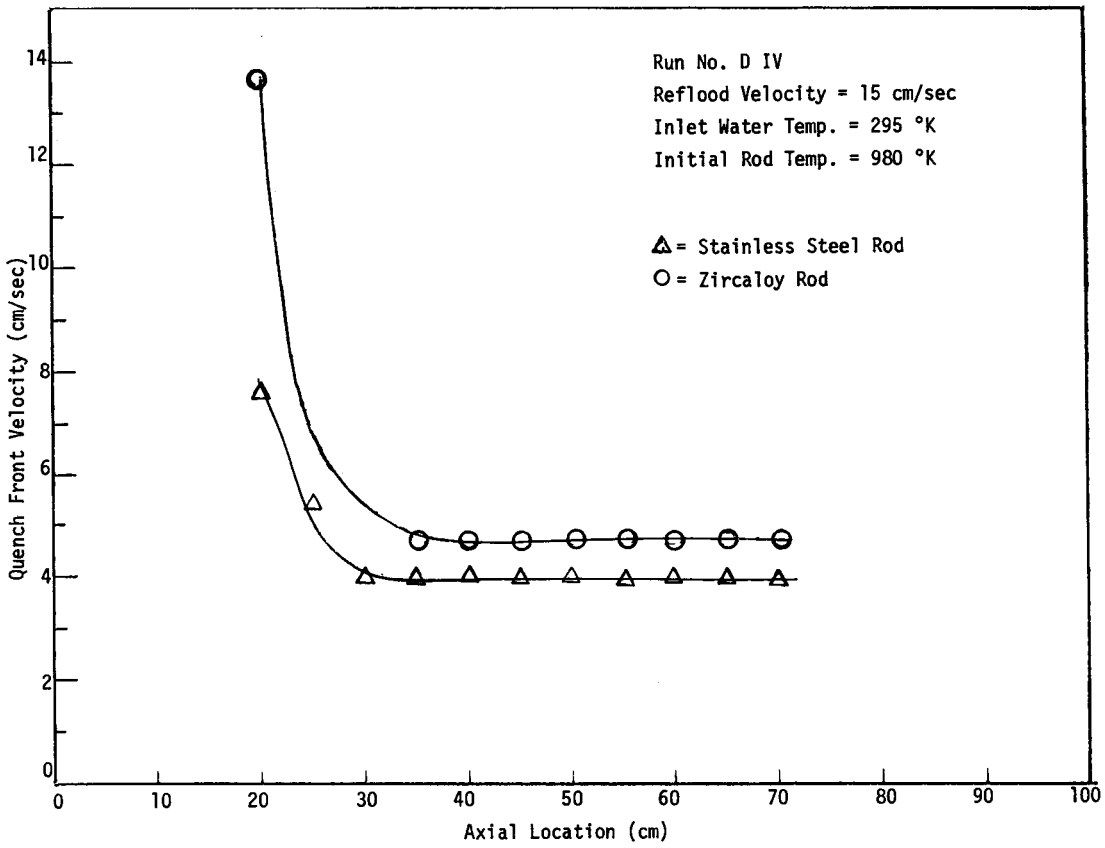

Figure B-31 Quench Front Velocity as a Function of Height

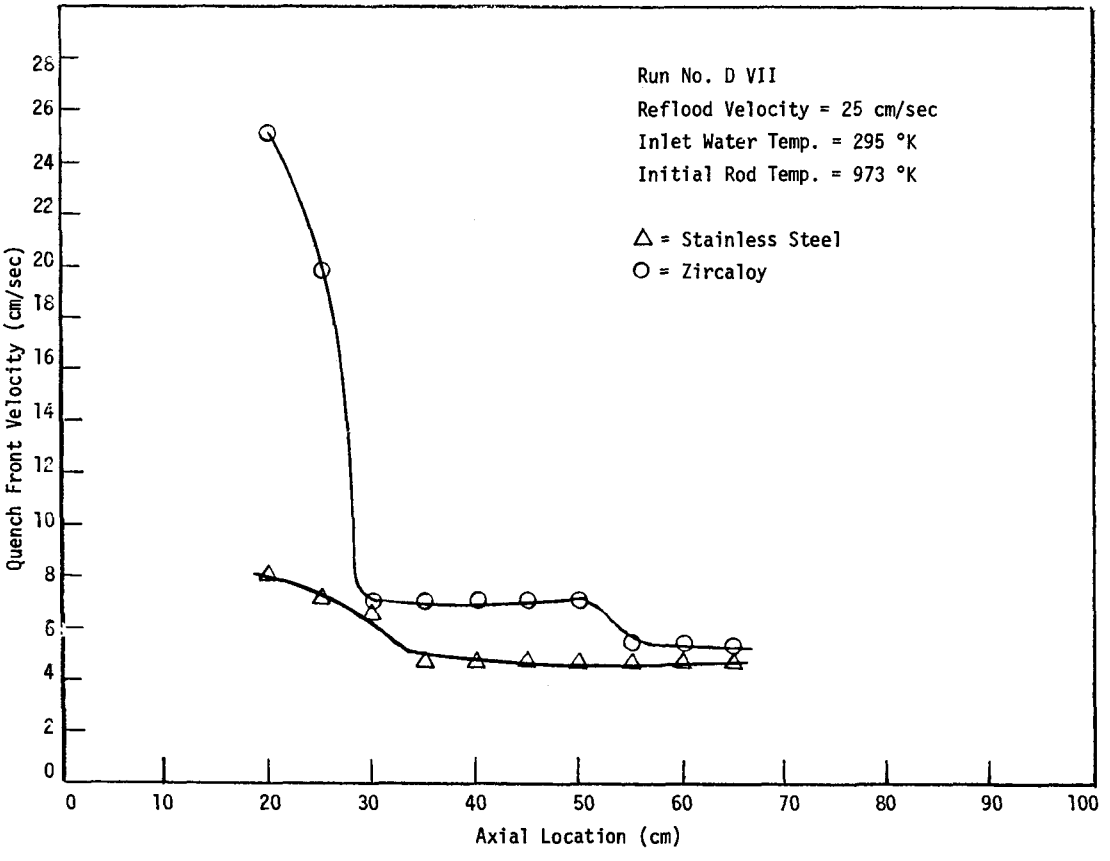

Figure B-32 Quench Front Velocity as a Function of Height

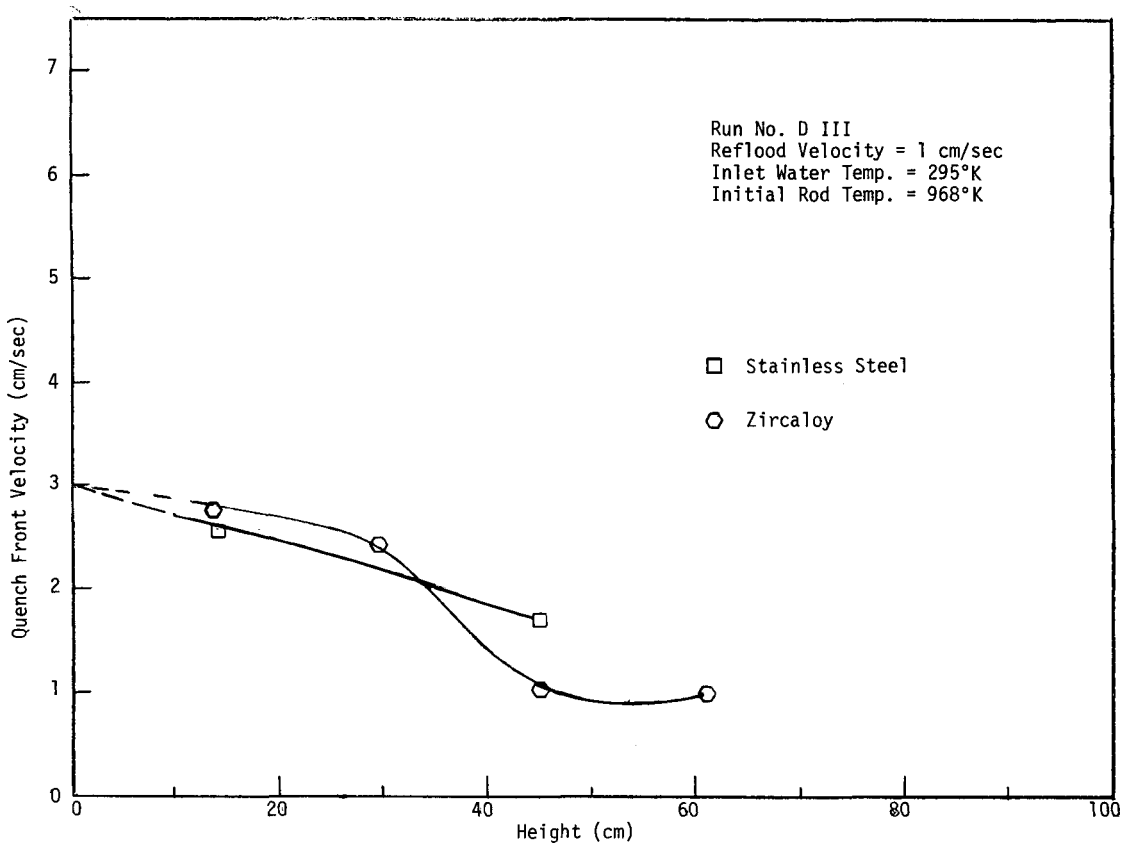

Figure B-33 Quench Front Velocity as a Function of Height

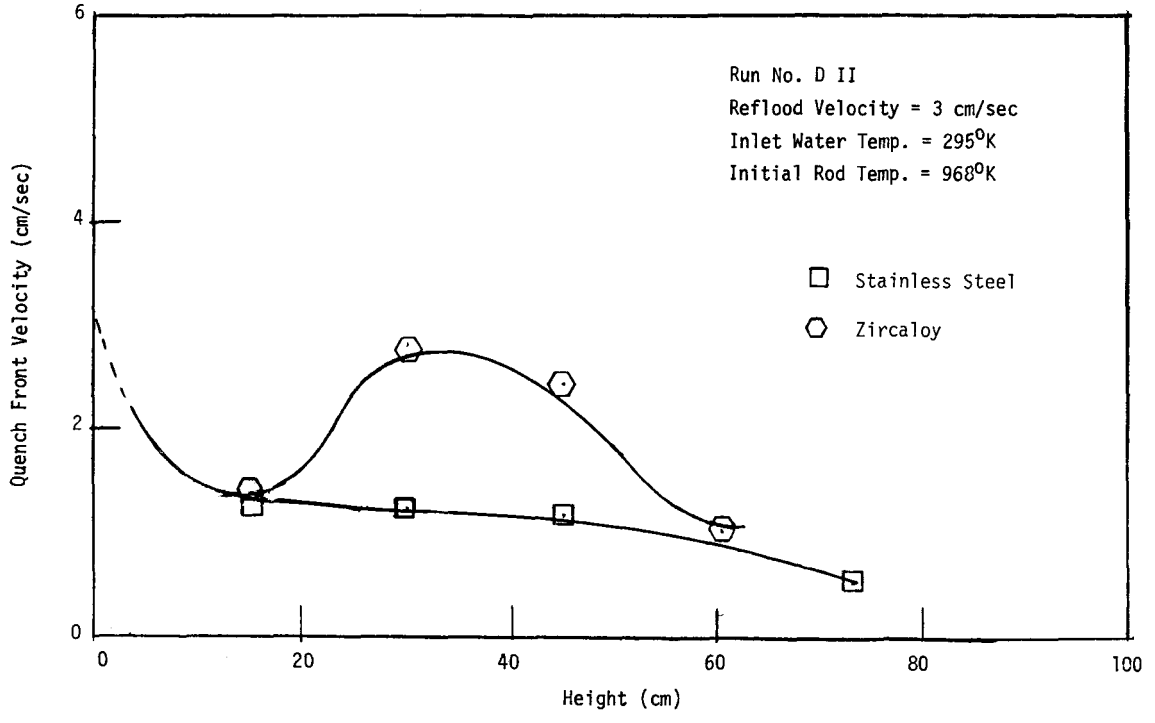

Figure B-34 Quench Front Velocity as a Function of Height

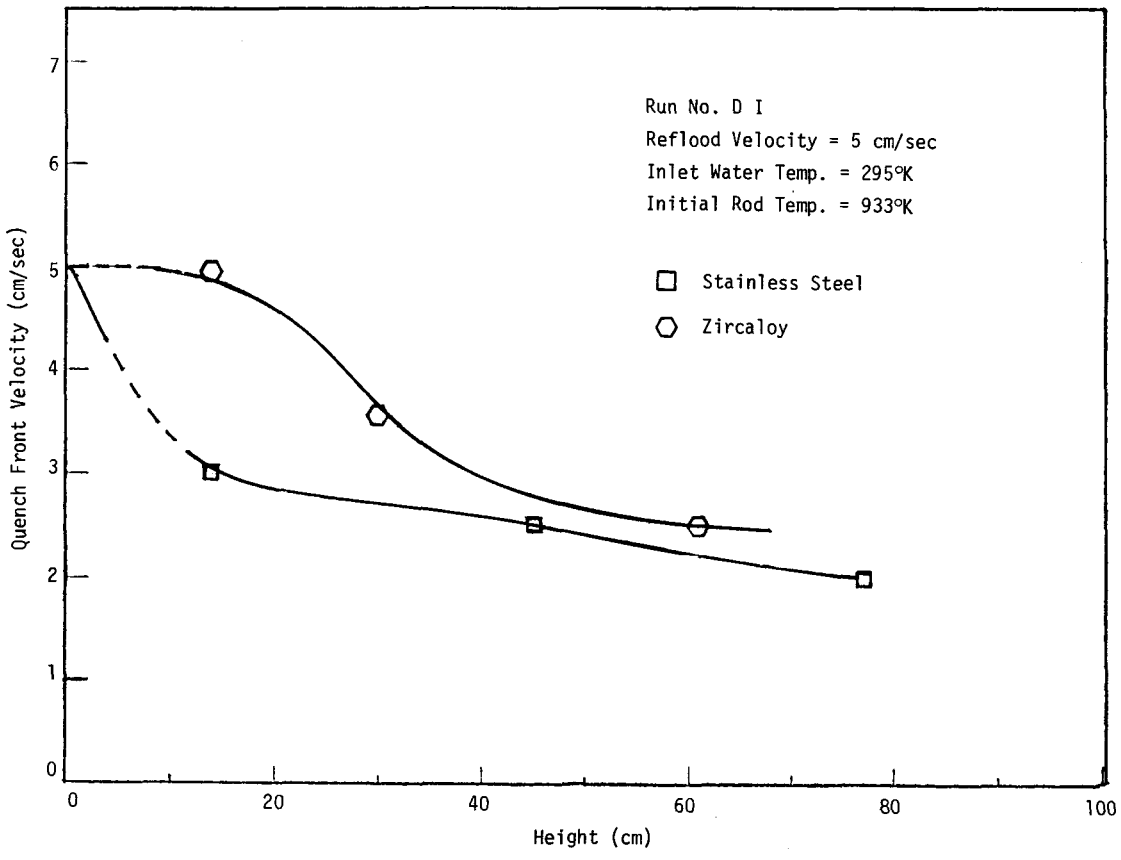

Figure B-35 Quench Front Velocity as a Function of Height

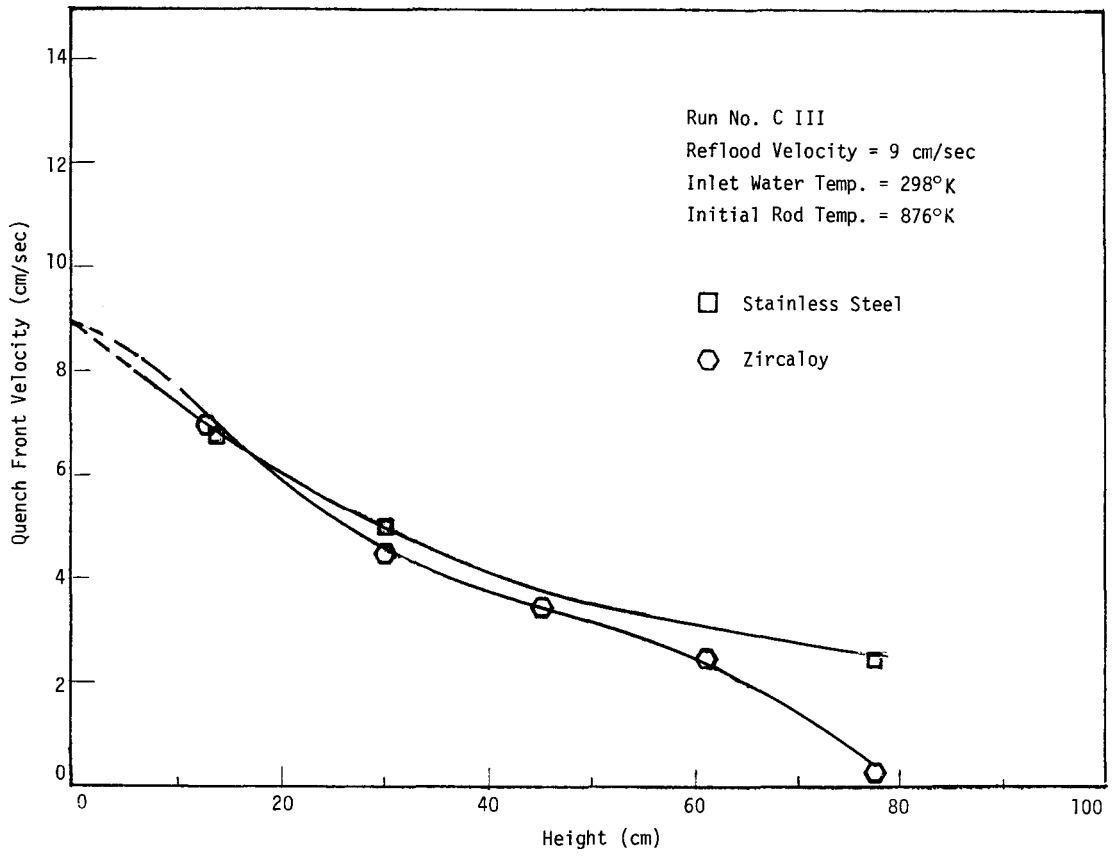

Figure B-36 Quench Front Velocity as a Function of Height

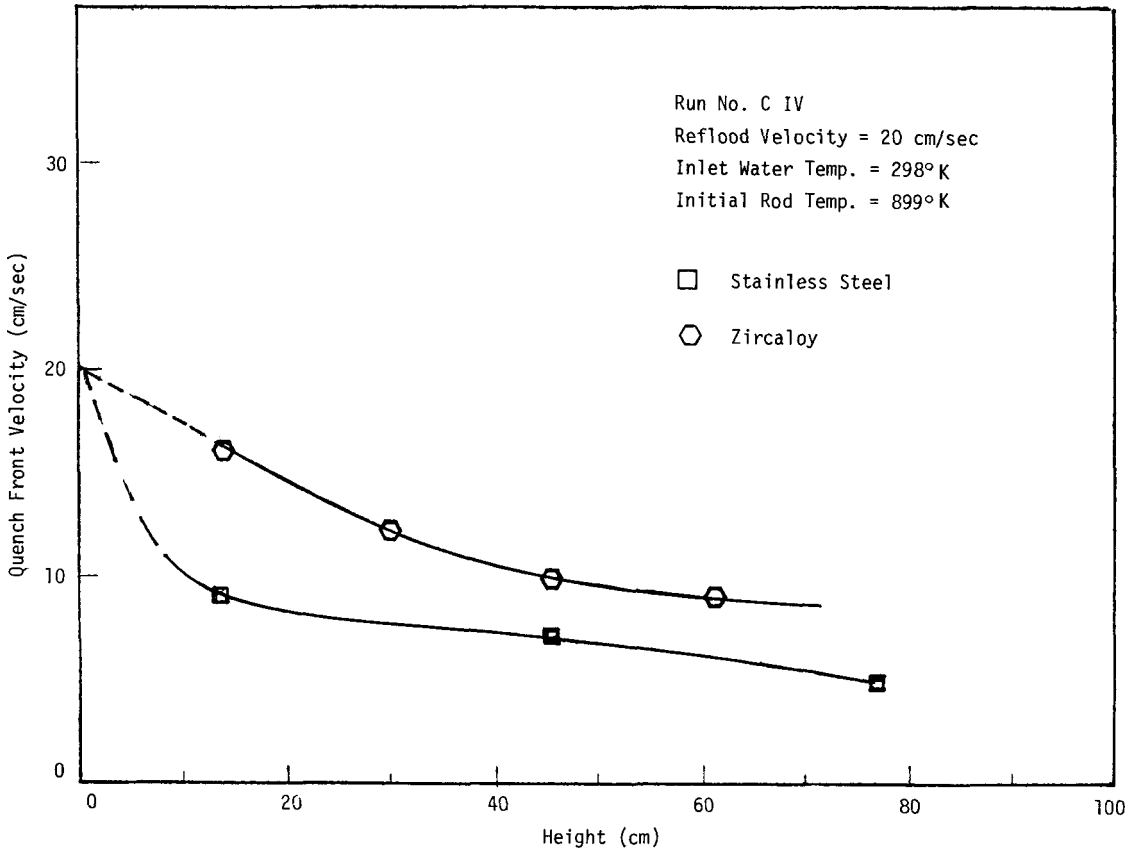

Figure B-37 Quench Front Velocity as a Function of Height

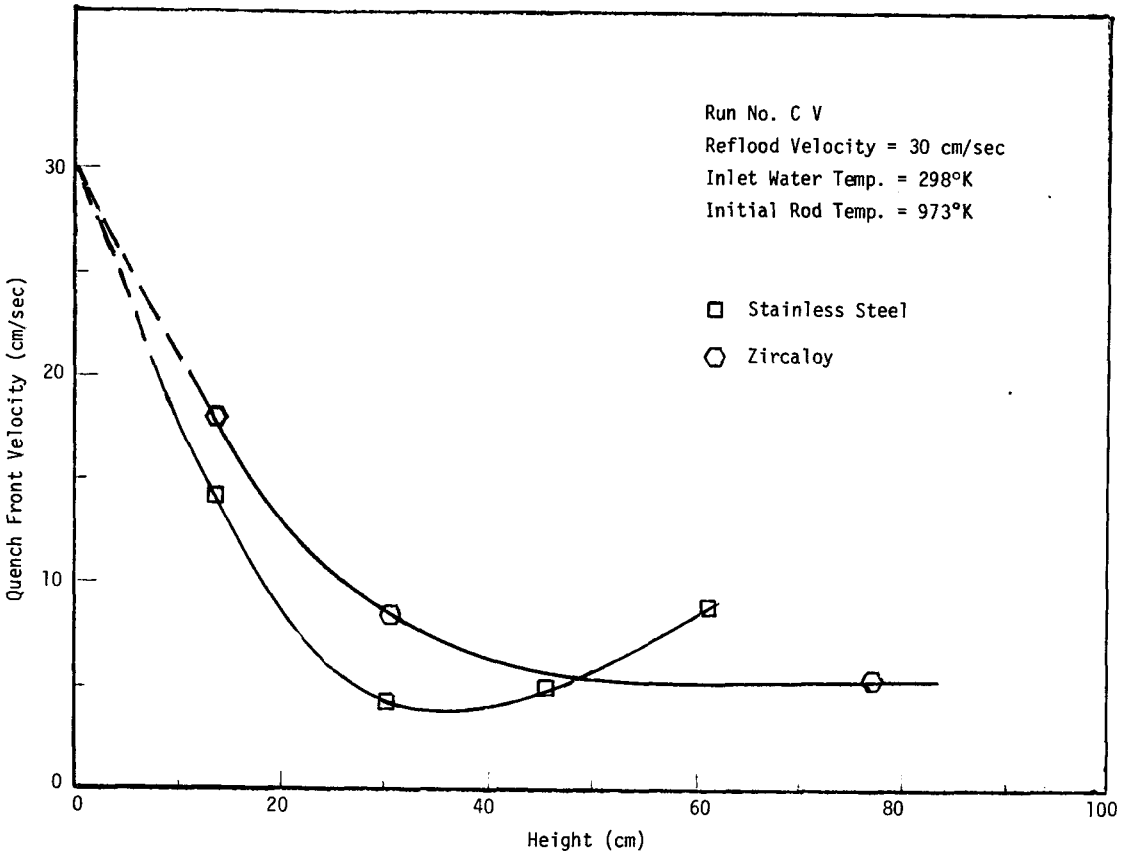

Figure B-38 Quench Front Velocity as a Function of Height

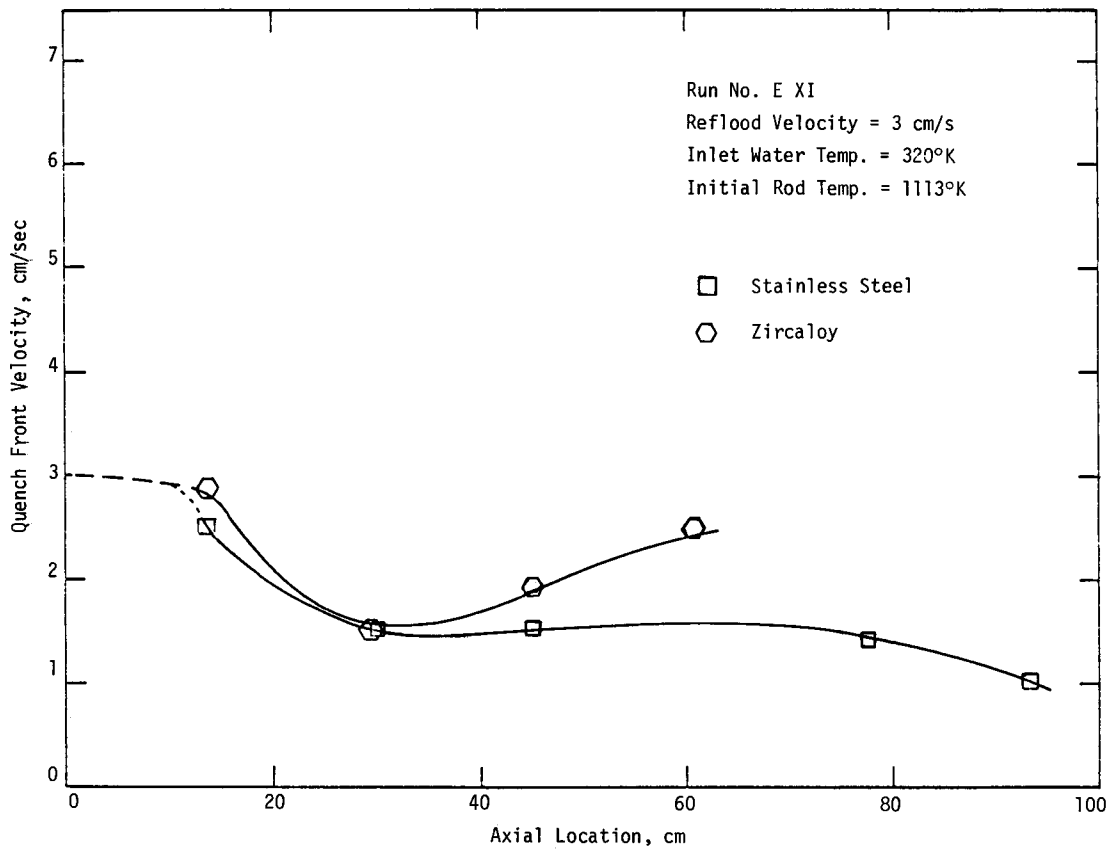

Figure B-39 Quench Front Velocity as a Function of Axial Location

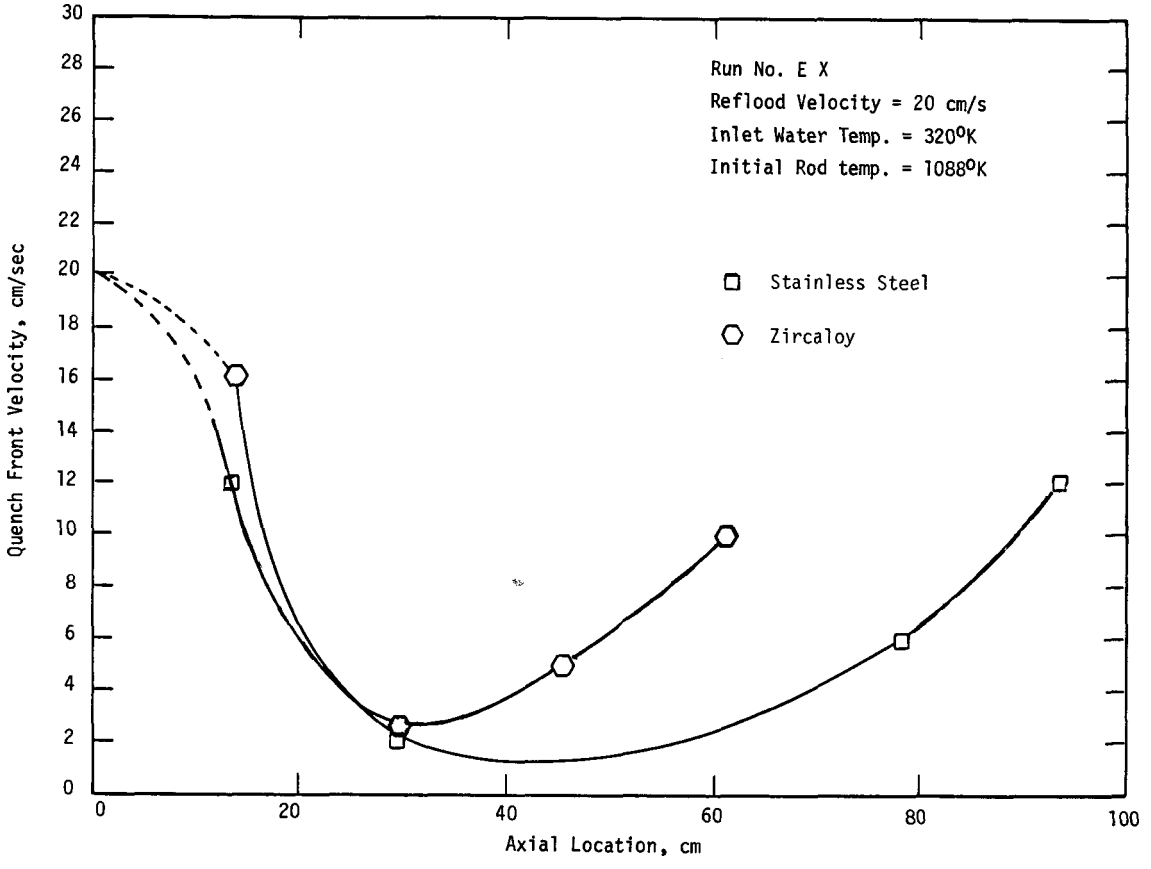

Figure B-40 Quench Front Velocity as a Function of Axial Location

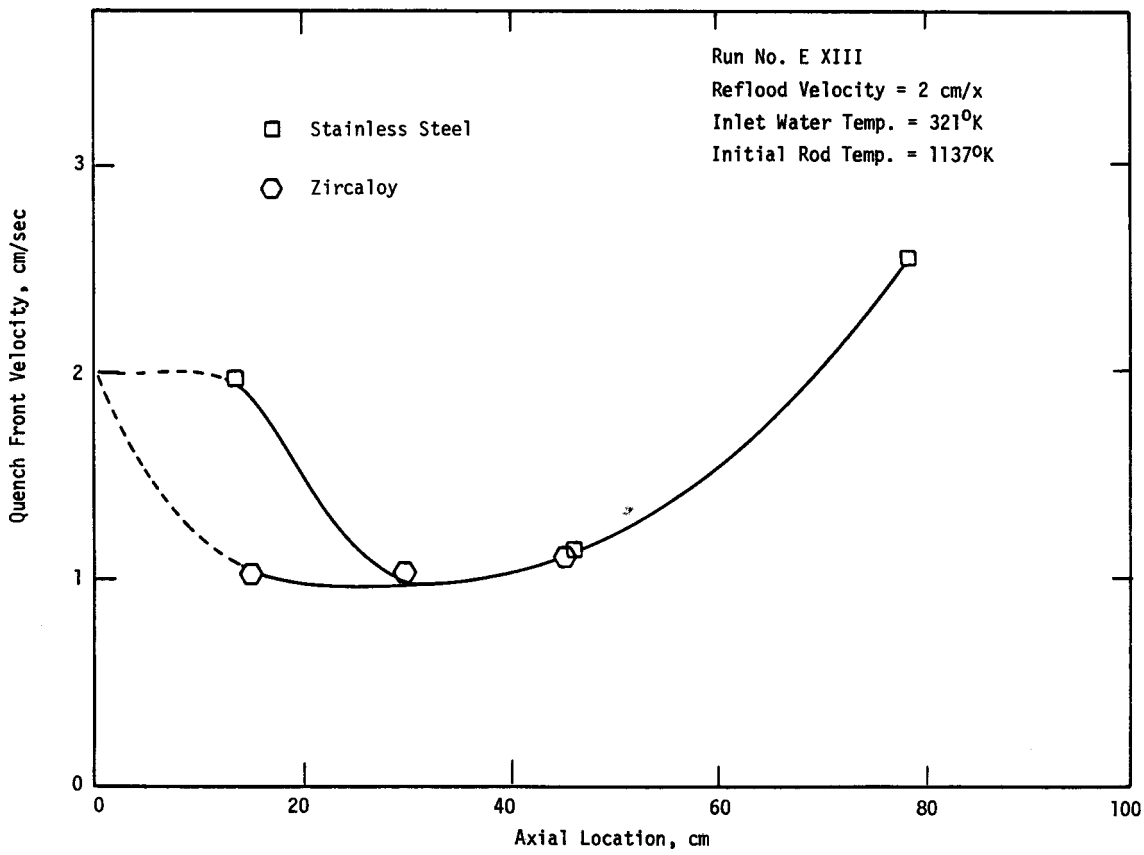

Figure B-41 Quench Front Velocity as a Function of Axial Location

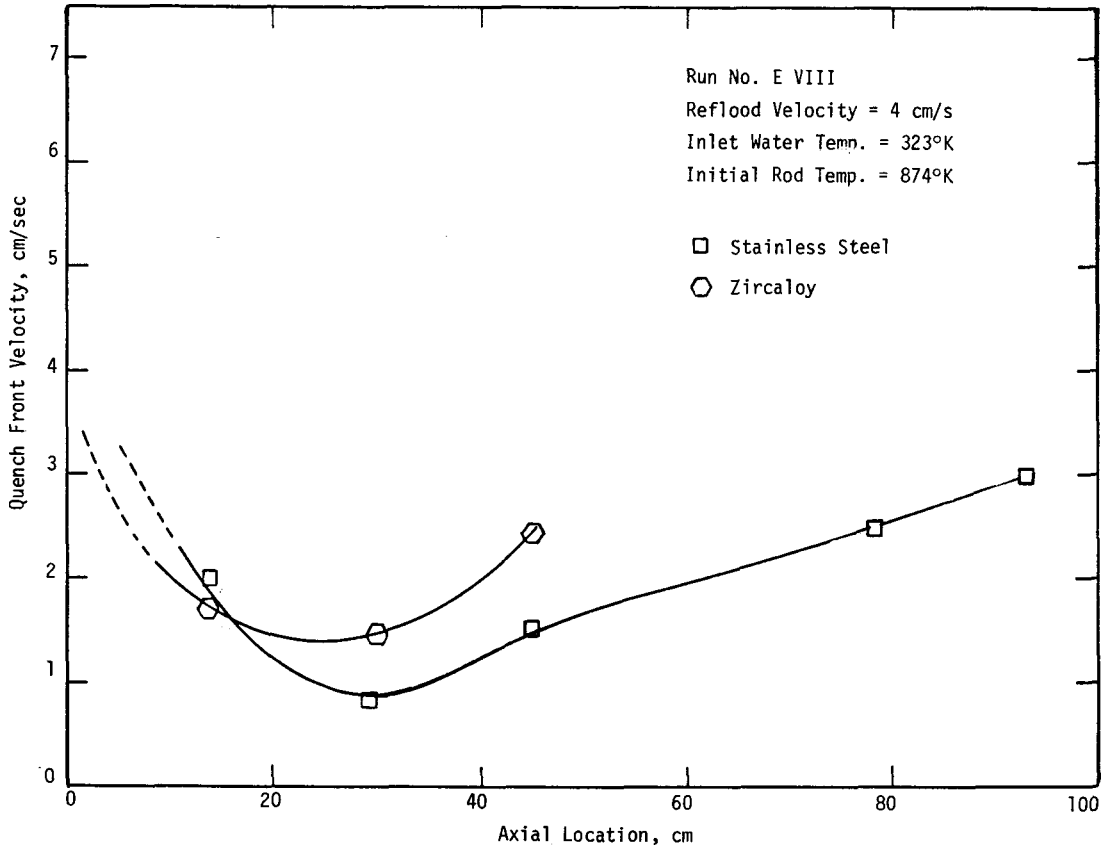

Figure B-42 Quench Front Location as a Function of Axial Location

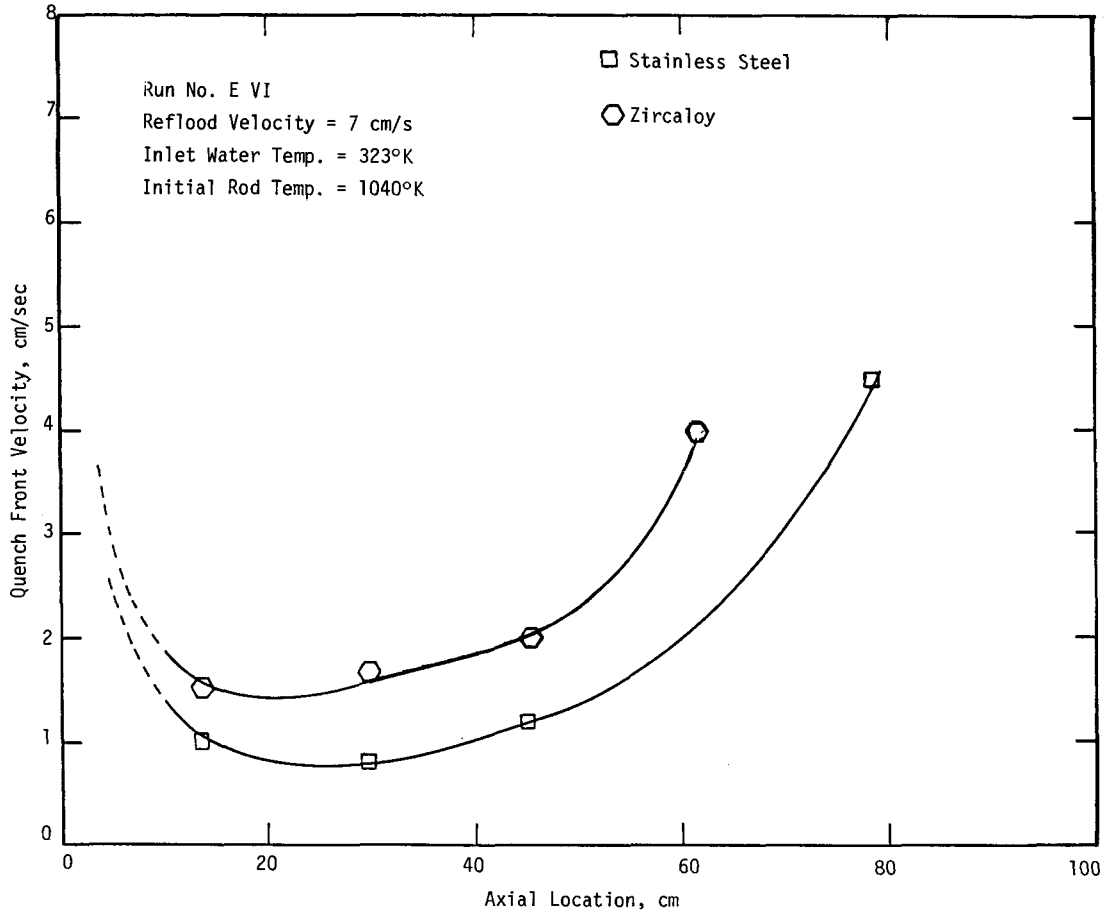

Figure B-43 Quench Front Velocity as a Function of Axial Location

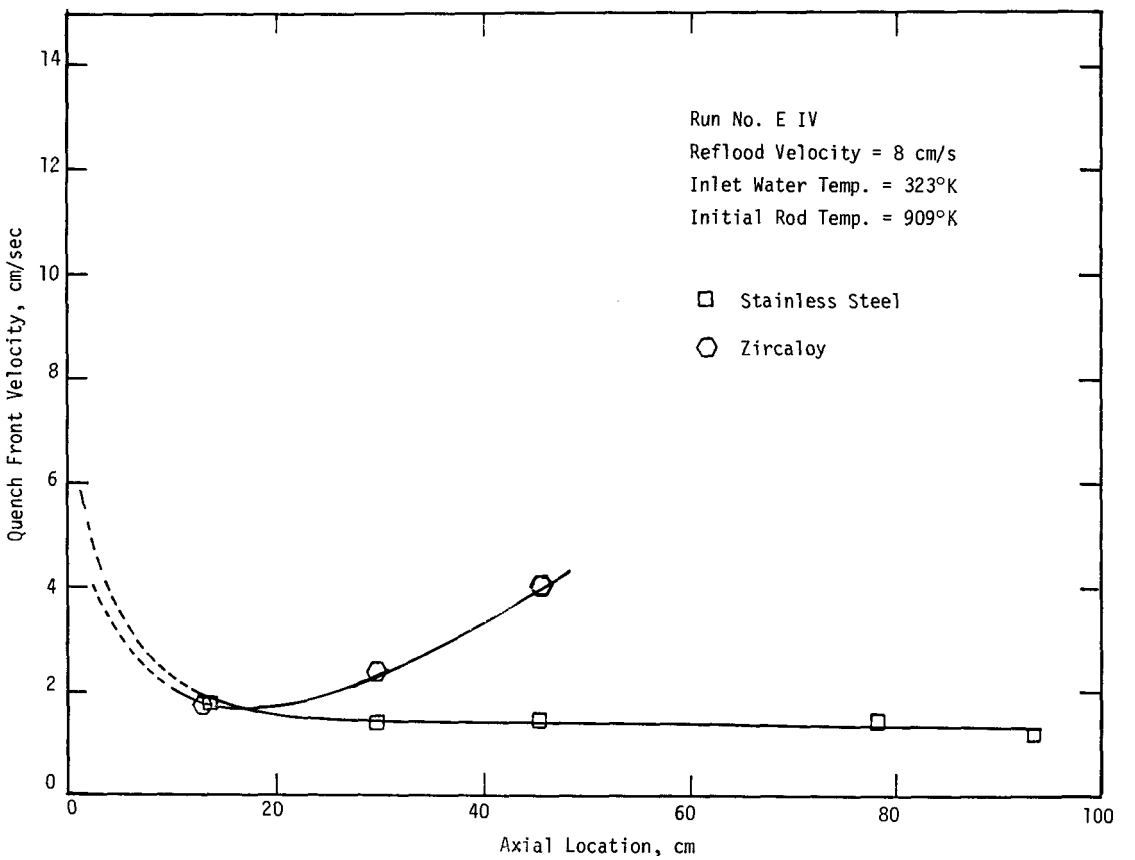

Figure B-44 Quench Front Velocity as a Function of Axial Location

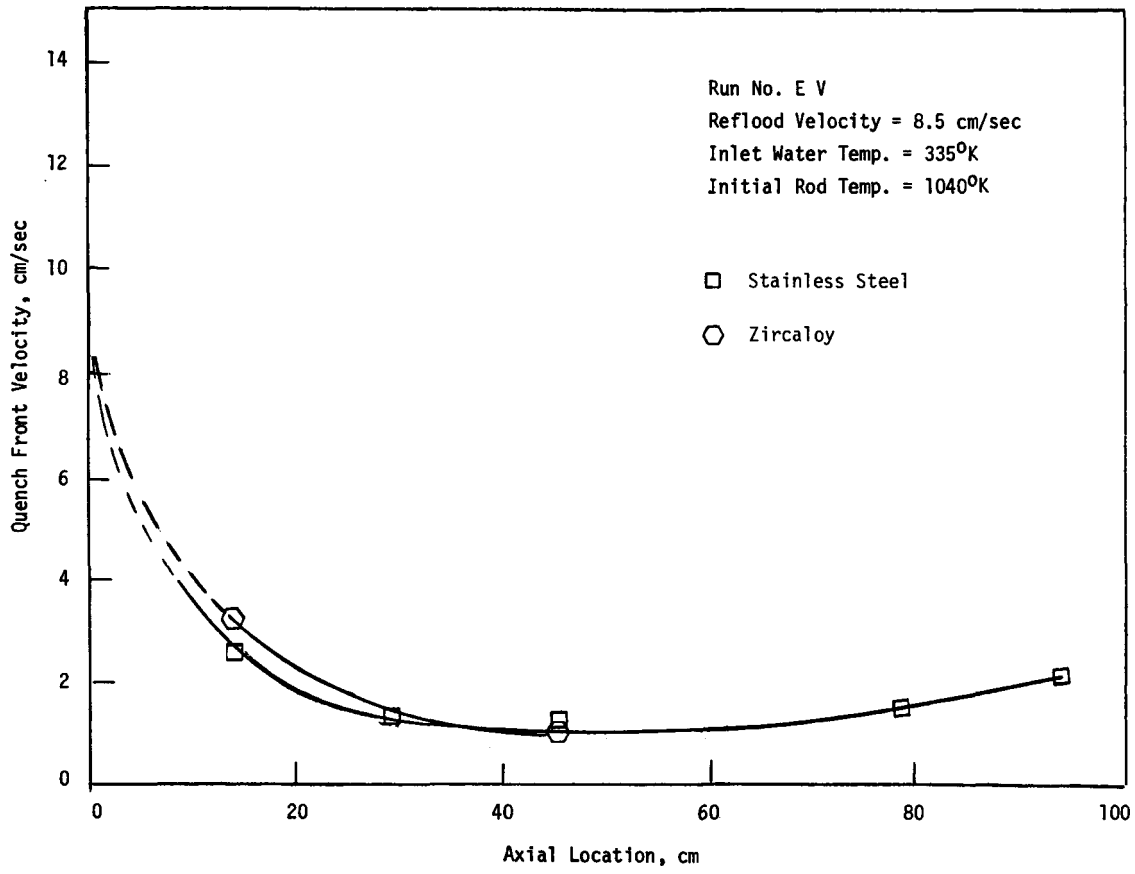

Figure B-45 Quench Front Velocity as a Function of Axial Location

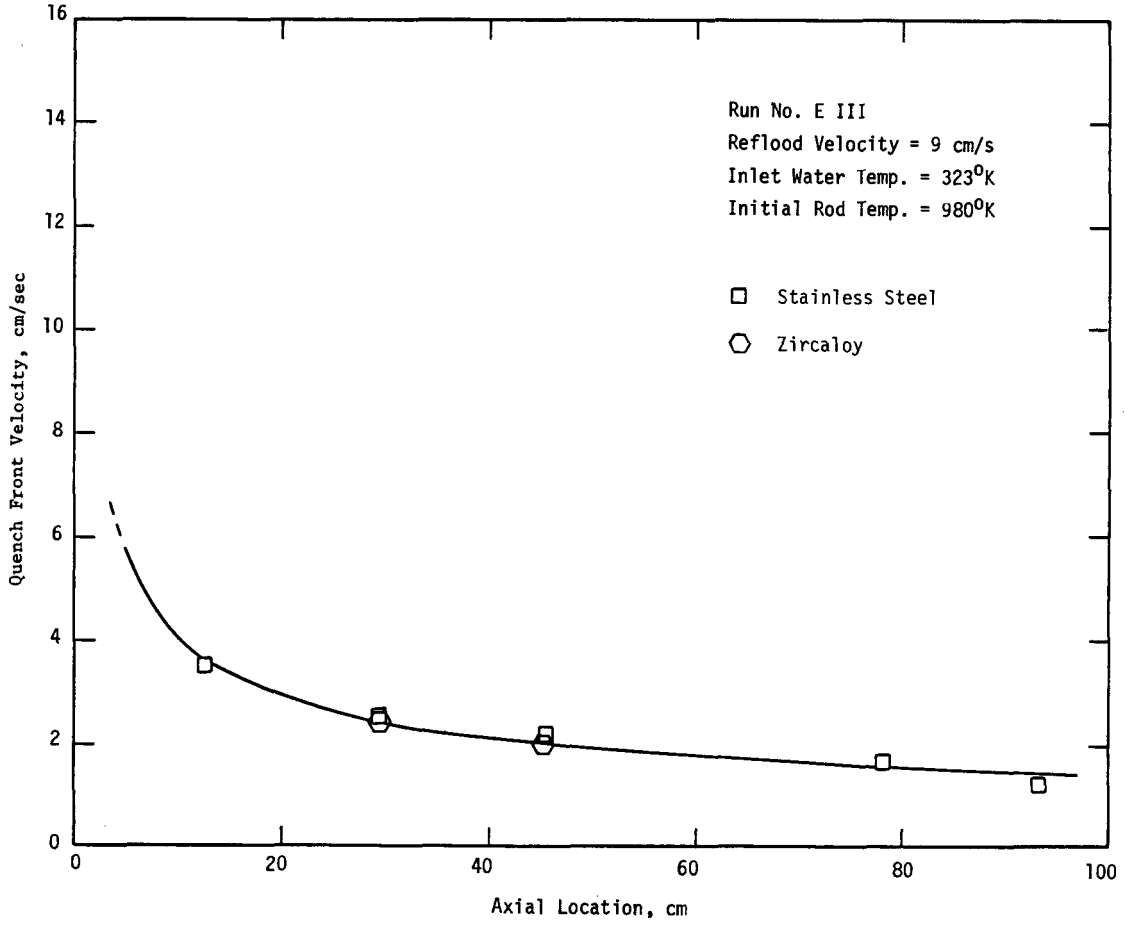

Figure B-46 Quench Front Velocity as a Function of Axial Location

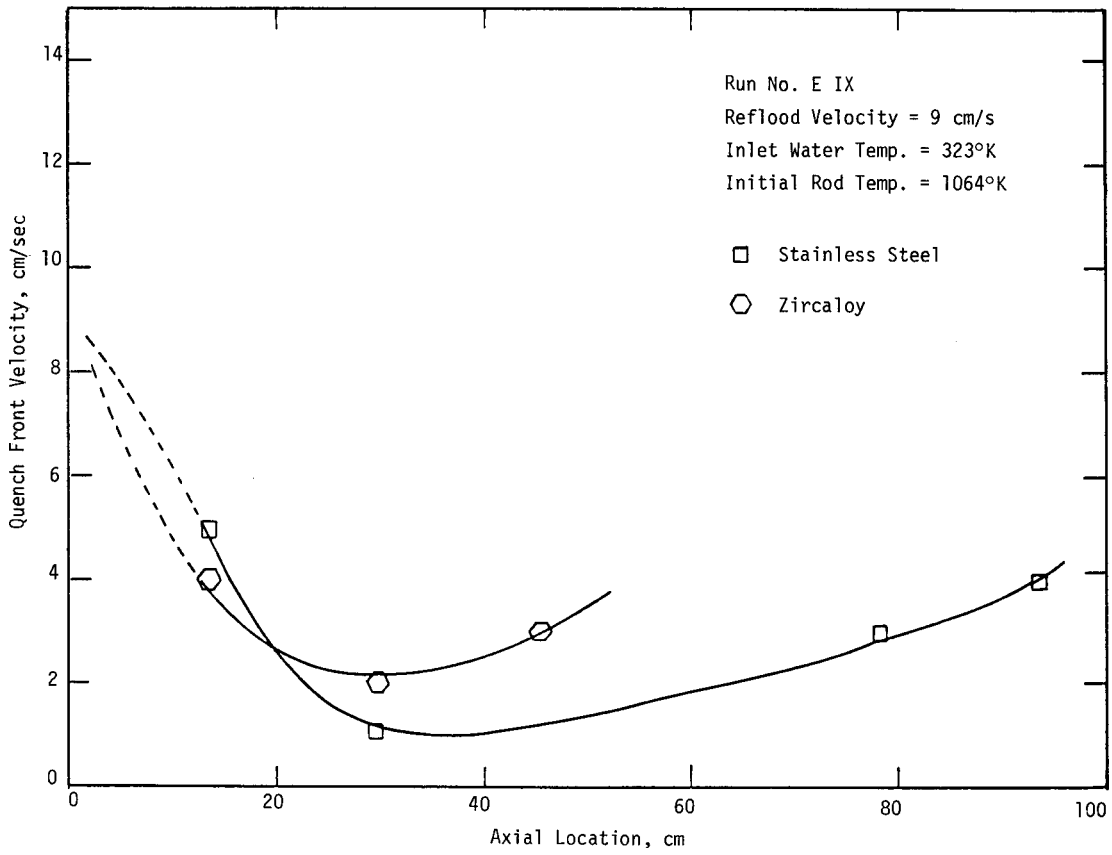

Figure B-47 Quench Front Velocity as a Function of Axial Location

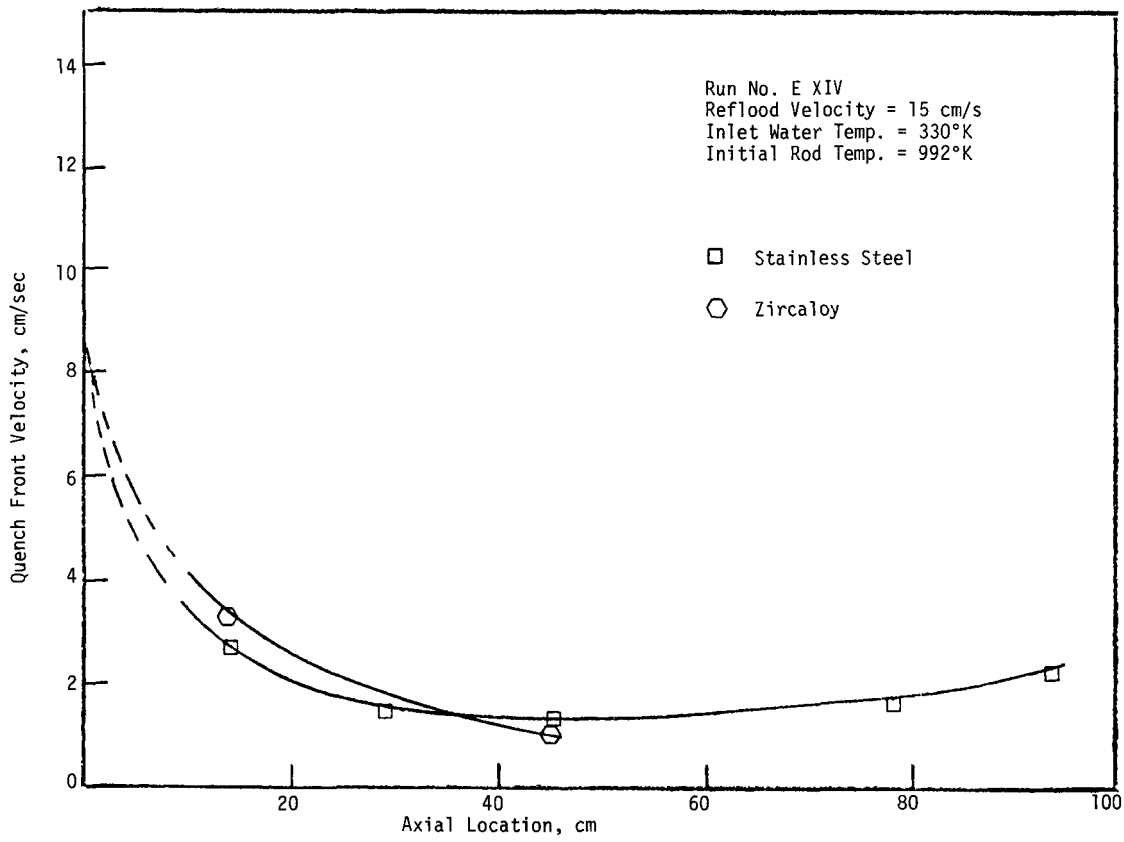

Figure B-48 Quench Front Velocity as a Function of Axial Location

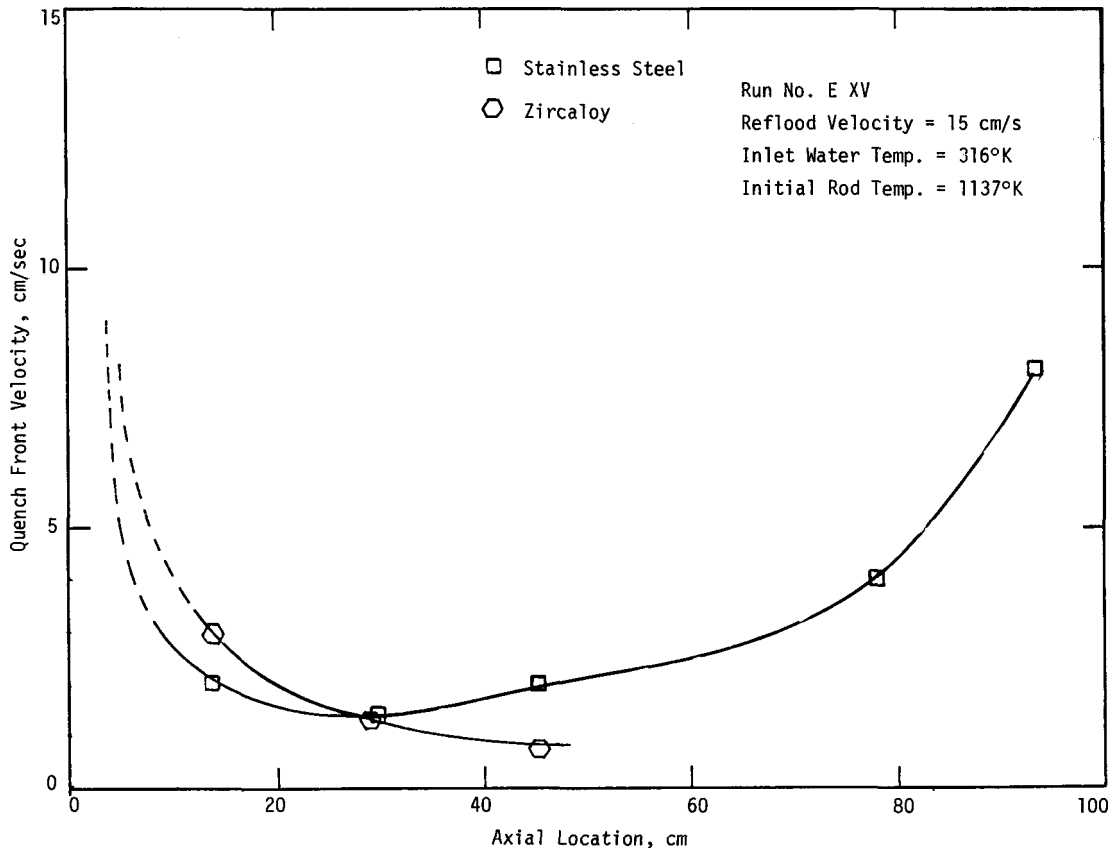

Figure B-49 Quench Front Velocity as a Function of Axial Location

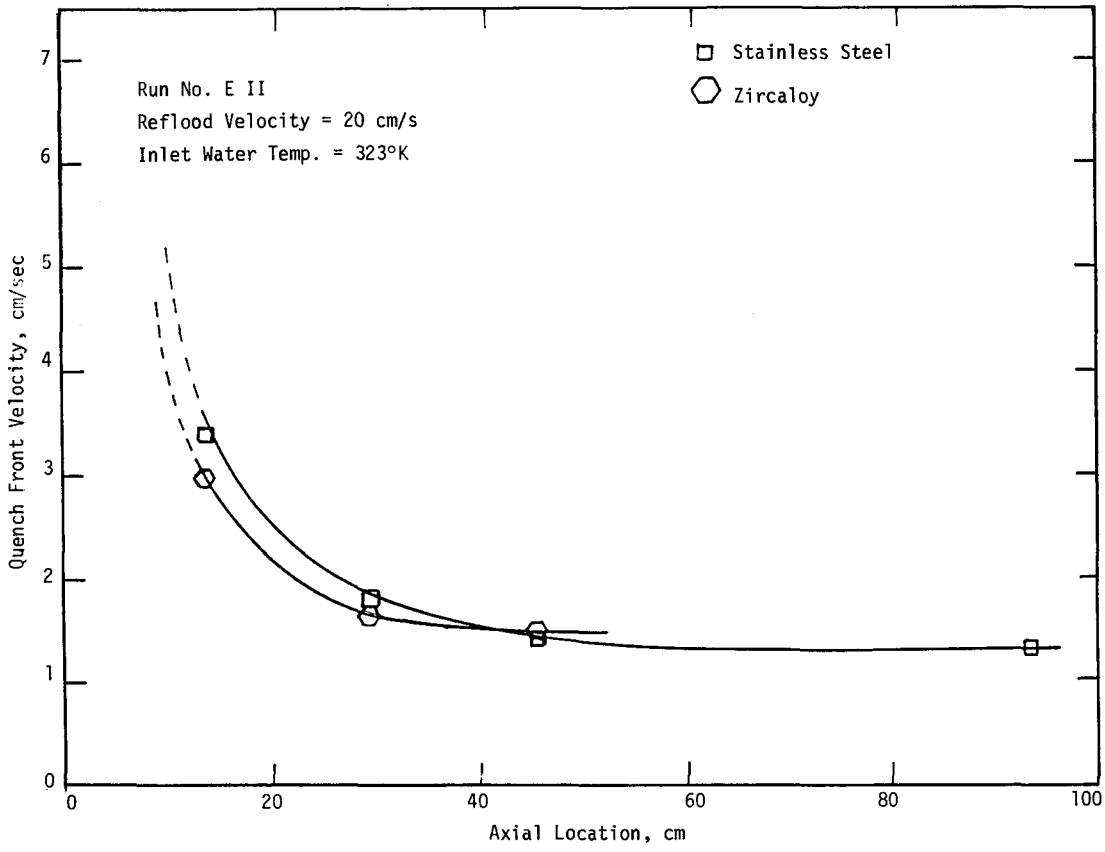

Figure B-50 Quench Front Velocity as a Function of Axial Location

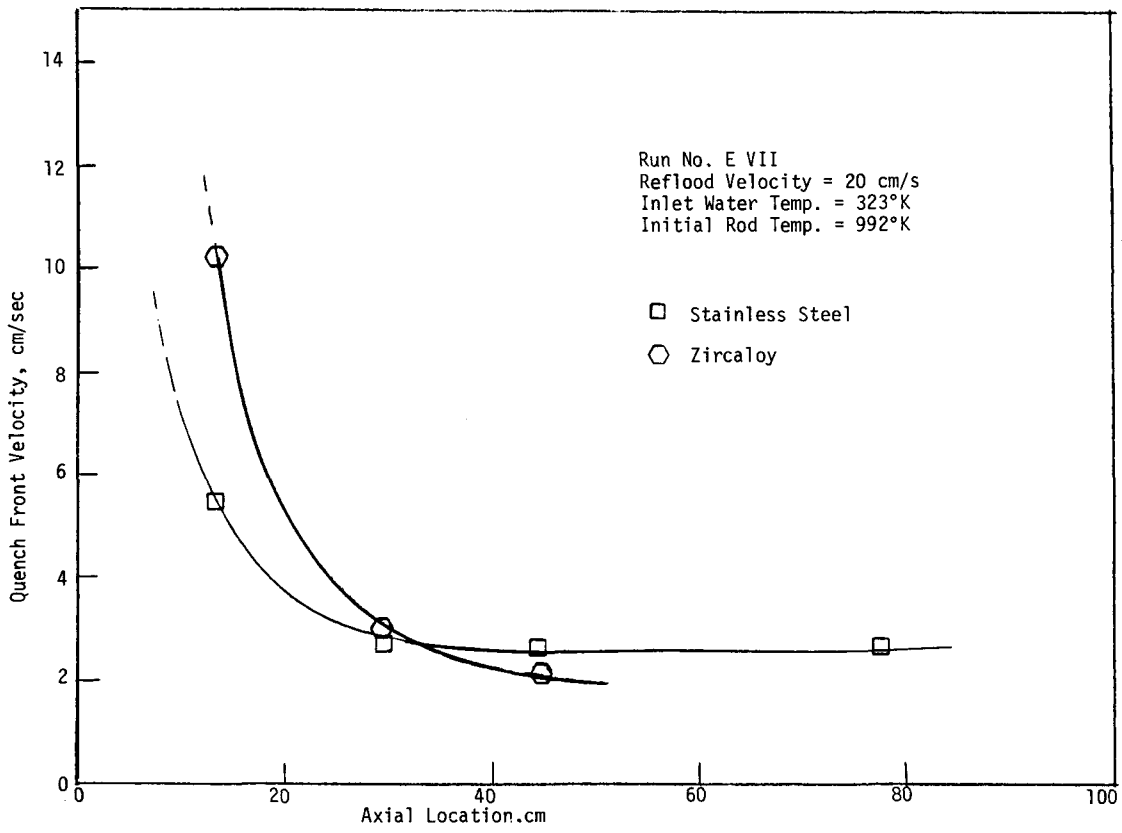

Figure B-51 Quench Front Velocity as a Function of Axial Location

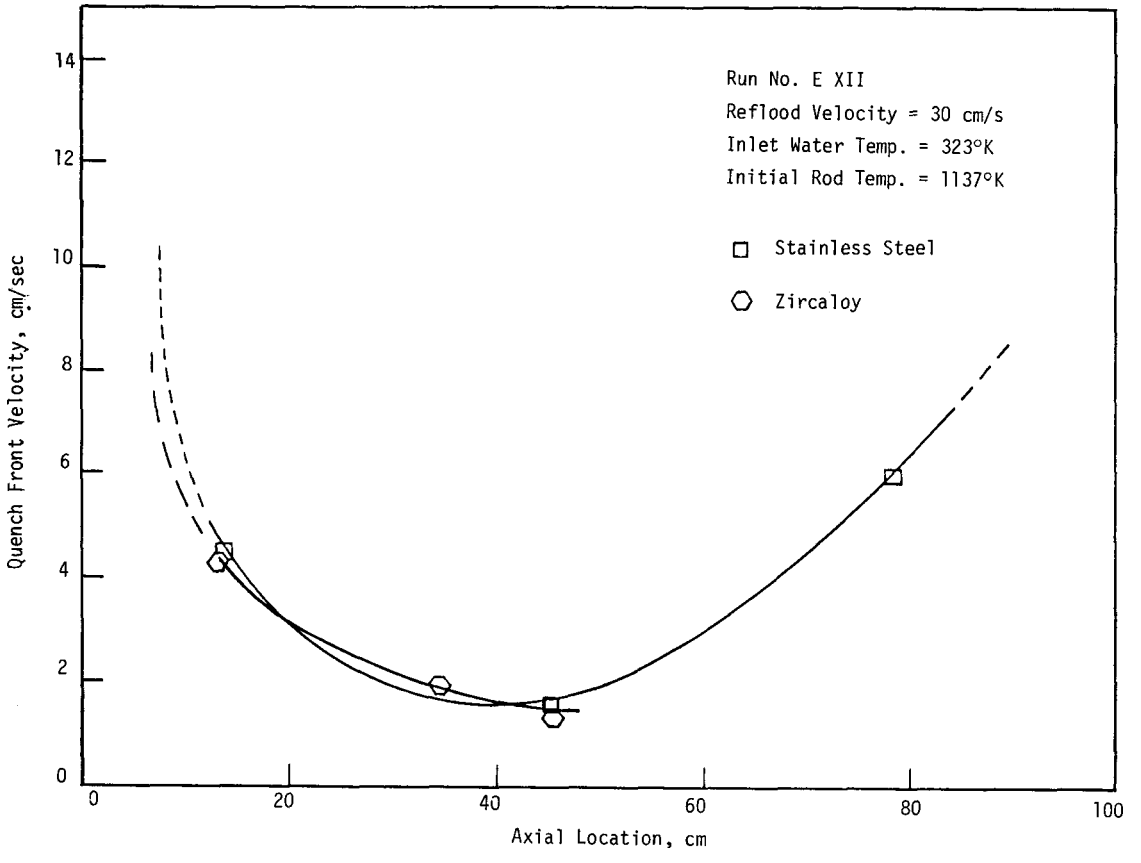

Figure B-52 Quench Front Velocity as a Function of Axial Location

APPENDIX C

TABULATION AND GRAPHICAL REPRESENTATION OF DATA FOR QUENCHING TEMPERATURE, QUENCH FRONT LOCATION AND QUENCH FRONT VELOCITY FOR A 4 ROD ZIRCALOY BUNDLE

A total of three runs were made with all zircaloy rod bundle. In these experiments initial rod wall temperature was about 1000 K while the flooding velocity was kept at 25 m/s. All the experiments were performed with inlet water subcooling of 75 K. The amount of oxidation of zircaloy rods in these experiments was determined by knowing the weight of the test specimen after each run.

QUENCH FRONT LOCATION

The quench front location on a fresh zircaloy rod bundle is plotted in Figure C-1 as a function of time. Figures C-2 and C-3 show the quench front locations on oxidized rod bundles.

QUENCH FRONT VELOCITY

The quench front velocities as reduced from quench front location data are plotted in Figures C-4 - C-6.

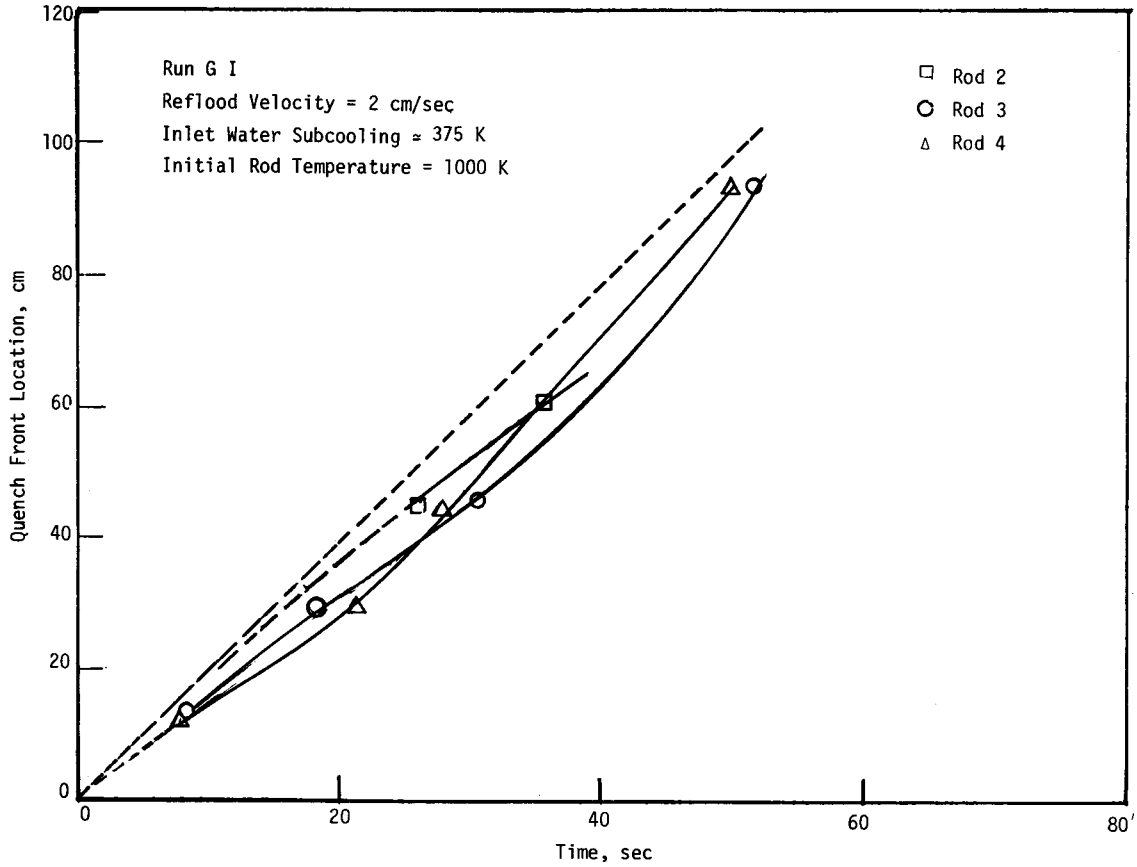

Figure C-1 Quench Front Location as a Function of Time for a Fresh Zircaloy 4 Rod Bundle

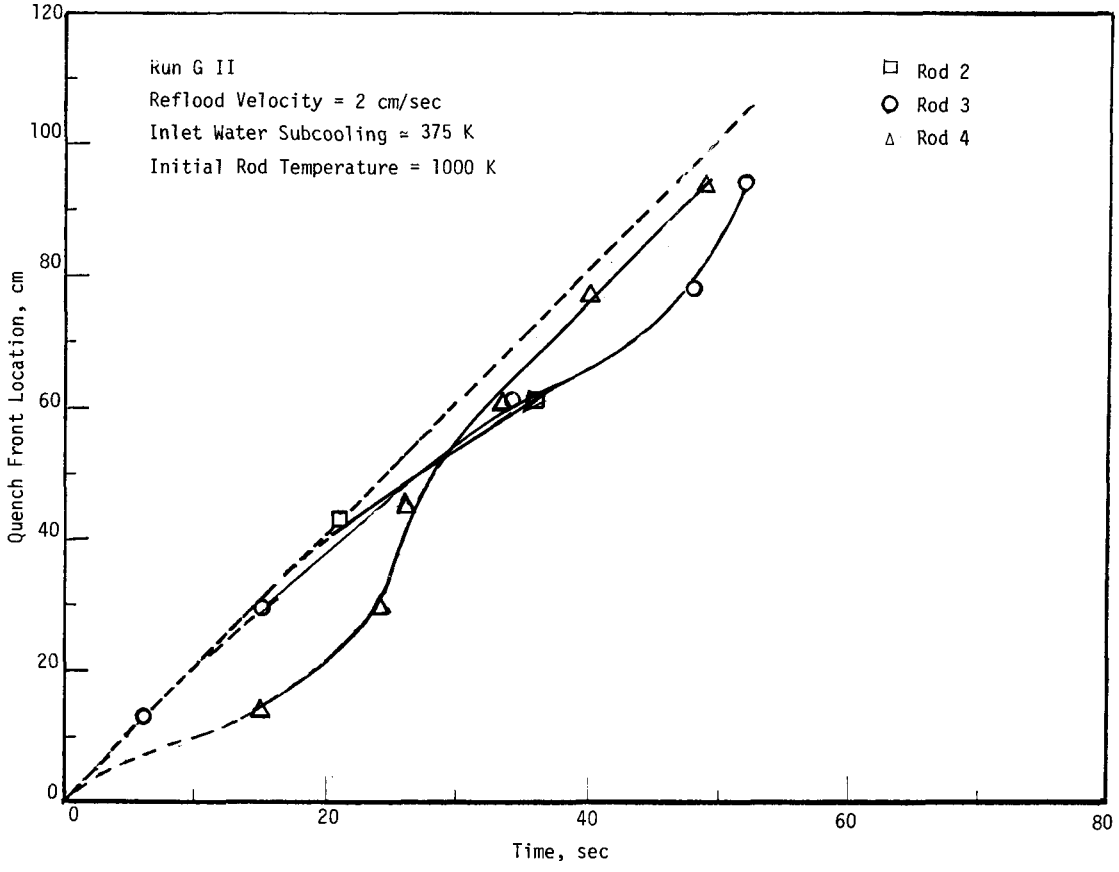

Figure C-2 Quench Front Location as a Function of Time for a Mildly Oxidized Zircaloy 4 Rod Bundle

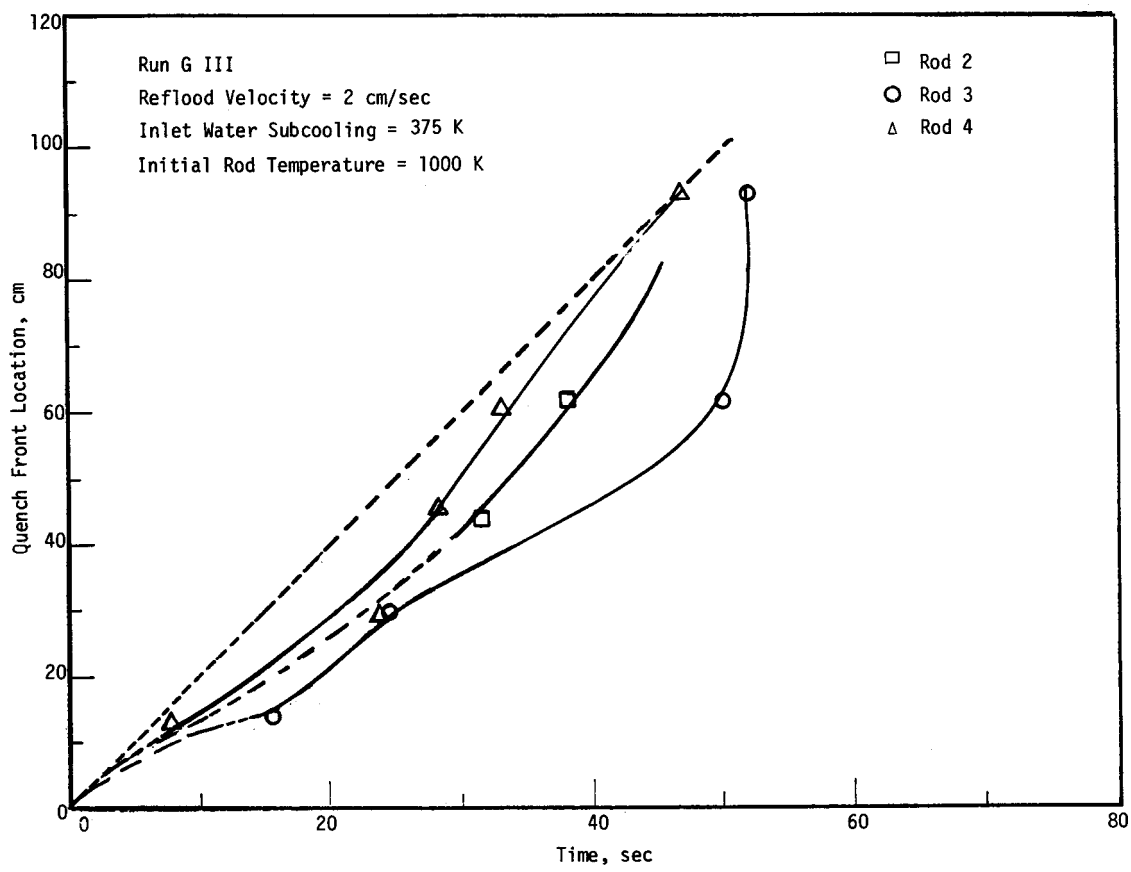

Figure C-3 Quench Front Location as a Function of Time for a Highly Oxidized Zircaloy 4 Rod Bundle

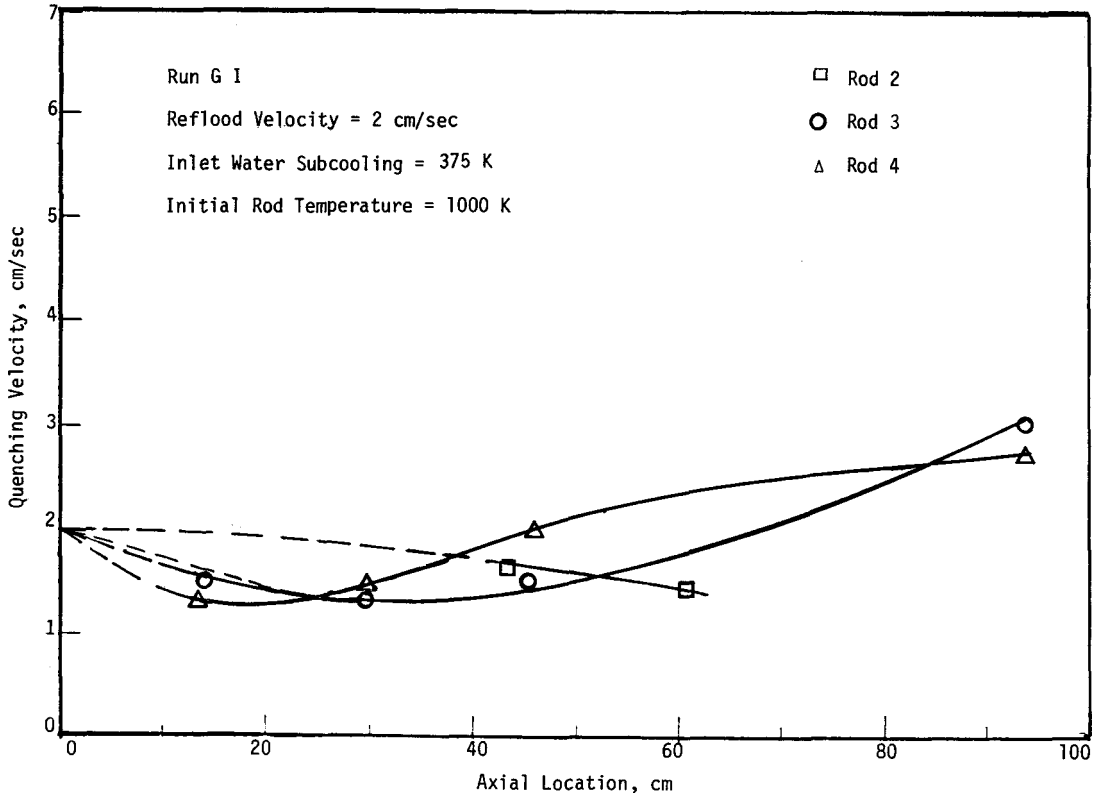

Figure C-4 Quench Front Velocity as a Function of Axial Location for a Fresh Zircaloy 4 Rod Bundle

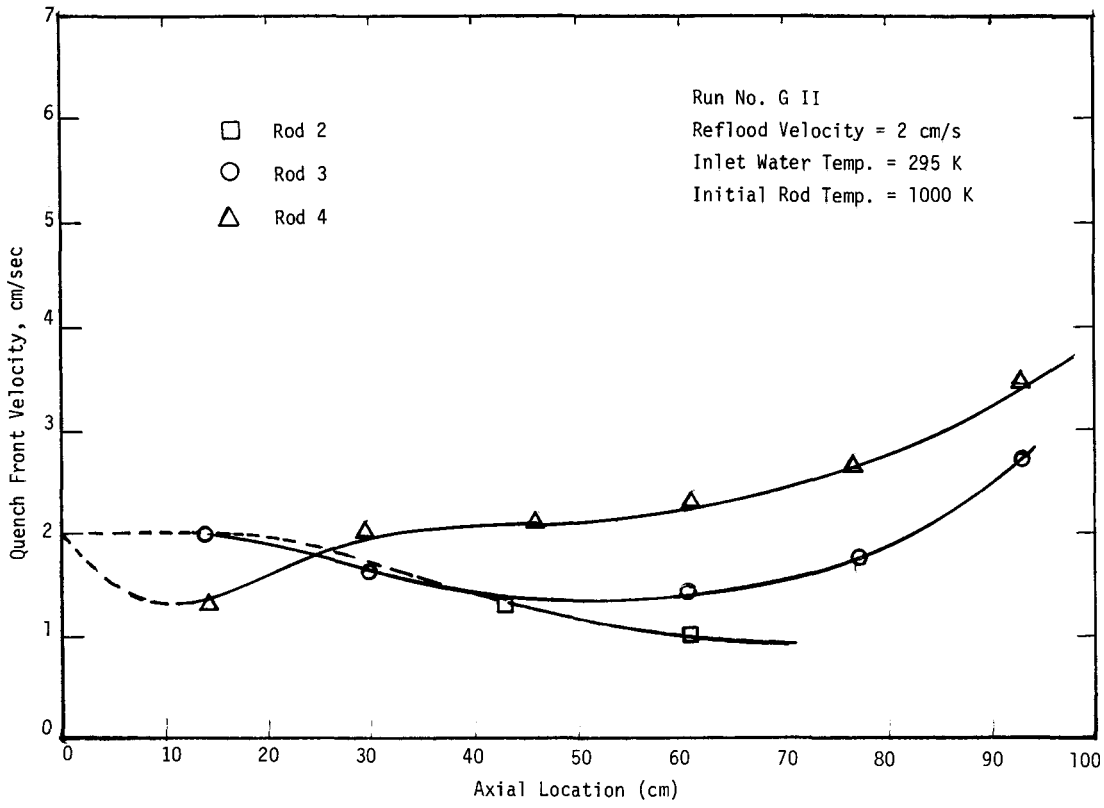

Figure C-5 Quench Front Velocity as a Function of Axial Location for a Mildly Oxidized Zircaloy 4 Rod Bundle

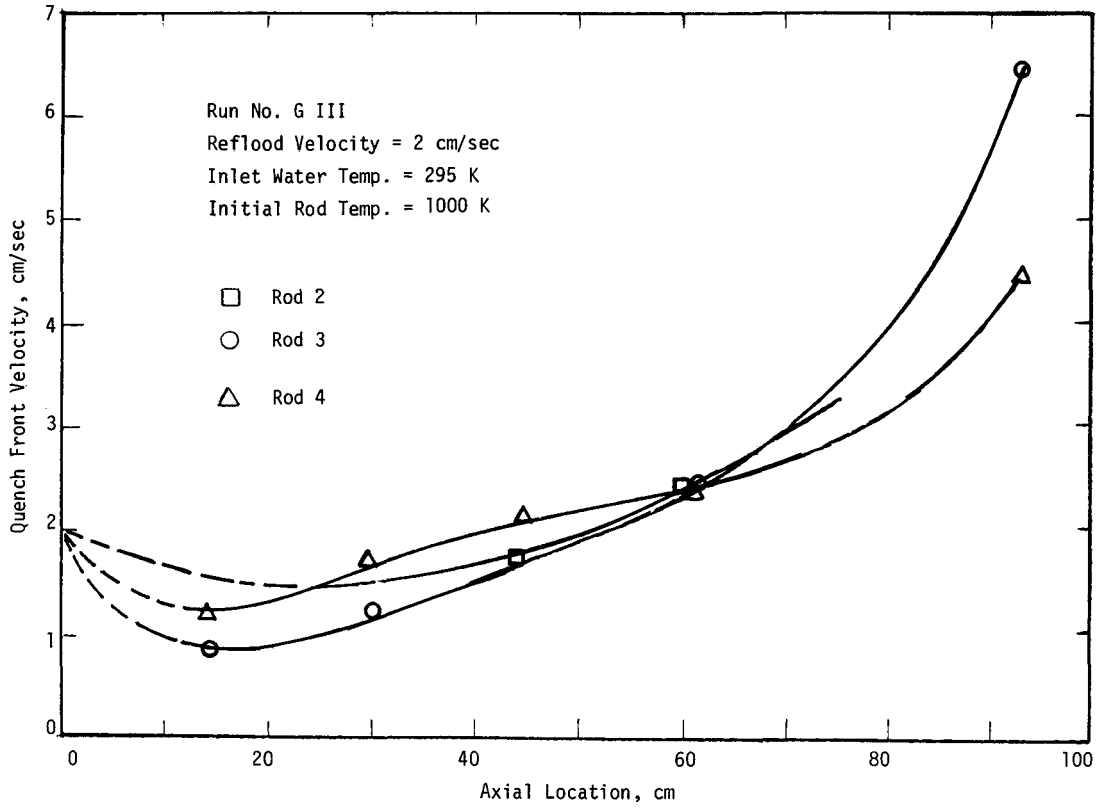

Figure C-6 Quench Front Velocity as a Function of Axial Location for a Heavily Oxidized Zircaloy 4 Rod Bundle

APPENDIX D

TABULATION AND GRAPHICAL PRESENTATION OF DATA FOR QUENCHING TEMPERATURE, QUENCH FRONT LOCATION AND QUENCH FRONT VELOCITY FOR A 4 ROD BUNDLE CONTAINING TWO ZIRCALOY AND TWO RODS FROM FLECHT EXPERIMENTS

A total of ten flooding experiments were performed with a 4 rod bundle containing two zircaloy rods and two rods from FLECHT experiments. Rods from the FLECHT program were not instrumented because the thermocouples were broken loos during cutting of the rods to a height suited for the present test set up. In these experiments the initial temperature of the zircaloy rods was varied from 945 to 1047 K while the flooding velocity was varied from 2 to 30 cm/s. Subcooling of water at the inlet was generally 78 K, however in a few experiments subcooling was decreased up to about 47 K. Test parameters are listed in Table D-1.

QUENCH FRONT LOCATION

Quench front locations obtained from movies for stainless steel (FLECHT) rods and zircaloy rods are plotted in Figures D-1, D-2 and D-3. In these figures, the quench front data as interpreted from output of the thermocouples are also plotted. The quench front location data obtained only from thermocouples for the cases in which no movies were made are plotted in Figures D-4 - D-10. Figures D-4 - D-7 correspond to the case when subcooling of water at the inlet was 78 K.

QUENCH FRONT VELOCITY

Quench front velocities as reduced from quench front location data are plotted in Figures D-11 - D-20.

Table D-1

TEST RUNS WITH TWO RODS (STAINLESS STEEL) FROM FLECHT EXPERIMENTS AND TWO ZIRCALOY RODS

Run Number	Reflood Velocity (cm/s)	Inlet Water Temp.(K)	Initial Tube Temp.(K)	Movie Data
F-I	10	295	957	Yes
F-II	10	295	957	No
F-III	30	295	957	Yes
F-IV	2	295	945	No
F-V	2	295	957	Yes
F-VI	2	323	957	No
F-VII	10	295	957	Yes
F-VIII	2	295	957	Yes
F-IX	10	317	1047	No
F-X	30	326	1026	No

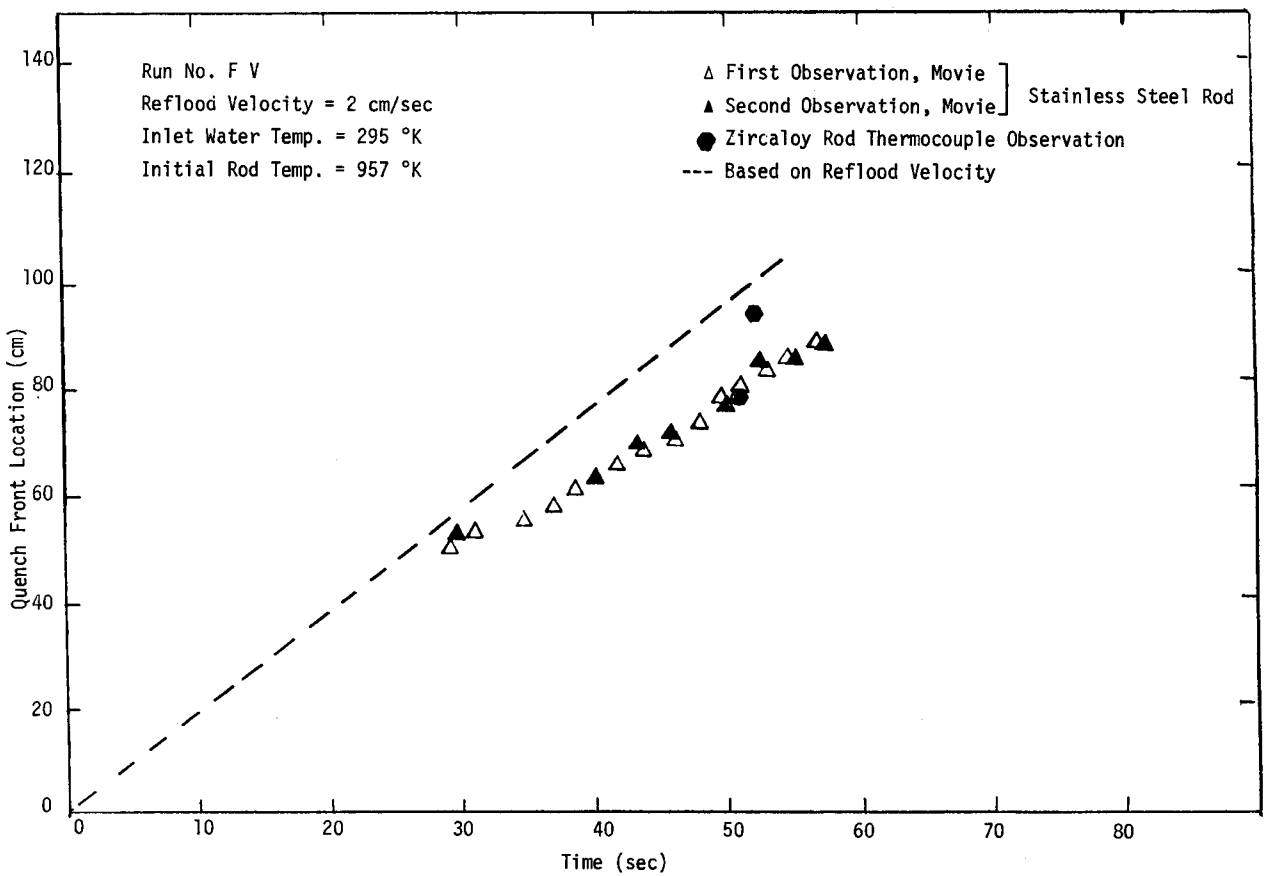

Figure D-1 Quench Front Location as a Function of Time

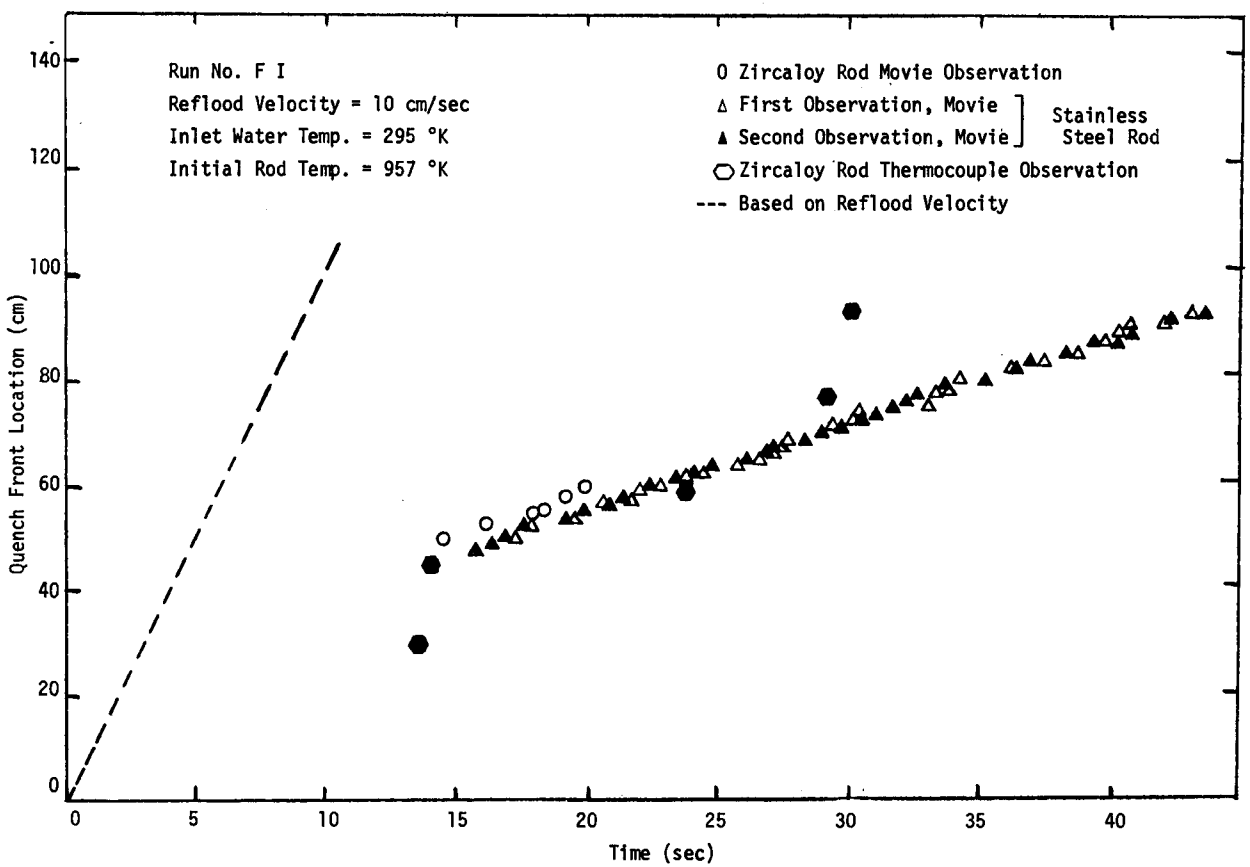

Figure D-2 Quench Front Location as a Function of Time

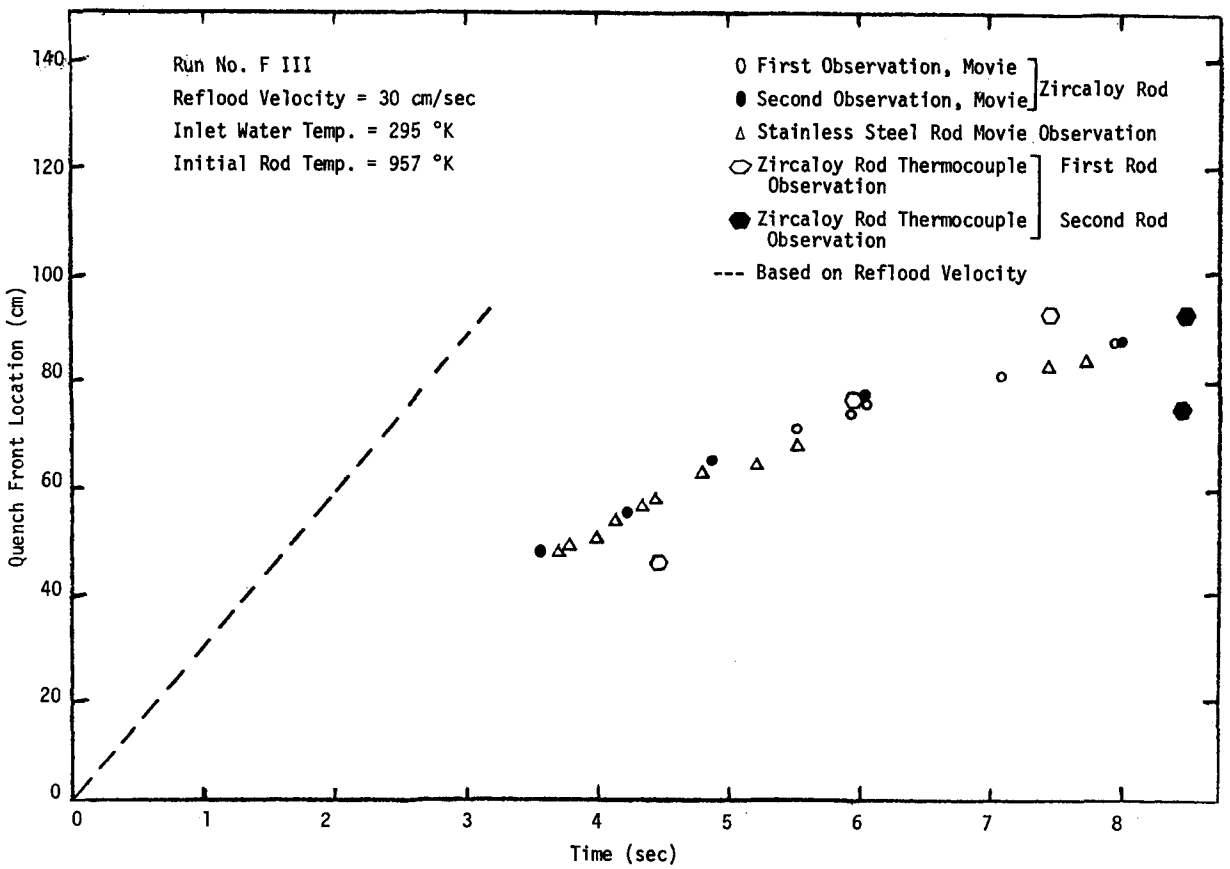

Figure D-3 Quench Front Location as a Function of Time

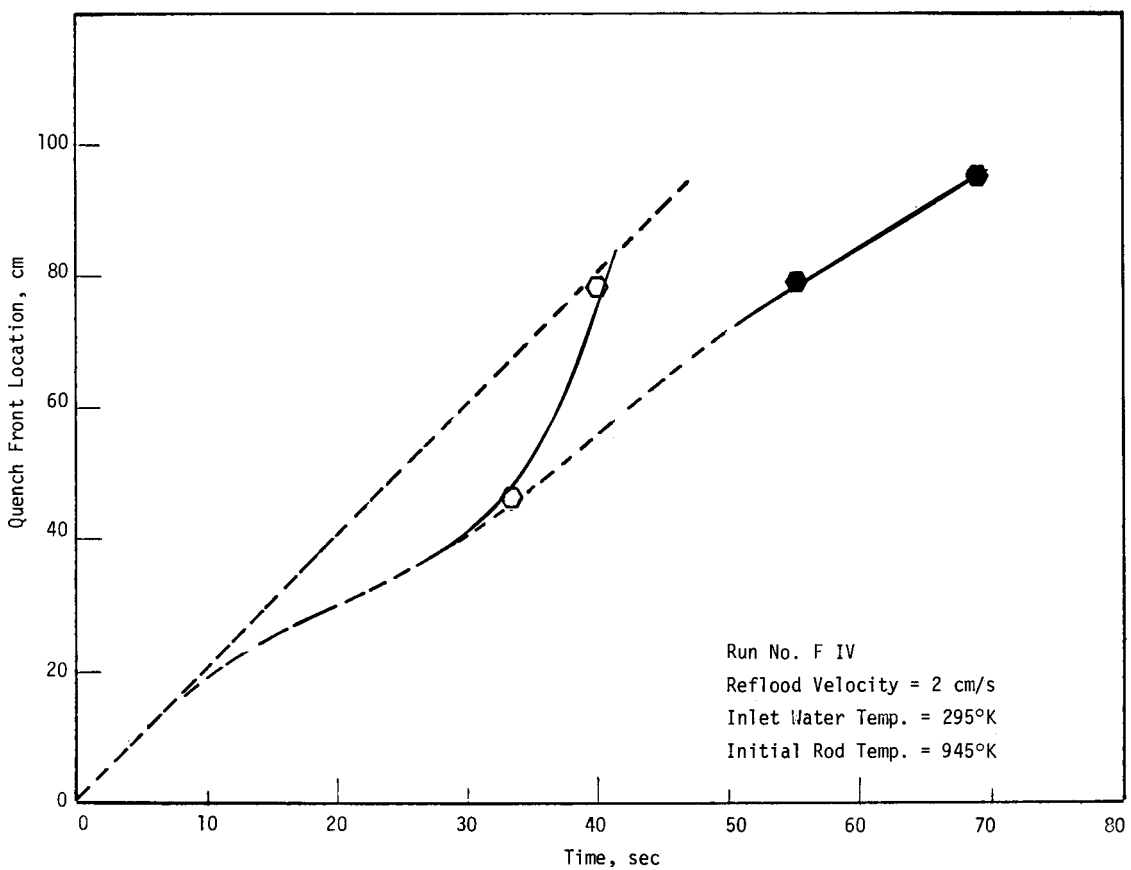

Figure D-4 Quench Front Location as a Function of Time

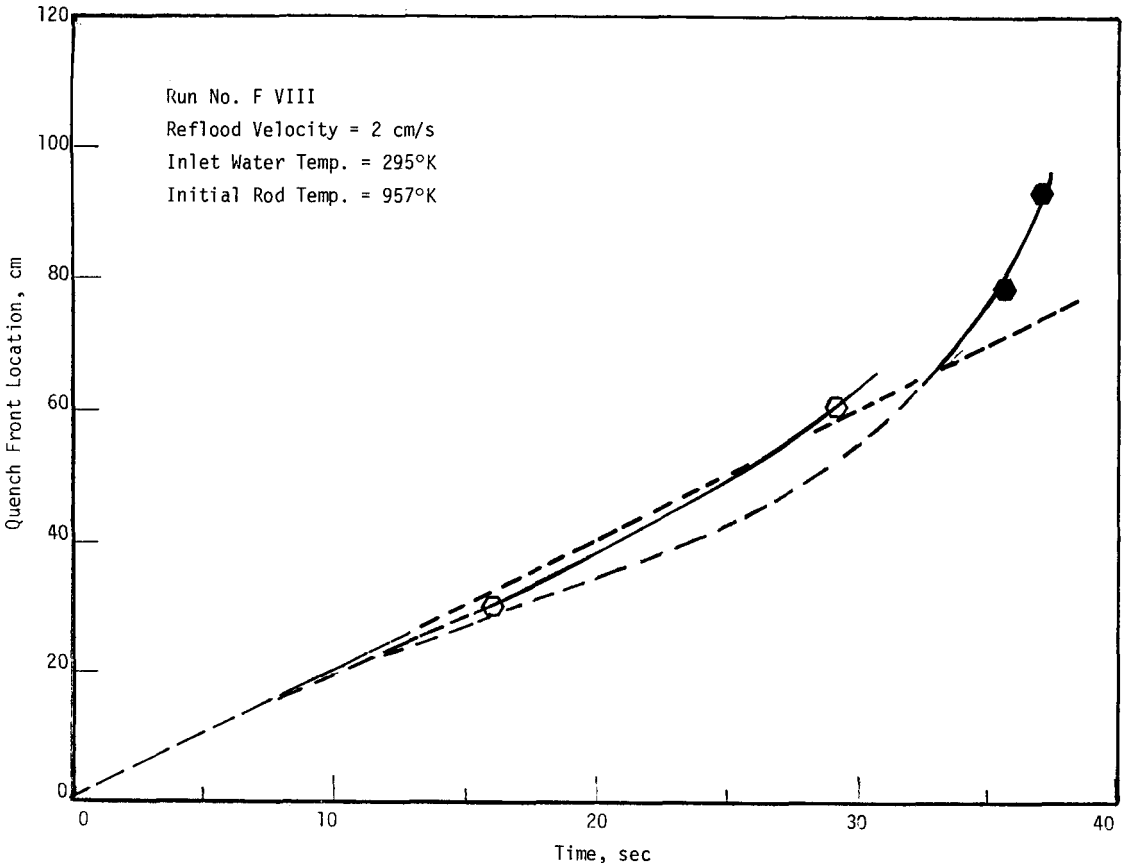

Figure D-5 Quench Front Location as a Function of Time

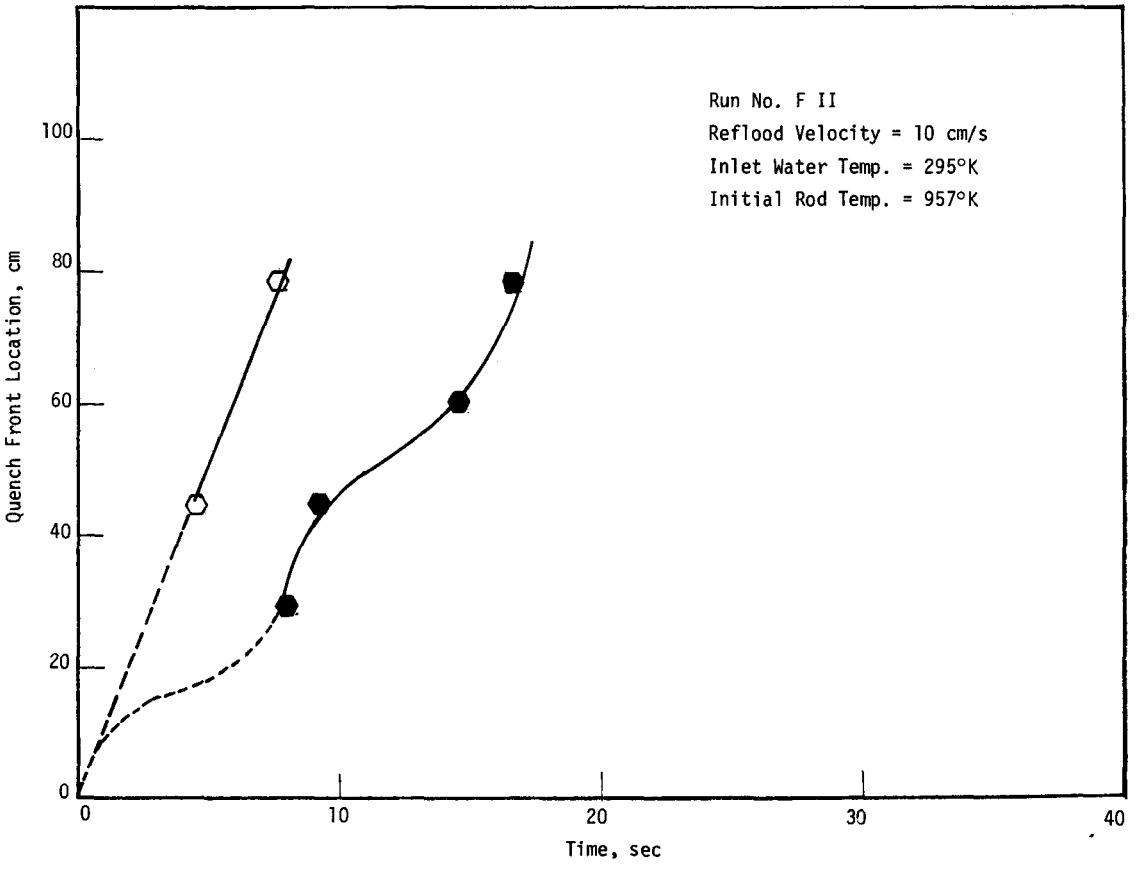

Figure D-6 Quench Front Location as a Function of Time

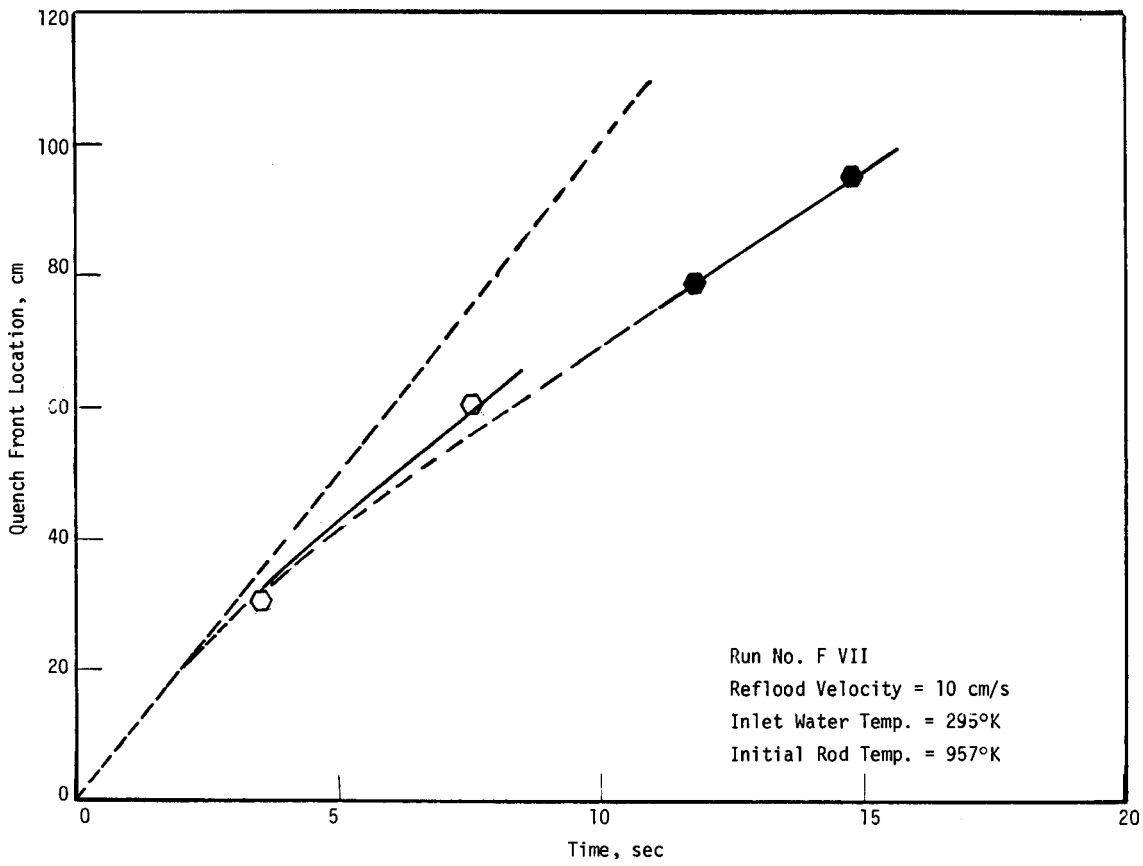

Figure D-7 Quench Front Location as a Function of Time

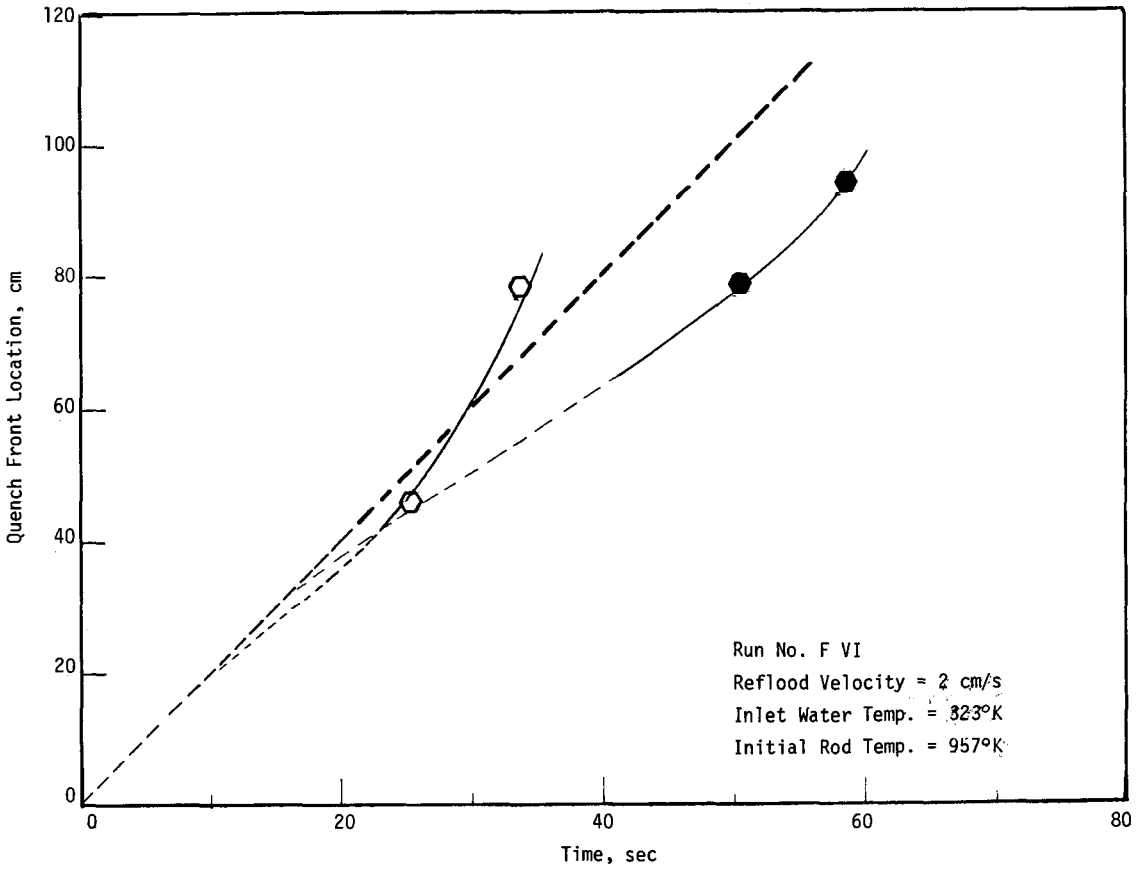

Figure D-8 Quench Front Location as a Function of Time

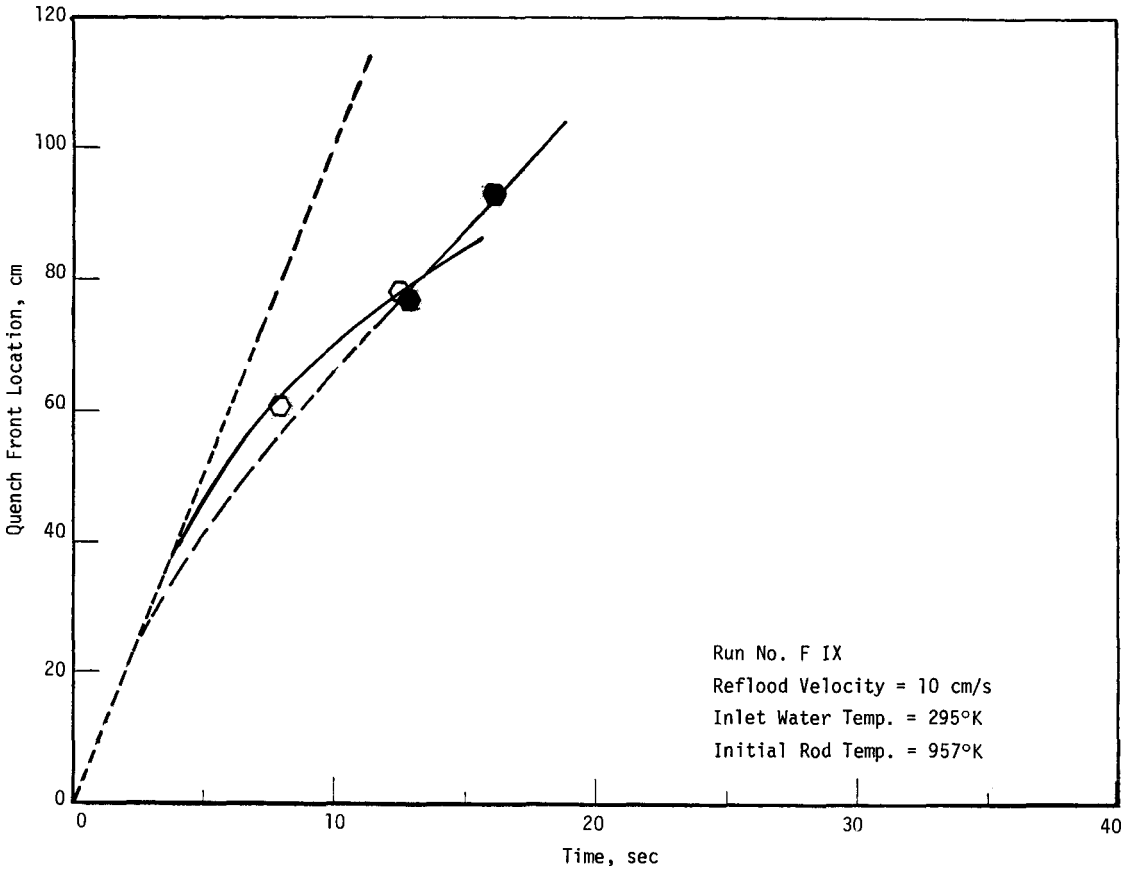

Figure D-9 Quench Front Location as a Function of Time

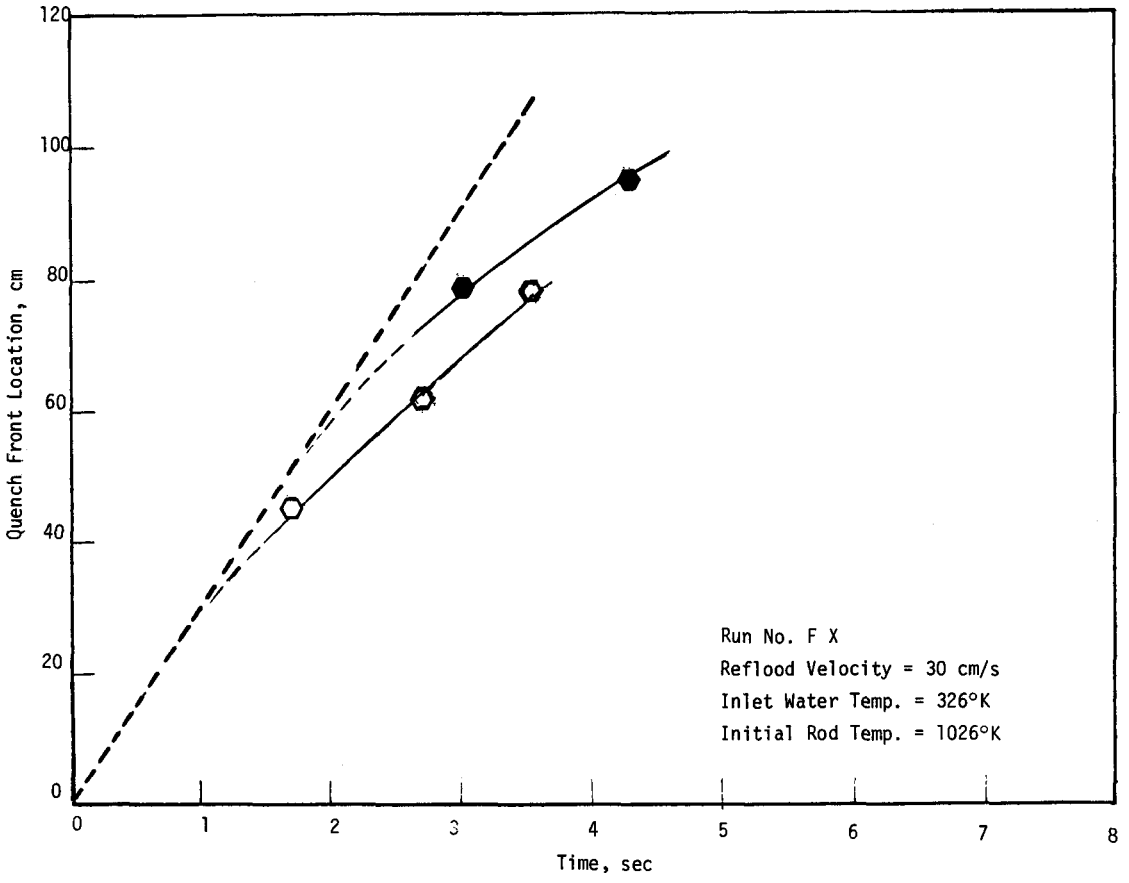

Figure D-10 Quench Front Location as a Function of Time

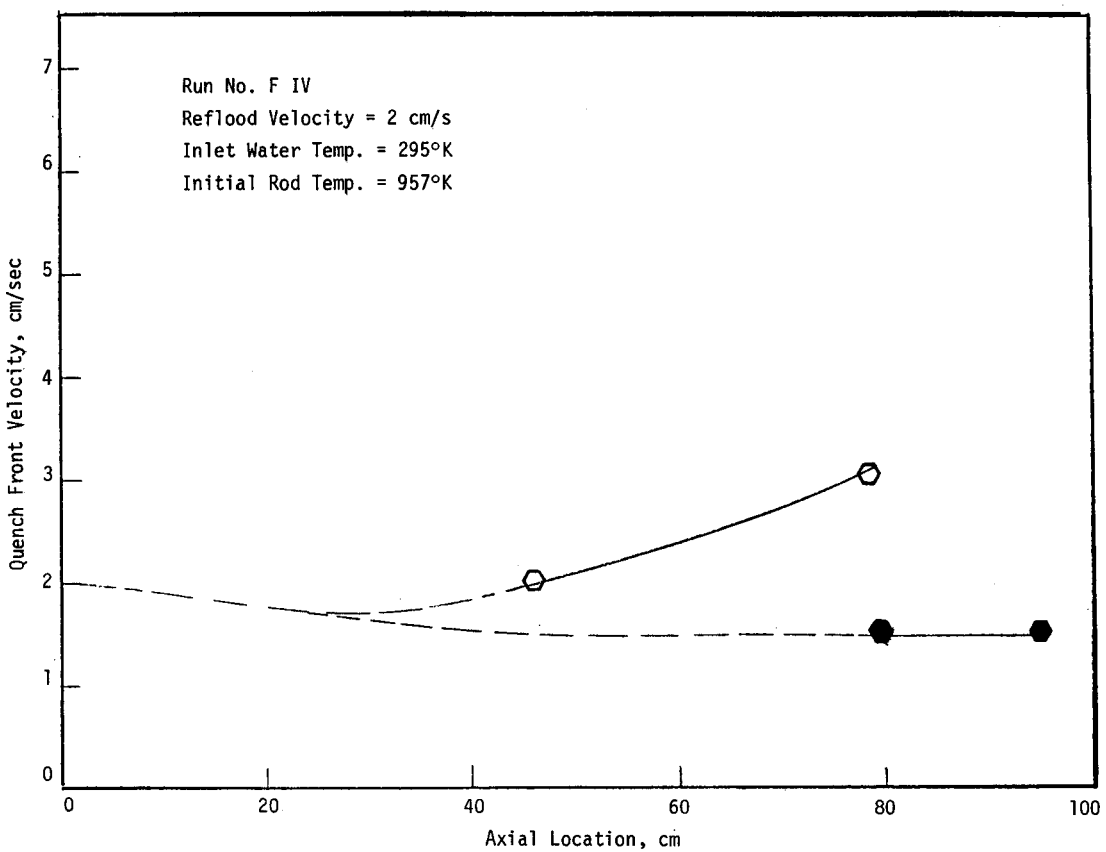

Figure D-11 Quench Front Velocity as a Function of Axial Location

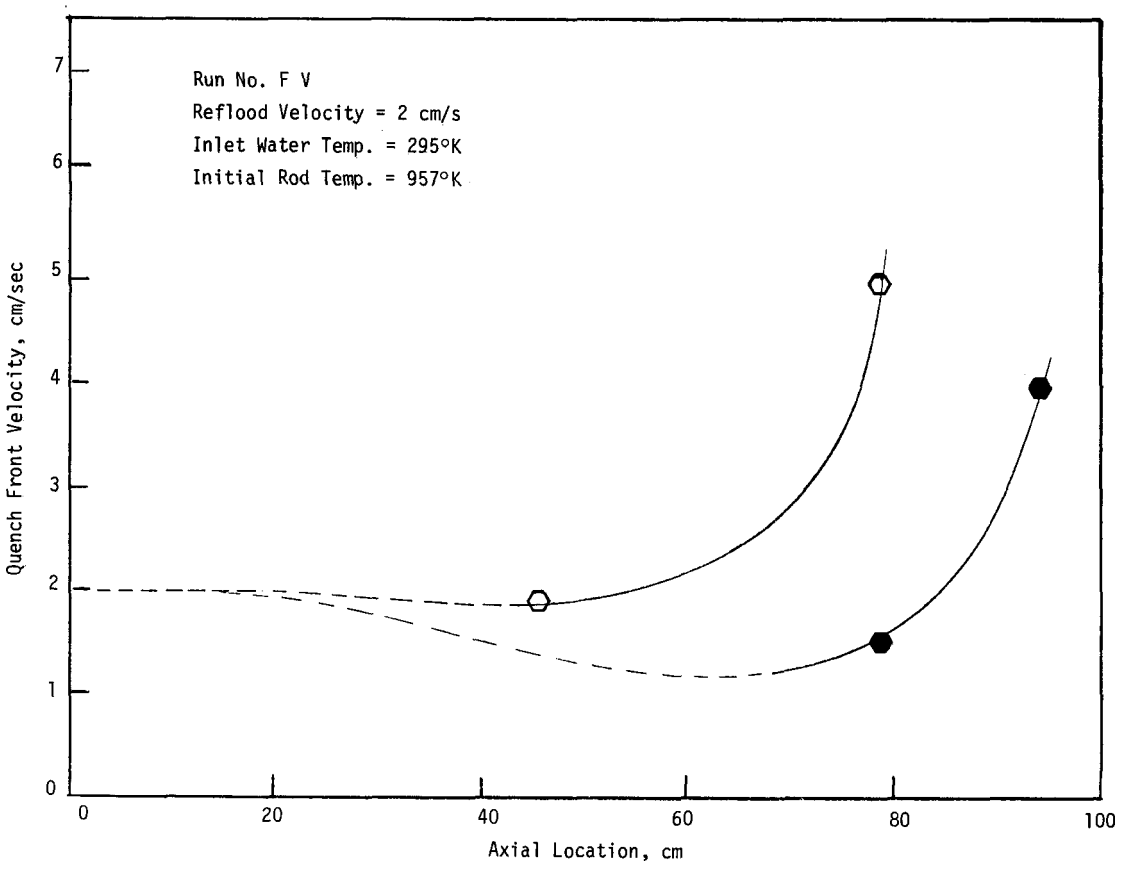

Figure D-12 Quench Front Velocity as a Function of Axial Location

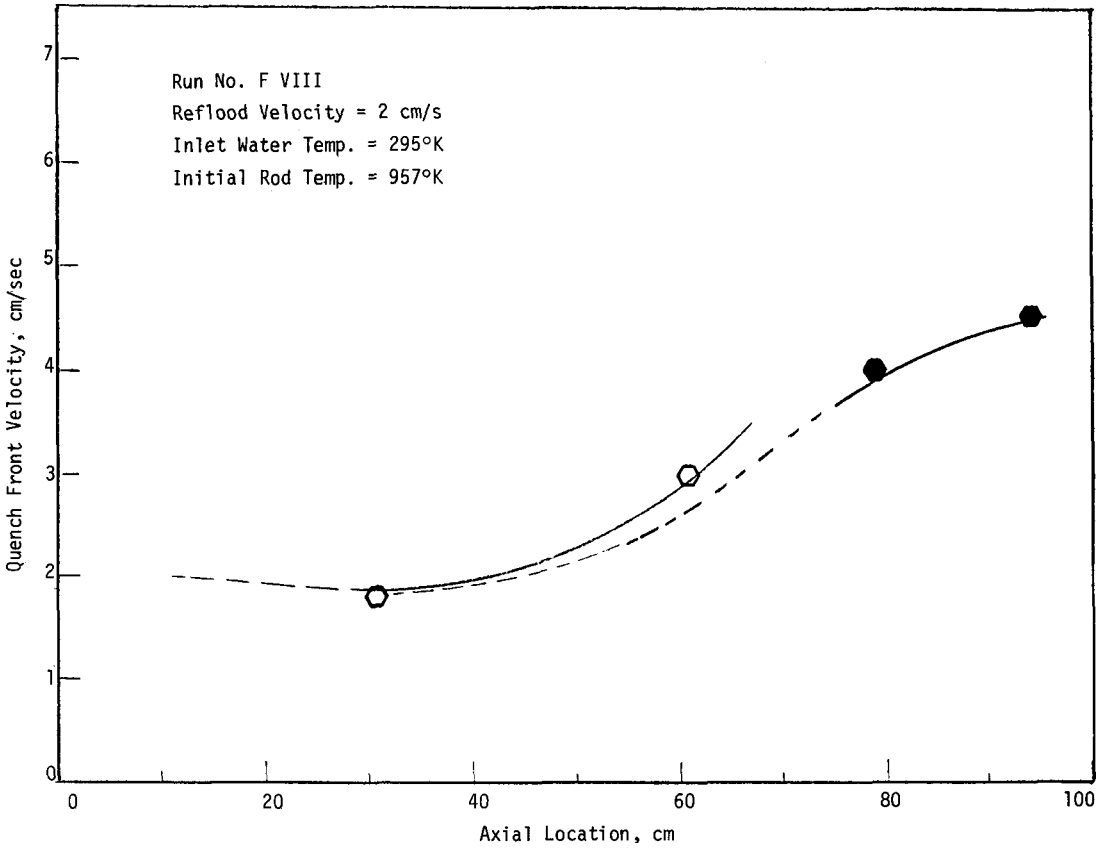

Figure D-13 Quench Front Velocity as a Function of Axial Location

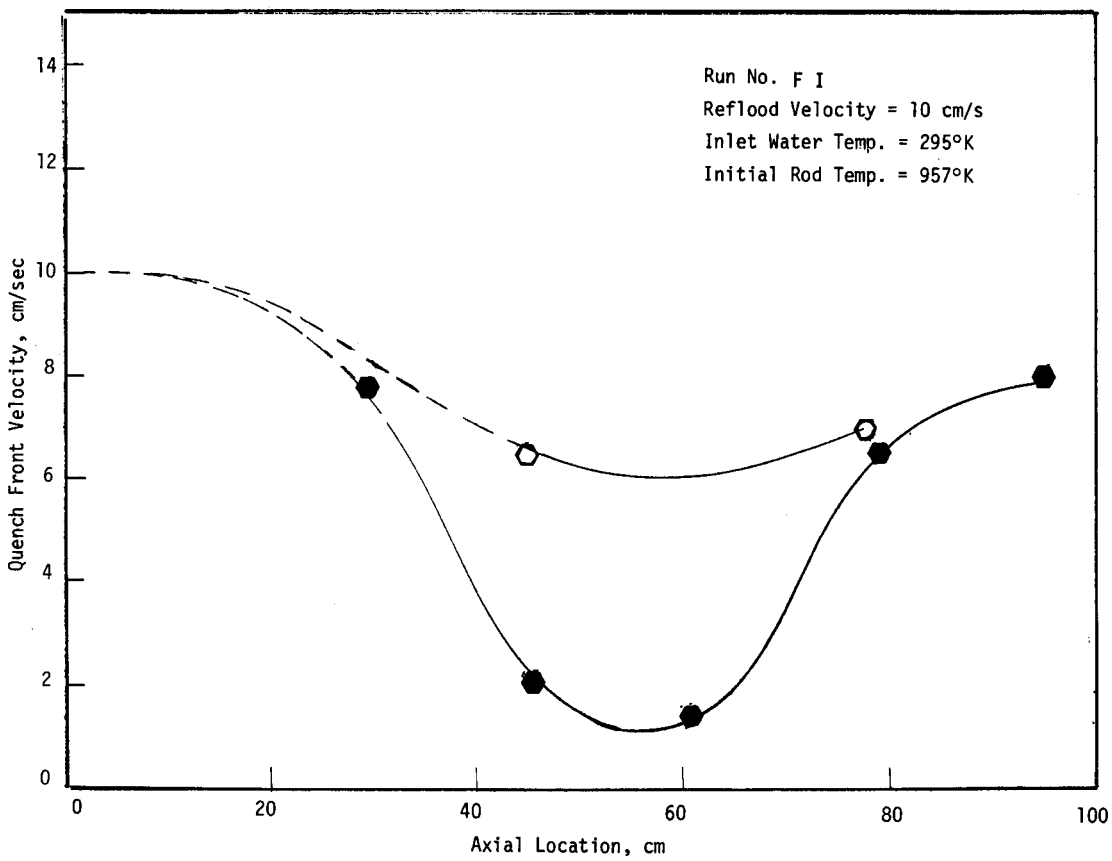

Figure D-14 Quench Front Velocity as a Function of Axial Location

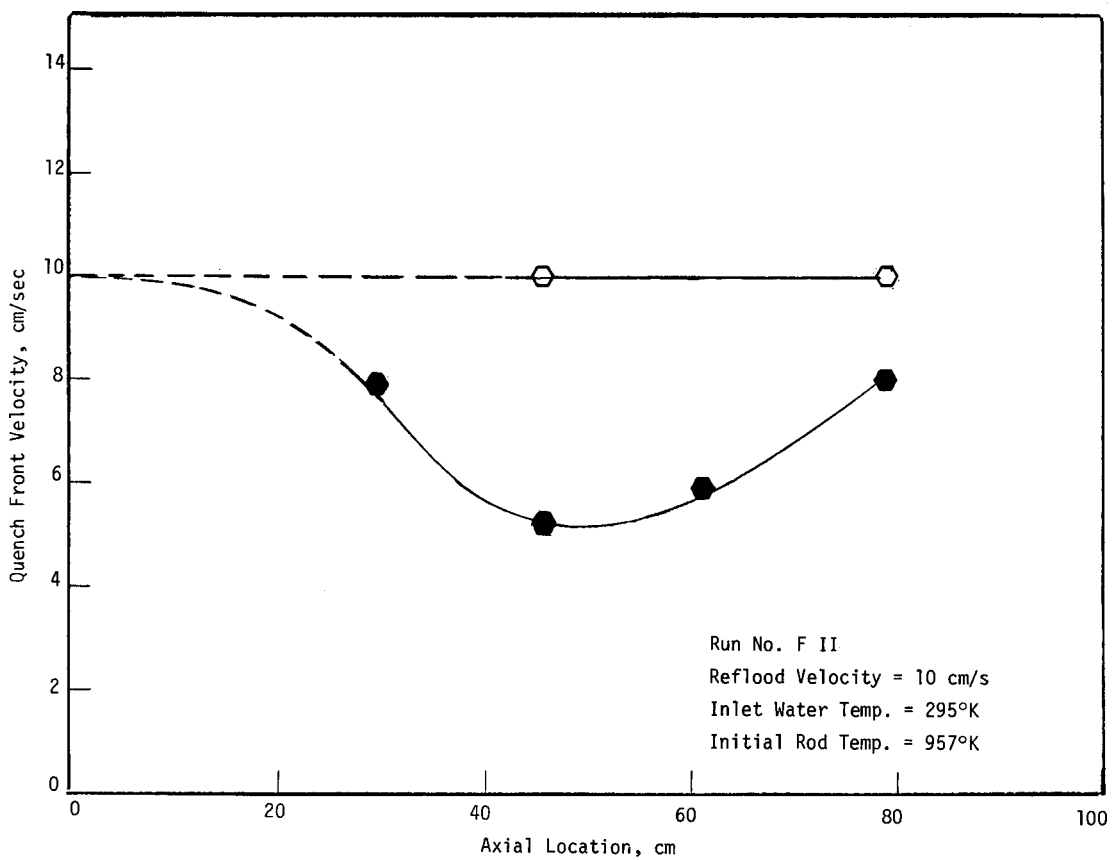

Figure D-15 Quench Front Velocity as a Function of Axial Location

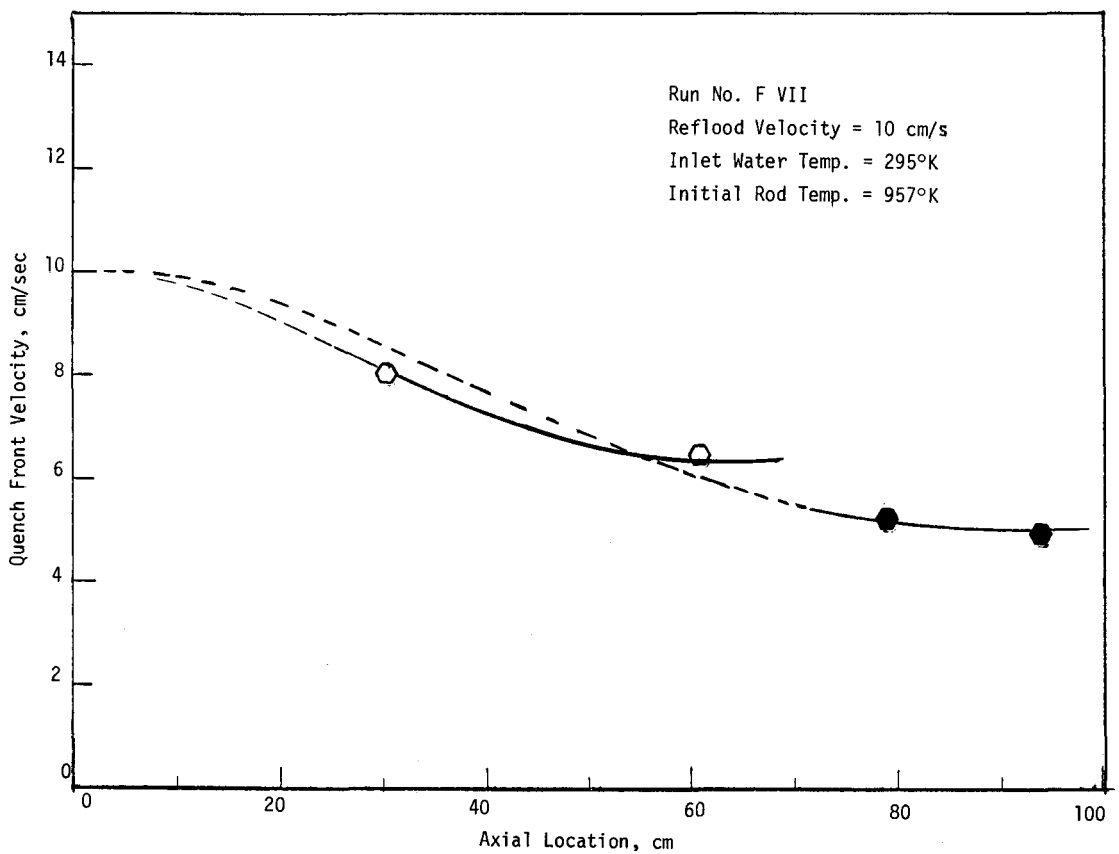

Figure D-16 Quench Front Velocity as a Function of Axial Location

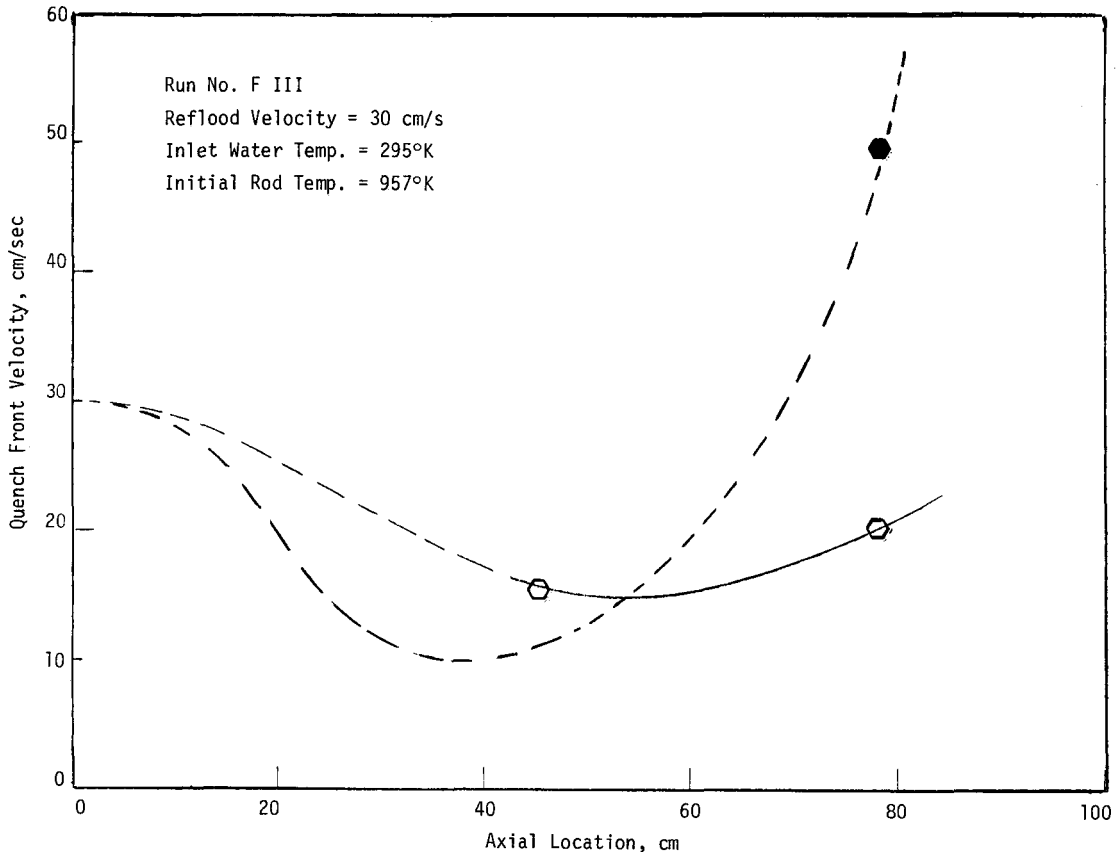

Figure D-17 Quench Front Velocity as a Function of Axial Location

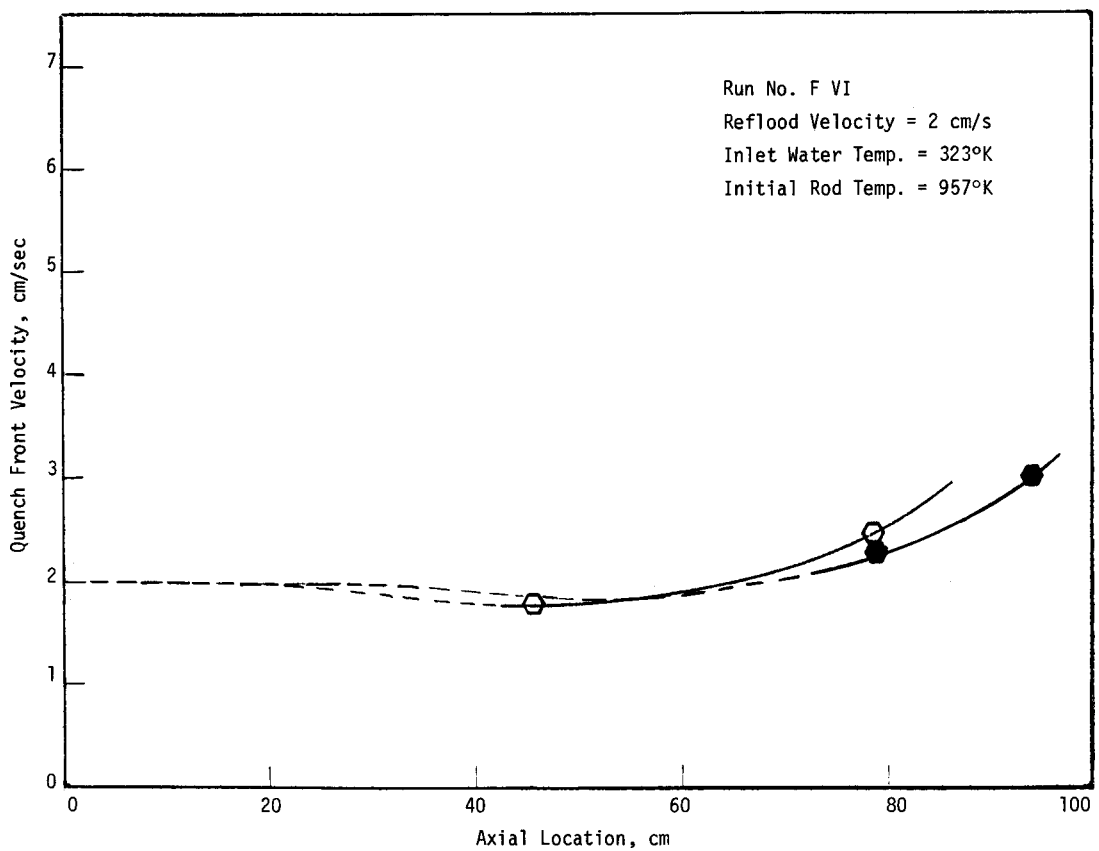

Figure D-18 Quench Front Velocity as a Function of Axial Location

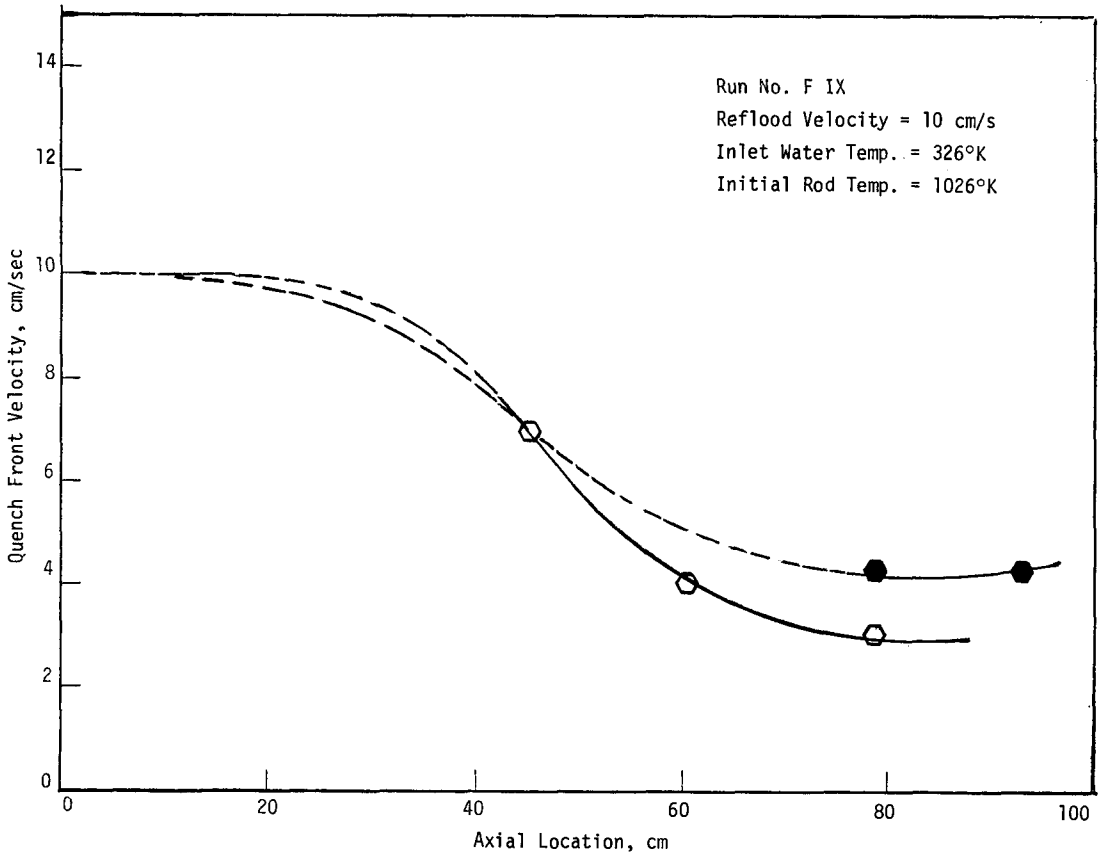

Figure D-19 Quench Front Velocity as a Function of Axial Location

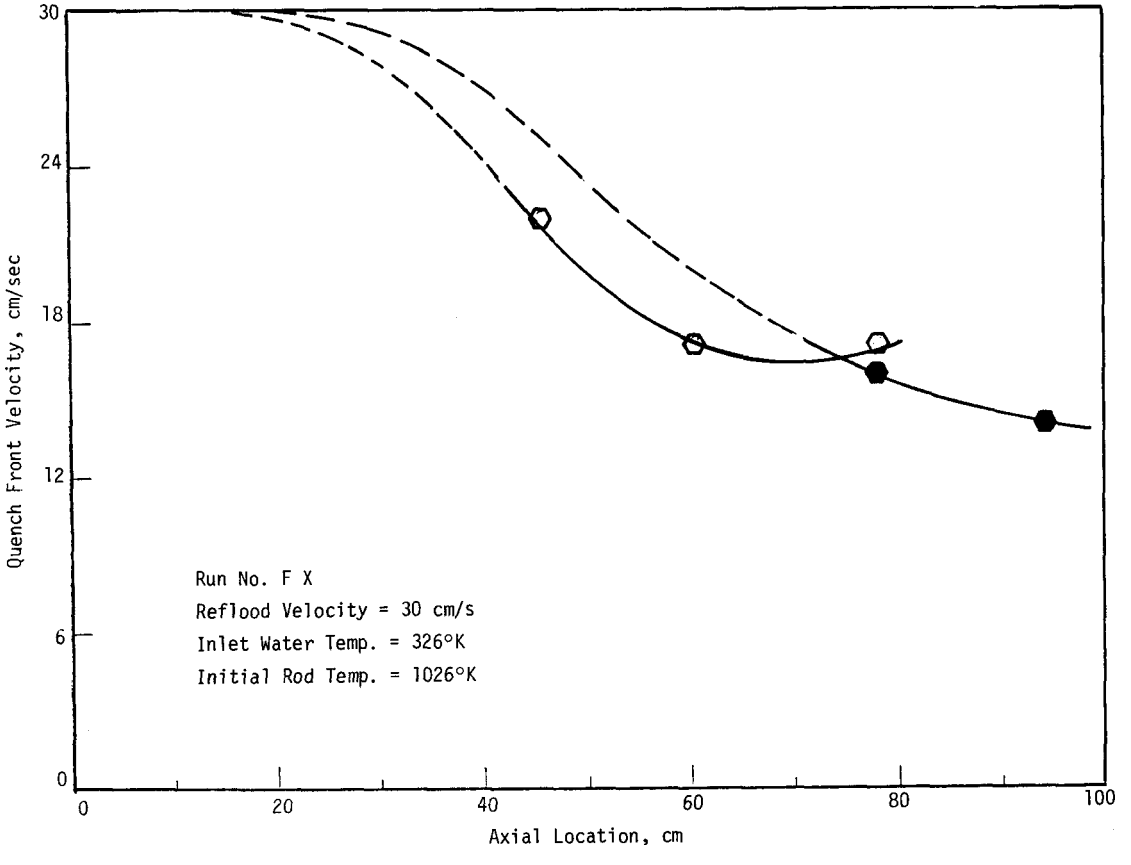

Figure D-20 Quench Front Velocity as a Function of Axial Location

APPENDIX E

COMPARISON OF THE THERMOPHYSICAL PROPERTIES OF ALUMINA AND UO_2

The thermophysical properties of the alumina insulators are compared below with the thermophysical properties of UO_2.

	Density, ρ gm/cm^3	Thermal Conductivity, k $W/m^2\ °C$	Thermal Capacity, c_p $W\ s/m\ °C$	$\sqrt{\frac{(k\rho c_p)UO_2}{(k\rho c_p)Alumina}}$
Alumina	3.2	20.9	≃0.78	≃0.7
UO_2	≃10.0	10.2	0.234	